CV AND DLTS ANALYSIS OF MATERIALS FOR

MICROELECTRONIC APPLICATIONS

THESIS

Presented to the Graduate Council
of Texas State University-San Marcos
in Partial Fulfillment
of the Requirements

for the Degree

Master of SCIENCE

by

Christopher Lohn, B.S.

San Marcos, Texas
May 2008

CV AND DLTS ANALYSIS OF MATERIALS FOR

MICROELECTRONIC APPLICATIONS

Committee Members Approved:

_____
Wilhelmus J. Geerts, Chair

_____
Terry Golding

_____
Carl A. Ventrice, Jr.

Approved by:

_____
J. Michael Willoughby
Dean of the Graduate College

DEDICATION

To my loving wife, Vlada, who has put up with me for

over six years and our furry children.

A theory is something nobody believes, except the person who made it.

An experiment is something everybody believes, except the person who made it.

-- Albert Einstein

ACKNOWLEDGEMENTS

TABLE OF CONTENTS

LIST OF TABLES

LIST OF FIGURES

CHAPTER 1

INTRODUCTION

Deep level traps occur due to defects in the crystal structure of semiconductors and reside near the center of the band. These traps are generally unwanted and affect the operation of electrical and optoelectrical devices such as transistors, light-emitting diodes and photovoltaic cells. Deep level transient spectroscopy (DLTS), pioneered by David V. Lang in 1974, is a powerful technique used to characterize those traps. The measurement technique measures the capacitance transients of simple devices such as diodes, MOS-Capacitors, and MOSFETs, after applying a bias pulse. DLTS provides information on the trap density, the capture cross section, and the position of the trap in the bandgap. DLTS is best used to characterize traps that lie deep in the bandgap. While many techniques exist to characterize shallow level traps, they lack the ability to probe deep traps, in which case DLTS is used.

The DLTS system at the Department of Physics is the minimum configuration of a commercial instrument manufactured by SULA technologies. It is furnished with a fast capacitance meter and two correlators. It uses a closed-cycle refrigerator system to vary the temperature of the sample between 10 and 700 Kelvin. DLTS experiments using ratewindow analysis performed with the original system are very time consuming. A typical temperature scan from 60-400 K, including cool down time, will take

approximately 7 hours. Since the system is only furnished with two correlators, at least

seven to ten temperature scans are necessary to get sufficient data to fully characterize a

sample. In order to reduce the measurement time, the original system was modified to

allow the measurement capacitance transient waveforms over the temperature range. The

new setup uses a new National Instruments data acquisition board as well as new

software developed by Semetrol. The improved setup allows samples to be characterized

with a single temperature scan, resulting in a large reduction in measurement time. The

software of the new system was tested extensively and suggestions for improvement were

relayed back to Semetrol resulting in a very powerful instrument.

This thesis gives a description of the new DLTS system setup, describes the

changes made to the original Sula system, and contains the results of preliminary

measurements on several diodes. An overview of the DLTS measurement technique and

standard operating procedures for the new system are also included.

CHAPTER 2

THEORY OF SOLIDS

2.1   Structure of Matter – Fundamental Level

It was once thought that atoms were indivisible and the smallest building block of matter. As we have come to learn, atoms are constructed of three subatomic particles- electrons, protons and neutrons. We can begin to understand solids by starting at the level of fundamental particles and the forces that act upon them. The four fundamental forces that act on all particles are the *gravitational force*, *electromagnetic force*, *strong force* and *weak force*. Due to the small mass of the particles, the effect of the gravitational force is so small that we can ignore it. The electromagnetic force acts on all charged particles. The strong force acts on hadrons and is responsible for binding the atomic nucleus together, while the weak force acts on all particles.

The basic building blocks of hadrons are quarks. Hadrons are made up of two subfamilies of particles, the baryons (p, n, Λ^0, Σ^+, Σ^0, Σ^-, Ξ^0, Ξ^-) with spin quantum number ½ and the mesons (π^0, π^+, K^+, K^0, η, η') with spin 0. The origins of the quark began in 1961 when Murray Gell-Mann and Yuval Ne'eman working independently, proposed the Eightfold Way patterns which can be seen in figure 2.1, when the property strangeness, denoted by the strangeness quantum number *S* is plotted versus charge, *Q*. Later in 1964, Gell-Mann and George Zweig independently observed that the Eightfold

Way pattern could be easily understood if the hadrons were built of subunits, which Gell-Mann named quarks. In 1969, Murray Gell-Mann was awarded the Nobel prize in physics for the "classification of elementary particles and their interactions".[1]
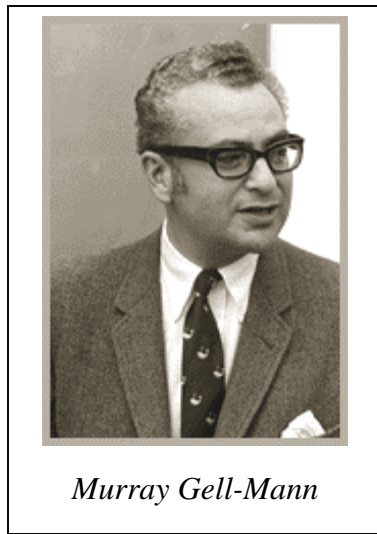
Murray Gell-Mann
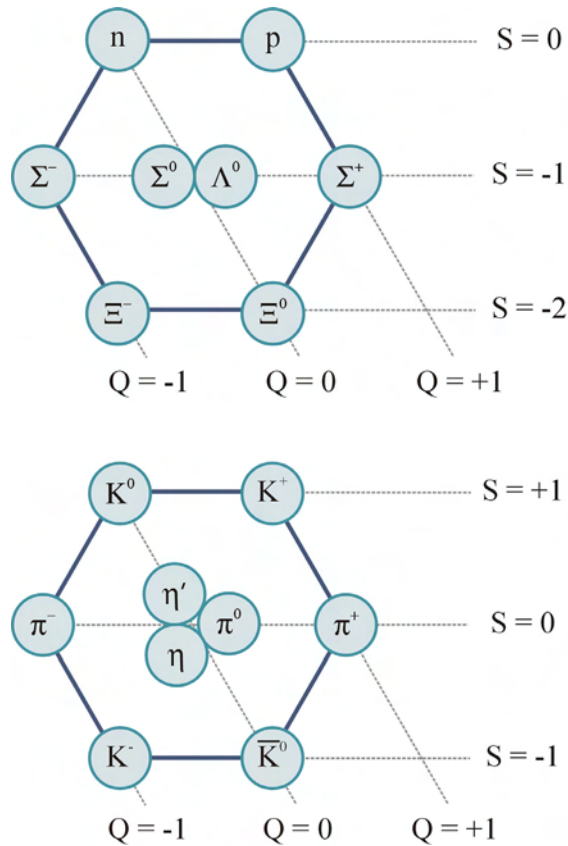
Figure 2.1
Eightfold Way Patterns[1]

There are six quarks, which have been named *up*, *down*, *strange*, *charm*, *top* and *bottom*. The baryons, which include protons and neutrons, are made up of a combination of three quarks and the mesons are made of a quark and antiquark pair.[2] As shown in figure 2.2, the combination of quarks making up the particles inside the atomic nucleus, the neutron and proton, gives a net charge of 0 and +1 respectively. The final component of an atom, the electron, is a member of the lepton family and has a charge of –1.

Table 2.1
Quarks[1,2]

Particle	Symbol	Charge	Strangeness	Antiparticle*
Up	u	+2/3	0	$\bar{u}$
Down	d	-1/3	0	$\bar{d}$
Strange	s	-1/3	-1	$\bar{s}$
Charm	c	+2/3	0	$\bar{c}$
Bottom	b	-1/3	0	$\bar{b}$
Top	t	+2/3	0	$\bar{t}$
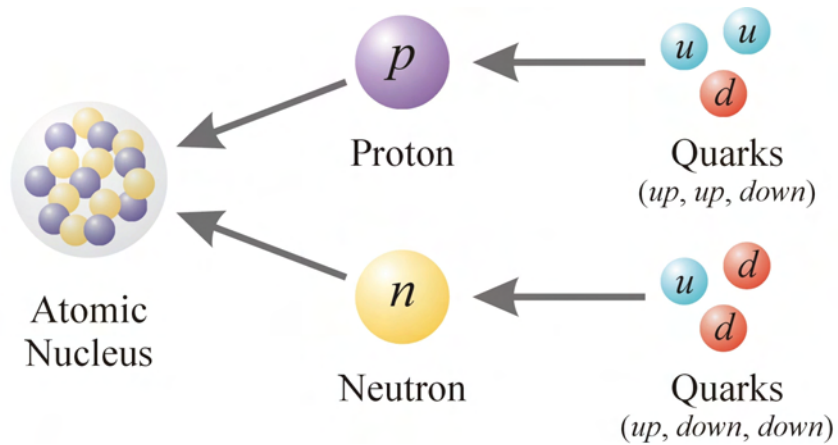
Figure 2.2
Formation of the Atomic Nucleus from Quarks[2]

Our basic understanding of the atomic model has its origin in the discovery of the electron by Joseph John Thomson in 1897. Working with a cathode ray tube, Thomson demonstrated the "rays" which caused the tube to glow were actually negatively charged particles he named corpuscles. The name was later changed to electron, a word derived from the Greek word for amber (ἤλεκτρον), which was a material the Greeks had used to investigate electrical phenomena. In 1906, Thomson received the Nobel Prize in physics

for his work in "conduction of electricity by gases". Later Thomson would put forth his proposed model for the structure of the atom.

Joseph John Thomson
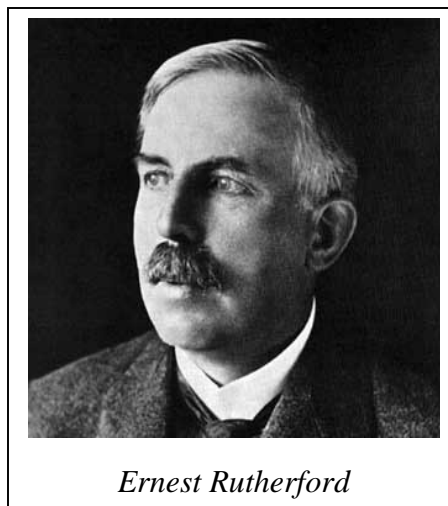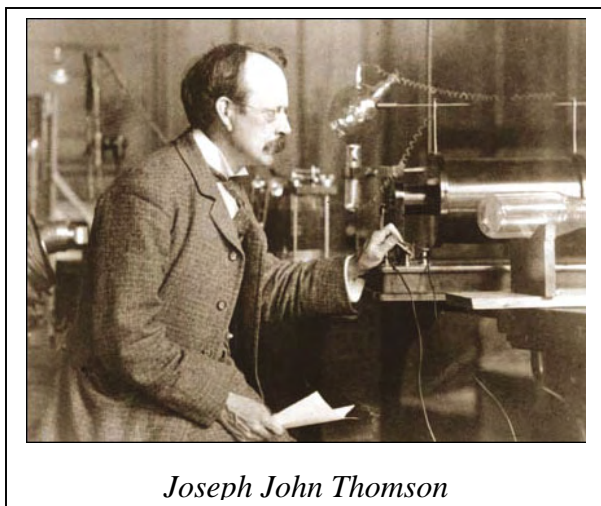
Ernest Rutherford

Although no one had made a convincing discovery of the proton as Thomson had done with the electron, the credit for the discovery of the proton went to one of Thomson's student, Ernest Rutherford. In 1918, Rutherford noticed that when alpha particles were shot into nitrogen gas, the scintillator showed the signature of a hydrogen nuclei (proton and neutron pair). His most notable contribution is the gold foil experiment which resulted in the discovery of the nucleus. In 1908, Rutherford received the Nobel Prize in chemistry for his "investigations into the disintegration of the elements, and the chemistry of radioactive substances".

In 1920, Rutherford predicted the existence of the neutron, the third and final particle comprising the atom. Building on the work done by Walther Bothe (Physics Nobel Laureate-1954) and H. Becker in 1930 and Irène Joliot-Curie and Frédéric Joliot (Chemistry Nobel Laureates-1935) in 1932 who had thought they were working with gamma ray radiation, James Chadwick proved that the radiation was not gamma rays. In 1932, Chadwick carried out a series of experiments and bombarded various gases in a

cloud chamber with the radiation and observed the recoiling nuclei. From his experiments, he determined the radiation was in fact the neutron which Rutherford had predicted. For his "discovery of the neutron", Chadwick received the Nobel Prize in physics in 1935.

James Chadwick
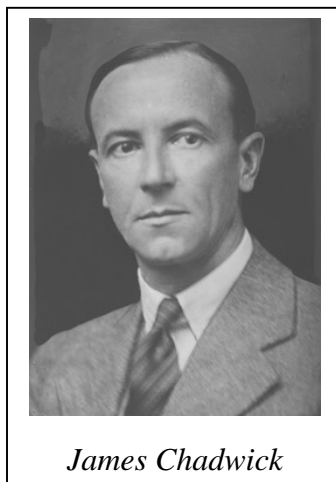
2.2   Atoms

Although much of understanding of atoms has come about during the 20th century, the concept of atoms originated approximately 2400 years ago. Around the year 400 B.C., the Greek philosopher, Democritus conceived the idea that all material bodies are made of particles too small to be seen by the human eye. He called the particles atoms (άτομος) or indivisibles. Democritus believed that there were four kinds of atoms-stone (heavy and dry), water (heavy and wet), air (cold and light), and fire (hot and slippery). He believed that all matter was composed of a combination of these four atoms. The soil was composed of stone and water atoms. Plants which grew in the soil and required water and sunlight (fire atoms) for growth, consisted of soil, water and fire atoms. Once the plants dried and all of the water atoms were removed, the plants could be burned thus liberating the fire atoms and leaving behind ash (stone atoms).[3]

Democritus
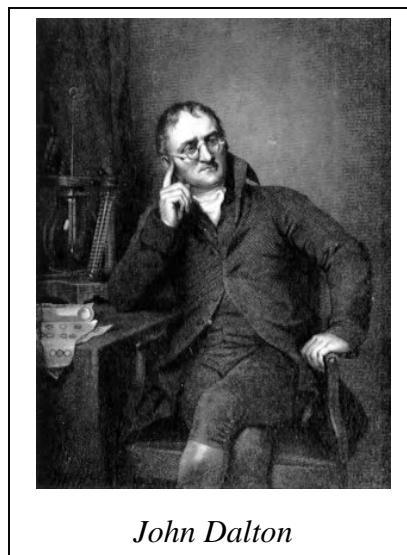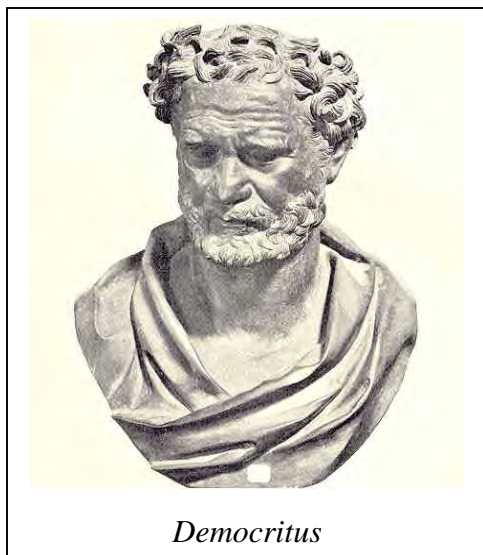
John Dalton

In the early 19th century, atomic theory was further advanced by chemist John Dalton. His postulates based on experimentation and chemical laws known at the time, provided the foundation for atomic theory and resemble a more modern view of the atom. The main points of Dalton's atomic theory are:[4,5]

I. All matter is composed of indivisible particles called atoms. Atoms maintain their identity through physical and chemical change.

II. An element is a type of matter composed of only one kind of atom with each atom of the element having the same properties - mass, chemical, physical, etc.

III. A compound is a type of matter composed of atoms of two or more elements chemically combined in fixed proportions.

IV. A chemical reaction consists of the rearrangement of the atoms present in the reacting substances to give new chemical combinations present in the substances formed by the reaction. Atoms are not created, destroyed or broken into smaller particles by the chemical reaction.

Although Dalton's work laid the foundation for chemistry, he lacked the tools necessary to investigate the structure of the atom itself. This would occur approximately 50 years after his death.

In 1904, approximately seven years after discovering the electron, J. J. Thomson put forth what has become known as the "plum pudding" model. Thomson described the model of the atom as a "number of negatively electrified corpuscles (electrons) enclosed in a sphere of uniform positive electrification".[6] He believed that the electrons moved about on rings enclosed by a cloud of positive charge. This was later disproved in 1909 by Rutherford's gold foil experiment.

Under the direction of Rutherford, Hans Geiger and Ernest Marsden shot alpha particles at a piece of gold foil. They observed that some of the alpha particles were deflected at very large angles and in some cases recoiled backwards. From the results, Rutherford deduced that Thomson's model was incorrect and that the atoms are comprised of mostly empty space with the positive charge (protons) and mass of the atom concentrated in the nucleus.
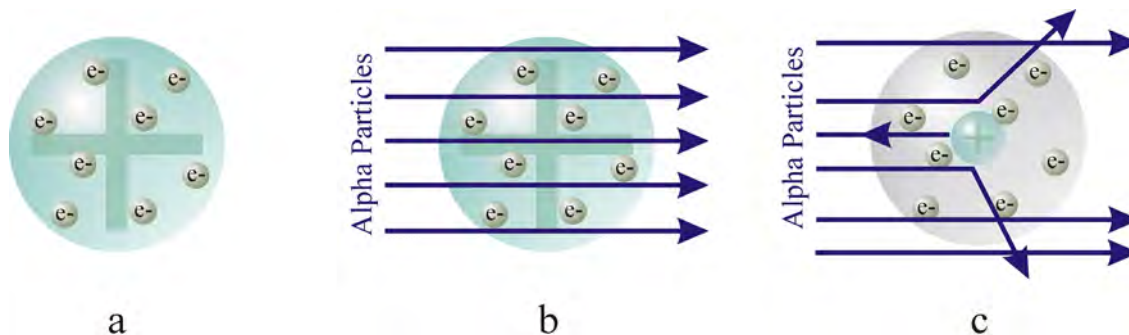
Figure 2.3
Early Atomic Model: a) Thomson's "Plum Pudding" model; b) Alpha particles
penetrating "Plum Pudding" model; c) Rutherford's results and model

It was believed that the positive charge concentrated at the center provided the Coulombic attraction for the electrons orbiting the nucleus and the electrons stayed in lasting, stable orbits. This planetary model of the atom presented two problems. As the electrons orbited the nucleus, they would lose energy in the form of electromagnetic

radiation and ultimately spiral inward crashing into the nucleus and thus causing an end to all matter. Secondly, the hydrogen spectrum which had been known for some time, did not exhibit the continuous spectrum of a decaying electron. The solution was provided by Niels Bohr, a student working in Rutherford's laboratory.

During this time, many scientists were working with hydrogen since it was the simplest element and easily understood. Various parts of the discrete spectrum had been measured and are named after the scientist (Lyman, Balmer, Paschen, Brackett) who reported them. Johann Balmer published a simple equation (2.1) governing the hydrogen spectrum in the visible region (λ = 410.12, 434.05, 486.13, 656.28 nm).

$$\lambda = B\left(\frac{m^2}{m^2 - n^2}\right) \qquad \text{where } B = 3.6456 \text{ x } 10^{-7} \text{ m, } m > 2 \text{ and } n = 2 \qquad (2.1)$$

This was later generalized for all transitions of hydrogen by Johannes Rydberg into what has become known as the Rydberg formula, equation (2.2).

$$\frac{1}{\lambda} = R\left(\frac{1}{m^2} - \frac{1}{n^2}\right) \qquad \text{where } R = 1.097373 \text{ x } 10^7 \text{ m}^{-1} \text{ and } m < n \qquad (2.2)$$

Some thought there may be a relationship between the structure of the atom and the spectrum it emits. Upon discussing the equations governing the hydrogen spectrum with a friend, Bohr hit upon the solution – the electron energy is quantized. When the electron receives energy and is stimulated, the electron is excited into a higher energy orbit further away from the nucleus until it decays to a lower energy orbit thus emitting electromagnetic radiation. Bohr's original model with concentric circular quantum orbits was later generalized by Arnold Sommerfeld to include elliptical orbits. The model does have some limitations and has subsequently been replaced by quantum mechanics.
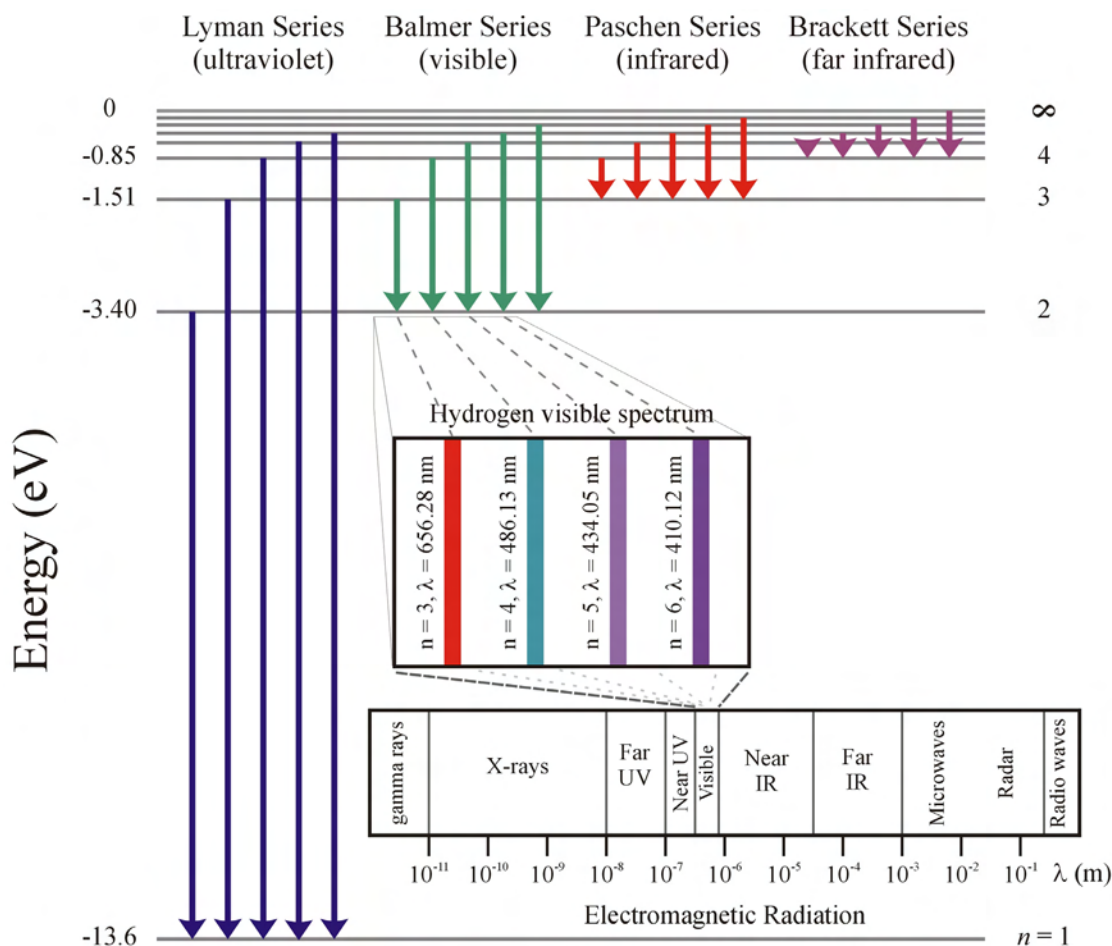
Figure 2.4
Energy Level Diagram for Hydrogen Spectrum

From Bohr's postulates regarding atomic structure, we get the principal quantum

number, *n*, which is used to describe the orbital energy level. Sommerfeld's modification

to the model, the addition of the elliptical orbits, added an additional degree of freedom

to the orbits. This modification required a second quantum number, *l*, to describe the

angular momentum. A new problem with the model then arose, it was long known that

light emitted from the from the atom was affected by magnetic fields. Pieter Zeeman

(Physics Nobel Laureate-1902) observed in 1896, that the sodium spectrum experienced a

broadening of the spectral lines under the influence of a magnetic field. As the electron

1st Orbit

2nd Orbit

3rd Orbit

1st Orbit
(1 circular)

2nd Orbit
(1 circular, 3 elliptical)

3rd Orbit
(1 circular, 8 elliptical)

a

b
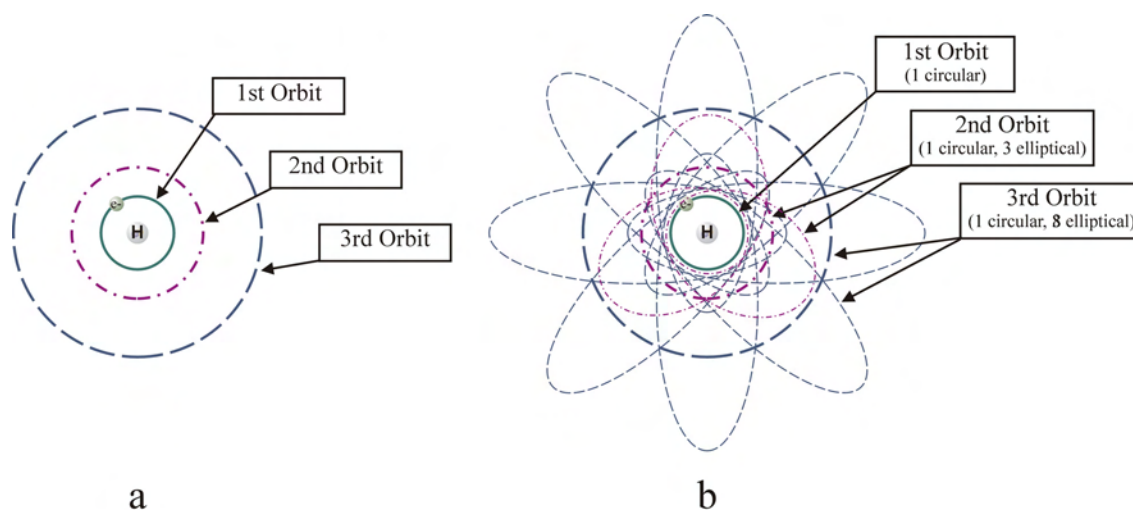
Figure 2.5
Atomic Model: a) Bohr Model of Hydrogen;
b) Bohr-Sommerfeld Model of Hydrogen

No Magnetic Field   External Magnetic Field

$m_l = 1$

$m_l = 0$

$m_l = -1$

$n = 2$
($2p$ orbital)

$n = 1$
($1s$ orbital)

Resulting
spectrum
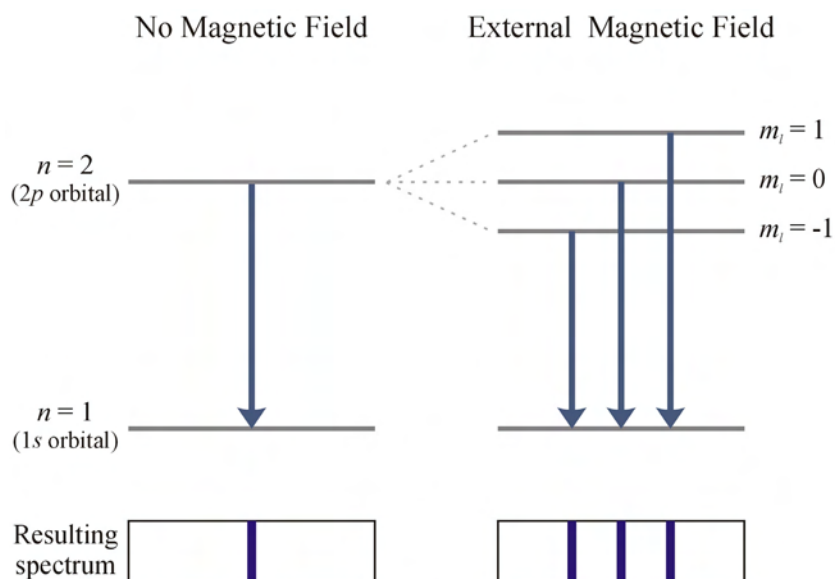
Figure 2.6
The Zeeman Effect

orbits the nucleus, it behaves as a current loop and produces a magnetic moment and thus

the electron is influenced by an external magnetic field. This required that the electron to

have a third quantum number, m_l, the magnetic quantum number. Finally, to match

experimental results, a fourth quantum number was added to account for the intrinsic

angular momentum due to the electron spining about its own own axis. The fourth

quantum number, m_s, spin angular momentum or spin of the electron takes the value ½

for spin up or -½ for spin down particles.

The electrons in an atom are therefore described by a set of four quantum

numbers. The rules governing these values can be seen in table 2.2. It is also important

to note that no two atomic electrons can be in the same quantum state, that is have the

same set of quantum numbers, as dictated by the Pauli Exclusion Principle put forth by

Wolfgang Pauli (Physics Nobel Laureate-1945). The set of quantum numbers can also be

used to determine the electron orbit (or shell) and the electron configuration of an atom as

shown in table 2.3 and table 2.4.

Table 2.2
Quantum Numbers

Name	Symbol	Value
principal quantum number	n	1, 2, 3, 4, …
orbital angular momentum quantum number	l	0, 1, 2, 3, … $(n\text{-}1)$
magnetic quantum number	m_l	0, ±1,±2, ..., ±l
spin angular momentum quantum number	m_s	±½

Table 2.3
Electron Shells

Orbital angular momentum quantum number, l	Electron shell designation	Name	Number of electron vacancies in shell
0	s	**s**harp	2
1	p	**p**rincipal	6
2	d	**d**iffuse	10
3	f	**f**undamental	14

Table 2.4
Electron configuration for iron ($1s^2 2s^2 2p^6 3s^2 3p^6 3d^6 4s^2$ - 26 electrons)[7]

electron	quantum number				
	n	l	m_l	m_s	
1	1	0	0	$+\frac{1}{2}$	1s electrons
2	1	0	0	$-\frac{1}{2}$	
3	2	0	0	$+\frac{1}{2}$	2s electrons
4	2	0	0	$-\frac{1}{2}$	
5	2	1	-1	$+\frac{1}{2}$	2p electrons
6	2	1	0	$+\frac{1}{2}$	
7	2	1	+1	$+\frac{1}{2}$	
8	2	1	-1	$-\frac{1}{2}$	
9	2	1	0	$-\frac{1}{2}$	
10	2	1	+1	$-\frac{1}{2}$	
11	3	0	0	$+\frac{1}{2}$	3s electrons
12	3	0	0	$-\frac{1}{2}$	
13	3	1	-1	$+\frac{1}{2}$	3p electrons
14	3	1	0	$+\frac{1}{2}$	
15	3	1	+1	$+\frac{1}{2}$	
16	3	1	-1	$-\frac{1}{2}$	
17	3	1	0	$-\frac{1}{2}$	
18	3	1	+1	$-\frac{1}{2}$	
19	3	2	-2	$+\frac{1}{2}$	3d electrons
20	3	2	-1	$+\frac{1}{2}$	
21	3	2	0	$+\frac{1}{2}$	
22	3	2	+1	$+\frac{1}{2}$	
23	3	2	+2	$+\frac{1}{2}$	
24	3	2	-2	$-\frac{1}{2}$	
25	4	0	0	$+\frac{1}{2}$	4s electrons
26	4	0	0	$-\frac{1}{2}$	

2.3   Atomic Bonding

When two atoms are brought close together, the valence electrons in the atoms and the positively charged nucleus begin to interact. As the two atoms are brought in close proximity, like charges such as the valence electrons of the atoms or their nuclei will produce a repulsive force between the two atoms while the nucleus of an atom and the electrons of the second atom create an attractive force. A chemical bond is formed between the two atoms if the energy of the system (two atoms) is more favorable and thus more stable than if the atoms were separated. That is to say that a bond will be formed when the net force is equal to zero and the energy is minimized assuming that it is less than if the two atoms were separated. The bond length (r_o) between the atoms is when this condition is met.
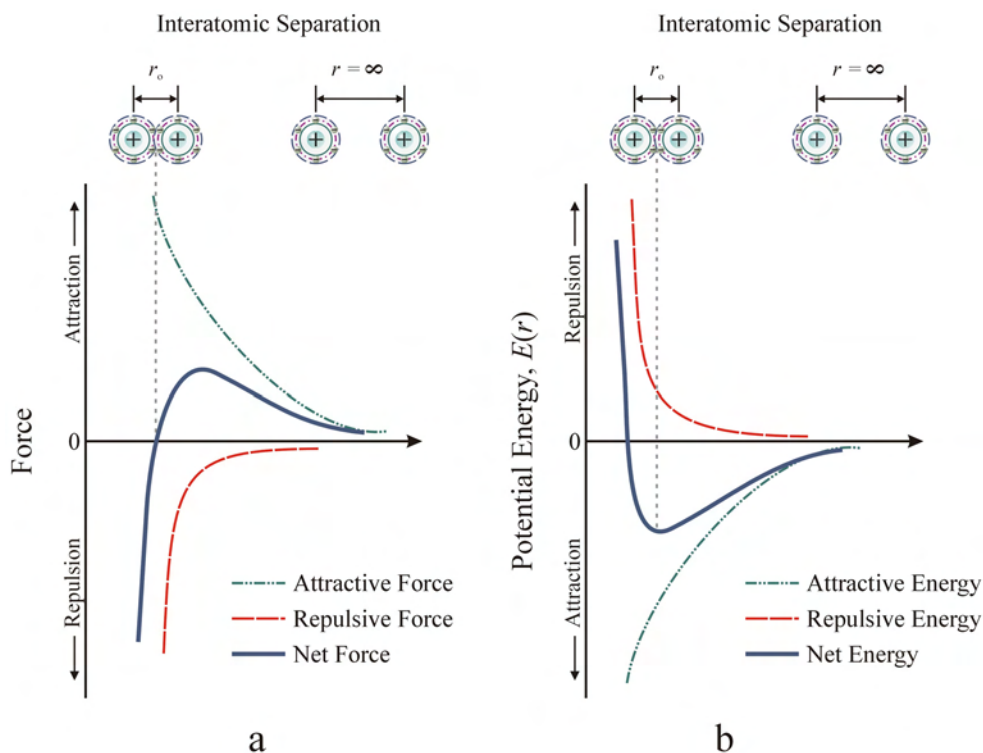
Figure 2.7
Atomic Bonding: a) Force vs. Interatomic Separation;
b) Potential Energy vs. Interatomic Separation

2.3.1   Primary Bonds

Covalent bonding occurs when neighboring atoms share a valence electrons pair, thus minimizing the energy of the system. In the case of the simplest element, hydrogen with an electron configuration of $1s$, a diatomic molecule is formed when two hydrogen atoms are brought together to share their $1s$ electrons. Carbon with the electron configuration of $1s^2 2s^2 2p^2$, shares one valence electron with each of the four neighboring carbon atoms. The bond energy is highest for covalent bonds, resulting in very hard materials with high melting points and being insoluble in nearly all solvents. The directional nature and strength of the bond results in covalently bonded materials being non-ductile and non-malleable. As a result, these materials will fracture under a strong applied force. Since all valence electrons are locked in the atomic bonds and not free to move under an applied electric field, such materials exhibit poor electrical conductivity.

Ionic bonding, also known as electrovalent bonding, generally takes place between metallic (electropositive) and nonmetallic (electronegative) elements. One atom will give up valence electron(s), becoming a positively charged ion (cation) in order to obtain a stable electron configuration. The second species of atom will accept the electron(s), forming a negatively charged ion (anion) in order to obtain a stable electron configuration. The oppositely charged ions will be pulled together due to the Coulombic force until it is balanced by the repulsive force between the electron shells of the two atoms, forming an ionic bond. Ionic bonding results in strong, but brittle materials, which are soluble in polar solvents. Ionic bonded materials are typically electrical insulators and have lower thermal conductivity compared to metals and covalently

bonded materials. The melting point of ionic bonded materials is usually higher than that
of metals.
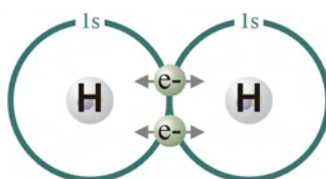
Hydrogen ($1s$) - Each atom shares an electron
to fill $1s$ shell (available states = 2)

a
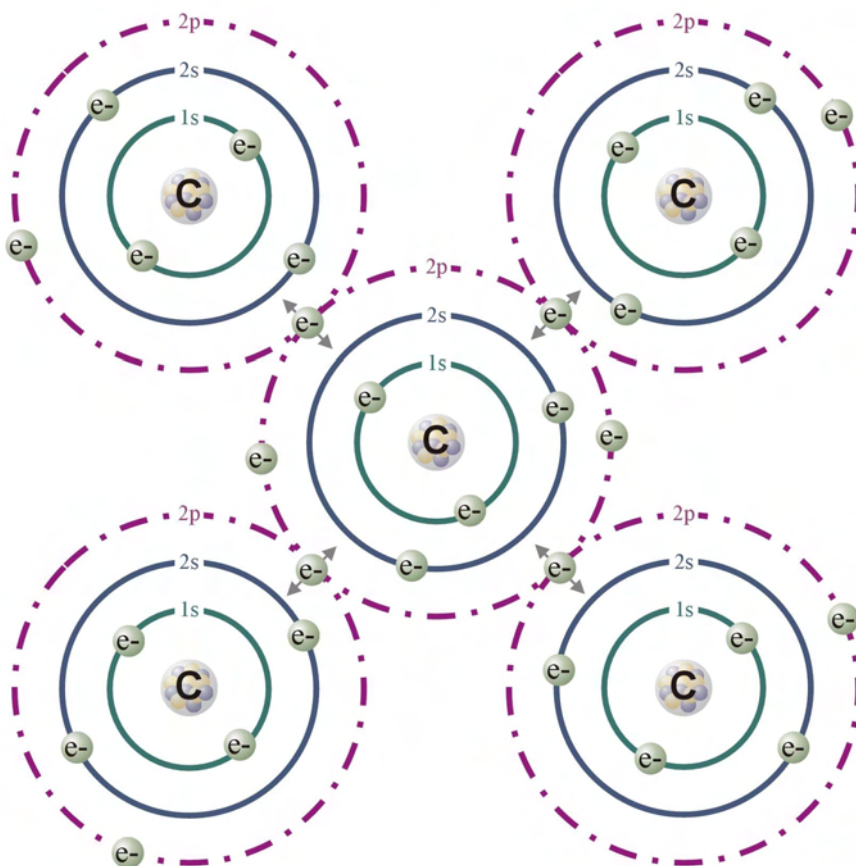
Carbon ($1s^2 2s^2 2p^2$) - Each neighboring atom shares one electron
with center atom to fill $2p$ shell (available states = 6)

b

Figure 2.8
Covalent Bonding: a) Diatomic Hydrogen Molecule; b) Carbon

+1 Ion   -1 Ion
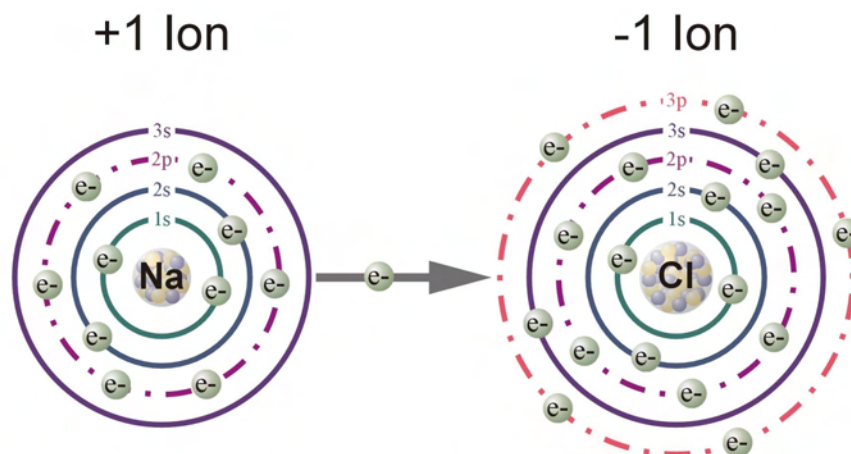
Sodium ($1s^2 2s^2 2p^6 3s^1$) gives up the $3s$ valence electron to achieve a stable electron configuration and becomes a positively charged ion. Chlorine ($1s^2 2s^2 2p^6 3s^2 3p^5$) accepts the electron to fill the $3p$ shell, achieving a stable electron configuration and becoming a negatively charged ion. The two atoms become bonded due to the Coulombic attraction between the ions.

a

-2 Ion   +2 Ion
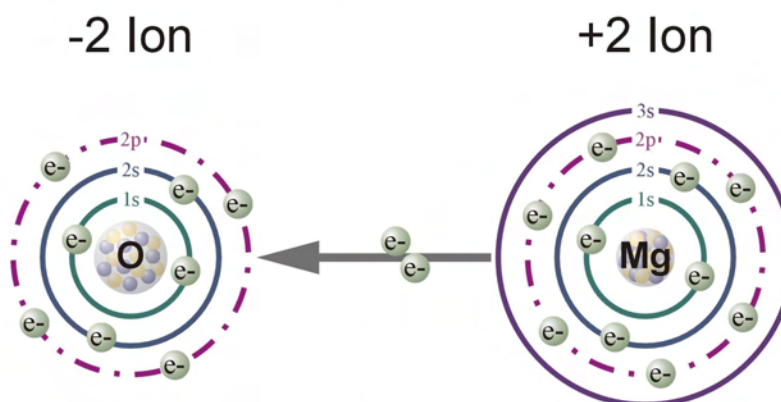
Magnesium ($1s^2 2s^2 2p^6 3s^2$) gives up the two $3s$ valence electrons to achieve a stable electron configuration and becomes a positively charged ion. Oxygen ($1s^2 2s^2 2p^4$) accepts the two electrons to fill the $2p$ shell, achieving a stable electron configuration and becoming a negatively charged ion. The two atoms become bonded due to the Coulombic attraction between the ions.

b

Figure 2.9
Ionic Bonding: a) Sodium Chloride (table salt); b) Magnesium Oxide

The third type of bonding, metallic bonding is when many metal atoms are brought together and the valence electrons become delocalized, forming an electron cloud, which is collectively shared by the metal ions. The sharing of the electron cloud results in non-directional bonding and close packing of the metal ions and thus higher densities for metals. The non-directional bonding and freedom of electron and ion movement makes metals ductile (and malleable), and gives the material high electrical and thermal conductivity.
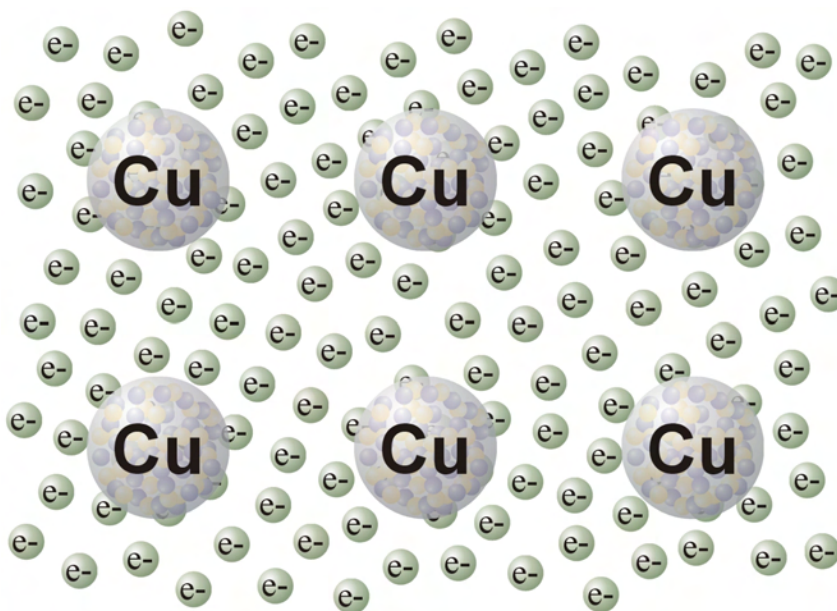
Figure 2.10
Metallic Bonding: Copper

2.3.2   Secondary Bonds

Secondary bonds are weak compared to primary bonds. In contrast to primary bonding, when bonds are formed due to minimization of force and potential energy, secondary bonding occurs due to the attraction between electric dipoles contained in atoms or molecules. Secondary bonds are often referred to as van der Waals bonds due

to the van der Waals force responsible for the bonding. Secondary bonding may occur as one of two types of bonding involving fluctuating dipoles or permanent dipoles.

The liquefaction and solidification of noble gases, which have a filled outer valence electron shell, is due to the bonding of fluctuating dipoles. At any given moment there is an asymmetrical distribution of negatively charged electrons around the positively charged nucleus resulting in an electric dipole. The electron distribution and creation of a dipole is also influenced by neighboring atoms. Once the dipoles are formed, attraction between the dipoles occurs and very weak bonds are formed.
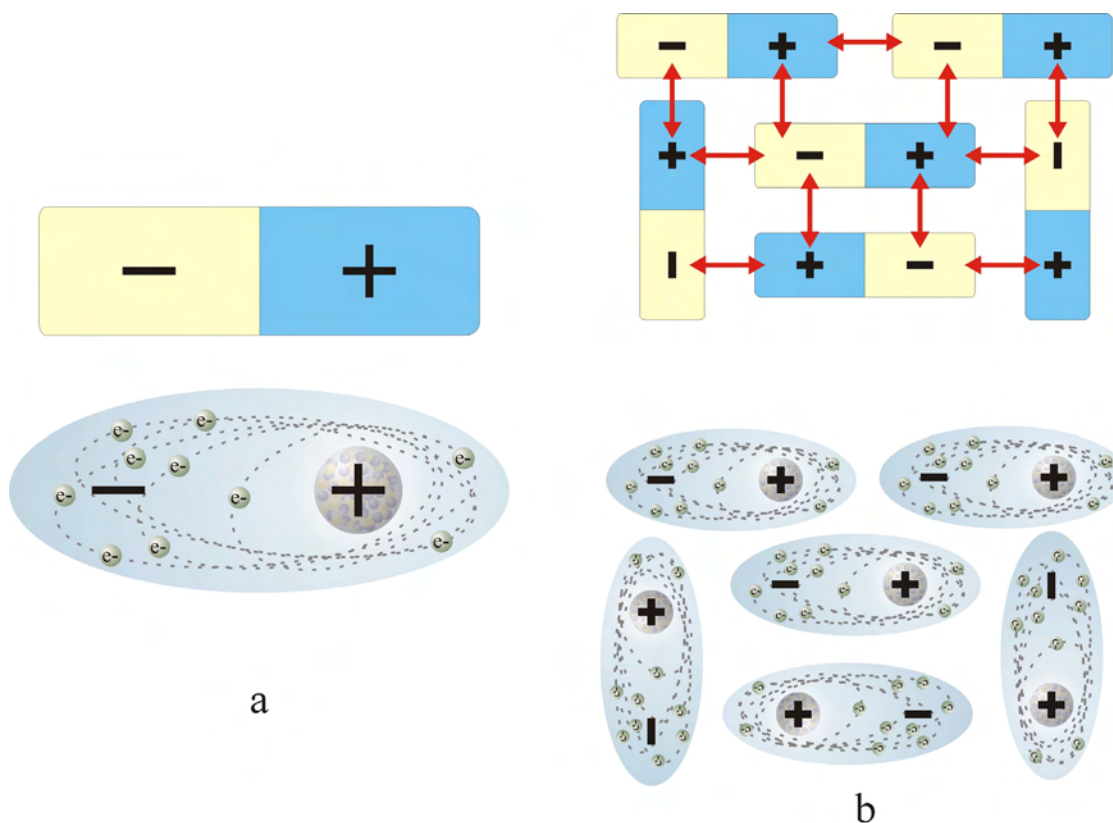
Figure 2.11
Secondary Bonding - Fluctuating Dipole: a) Atom forming a fluctuating dipole;
b) Fluctuating dipole formation of a solid

Permanent dipoles occur due to the arrangement of atoms in the molecule itself. If we consider methane (CH_4), we see a symmetrical arrangement of the four C-H bonds resulting in no net dipole. However, if we replace one hydrogen atom with a chlorine atom to form a chloromethane molecule (CH_3Cl), a dipole would form along the axis of the C-Cl bond. The dipole created would allow the molecule to bond with other molecular dipoles.

Hydrogen bonding is a special case of permanent dipole bonding when polar bonds O-H and N-H interact with electronegative atoms. Hydrogen bonding can be seen in water molecules (H_2O) where a dipole is created between oxygen and two hydrogen atoms. A general list of properties associated with each bonding type can be seen in table 2.5.

a   b
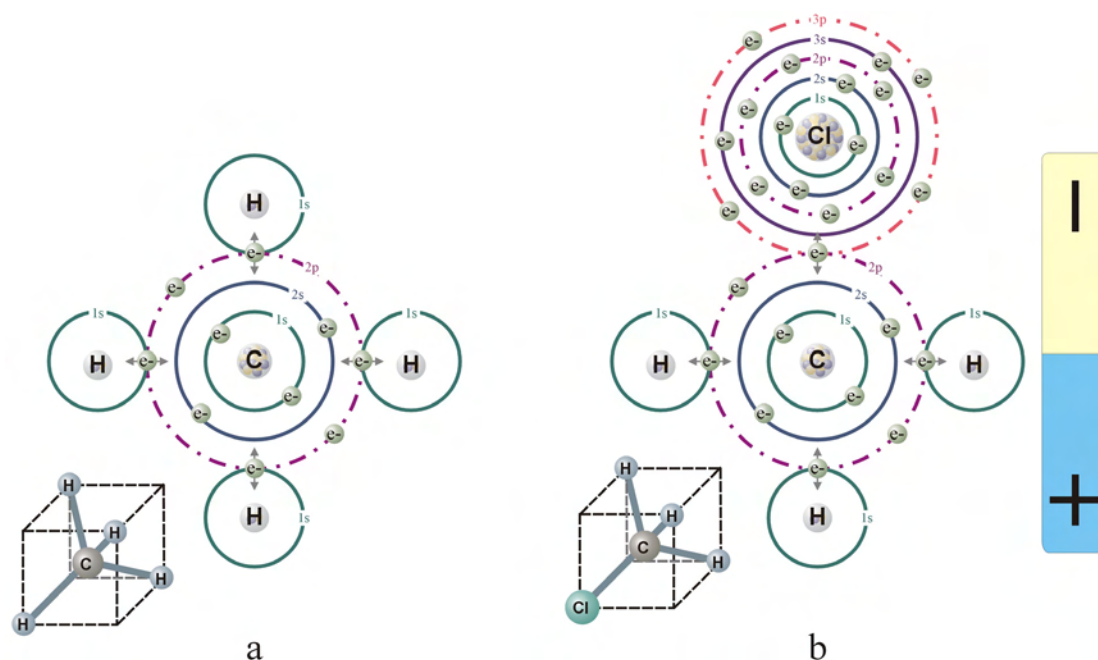
Figure 2.12
Secondary Bonding - Permanent Dipole: a) Methane (CH₄);
b) Chloromethane (CH₃Cl)
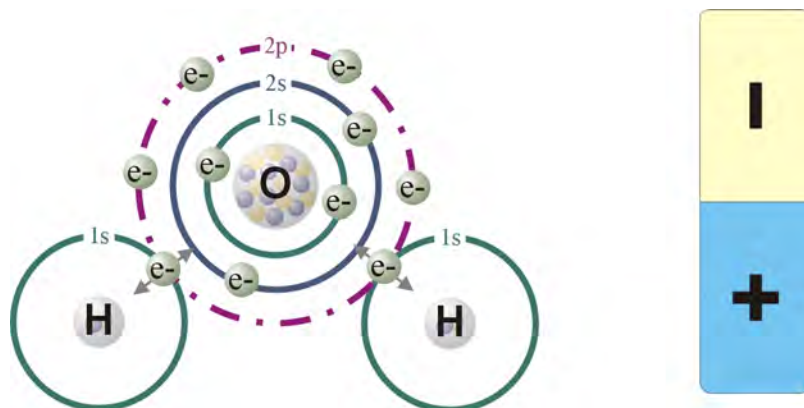
Figure 2.13
Secondary Bonding – Hydrogen Bonding

Table 2.5
Bonding Properties[8]

Covalent Bonding	Ionic Bonding	Metallic Bonding	Van der Waals Bonding	Hydrogen Bonding
Strongest bond			Weakest bond	Weak bond
Materials are hard, will fracture under applied force, nonductile, nonmalleable	Hard and brittle, cleavable	Ductile, malleable		Some ductility
Large elastic modulus	Large elastic modulus	Large elastic modulus	Low elastic modulus	Low elastic modulus
Highest melting point	High melting point, greater than metals	Low melting point	Low melting point	Low melting point
Poor electrical conductivity	Generally electrical insulator, may conduct at high temperature	Excellent electrical conductivity	Electrical insulator	Electrical insulator
Moderate thermal condcutivity	Low thermal conductivity compared to covalent and metal bonds	Good thermal conductivity	Poor thermal conductivity	Poor thermal conductivity

2.4   Energy Bands

In going from a gas to a solid, the atoms of the material become more closely packed. As the atoms are brought close together in forming a solid, the outer valence electrons of neighboring atoms begin to interact. As the interatomic spacing is further reduced, the inner energy levels also become affected by the electrons of other atoms. The Pauli Exclusion Principle dictates that no two electrons in the system can have the same quantum state, that is have the same set of quantum numbers. Since there are many atoms in the solid, the discrete energy levels of the individual atoms begin to split into many closely spaced sublevels which form continuous energy bands. The band into which the ground state valence band splits is termed the valence band, while the first excited state, the level immediately above the valence band is termed the conduction band. The valence band is filled with electrons, while the conduction band may or may not be occupied by electrons at any given time, similar to the excited state of a free atom. The inner levels below the valence band also split into bands, which are more narrow because the wavefunctions of the inner electrons of neighboring atoms have less overlap. The inner bands are often omitted when describing the band structure of a material because they have little effect on the electronic transport properties of the solid.[10] The energy gap between the valence band and the conduction band is known as the bandgap (E_g). In this energy range no stationary electron states exist. The bandgaps and band widths will vary from the inner levels to the conduction band. The bandgap between the valence band and conduction band is of most importance, contributing the properties of the material, while bandgaps between the lower levels are often ignored.

An example of energy band formation in carbon can be seen in figures 2.14 and 2.15. This figure shows the theoretical band structure of diamond as a function of the lattice parameter. When the atoms are separated by a large distance, the electronic structure is similar to that of individual atoms. Bringing the atoms closer together, as in a solid, causes neighboring atoms to interact and the wavefunctions will overlap resulting in the energy levels splitting into energy bands. An isolated carbon atom in the ground state has an electron configuration of $1s^2 2s^2 2p^2$ resulting in two $1s$ states, two $2s$ states, six $2p$ states and higher states. If there are N atoms in the solid there will be $2N$ $1s$ states, $2N$ $2s$ states and $6N$ $2p$ states. As the interatomic spacing is reduced, the energy levels will split into bands. The $2s$ and $2p$ bands will merge as the spacing is reduced, until they reach equilibrium at the bond distance forming the valence and conduction bands each with $4N$ states separated by the bandgap, E_g.[9]
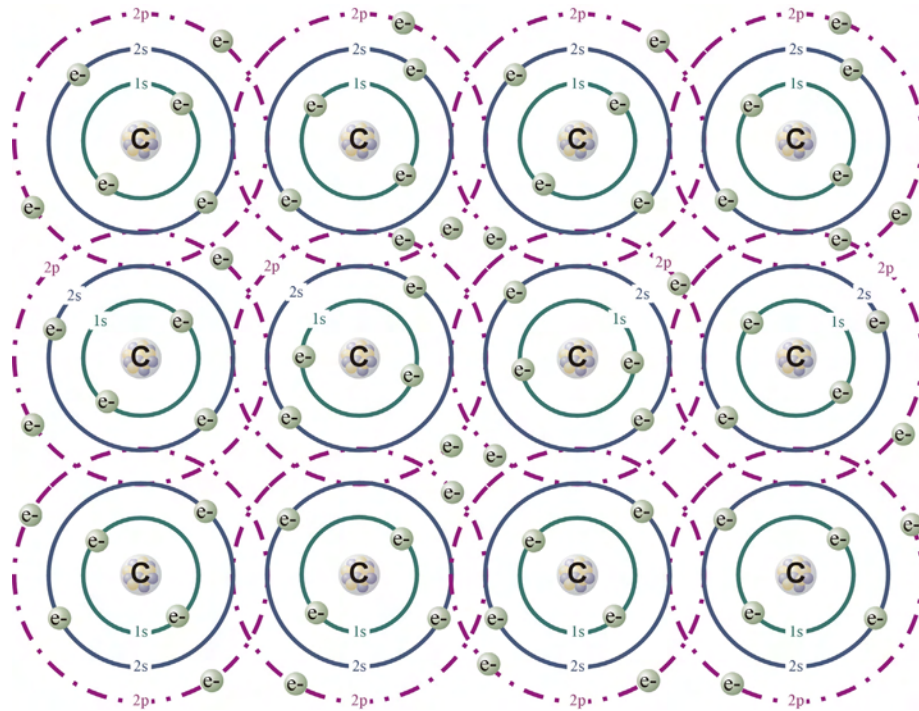
Figure 2.14
Formation of solid: Carbon ($1s^2 2s^2 2p^2$)
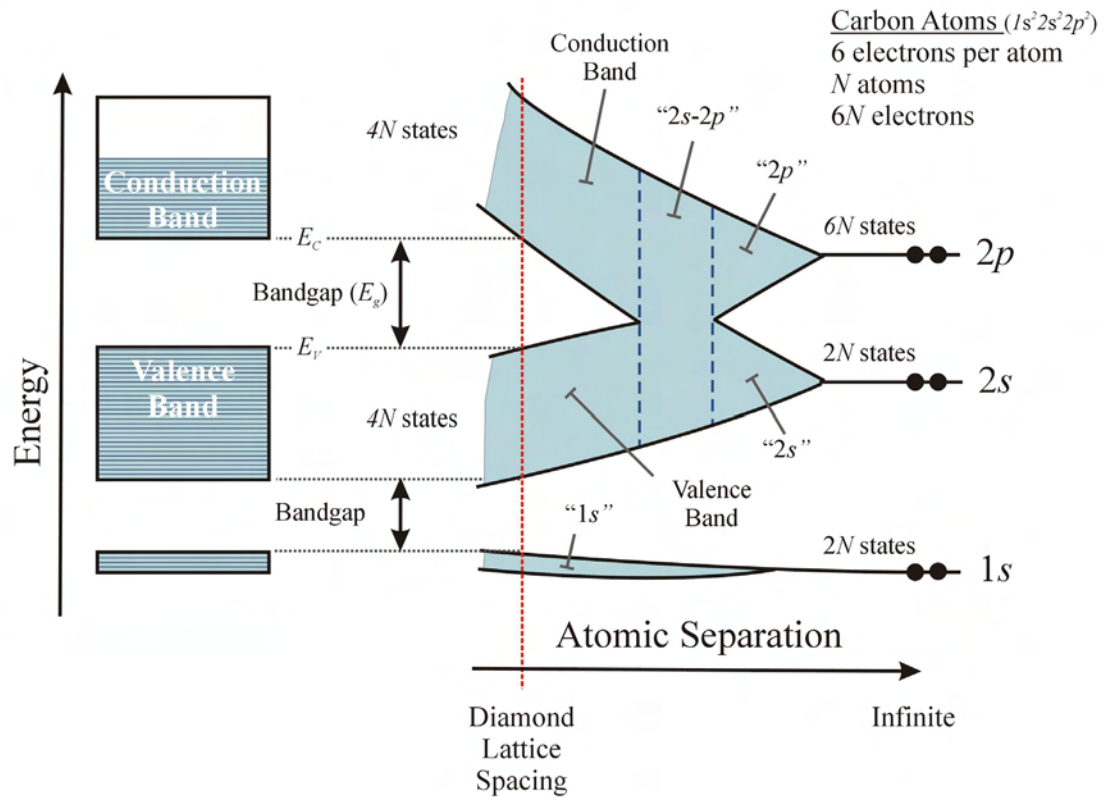
Figure 2.15
Energy Band Formation: Carbon $(1s^2 2s^2 2p^2)^9$

The energy band structure defines the electric transport properties of a material resulting in conductors, semiconductors and insulators. Under an applied electric field, for a material to be able to conduct, there must be empty states available for the electron to fill. For this reason conductors generally have partially filled bands or overlapping partially filled bands which provide the necessary empty states for electrons to fill. Insulators and semiconductors have filled valence bands and empty conduction bands separated by a bandgap, which do not provide the empty states to allow for charges to move and thus result in electrical conduction. The difference in band structure which distinguishes insulators from semiconductors and makes conduction possible in semiconductors is the width of the bandgap. Insulators have a larger bandgap, which

prevents the electron at room temperature from gaining enough energy to traverse the bandgap from valence band to the conduction band. In the case of semiconductors, at T=0K the valence band is completely filled and the conduction band is empty. However at higher temperatures, electrons can gain enough energy to jump the narrow bandgap into the conduction band and contribute to electrical conduction.
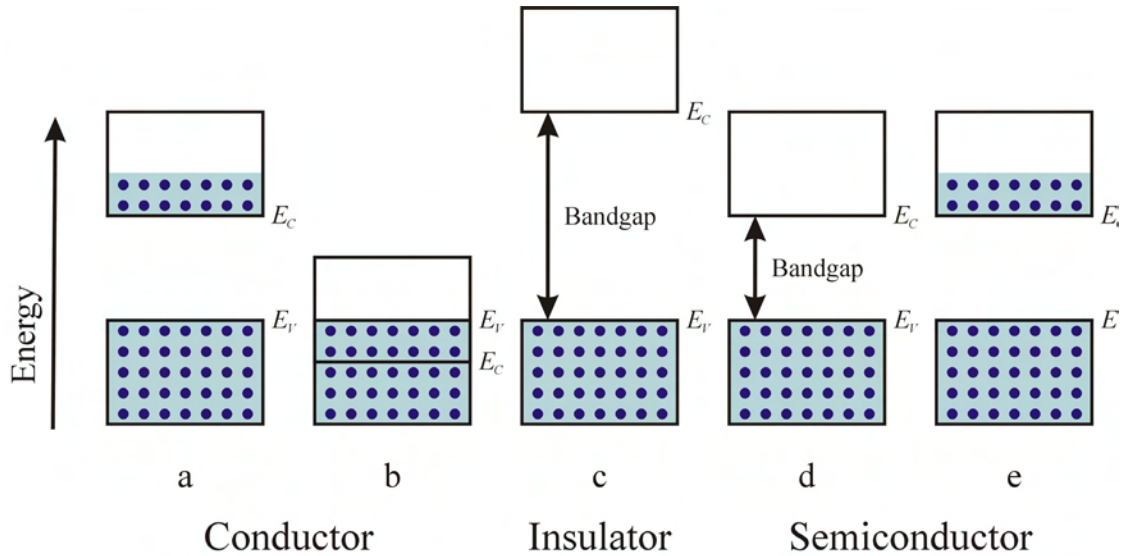
Figure 2.16
Band Structure - Conductors, Insulators and Semiconductors:
a) Conductor with partially filled bands; b) Conductor with overlapping bands;
c) Insulator; d) Semiconductor at T=0K; e) Semiconductor at T=300K

The distribution of electrons in the bands among available states also influences the physical properties of materials and systems. Electrons in solids are fermions, which obey Fermi-Dirac statistics. Their distribution over the range of allowed energy states is governed by the Fermi-Dirac distribution function, equation 2.3, where k_B is the Boltzman constant (8.62×10^{-5} eV/K), T is the temperature, E_F is a reference known as the Fermi energy (or Fermi level) and E is the energy of interest.

$$f(E) = \frac{1}{1 + e^{(E - E_F)/k_B T}}$$

(2.3)

The Fermi-Dirac distribution function gives the probability of that a state is occupied at a particular energy level. We know by examination that the probability of an electron occupying the Fermi energy is ½ or when $E = E_F$, the distribution function reduces to ½.

$$\text{when } E = E_F \quad f(E_F) = \frac{1}{1 + e^{(E_F - E_F)/k_B T}} = \frac{1}{1 + e^{(0)/k_B T}} = \frac{1}{1 + 1} = \frac{1}{2} \tag{2.4}$$

Another way of understanding Fermi-Dirac distribution function is to examine the influence of temperature on the electron distribution. At $T = 0K$, when $E < E_F$ the probability function $f(E)$ becomes 1 and when $E > E_F$ the function becomes 0, meaning that all available states up to the Fermi level are filled with electrons and all the states above the Fermi level are empty at $T = 0K$.

$$\text{when } E < E_F \text{ and } T = 0K \qquad f(E) = \frac{1}{1 + e^{(E - E_F)/k_B T}} \rightarrow \frac{1}{1 + 0} = 1 \tag{2.5}$$

$$\text{when } E > E_F \text{ and } T = 0K \qquad f(E) = \frac{1}{1 + e^{(E - E_F)/k_B T}} \rightarrow \frac{1}{1 + \infty} = 0 \tag{2.6}$$

As T increases above 0K, so does the probability of finding an occupied state above the Fermi level and there is a corresponding probability [1 - $f(E)$] of finding empty states below the Fermi level.
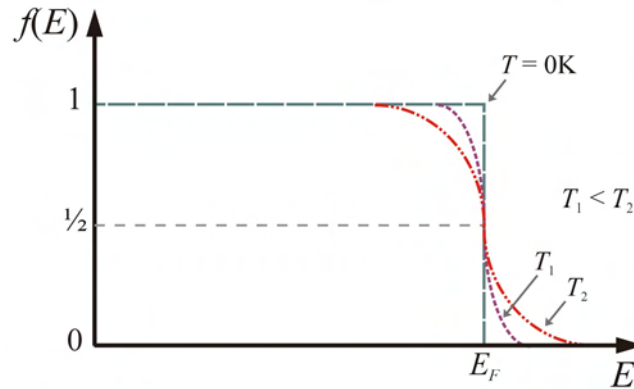
Figure 2.17
Fermi-Dirac Distribution Function

For a conductor, all available states are filled up to the Fermi level, alternatively this can be seen as the Fermi level residing just above the upper most filled state. In an intrinsic (pure) semiconductor the Fermi level is near the center of the band gap. However if impurities (dopants) are added to the intrinsic semiconductor forming an extrinsic semiconductor, the material may become an n-type or p-type material and the Fermi level is shifted. The Fermi level will shift closer to the conduction band in an n-type material and closer to the valence band in a p-type material.
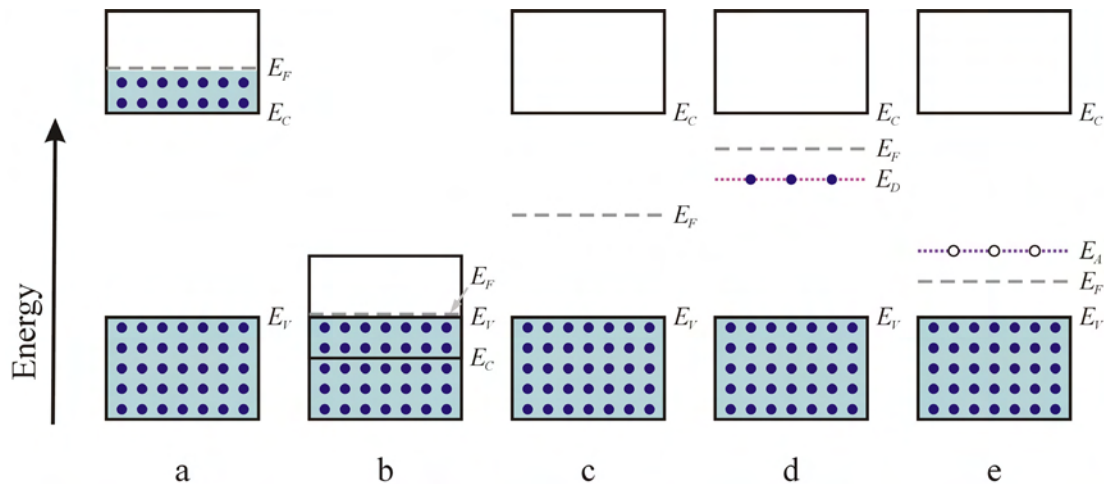
Figure 2.18
Fermi Level in Conductors and Semiconductors: a) Fermi level in a conductor;
b) Fermi level in a conductor; c) Fermi level in an intrinsic semiconductor;
d) Fermi level in an n-type semiconductor with donor energy level;
e) Fermi level in a p-type semiconductor with acceptor energy level

If we consider a group IV element such as silicon and add phosphorous, a group V element, four of the five phosphorous valence electrons will bond with neighboring silicon atoms leaving the fifth electron loosely bound to the phosphorous atom. At room temperature, this fifth electron bond easily breaks allowing the electron to move freely through the crystal. The electron may absorb the energy of a phonon and be excited into

the conduction band. This results in electrons in the conduction band, producing an n-type material. The energy level of this donor electron is just under the conduction band edge in the bandgap. Only a small amount of energy is needed to move the electron into the conduction band.
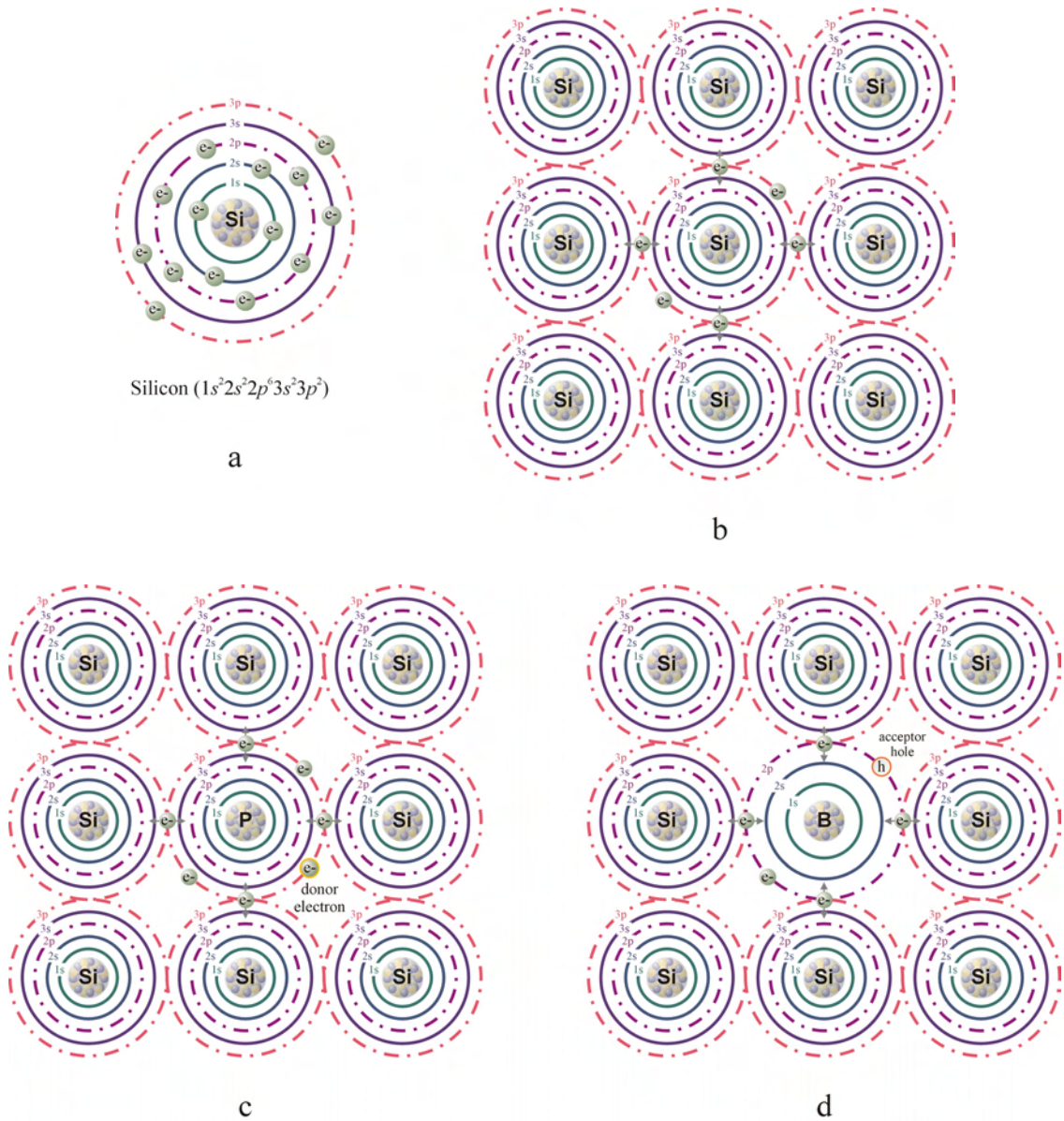
Figure 2.19
Intrinsic and Extrinsic Silicon Semiconductor:
a) Structure of silicon atom; b) Covalently bonded intrinsic silicon;
c) Phosphorous doped n-type silicon; d) Boron doped p-type silicon

Similarly, if a group III element such as boron is added to silicon this will create

an electron vacancy. The presence of acceptor impurities creates a p-type material, and

the acceptor energy levels are located just above the valence band within the bandgap. At

room temperature, electrons in the valence band can easily gain enough energy to fill the

acceptor states and thus create a vacancy in valence band. Such a vacancy is called a

hole since it can move freely through the material. Strictly speaking, a hole is not a

positive charge, but the absence of an electron and contributes to conduction whereas the

bonded electrons cannot.

In metallic bonding the valence electrons form an electron "gas" surrounding the

positively charged atomic cores. Generally the valence electron is held within the surface

of the material due to two things: (a) the electric field created between the row of

positively charged cores and the electron cloud at the surface; and (b) the positive net

charge caused by the escaping electron will create an attractive force to pull the electron
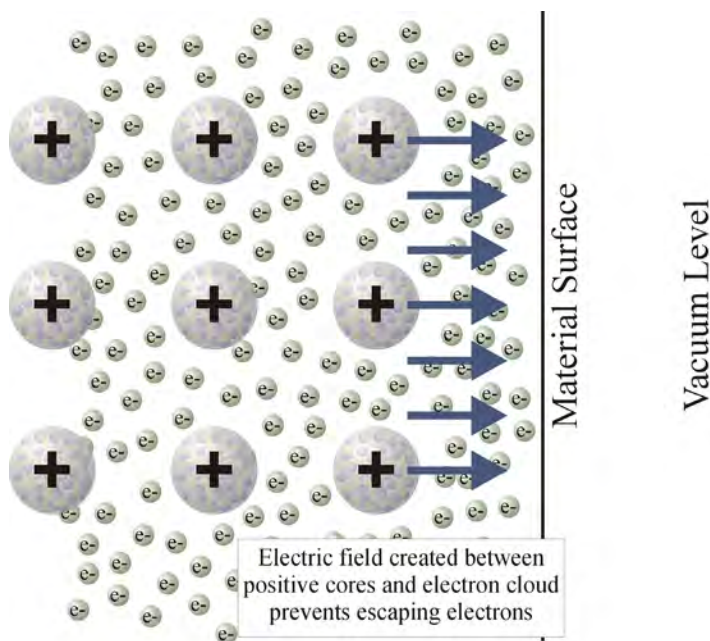
Figure 2.20
Electric Field preventing Electrons from Escaping to the Vacuum Level

back. If the electron escapes the material, it is said to be in the vacuum level. This energy necessary for "escaping" is known as the work function of the material (Φ) and is the difference in energy between the Fermi level and vacuum level. Both metals and semiconductors have a work function and are denoted Φ_m and Φ_s, respectively. In addition to the work function, semiconductors also have and electron affinity (χ), which is the least amount of energy necessary to remove an electron from the atom. The electron affinity is the difference in energy between the bottom of the conduction band (E_C) and the vacuum level.
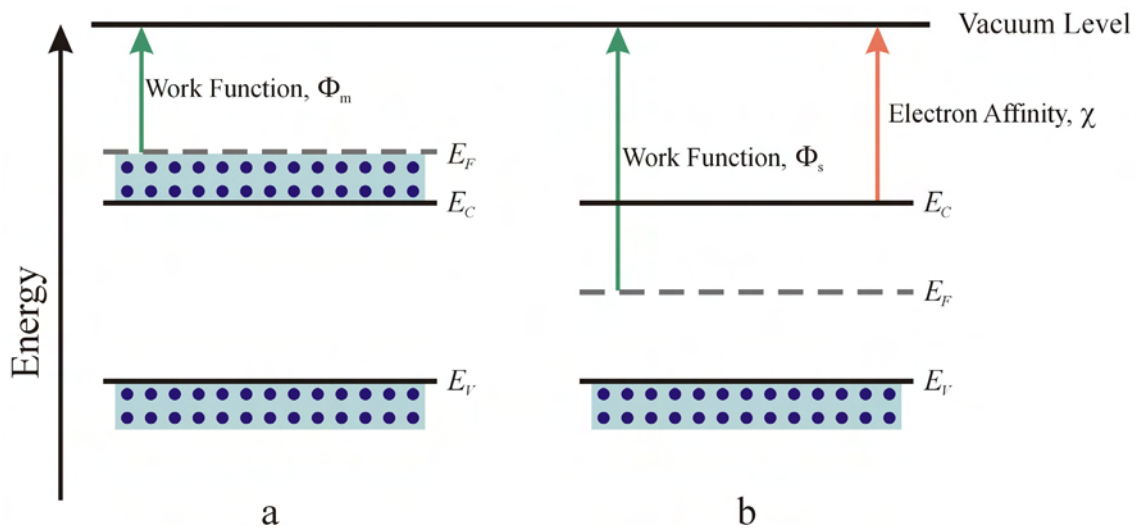
Figure 2.21
Work Function and Electron Affinity: a) Work function in a conductor (metal);
b) Work function and electron affinity in a semiconductor

2.5   Crystal Structure

Solids exist as crystalline, polycrystalline and amorphous forms. In crystalline form, atoms are arranged in the material in a periodic arrangement exhibiting long-range order. The infinite periodic array of geometric points defines the lattice within the material. The periodic crystal is formed by placing identical groups of atoms, known as

CUBIC

$a = b = c$

$\alpha = \beta = \gamma = 90°$

simple cubic

body-centered cubic

face-centered cubic

TETRAGONAL

$a = b \neq c$

$\alpha = \beta = \gamma = 90°$

simple tetragonal

body-centered tetragonal

HEXAGONAL

$a = b \neq c$

$\alpha = \beta = 90°, \gamma = 120°$

ORTHORHOMBIC

$a \neq b \neq c$

$\alpha = \beta = \gamma = 90°$

simple orthorhombic

body-centered orthorhombic

base-centered orthorhombic

face-centered orthorhombic

RHOMBOHEDRAL

$a = b = c$

$\alpha = \beta = \gamma \neq 90°$

TRICLINIC

$a \neq b \neq c$

$\alpha \neq \beta \neq \gamma \neq 90°$

MONOCLINIC

$a \neq b \neq c$

$\alpha = \beta = 90°, \gamma \neq 90°$

simple monoclinic

base-centered monoclinic

a, b, c - lengths

α, β, γ - angles

Figure 2.22
Bravais Lattices

the basis, at each lattice point. There are many distinct lattice patterns occurring in solids with differing atomic spacing and thus different lattice parameters. There are 14 distinct lattice patterns occurring in 7 geometric systems known as a Bravais lattice. Polycrystalline materials are a collection of small volumes in various orientations known as grains, which exhibit crystallinity within the grain. Such materials exhibit short-range order within the grain, while the boundaries of the grains create strained and dangling bonds. Similar to the plum pudding model, another popular desert, the rice krispy treat, can be used to describe polycrystalline materials. Grains (puffed rice) of various size and orientation make up the solid. Amorphous materials do not exhibit any long-range order and similar to polycrystalline materials, contain strained or dangling bonds.
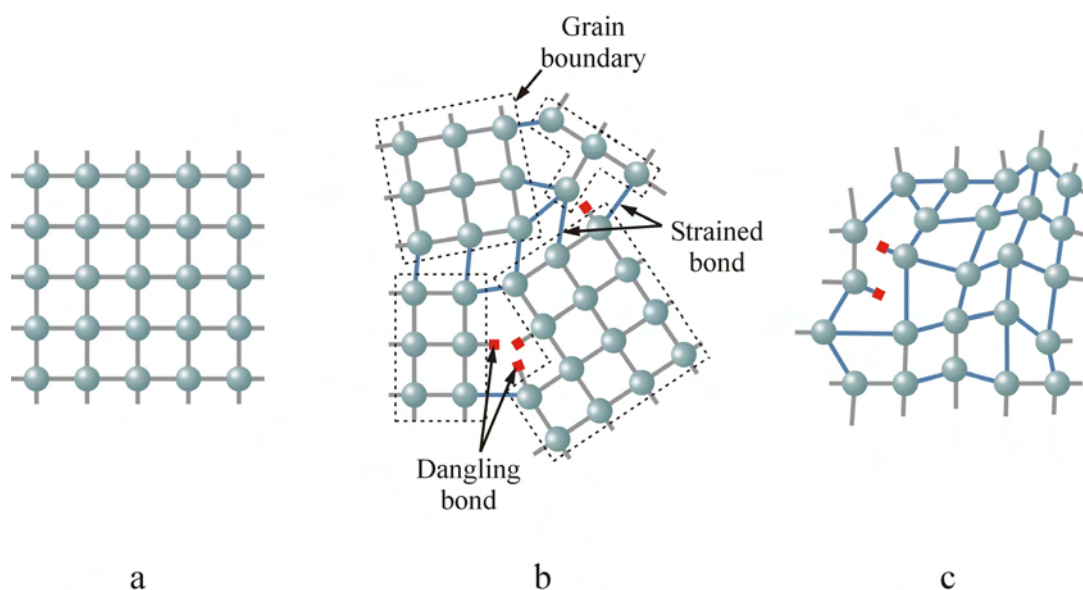
Figure 2.23
Structure of Solids: a) Crystalline; b) Polycrystalline; c) Amorphous

A perfect crystalline solid does not exist and often defects in the crystal structure occur due to crystal growth and subsequent processing. Defects affect the mechanical and electrical properties of the material. It is important to note that a defect in the crystal

is not necessarily a negative attribute and often defects are created intentionally to produce desired effects such as gettering for trapping contaminants and doping to affect conductivity. Defects are classified by their dimensionality as point defects (0-dimensional), line defects (1-dimensional), area defects (2-dimensional) and volume defects (3-dimensional).

Point defects are so named because they exist at a point within the crystal and do not extend in any direction, however point defects may agglomerate and grow into line defects. Vacancies and interstitials are two common point defects. Vacancies are when an atom is missing from a lattice site. Interstitials occur when atoms do not occupy a lattice site, but all sites around it are filled. The case where an atom moves from a lattice site to an interstitial position, leaving a vacancy is called a Frenkel defect.
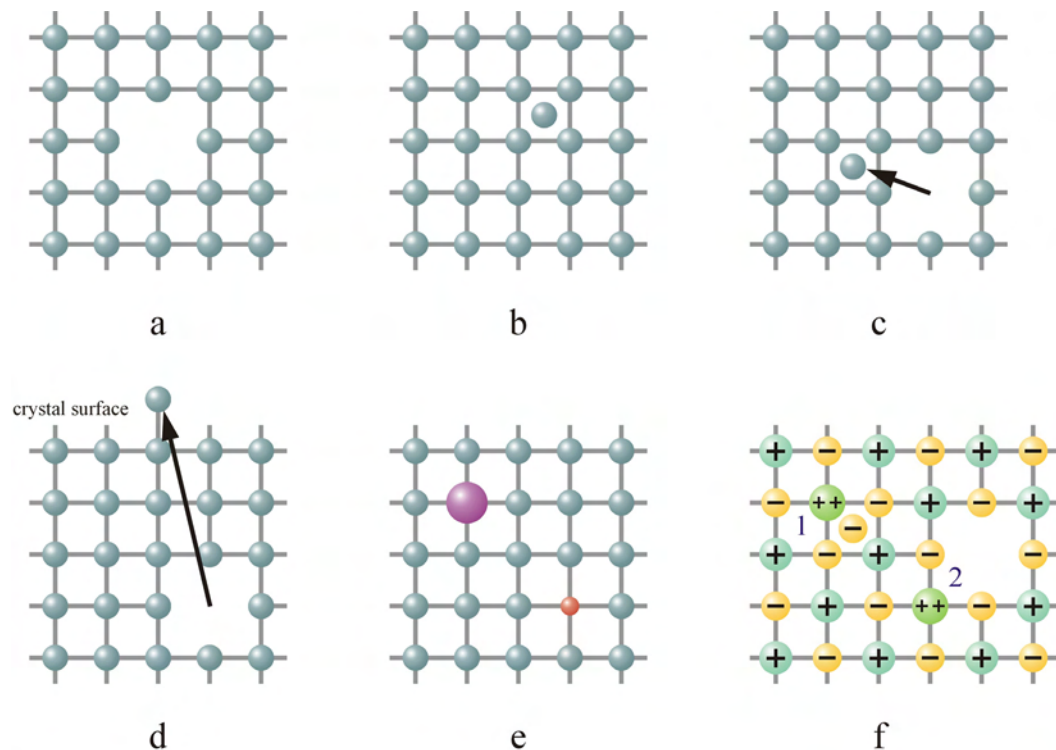
Figure 2.24
Point Defects: a) Vacancy; b) Interstitial; c) Frenkel; d) Schottky; e) Substitutional impurities; f) Substitutional impurity-ionic (1) Interstitial (2) Vacancy

If the atom moves from a lattice site to the surface of the crystal, leaving a vacancy, it is known as a Schottky defect. Often different species of atoms are added to the crystal (doping) to occupy bonding sites to produce desired effects. Since the impurity is of different size than other atoms within the lattice, this creates strain around the substitutional impurity due to the atomic bonding. In the case of ionic bonding, the impurity may have a different ionization than other ions in the crystal and create a vacancy or interstitial defect in order to maintain charge neutrality of the crystal.

Line defects include edge dislocation, dislocation loops and screw defects. Point defects can move around the crystal and agglomerate in one location forming line defects. These line defects can then move through the crystal in processes known as glide and
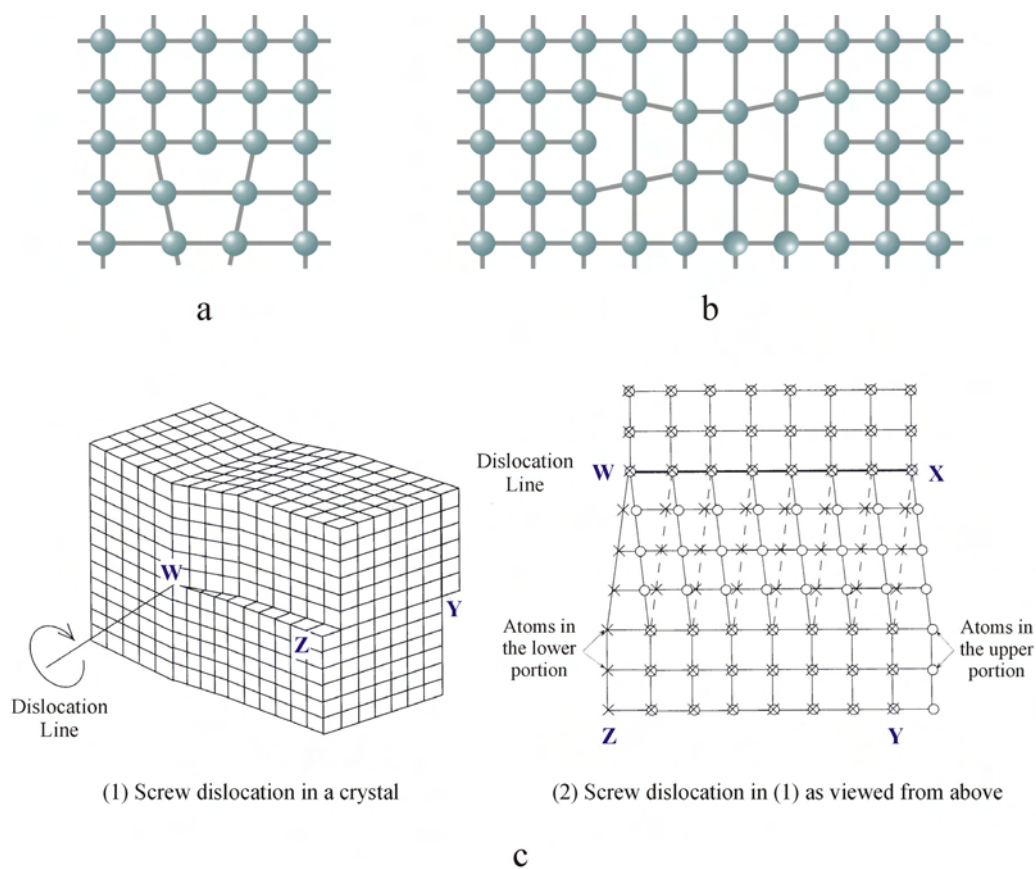
Figure 2.25
Line Defects: a) Edge dislocation; b) Dislocation loop; c) Screw dislocation[8]

climb. Glide is when the line of defects moves through the crystal in a direction other than along the line of defects. If the line of defects grows or shrinks along the line or moves along the line, it is known as climb.[11]
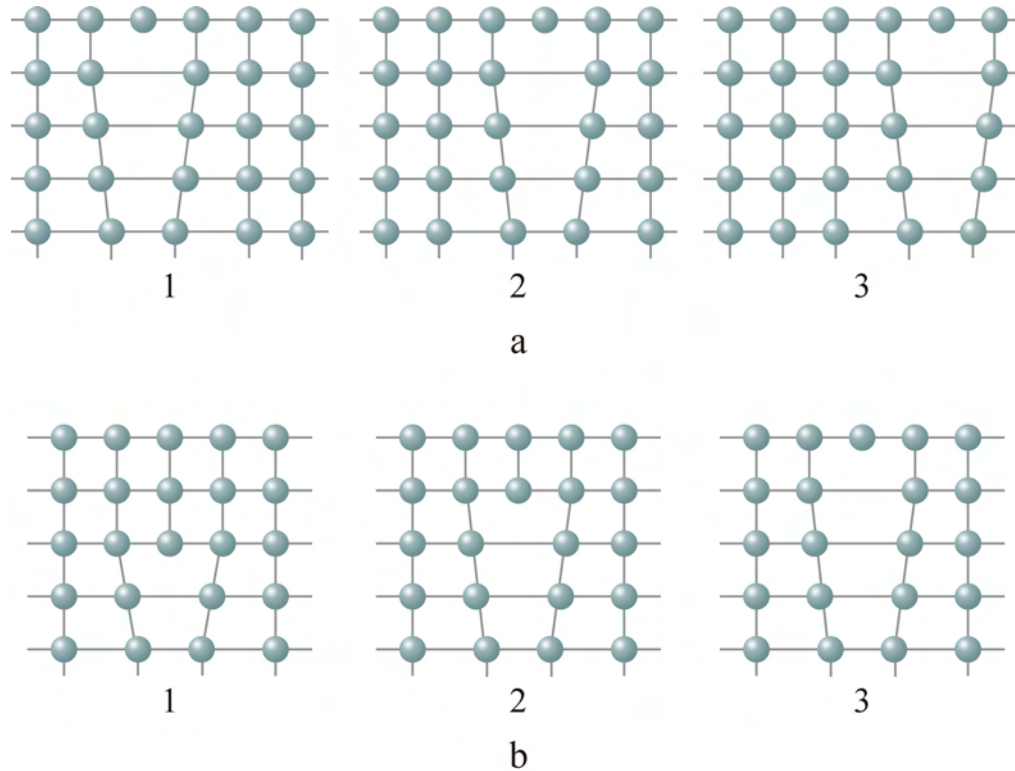
Figure 2.26
Line Defect Movement through a Crystal: a) Glide; b) Climb

Area defects include stacking faults, twins and grain boundaries. Stacking faults occur when an extra plane is inserted into the crystal lattice or a plane is removed from the crystal lattice disturbing the periodic order of the planes. Insertion of an extra plane creates an extrinsic stacking fault and removal of a plane creates an intrinsic stacking fault. Grain boundaries are formed in polycrystalline materials and may form due to an array of edge dislocations. The grains consist of single crystalline material that is oriented in different directions forming voids in between the grains. The voids may contain interstitials, vacancies, and dangling or strained bonds.
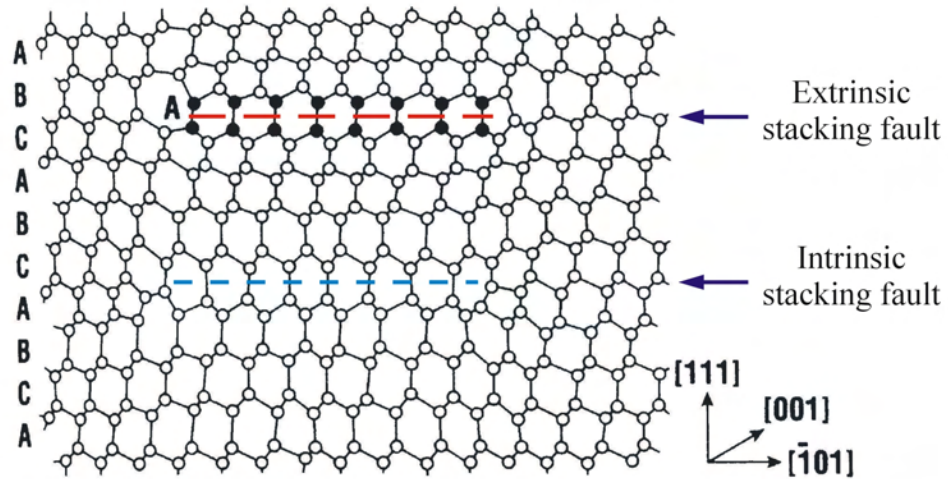
An intrinsic stacking fault is the removal of part of a plane of atoms in the {111} directions. An extrinsic stacking fault is the addition of a partial plane of atoms in the {111} directions. The labels A, B, and C correspond to the three different (111) planes in the diamond lattice (*silicon*).

a
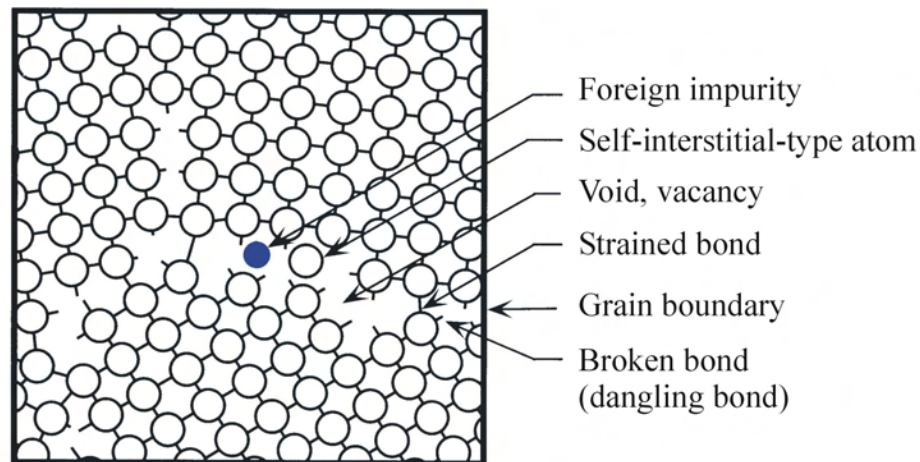
The grain boundaries have broken bonds, voids, vacancies, strained bonds and interstitial-type atoms. The structure of the grain boundaries have higher energies than those within the grains.

b

Figure 2.27
Area Defects: a) Stacking faults[11]; b) Grain boundaries[8]

Volume defects occur as voids, local amorphous regions and precipitates. Precipitates originate as point defects and nucleate into a larger volume of impurities. Precipitates are usually unwanted, but can serve a useful purpose in semiconductor electronics. If away from active areas, oxygen precipitates serve as gettering devices and attract and trap impurities in the crystal thereby minimizing the effect of the impurities on device performance.

Defects within the crystal structure cause mechanical stress and can lead to the material fracturing or films delaminating from a substrate. Stresses built up from the layering of films can also lead to warpage and process variation across the surface. Defects also impact the electrical properties of the material and introduce discrete energy levels within the bandgap.[13] Defects such as metal precipitates crossing a p-n junction boundary increase reverse bias leakage currents across the boundary. Defects also increase leakage currents across insulators and lead to lower breakdown voltages. In conductive materials, defects cause charge trapping and reduce minority carrier lifetime, which may degrade device operation.[12]

CHAPTER 3

RECTIFYING JUNCTIONS

3.1   Formation and Band Structure of a p-n Junction

The diode is an electrical component commonly used in circuits. They are typically two-terminal devices which possess the characteristics of rectification, that is they allow current flow in one direction (forward biased), but prevent current flow in the opposite direction (reverse biased). There are many types of diodes, but the p-n junction is perhaps the most fundamental, which can be used as a circuit element and is necessary for metal-oxide-semiconductor field-effect transistor (MOSFET) and bipolar junction transistor (BJT) operation.

A p-n junction is formed in a single crystalline semiconductor by doping one region with acceptor atoms, forming a p-type region and then doping an adjoining region with donor atoms creating an n-type region. In the p-type region there are many free holes (majority carriers) and a few free electrons (minority carriers), similarly the n-type region will have many free electrons (majority carriers) and a few free holes (minority carriers). Due to the difference of available carriers in each region, a carrier concentration gradient is formed across the junction causing holes from the p-type material to diffuse into the n-type material and electrons from the n-type material to diffuse into the p-type material. Once the majority carriers diffuse across the junction

they will recombine and disappear (i.e. holes diffusing from the p-type region will recombine with electrons in the n-type region). However, this process does not continue indefinitely due to the creation of an internal electric field, which opposes the diffusion. As the holes and electrons recombine, they leave behind ionized dopant atoms near the junction. As the holes leave the p-type material, they leave negatively charged acceptor ions behind, which are held in a fixed position. Similarly, the diffusion of electrons from the n-type material leaves behind fixed positively charged donor ions. The electric field created between the ionized atoms in the depletion area prevents further diffusion of carriers across the junction. This built-in electric field creates what is known as the
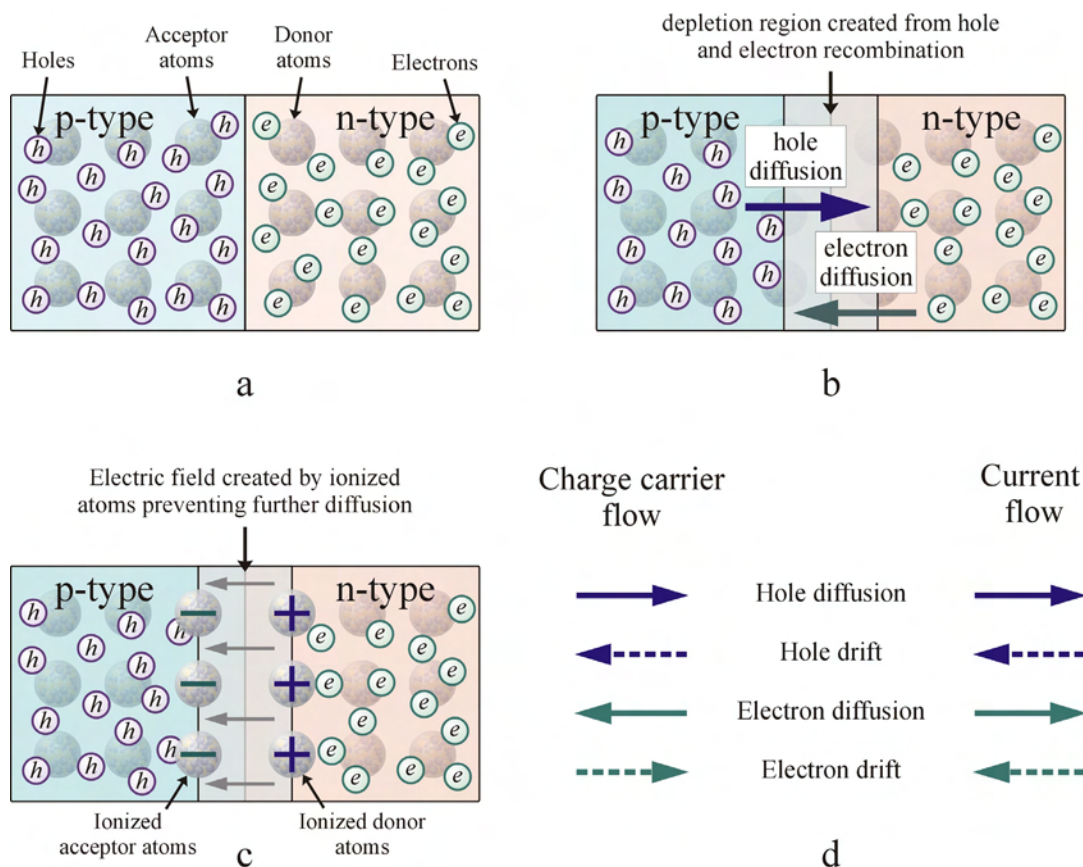
Figure 3.1
p-n Junction: a) p-type and n-type material forming junction;
b) Hole and electron diffusion due to carrier concentration gradient; c) Electric field
created by ionized atoms; d) Summary of charge carrier and current flow

built-in potential or contact potential, V_o. Since the junction area contains no free mobile charges it is called the depletion region. It is also referred to as the space charge region, since it contains positive charge on the n-side and negative charge on the p-side of the junction. The total net charge of the depletion region is zero.

The p-n junction can also be understood in terms of a band diagram. If we consider the p-type and n-type regions separately, we know that the electronic band structure is similar since it is the same material and the only difference will be the dopant states and the position of the Fermi level in each material. Under equilibrium conditions, as the materials are brought into contact, free electrons will flow from the n-type semiconductor to the p-type semiconductor and free holes from the p- type semiconductor will flow into the n-type semiconductor. As a result of charge transfer, the band structure of the n-type semiconductor will shift down and the band structure of the p-type semiconductor will shift up. Net charge transfer will continue until the Fermi level is aligned across the junction. A step is formed in the conduction and valence bands in the junction. The height difference of this step is qV_o, where V_o is the built-in potential.
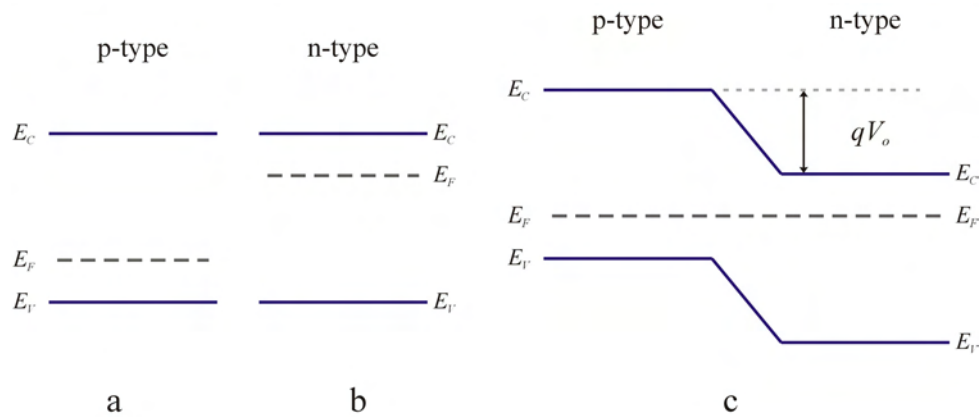
Figure 3.2
Band Structure: a) Band structure of p-type semiconductor;
b) Band structure of n-type semiconductor; c) Band structure of p-n junction

3.2   Effect of Carrier Concentration on Built-in Potential

By understanding the effect of the doping concentration on the built-in potential, a device with a specific "turn on" voltage can be fabricated. Under equilibrium conditions there is no net current flow across the junction. The majority carriers, free holes (free electrons) in the p-type (n-type) region will keep diffusing into the n-type (p-type) region due to the concentration gradient. At the same time, minority carriers such as holes (electrons) in the n-type (p-type) region will drift under the influence of the electric field into the p-type (n-type) region. This is represented in equation 3.1 for the holes, by summing up the hole drift current [$q\mu_p p(x)E(x)$] due to the electric field and the hole diffusion current [$D_p\, dp(x)/dx$] due to the concentration gradient.

$$J_p(x) = q\left[\mu_p p(x)E(x) - D_p \frac{dp(x)}{dx}\right] = 0 \qquad (3.1)$$

which be rearranged into:

$$\mu_p p(x)E(x) = D_p \frac{dp(x)}{dx} \qquad (3.2)$$

$$\frac{\mu_p}{D_p} E(x) = \frac{1}{p(x)} \frac{dp(x)}{dx} \qquad (3.3)$$

The electric field, $E(x)$ can be written as the potential gradient across the depletion region as:

$$E(x) = -\frac{dV(x)}{dx} \qquad (3.4)$$

From Albert Einstein's famous 1905 paper over Brownian motion[14], we have the Einstein relationship,

$$D = \frac{\mu k_B T}{q} \tag{3.5}$$

where D is the diffusion constant, μ is the mobility, k_B is the Boltzman constant (8.62 x 10^{-5} eV/K), T is the absolute temperature and q is elementary charge (1.60 x 10^{-19} C).

This allows us to substitute for the term $\frac{\mu_p}{D_p}$ and equation 3.3 becomes:

$$-\frac{q}{k_B T} \frac{dV(x)}{dx} = \frac{1}{p(x)} \frac{dp(x)}{dx} \tag{3.6}$$

The built-in potential can be determined by integrating over the appropriate limits (eq. 3.7), where V_n and V_p are the voltages at the edges of the depletion region in the n-type and p-type material. The limits of the second integral in equation 3.7, p_n and p_p are the equilibrium hole concentration in the n-type and p-type material respectively.

$$-\frac{q}{k_B T} \int_{V_p}^{V_n} dV = \int_{p_p}^{p_n} \frac{1}{p} \, dp \tag{3.7}$$

$$-\frac{q}{k_B T}(V_n - V_p) = \ln p_n - \ln p_p \tag{3.8}$$

Since the built-in potential is the difference in voltage over the depletion region we know that $V_o = V_n - V_p$ and equation 3.8 becomes:

$$\frac{q}{k_B T} V_o = \ln\left(\frac{p_p}{p_n}\right) \tag{3.9}$$

The built-in potential can be expressed as:

$$V_o = \frac{k_B T}{q} \ln\left(\frac{p_p}{p_n}\right) \tag{3.10}$$

If we consider the junction to be made up of N_A acceptor atoms in the p-material and N_D donor atoms in the n-material, equation 3.10 can be rewritten as:

$$V_o = \frac{k_B T}{q} \ln\left(\frac{N_A}{n_i^2/N_D}\right) = \frac{k_B T}{q} \ln\left(\frac{N_A N_D}{n_i^2}\right) \qquad (3.11)$$

If the doping concentration of the device is known, then equation 3.11 can be used to substitute for the built-in potential, V_o. Similarly, the free electron concentration can be expressed in terms of the built-in potential and can be extended to include the electron concentration in each region.

$$\frac{p_p}{p_n} = \frac{n_n}{n_p} = \exp\left(\frac{qV_o}{k_B T}\right) \qquad (3.12)$$

3.3 Depletion Region Width and Electric Field

Within the depletion region there are no free charge carriers due to the electric field, all charge occurs due to the ionized acceptor and donor atoms. If we consider the junction interface to be at $x = 0$ and the depletion region extends into the p-type material a distance x_p and into the n-type material a distance x_n, then the total width of the depletion region, W, is the sum of x_p and x_n.

$$W = |x_p| + |x_n| \qquad (3.13)$$
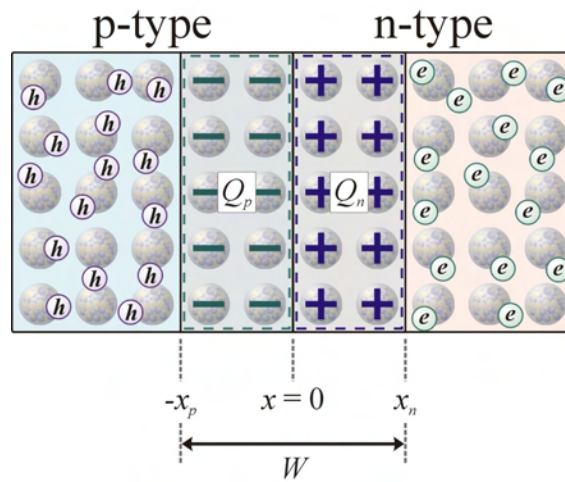
Figure 3.3
Depletion Region Width

The negative charge provided by the ionized acceptor atoms in the depletion region extending into the p-type material ($x = 0$ to $-x_p$) can be represented as Q_p. Similarly, the positive charge provided by ionized donor atoms in the depletion region extending into the n-type material ($x = 0$ to $-x_n$) can be represented by Q_n. Since the total material is neutral we assume charge neutrality in the depletion region, therefore:

$$Q_p + Q_n = 0 \qquad (3.14)$$

or

$$|Q_p| = |Q_n| \qquad (3.15)$$

The charge provided by the ionized atoms can be determined from the dopant concentration (N_A and N_D) and the volume of the depletion region extending into the p-type and n-type regions.

$$Q_p = -q\,N_A\,A\,x_p \qquad (3.16)$$

$$Q_n = q\,N_D\,A\,x_n \qquad (3.17)$$

Equation 3.15 can be rewritten as:

$$q\,N_A\,A\,x_p = q\,N_D\,A\,x_n \qquad (3.18)$$

which reduces to:

$$N_A\,x_p = N_D\,x_n \qquad (3.19)$$

The manipulation of equation 3.19 will yield the depletion width into the p-type material, x_p and the depletion width into the n-type material, x_n in terms of the total depletion width, W and the acceptor (N_A) and donor (N_D) concentrations.

$$N_A\,x_p + N_D\,x_p = N_D\,x_n + N_D\,x_p \qquad (3.20)$$

$$x_p(N_A + N_D) = N_D(x_n + x_p) \qquad (3.21)$$

$$x_p(N_A + N_D) = N_D W \tag{3.22}$$

$$x_p = \frac{N_D W}{(N_A + N_D)} \tag{3.23}$$

by similar means, the depletion region into the n-type material can be obtained:

$$x_n = \frac{N_A W}{(N_A + N_D)} \tag{3.24}$$

In order to gain an understanding of how the built-in potential and depletion width are

related, we must examine the electric field created by the ionized atoms which

incorporates both. We can begin with applying Gauss' Law on the cylinder (see figure

3.4). We know by observation that the electric field points in the $-x$ direction and that the

field is zero at the depletion region boundaries extending into the p-type and n-type

material ($E = 0$ for $x \le x_p$ and $x \ge x_n$).

$$\oint_s \bar{E} \cdot \hat{n}\, da = \frac{1}{\varepsilon_s \varepsilon_o} \int_V \rho\, dV = \frac{Q_{Enclosed}}{\varepsilon_s \varepsilon_o} \tag{3.25}$$
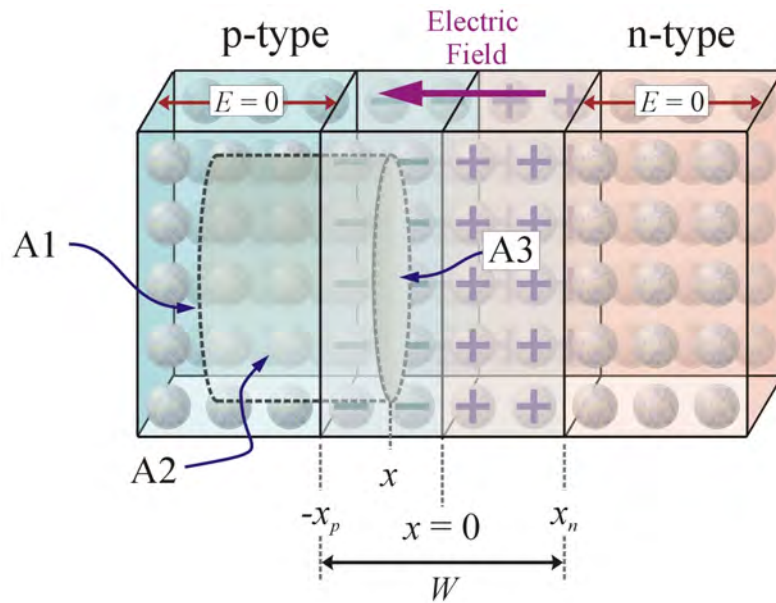
Figure 3.4
Gauss' Law: p-side of junction

From the diagram we see that surface A1 has no electric field and thus no flux normal to the surface and surface A2 is parallel to the electric field, so only surface A3 contributes to the integral because the electric field is normal to the surface. The electric field in the region from x_p to $x = 0$ becomes:

$$-E(x)A = \frac{qN_A}{K_s\varepsilon_o}(x - x_p)A \qquad \text{for } x_p \leq x \leq 0 \qquad (3.26)$$

$$E(x) = \frac{qN_A}{K_s\varepsilon_o}(x_p - x) \qquad (3.27)$$

We can extend the Gaussian surface into the n-type material to include positive charge from the ionized donor atoms.
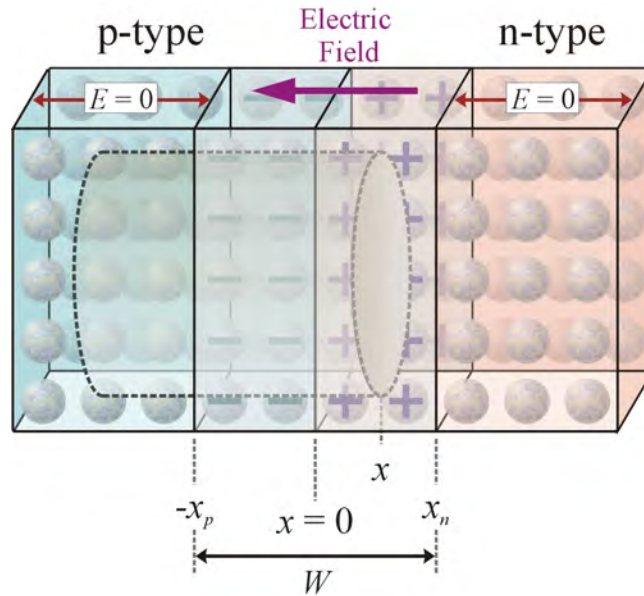
Figure 3.5
Gauss' Law: p and n-side of junction

$$-E(x)A = -\frac{qN_A}{K_s\varepsilon_o}x_p A + \frac{qN_D}{K_s\varepsilon_o}x A \qquad \text{for } 0 \leq x \leq 0 \, x_n \qquad (3.28)$$

From equation 3.19, this becomes:

$$-E(x)A = -\frac{qN_D}{K_s\varepsilon_o}x_n A + \frac{qN_D}{K_s\varepsilon_o}x A \qquad (3.29)$$

which reduces to equation 3.30.

$$E(x) = \frac{qN_D}{K_s\varepsilon_o}(x_n - x) \qquad (3.30)$$

From the results of equations 3.27 and 3.30, we see the maximum electric field occurs at

x = 0.

$$E_{MAX} = \frac{qN_A}{K_s\varepsilon_o}x_p = \frac{qN_D}{K_s\varepsilon_o}x_n \qquad (3.31)$$

A plot of the charge distribution and resulting electric field can be seen in figure 3.6.

Using equation 3.4, we can determine the built-in potential from the electric field across

the depletion region.

$$-Vo = -\Delta V(x) = \int_{-x_p}^{x_n} E(x)\,dx \qquad (3.32)$$

By inspection we know that the integral of the electric field over the depletion width is

the shaded area in figure 3.6-c defined by the $E(x)$ curve and the x-axis.

$$V_o = \frac{E_{MAX}(x_p + x_n)}{2} \qquad (3.33)$$

$$V_o = \frac{E_{MAX}\,x_p}{2} + \frac{E_{MAX}\,x_n}{2} \qquad (3.34)$$

From equation 3.31

$$V_o = \frac{qN_A x_p}{2K_s\varepsilon_o}x_p + \frac{qN_D x_n}{2K_s\varepsilon_o}x_n \qquad (3.35)$$

$$V_o = \frac{q}{2K_s\varepsilon_o}\left[N_A x_p^2 + N_D x_n^2\right] \qquad (3.36)$$
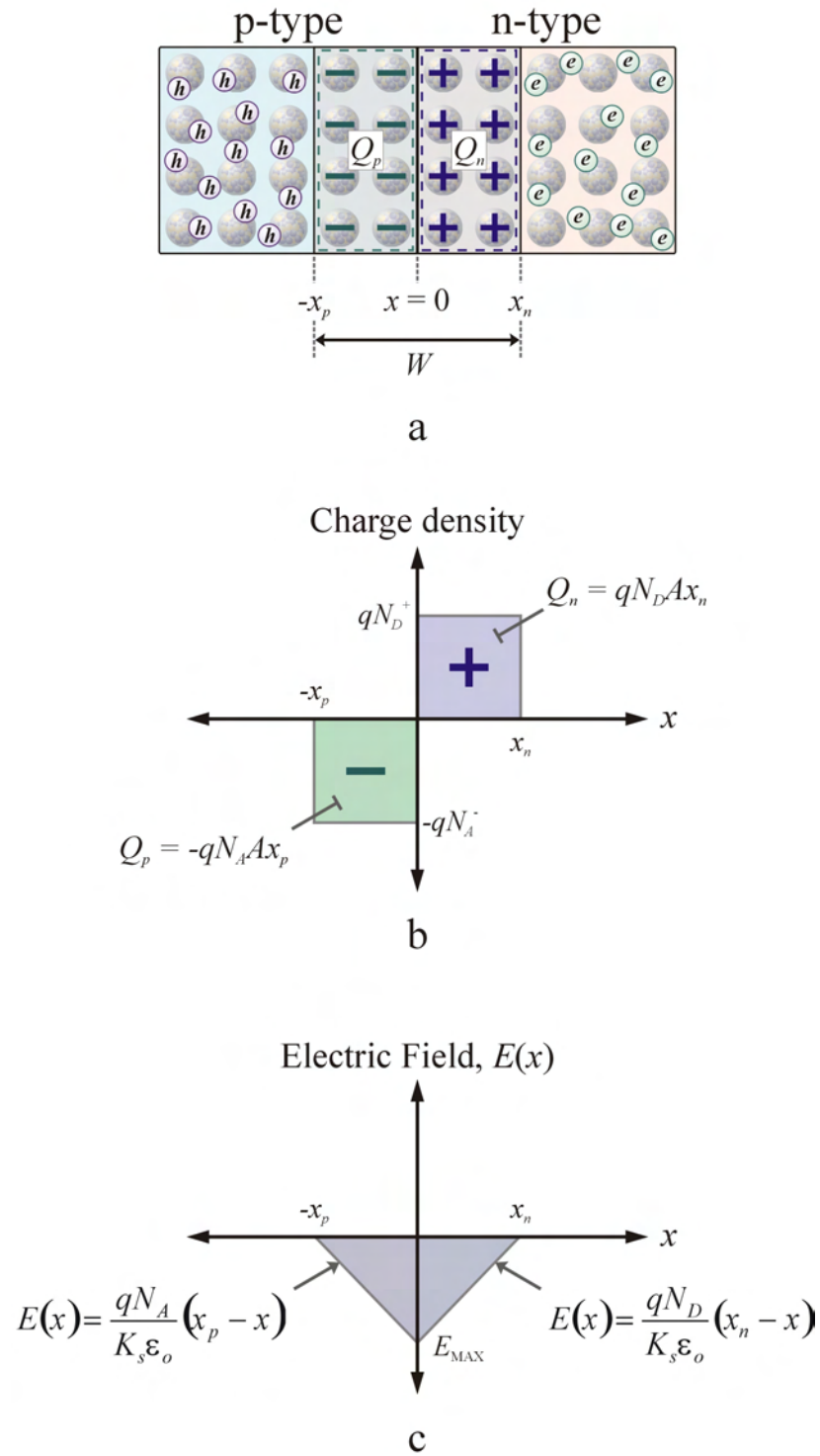
Figure 3.6
Symmetric p-n Junction: a) Physical p-n junction; b) Charge distribution in depletion
region; c) Electric field in the depletion region

From equations 3.23 and 3.24

$$V_o = \frac{q}{2K_s\varepsilon_o}\left[N_A\left(\frac{N_D W}{N_A + N_D}\right)^2 + N_D\left(\frac{N_A W}{N_A + N_D}\right)^2\right] \quad (3.37)$$

$$V_o = \frac{qW^2}{2K_s\varepsilon_o}\left[\frac{N_A N_D^2 + N_D N_A^2}{(N_A + N_D)^2}\right] \quad (3.38)$$

$$V_o = \frac{qW^2}{2K_s\varepsilon_o}\left[\frac{N_A N_D(N_A + N_D)}{(N_A + N_D)^2}\right] \quad (3.39)$$

$$V_o = \frac{qW^2}{2K_s\varepsilon_o}\left[\frac{N_A N_D}{N_A + N_D}\right] \quad (3.40)$$

We can use equation 3.40 to solve for the depletion width in terms of the built-in potential and doping concentration,

$$W^2 = \frac{2K_s\varepsilon_o V_o}{q}\left[\frac{N_A + N_D}{N_A N_D}\right] \quad (3.41)$$

$$W = \left[\frac{2K_s\varepsilon_o V_o}{q}\left(\frac{N_A + N_D}{N_A N_D}\right)\right]^{1/2} = \left[\frac{2K_s\varepsilon_o V_o}{q}\left(\frac{1}{N_D} + \frac{1}{N_A}\right)\right]^{1/2} \quad (3.42)$$

where V_o is determined by the work function difference of the n-material and p-material or by the doping concentration using equation 3.11.

One useful feature of the p-n junction is the property of rectification, allowing current to flow in one direction under forward bias, when the applied voltage is greater than the built-in potential ($V_A \geq V_o$). We can understand this property by examining the effect the applied bias has on the depletion region width. We can make the assumption that most of the applied voltage to the device occurs across the depletion region. There is a small voltage drop across the p-type and n-type material when current flows through the

device, but the length of each region is relatively small and the doping is generally high to minimize resistance.

If the applied voltage to the p-type material electrode is high with respect to the n-type material electrode, the device is forward biased and the applied voltage (from p to n) is considered positive. If the voltage applied to n-type material electrode is higher with respect to the p-type material electrode, the device is reversed bias and the applied voltage (from p to n) is considered negative. The applied voltage, V_A can be incorporated into equation 3.42 and the depletion width can be determined from:

$$W = \left[\frac{2K_s\varepsilon_o}{q} \left(\frac{N_A + N_D}{N_A N_D} \right) (V_o - V_A) \right]^{1/2} = \left[\frac{2K_s\varepsilon_o}{q} \left(\frac{1}{N_D} + \frac{1}{N_A} \right) (V_o - V_A) \right]^{1/2} \qquad (3.43)$$

The effect of the applied bias on depletion width and band structure can be seen in figure 3.7.
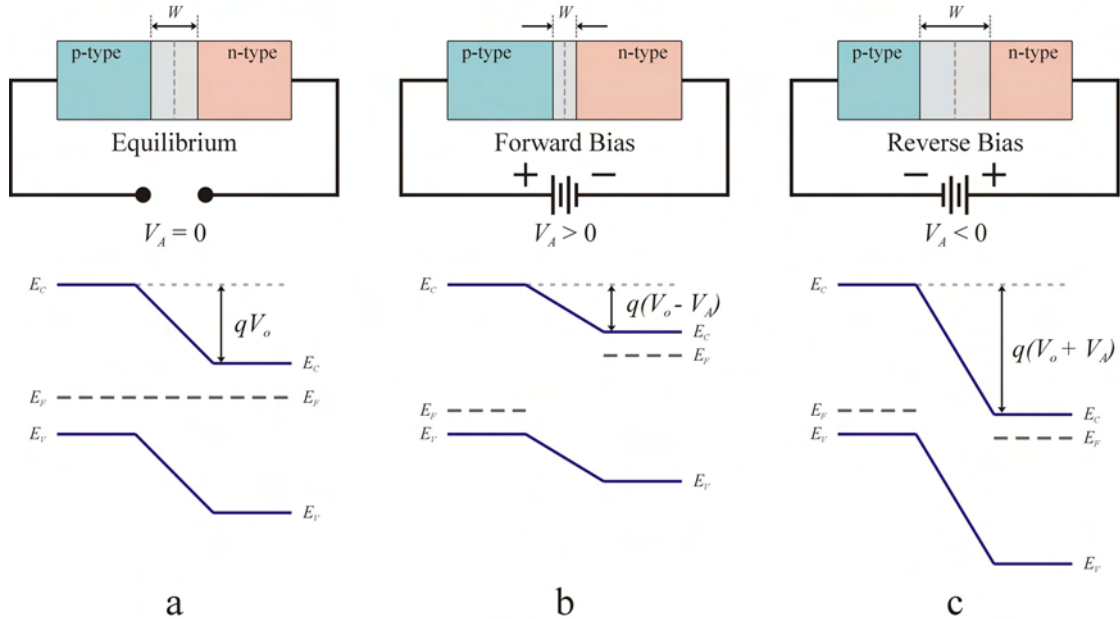
Figure 3.7
p-n Junction Depletion Width and Band Diagram:
a) Equilibrium; b) Forward bias; c) Reverse bias

It should be noted that N_A and N_D in equation 3.43 actually represent the charge densities in the p-side and n-side of the depletion area, respectively. If the only states in the bandgap are the acceptor and donor states and the temperature is high enough so that all dopants are ionized, these charge densities are indeed N_A and N_D and equation 3.43 is valid. In the case other states are present in the bandgap, equation 3.43 needs to be adapted and the width of the depletion area will depend on the charging of these states.

3.4   Junction Capacitance

The depletion region is depleted of free charge carriers and acts like a dielectric creating a capacitance across the junction. Due to the geometry of the junction, the junction capacitance can be thought of as a parallel plate capacitor described by the following equation:

$$C_j = \frac{K_s \varepsilon_o A}{W} \tag{3.44}$$

Since the depletion region width varies with doping concentration and applied bias, the junction capacitance will also vary with these parameters:

$$C_j = K_s \varepsilon_o A \left[\frac{q}{2K_s \varepsilon_o} \left(\frac{N_A N_D}{N_A + N_D} \right) \left(\frac{1}{V_o - V_A} \right) \right]^{1/2} \tag{3.45}$$

$$C_j = A \left[\frac{qK_s \varepsilon_o}{2(V_o - V_A)} \left(\frac{N_A N_D}{N_A + N_D} \right) \right]^{1/2} \tag{3.46}$$

Equations 3.45 and 3.46 are valid when the device is reverse biased ($V_A \le 0$).

Equation 3.46 is useful in determining the built-in potential and may lead to determining the doping concentration. If the applied bias is varied and the junction capacitance is measured, the built-in potential can be determined from a plot of $1/C_j^2$ versus applied voltage.
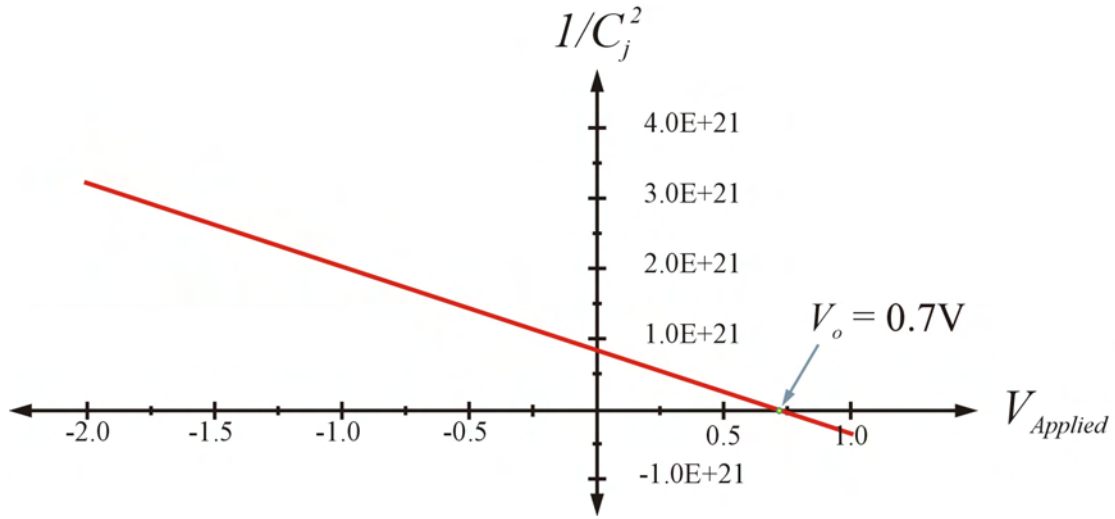
Figure 3.8
$1/C_j^2$ versus $V_{Applied}$

$$\frac{1}{C_j^2} = \frac{1}{A^2}\left[\frac{2(V_o - V_A)}{qK_s\varepsilon_o}\left(\frac{N_A + N_D}{N_A N_D}\right)\right] = \left[\frac{2}{A^2 qK_s\varepsilon_o}\left(\frac{1}{N_D} + \frac{1}{N_A}\right)\right](V_o - V_A) \qquad (3.47)$$

At $1/C_j^2 = 0$ (*x*-intercept), the built-in potential can be determined since $V_A = V_o$. At the

y-intercept, $V_A = 0$ and the expression for doping concentration becomes:

$$\frac{1}{N_D} + \frac{1}{N_A} = \frac{qA^2 K_s\varepsilon_o}{2C_j^2 V_o} \qquad (3.48)$$

If the junction is asymmetrically doped such that $N_D \gg N_A$ then $1/N_D \rightarrow 0$ and the

acceptor doping concentration can be determined.

$$N_A = \frac{2C_j^2 V_o}{qA^2 K_s\varepsilon_o} \qquad (3.49)$$

Equations 3.45 through 3.49 assume that the only states in the bandgap are

acceptor and donor states and that all dopants are ionized. If these conditions are not met,

then equations 3.45 through 3.49 are no longer valid. For example, at low temperatures,

not all dopants are expected to be ionized, resulting in lower space charge densities,

wider depletion width and thus lower capacitance values. Another example when the equations are not valid is when in addition to the acceptor and donor states, deep level states are also present in the bandgap. These deep level states are caused by the presence of other impurities or lattice defects. The charge state of these deep level defects depends on the bias voltage, making N_A and N_D (real charge density in the p-side and n-side of the depletion area) bias voltage dependent. As discussed in chapter 4, the bias voltage dependence provides a novel technique in identifying and characterizing the deep level defects.

3.5   IV Characteristics

A plot of the IV characteristics of a p-n junction diode can be seen in figure 3.9 and the resulting band diagrams can be seen in figure 3.10. At equilibrium ($V_A = 0$), a potential barrier prevents appreciable current flow. When the device is forward biased and the applied voltage is sufficient enough ($V_A \geq V_o$), the potential barrier is removed and the depletion region width goes to zero. This allows a large number of charge carriers to diffuse across the junction and contribute to the current and hence a large current under forward bias.

As stated earlier, the p-n junction acts as a rectifier and allows current flow under forward bias when $V_A \geq V_o$, but not under reverse bias when $V_A < V_o$. This is not entirely accurate. Under reverse bias there is a small drift current that occurs due to minority charge carriers drifting into the depletion region and being swept away by the electric field. This is often referred to as the reverse bias leakage current and is quite small compared to the forward biased current.
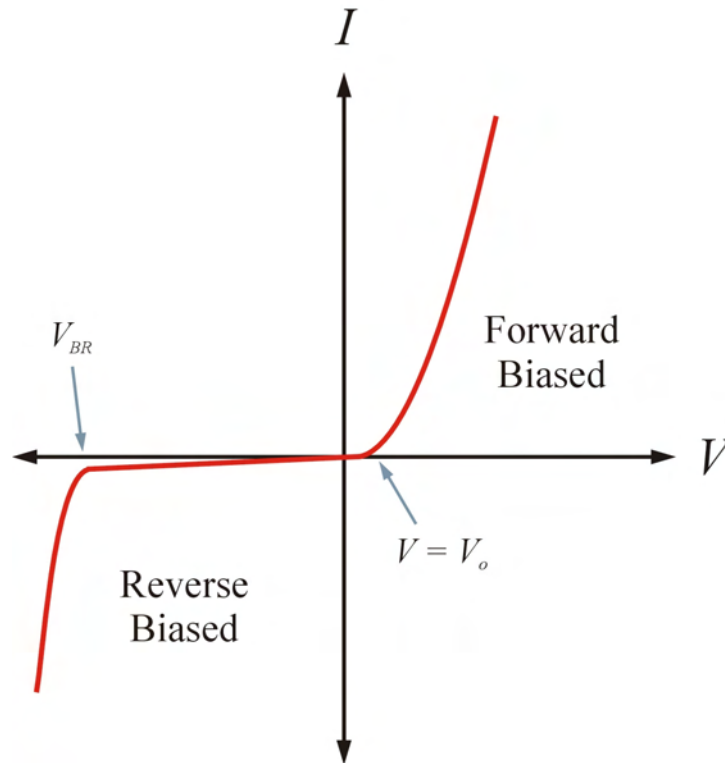
Figure 3.9
IV Characteristics of p-n Junction

As shown in figure 3.9, at large reverse bias (V_{BR}), breakdown occurs and

produces a large current in the opposite direction to the forward bias current. This

breakdown may occur due to the Zener effect seen in heavily doped junctions or as

avalanche breakdown seen in lightly doped junctions. If breakdown (Zener or avalanche)

occurs, for limited currents this will not destroy the device and in some cases the

breakdown properties of the device are used in protecting the circuit. Damage to the

device can occur at higher currents due to heating and may happen whether the device is

forward or reverse biased. In Zener breakdown, as reverse bias is applied and band

bending occurs, the conduction band of the n-type material will be pulled below the

valence band of the p-type material. If the electrons in the p-type material valence band

have enough energy they may tunnel through the bandgap to the n-type material

conduction band and contribute to the reverse bias current as shown in figure 3.10-c.
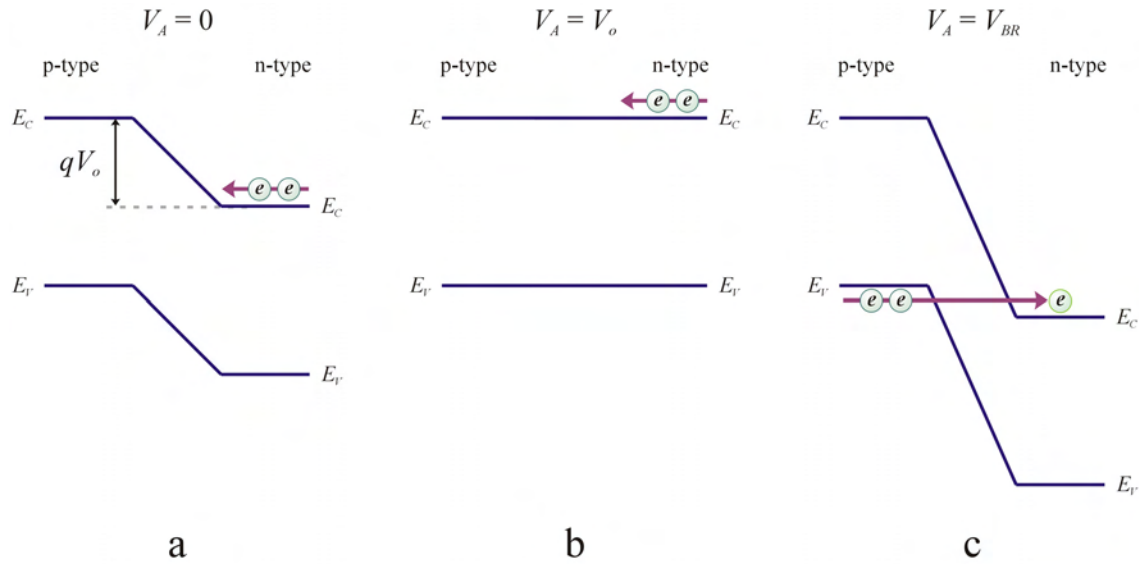
Figure 3.10
p-n Junction Band Diagram: a) Equilibrium;
b) Forward bias ($V_A = V_o$); c) Zener breakdown under reverse bias ($V_A = V_{BR}$)

The second breakdown mechanism, avalanche breakdown, is due to collisions

from drifting charge carriers. Under large reverse bias, the electric field within the

depletion region will become large. If an electron drifts into the depletion region and

comes under the influence of the large electric field, the electron may gain sufficient

kinetic energy to collide with the lattice and knock an electron out of its bond. The

collision will create an electron-hole pair (EHP), which will also be influenced by the

electric field. The newly created charge carriers may collide and create more charge

carriers producing an avalanche effect. The charge carriers escaping the depletion region

will contribute to the reverse bias current.

(1) Energetic electron accelerated in electric field
(2) Electron hole pair created
(3) Original electron and EHP-electron swept to n-type material
(4) EHP-hole swept to p-type material

a

b
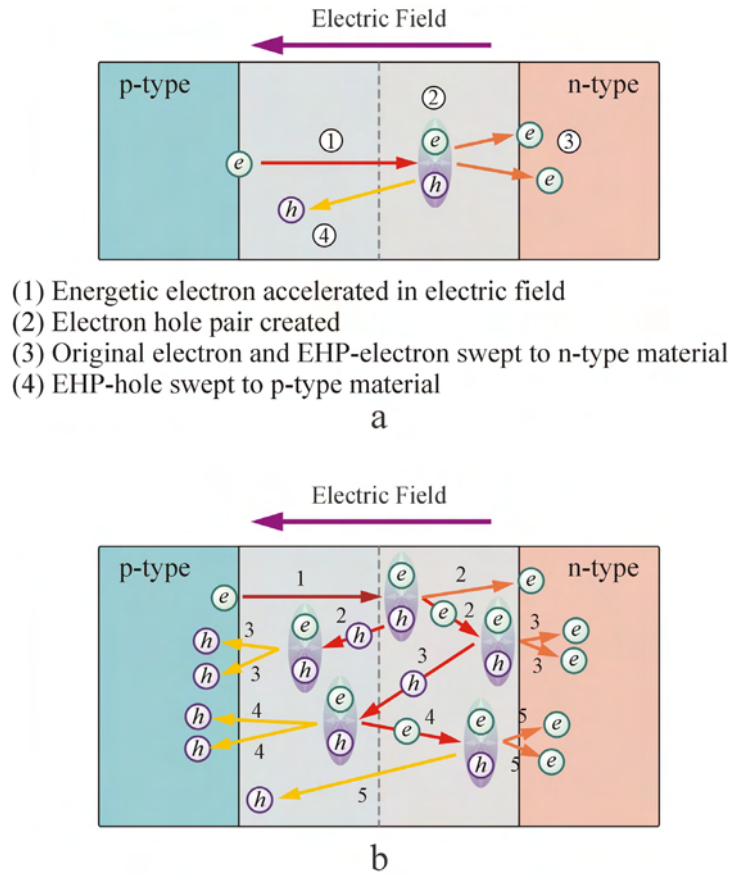
Figure 3.11
Avalanche Breakdown: a) Single EHP created; b) Sequential EHP's created

3.6   Asymmetrically Doped Junctions and Schottky Junctions

3.6.1   Asymmetrically Doped Junctions

In an asymmetrically doped junction, one side will be more heavily doped than the other ($N_A \gg N_D$ or $N_A \ll N_D$). In order to maintain equal amounts of charge within the depletion region on each side of the junction as dictated by equation 3.15 ($\left|Q_p\right| = \left|Q_n\right|$), the depletion region will shift accordingly, following equation 3.19 ($N_A x_p = N_D x_n$). An asymmetrically doped junction with charge density and electric field can be seen in figure 3.12 for the case $N_A \gg N_D$ for comparison to figure 3.6 (symmetrically doped junction).

p-type   n-type

Q_p Q_n

$-x_p$ $x = 0$ x_n

W

a

Charge density

qN_D^+

$Q_n = qN_D A x_n$

$-x_p$

$+$

x

x_n

$Q_p = -qN_A A x_p$

$-qN_A^-$

b

Electric Field, $E(x)$

$-x_p$ x_n

x

$E(x) = \dfrac{qN_A}{K_s \varepsilon_o}\left(x_p - x\right)$

E_{MAX}

$E(x) = \dfrac{qN_D}{K_s \varepsilon_o}\left(x_n - x\right)$

c
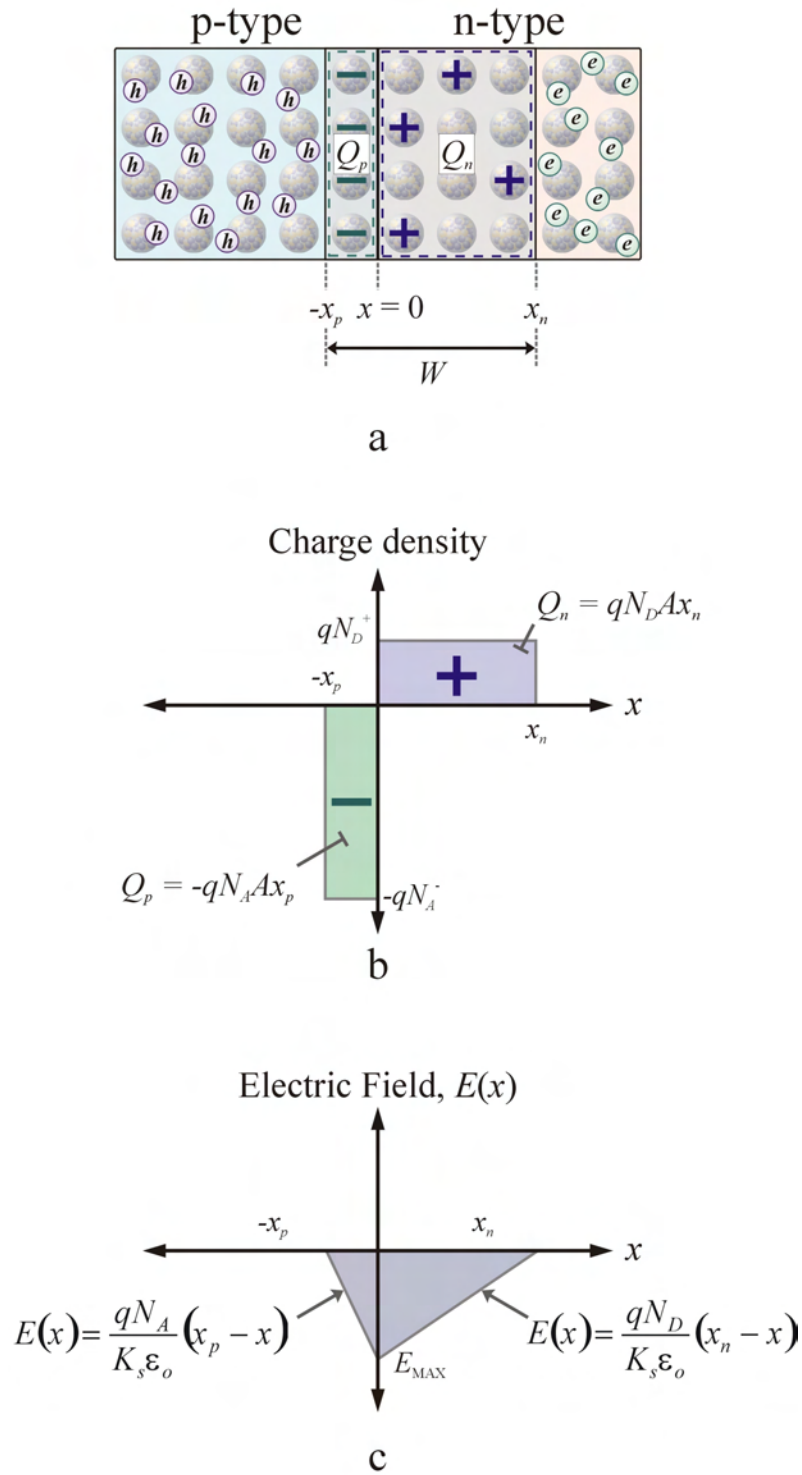
Figure 3.12
Asymmetric p-n junction: a) Physical p-n junction;
b) Charge distribution in depletion region; c) Electric field in depletion region

3.6.2   Schottky Junctions

A Schottky diode is a rectifying junction formed by a metal-semiconductor interface. The rectification properties of the junction arise due to the difference in work function of the two materials. If we consider a metal and an n-type semiconductor, we see the work function of the metal is greater than that of the semiconductor as seen in figure 3.13-a. When the two materials are brought together, charge transfer occurs to align the Fermi levels, leaving behind ionized donor atoms in the n-type material. As electrons leave the n-type material, a depletion region is formed at the junction extending into the n-type material. The Schottky junction can be viewed as an asymmetrically abrupt p-n junction with one side extremely heavily doped compared to the other. The
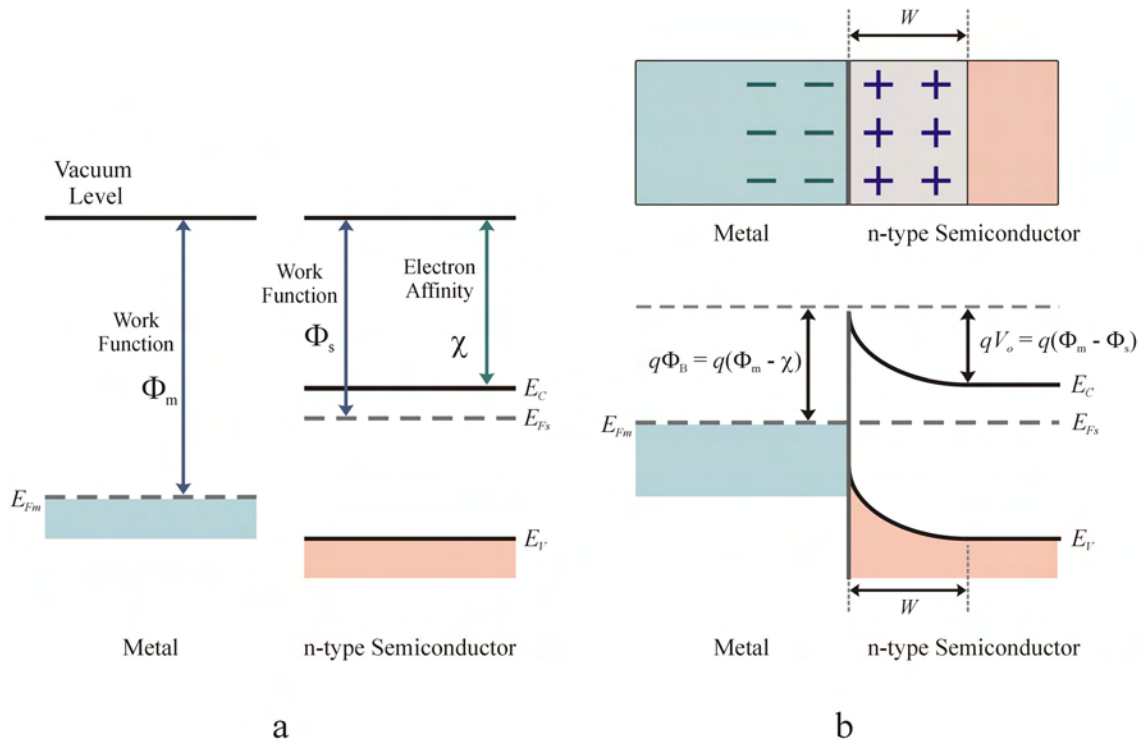
Figure 3.13
Schottky Junction - Metal to n-type Semiconductor ($\Phi_m > \Phi_s$):
a) Band diagram of metal and n-type semiconductor;
b) Band diagram of Schottky junction (metal to n-type semiconductor)

width of the depletion region in a Schottky junction can be estimated by treating it as an asymmetrically doped p-n junction and using the equations discussed previously, which are still valid for the Schottky junction. The built-in potential prevents further electron diffusion and a potential barrier is established, similar to the built-in potential of a p-n junction. The predicted barrier height, Φ_B is the difference in work function and the electron affinity ($\Phi_m - \chi$).

A Schottky barrier can also be formed between a metal and p-type semiconductor. The Fermi levels align, leaving ionized acceptor atoms in the p-type material, creating a depletion region which extends from the junction into the p-type material. The built-in potential prevents further diffusion of holes from the p-type material into the metal.
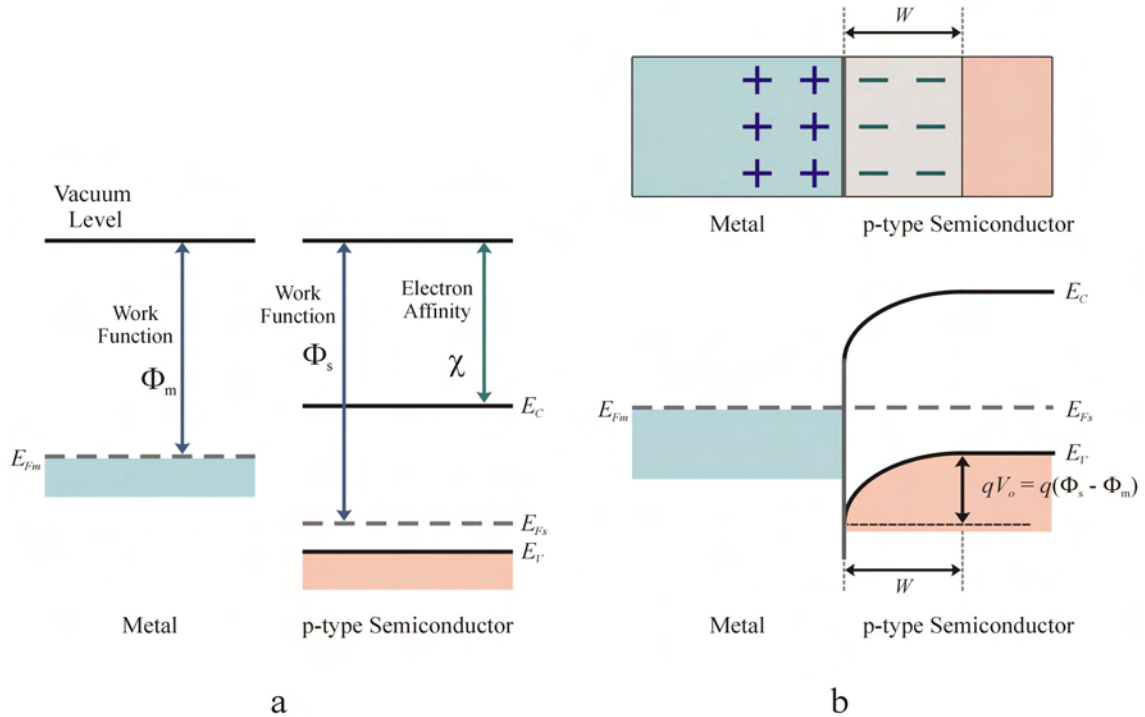
Figure 3.14
Schottky Junction - Metal to p-type Semiconductor ($\Phi_m < \Phi_s$):
a) Band diagram of metal and p-type semiconductor;
b) Band diagram of Schottky junction (metal to p-type semiconductor)

Electrical conduction through the junction occurs in a similar manner to a p-n junction. When forward bias is applied metal-n-type semiconductor junction, the band will shift allowing electrons to diffuse from the n-type material across the junction to the metal. If reverse bias is applied, the n-type material conduction band will be lowered, increasing the barrier and preventing electrons to diffuse across the junction.
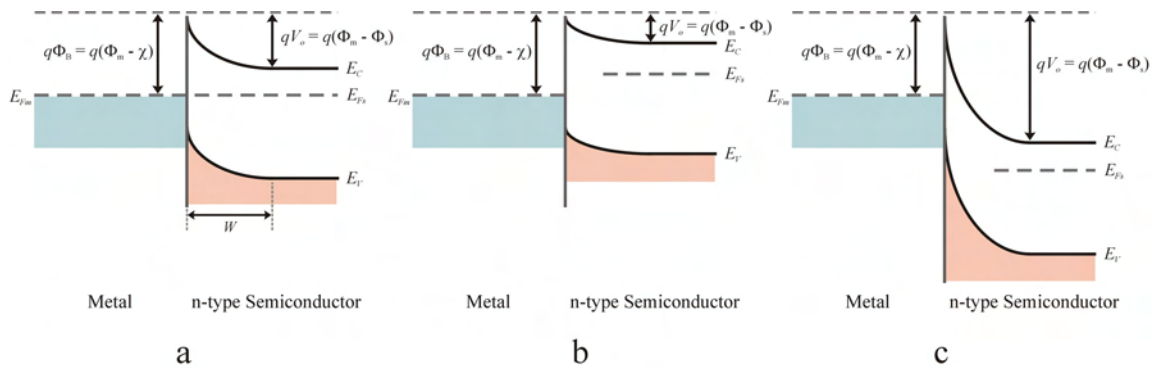
Figure 3.15
Schottky Junction Band Diagram: a) Equilibrium; b) Forward bias; c) Reverse bias

From figures 3.13 and 3.14, one would think that barrier height of the Schottky junction could be altered by using metals of varying work functions. However, it has been observed that the barrier height for common semiconductors (Ge, Si, GaAs and III-V compounds) is often relatively independent of the work function of the metal and consistency of the barrier height is attributed to Fermi level pinning.[13] At the metal-semiconductor interface dangling bonds and interface states exist, which pins the Fermi level at a fixed position, regardless of the metal used and ultimately affects the barrier height. Due to the phenomena of Fermi level pinning, doping density has little effect on the barrier height. However, the doping density does affect the depletion width. At low doping, the depletion width is wide and electrons require thermal energy to overcome the barrier and conduction is attributed to thermionic emission. At intermediate doping

levels, the electrons are thermally excited to a higher energy level where the barrier is

narrower and may tunnel through the barrier due the applied electric field in thermionic-

field emission. In highly doped materials, the barrier becomes narrow enough that

electrons may tunnel through the barrier under the influence of the applied electric field

in what is known as field emission.
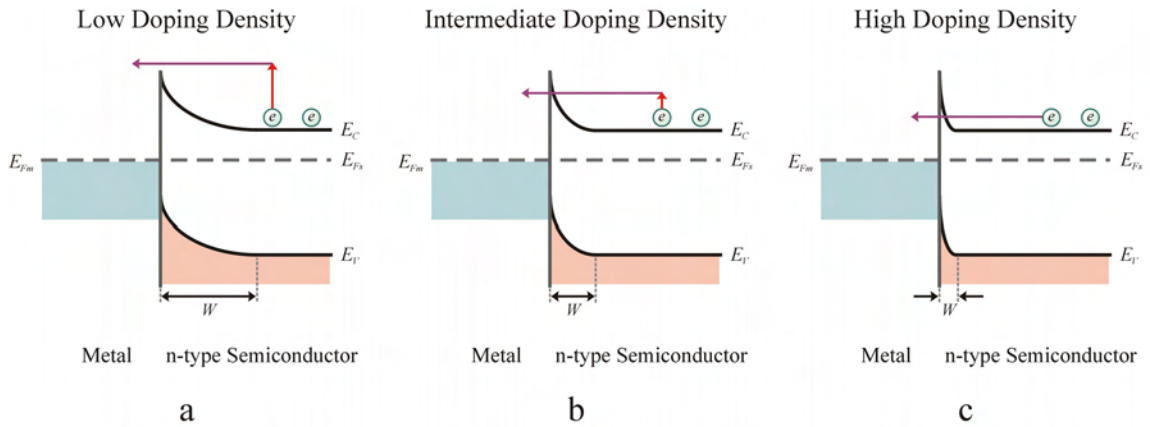
Figure 3.16
Conduction Mechanisms: a) Thermionic emission;
b) Thermionic-field emission; c) Field emission

CHAPTER 4

DEEP LEVEL TRANSIENT SPECTROSCOPY THEORY

4.1   Defect Levels

Defects within the crystal lattice create defect levels within the bandgap of the

semiconductor, which act as electron or hole traps depending on their occupancy. These

trap levels may be considered "shallow" level or "deep" level depending on their position

in the bandgap or more precisely the energy difference between the trap level and the

conduction or valence band edge. Substitutional impurities, such as dopants (ie. P, B, As

in Si), introduce defect levels just below the conduction band edge or just above the

valence band edge. These dopants, which affect the conduction properties of the

material, are considered electrically active and are classified as shallow level defects.

Deep level defects arise due to the substitutional impurities of other species of atoms,

vacancies, interstitials or a complex of other defects and produce trap levels further away

from the band edges, closer to the center of the bandgap.[15]

Shallow level traps are characterized by small ionization energies, which is of the

order of phonon energies.[16] These traps easily gain enough thermal energy at room

temperature (T = 300K, E = 0.02586 eV) to become ionized. A table of common donor

and acceptor ionization energies can be seen below in tables 4.1 and 4.2. Shallow level

defect states can be mapped out using techniques such as Hall effect, resistivity, and CV

measurements.[17] At low temperatures, DLTS is another method for detecting shallow

level defect states. One should be careful with analyzing data taken at low temperatures

as the resistance of the sample becomes considerable, causing errors in the determination

of the capacitance.[18]

Table 4.1
Donor Ionization Energies[19]

Ionization energies (meV) for common donors in Si, Ge and GaP

	P	As	Sb	Sn	Si	Te	Se	S	Ge
Germanium	12.9	14.2	10.3						
Silicon	45.5	53.7	42.7						
Gallium phosphide				65.5	82.1	89.8	102.0	104.1	200

Table 4.2
Acceptor Ionization Energies[19]

Ionization energies (meV) for common acceptors in Si, Ge, GaAs and GaP

	B	Al	Ga	In	Tl	C	Be	Mg	Zn	Cd	Si	Ge
Germanium	10.5	10.8	11.0	11.6	13.1							
Silicon	44.5	68.5	72	155								
Gallium aresnide						26.0	28.0	28.4	30.7	34.7	34.5	40.4
Gallium phosphide						48	50	53.5	64	96.5	203	258

Deep level defect states are often referred to as traps, recombination centers, generation centers, deep levels or deep impurities.[15,20] In common semiconductors, silicon and gallium arsenide, with bandgaps 1.1 and 1.4 eV respectively, deep level traps are more than about 0.05 eV from the band edges and are not thermally ionized at room temperature.[19] For this reason, acceptors just below the conduction band edge and donors just above the valence band edge are considered deep levels.

In contrast to the shallow level states, deep level states have large ionization energies, which implies a strong potential that acts to localize the charge carrier wave function near the defect site. As a consequence of the localization of real space is the delocalization of k-space, which results in two important properties of the deep level states. First, deep level states tend to be non-radiative recombination centers because the large extent of k-space allows the defect to couple strongly with a variety of phonons. In simple terms, recombination events at deep levels states leads to the release of energy in the form of phonons as opposed to photons. Second, the entire band structure must be involved in the description of the defect, making analysis more complicated. [15,20]

4.2   Deep Level Trap Characteristics

In a semiconductor, deep level traps may be defined as electron traps when the electron capture rate (c_n) is much larger than the hole capture rate (c_p). By similar reasoning, hole traps have a much larger hole capture rate than electron capture rate. A second parameter of the trap is the electron emission rate (e_n) and hole emission rate (e_p). If the electron emission rate is much larger than the hole emission rate, then the trap is likely to be free of electrons and capable of capturing them. A trap with $e_n \gg e_p$ is considered an electron trap and a trap with $e_p \gg e_n$ is considered a hole trap. Therefore

an electron trap mainly interacts with the conduction band and a hole trap mainly interacts with the valence band. In general, a recombination center is a trap that has both a large electron capture rate and large hole capture rate and a generation center has $e_n \sim e_p$.[20] Another convention for naming traps is by majority and minority charge carrier. Simply put, an electron trap is considered a majority carrier trap in n-type material and a minority carrier trap in p-type material and a hole trap is considered a majority carrier trap in p-type material and a minority carrier trap in n-type material.
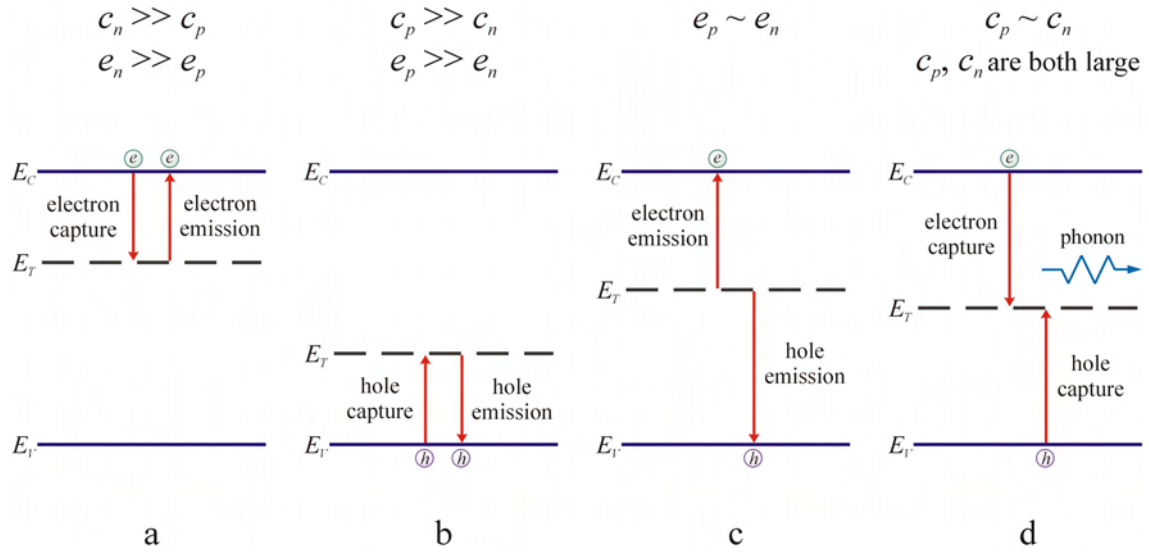
Figure 4.1
Traps: a) Electron trap; b) Hole trap;
c) Generation center; d) Recombination center

The electron capture process can be characterized by a capture cross section (σ_n) exposed to *n* electrons per unit volume moving with a thermal velocity of $<v_n>$. The trap is exposed to a flux of $n<v_n>$ per unit time. Given a trap density of N_T, at any given time, n_T of the traps are occupied. The number of electrons in a given time, Δt, captured by the remaining unoccupied states is:

$$\Delta n_T = \sigma_n \langle v_n \rangle n (N_T - n_t) \Delta t \qquad (4.1)$$

and the capture rate per unoccupied states is defined as:

$$c_n = \frac{(\Delta n_T / \Delta t)}{(N_T - n_T)} \tag{4.2}$$

which becomes:

$$c_n = \sigma_n \langle v_n \rangle n \tag{4.3}$$

Similarly, the hole capture rate is:

$$c_p = \sigma_p \langle v_p \rangle p \tag{4.4}$$

The thermal velocity is given by:[8,20]

$$\langle v \rangle = \sqrt{\langle v^2 \rangle} = \sqrt{\frac{3 k_B T}{m*}} \tag{4.5}$$

The effective mass ($m*$) can be approximated from the second order derivative of the

minima (conduction band) and maxima (valence band) of the E-k diagram from the

following:[9]

$$m* = \frac{\hbar^2}{d^2 E / dk^2} \tag{4.6}$$

The average effective masses for a few common semiconductors are given in table 4.3,

where m_o is electron rest mass (9.1093897 x 10^{-31} kg).

Table 4.3
Effective Masses for Common Semiconductors[9]

	Germanium	Silicon	Gallium arsenide
$m*_n$	0.55 m_o	1.1 m_o	0.067 m_o
$m*_p$	0.37 m_o	0.56 m_o	0.48 m_o

The free electron concentration, n, is determined from:

$$n = N_C \exp\left[\frac{-(E_C - E_F)}{k_B T}\right]$$ (4.7)

where N_C is the effective density of states at the edge of the conduction band.

$$N_C = 2\left[\frac{2\pi m_n^* k_B T}{h^2}\right]^{3/2}$$ (4.8)

The free hole concentration, p, used in equation 4.4 is determined from:

$$p = N_V \exp\left[\frac{-(E_F - E_V)}{k_B T}\right]$$ (4.9)

where N_V is the effective density of states at the edge of the valence band.

$$N_V = 2\left[\frac{2\pi m_p^* k_B T}{h^2}\right]^{3/2}$$ (4.10)

The emission rate can also be represented in mathematical terms. The electron emission rate for a trap is given by equation 4.11 and the hole emission rate is given by equation 4.12,

$$e_n = \frac{\sigma_n \langle v_n \rangle N_C}{g} \exp\left(-\frac{\Delta E}{k_B T}\right) = \frac{\sigma_n \langle v_n \rangle N_C}{g} \exp\left(-\frac{(E_C - E_T)}{k_B T}\right)$$ (4.11)

$$e_p = \frac{\sigma_p \langle v_p \rangle N_V}{g} \exp\left(-\frac{\Delta E}{k_B T}\right) = \frac{\sigma_p \langle v_p \rangle N_V}{g} \exp\left(-\frac{(E_T - E_V)}{k_B T}\right)$$ (4.12)

where the depth of the trap, ΔE, is the difference in energy between the trap level and the band edge to which the charge carrier is emitted. For an electron trap, $\Delta E = E_C - E_T$ and for a hole trap $\Delta E = E_T - E_V$. In equations 4.11 and 4.12, g is the degeneracy of the trap level. Equations 4.11 and 4.12 are often represented in literature in the form:

$$e_n = \gamma_n \sigma_n T^2 \exp\left(-\frac{\Delta E}{k_B T}\right)$$ (4.13)

where γ_n(Si) = 5.21 x 10^{20}, γ_p(Si) = 1.60 x 10^{21}, γ_n(GaAs) = 2.67 x 10^{20} and γ_p(GaAs) =

1.47 x 10^{21} cm^{-2}s^{-1}K^{-2}.[21]

4.3   Deep Level Trap Measurement

If a deep level trap is present in a sufficiently large concentration, it determines

the position of the Fermi level over a certain temperature range, therefore its

concentration and activation energy can be determined from the temperature dependent

Hall effect measurements. Most often, the deep level states are present in concentrations

orders of magnitude less than the shallow level impurities and consequently the Fermi

level is determined by shallow level impurities and therefore the Hall effect

measurements cannot be used. As a result of the low concentrations of deep states

compared to shallow states, measurement techniques that are sensitive to low

concentration of the deep states are necessary. These techniques rely on the transient

phenomena associated with charge carrier capture and emission from these deep states.

The time constant of the transient provides information about the rates of the process and

the amplitude provides information on the concentration of the deep states.[19]

Measurement of the transient nature of deep level traps depends on filling traps in

the depletion region by electrical or optical methods and observing the emission of these

filled traps as a function of the temperature. The transients due to majority traps can be

observed by filling the traps with a voltage pulse and then returning the device to its

original voltage. As seen in figure 4.2, the device is held at reverse bias and a filling

pulse with bias set to zero volts occurs. Following the filling pulse, the device is then

returned to the same reverse bias. During the filling pulse, the depletion width decreases

and the majority traps that are no longer in the depletion region are filled. Immediately

following the filling pulse when the reverse bias is applied, the traps will emit the charge

carriers with a characteristic time constant based on the temperature. Electrons emitted to

the conduction band are moved out of the depletion region by the internal electric field,

avoiding recapture. As a result of the emission of the trapped charge, the resulting

capacitance will exponentially decay back to it quiescent value following the pulse. The
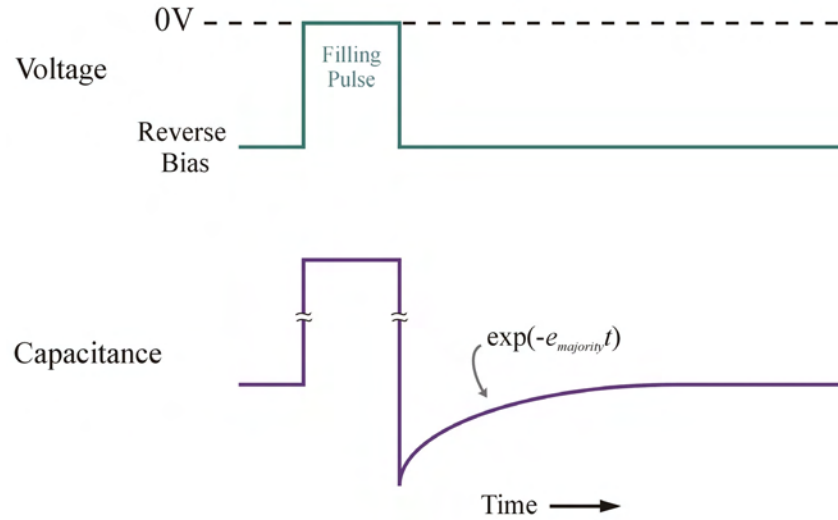
Figure 4.2
Majority Carrier Trap Biasing and Resulting Capacitance Transient

Figure 4.3
Majority Carrier Trap Band Structure: a) Under reverse bias; b) Bias pulsed to zero
volts and traps are filled; c) Under reverse bias and filled traps empty

band structure and filling of the electron traps (majority traps) can be seen in figure 4.3. Initially, the device is held at reverse bias (figure 4.3a) and traps below the Fermi level are filled. The bias is pulsed to zero volts and the traps in the space charge region are filled (figure 4.3b). After the device is returned to reverse bias, the traps will emit their charge (figure 4.3c). As the trapped charges are emitted back to the conduction band, the effective charge density increases in the depletion region, decreasing the depletion width and thus increasing the capacitance.

Minority traps can also be filled electrically in the same manner. However, the pulse used in filling traps is such that it will forward bias the device. Following the pulse, the capacitance of the device will decay back to the quiescent value with a characteristic time constant. The band structure and filling of the electron traps (minority
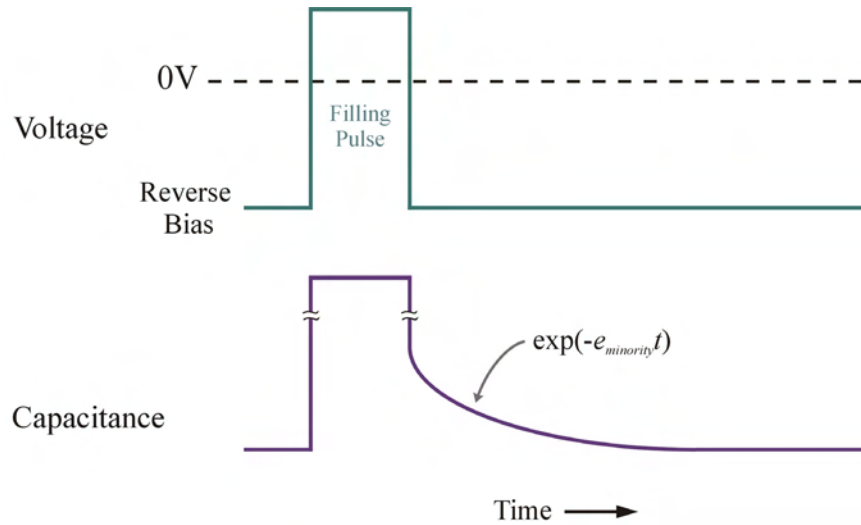
Figure 4.4
Minority Carrier Trap Biasing and Resulting Capacitance Transient

traps) can be seen in figure 4.5. In addition to electrical pulse filling, minority traps may also be filled by optical means by illuminating the reverse biased depletion region with photons ($hv < E_g$) and creating EHP's which fill the traps. As the electrons are emitted

back to the conduction band, the charge density decreases, increasing the depletion width and thus lowering the capacitance.
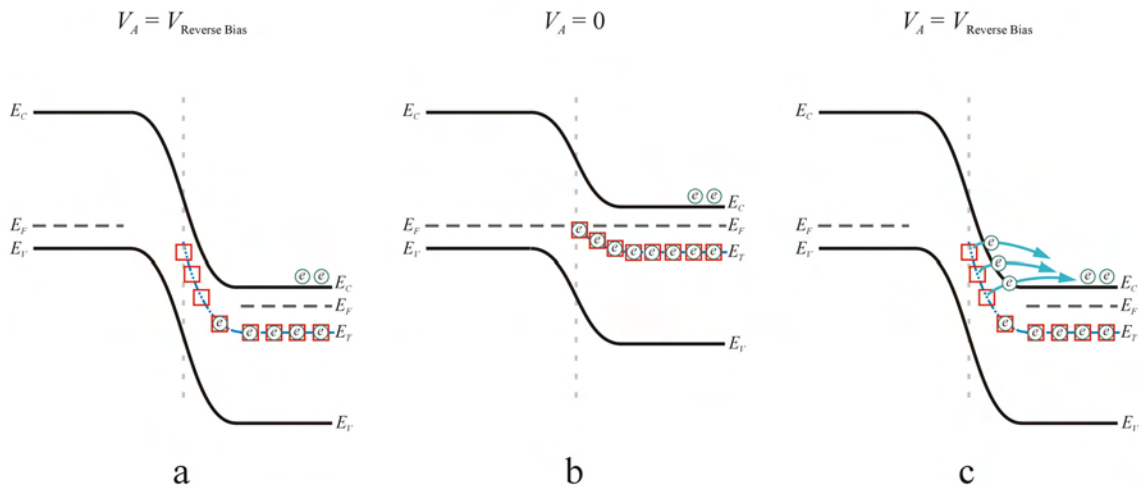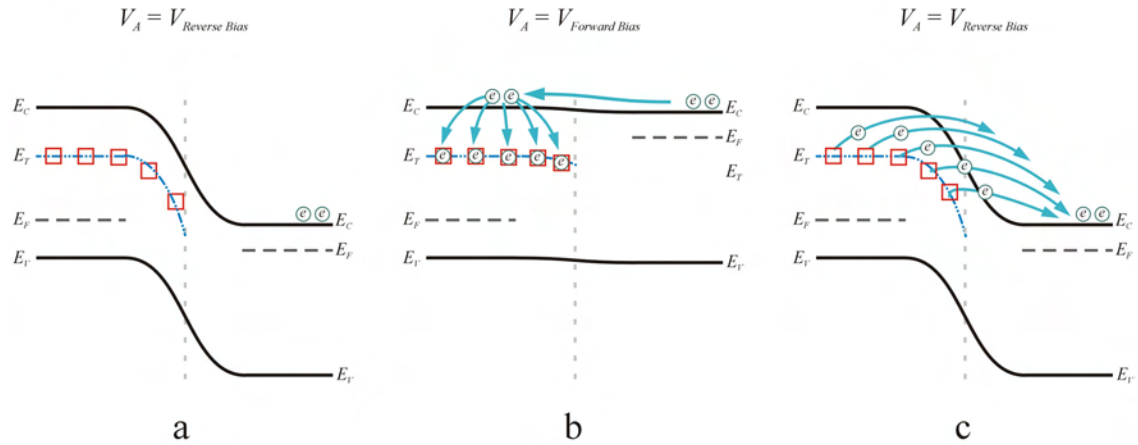

Figure 4.5
Minority Carrier Trap Band Structure: a) Under reverse bias;
b) Forward biased and traps are filled; c) Under reverse bias and filled traps empty

4.4   Early Techniques

Since the emission of trapped charged is temperature dependent, it naturally follows that changes in the current or capacitance of a material with deep level traps will also be temperature dependent. Early techniques employed thermally stimulated charges, which affect the measured electrical signal. The two techniques primarily used were thermally stimulated current (TSC) proposed by Driver and Wright in 1963 and later thermally stimulated capacitance (TSCAP) proposed by Caraballes and Lebailly in 1968.[16] During the measurement, the device is held at zero bias and cooled until the traps are filled with majority carriers. Alternately, the traps may be filled with minority carriers by optical injection or forward biasing the device and cooling it until the traps are filled. The device is then reverse biased and heated at a constant rate while the capacitance or current is measured. As the temperature is increased, the charges gain sufficient energy to escape the traps and contribute to the measurement. Steps in the

capacitance data or peaks in the current are observed as the traps emit the charges. The temperature of the current peak in the TSC curve or midpoint of the capacitance step in the TSCAP is related to the activation energy, $\Delta E = E_C - E_T$ or $\Delta E = E_T - E_V$, by

$$\Delta E = k_B T \ln\left[\frac{\gamma \sigma k_B T^4}{\beta\left(\Delta E + 2k_B T^4\right)}\right] \tag{4.14}$$

where T is the temperature , β is the heating rate, σ is the capture cross section and γ is defined in equation 4.13. The trap density is obtained from the area under the TSC peaks or step heights in the TSCAP curves. The equipment used in performing TSC and TSCAP measurements is simpler than DLTS, but the information obtained is limited and more difficult to interpret. TSC measurements are subject to leakage and steady state generation currents that arise due to the temperature increase while TSCAP measurements are less sensitive to device quality. A second disadvantage of the TSC measurement is that you are not able to distinguish whether a peak in the data is due to a minority or majority carrier trap.[13,16]

A sample containing a majority carrier trap concentration of N and a shallower minority carrier trap concentration of $2N$. The increase in current at the higher temperature in the TSC data is the dark current due to the steady state generation and leakage.
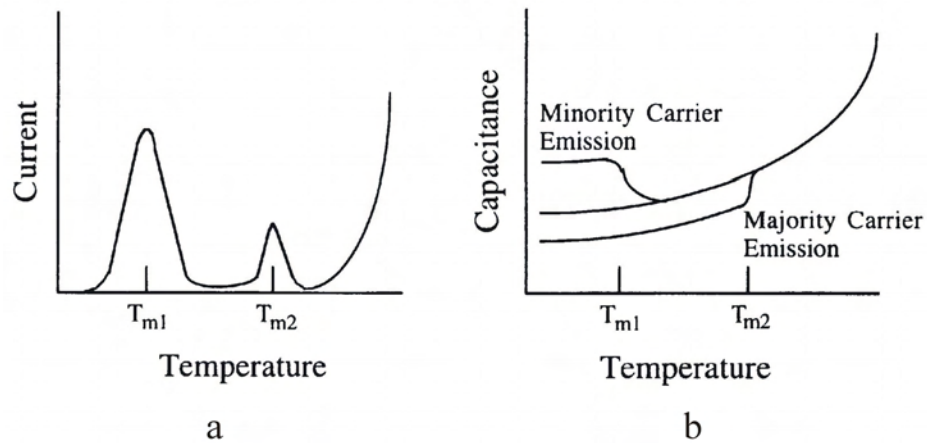
Figure 4.6
Early Measurement Techniques: a) Thermally stimulated current (TSC);
b) Thermally stimulated capacitance (TSCAP)[16]

4.5 Deep Level Transient Spectroscopy (Conventional Double Boxcar DLTS)

The early techniques used in measuring deep level traps were tedious and very time consuming. Most techniques were "single-shot" measurements which had to be repeated to gain additional information regarding the deep levels. The analysis of the transient behavior of deep level traps really came to fruition when automated data acquisition techniques were first used. The first technique, proposed by Lang in 1974, known as deep level transient spectroscopy (DLTS) made use of the dual-gated signal averager (double boxcar).[22] A block diagram of a basic DLTS system can be seen in figure 4.7. DLTS provides a method that quickly measures and analyzes capacitance transients and is able to distinguish between minority and majority carrier traps and
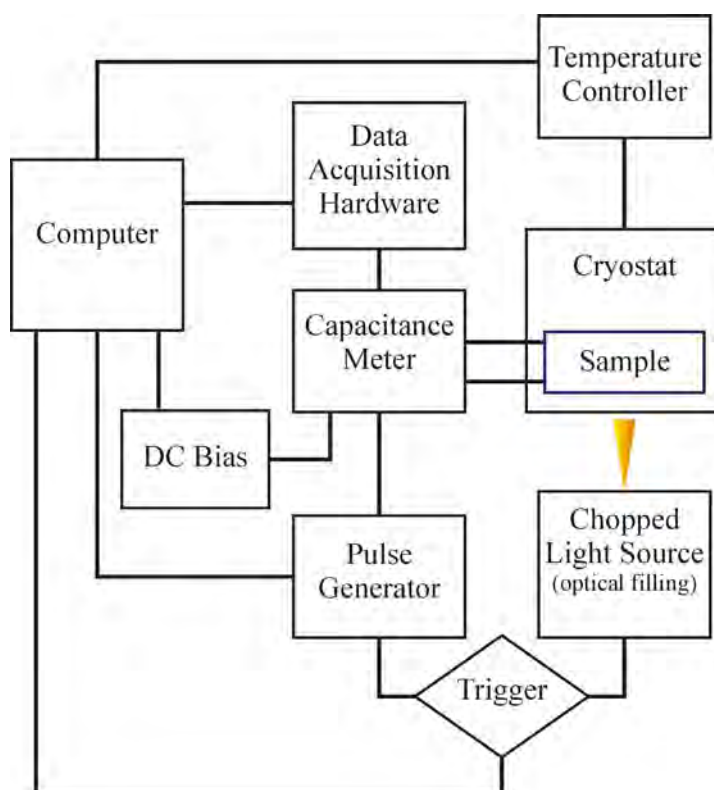
Figure 4.7
DLTS Block Diagram

provide information about the concentration, energy levels and capture rates of the traps. Furthermore, it is spectroscopic in nature, in that different traps can be resolved from one another and be reproducible in position when plotted against a single variable.[22] The same information can be gained by performing many transient capacitance measurements at several temperatures, and then compiling the information, which becomes rather laborious.

In a DLTS measurement, the device is held at reverse bias and then a voltage pulse is used to fill the traps. The device is then returned to reverse bias and the resulting capacitance transient is then measured. The double boxcar samples the capacitance at time t_1 and t_2 following the pulse. The sampling times t_1 and t_2 determine the ratewindow $(t_2 - t_1)$. This process is repeated as the temperature is increased. The difference between the sample capacitance at times t_1 and t_2, $(C(t_1) - C(t_2))$, can be plotted as function of the temperature to produce the DLTS signal as seen in figure 4.9.
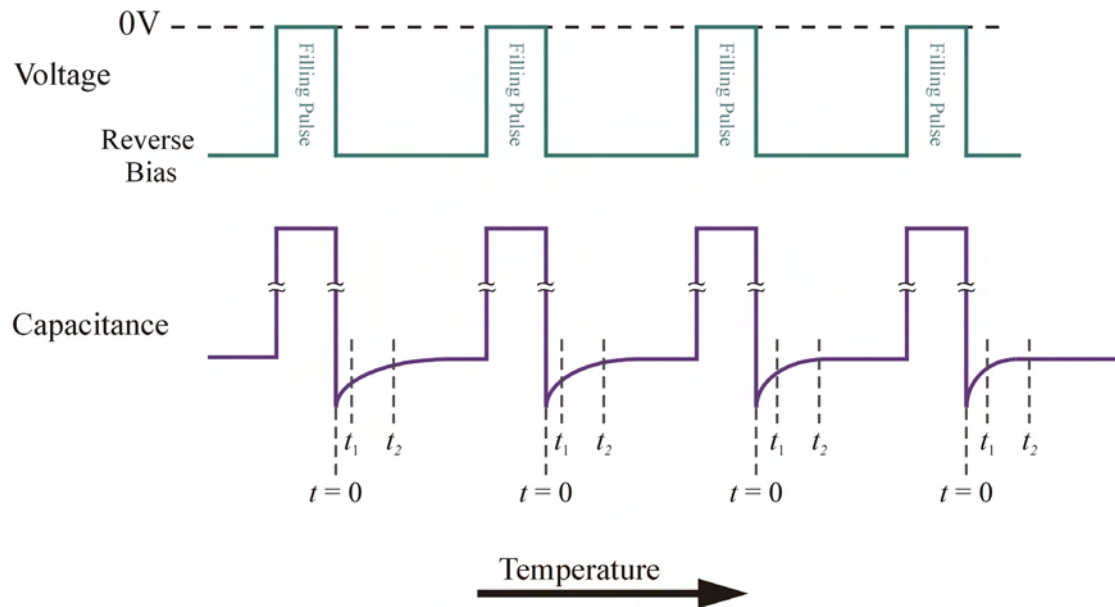
Figure 4.8
DLTS Measurement
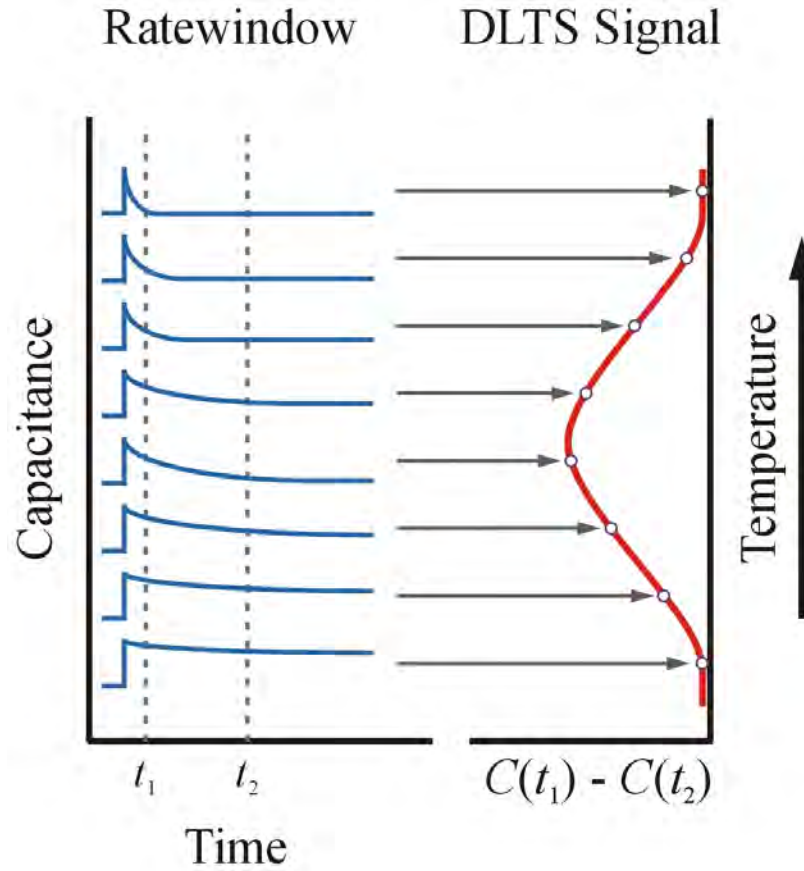
Figure 4.9
Ratewindow and DLTS Signal

If we assume that the capacitance transients following the filling pulse are exponential, then the capacitance as a function of time can be represented as:

$$C(t) = C(t = 0)\exp\left[\frac{-t}{\tau}\right] \tag{4.15}$$

where $\tau = 1/e_n$.[17] The sample capacitance at times t_1 and t_2 can then be represented as:

$$C(t_1) = C(t = 0)\exp\left[\frac{-t_1}{\tau}\right] \tag{4.16}$$

$$C(t_2) = C(t = 0)\exp\left[\frac{-t_2}{\tau}\right] \tag{4.17}$$

A function $S(T)$ can be defined as:

$$S(T) = \frac{C(t_1) - C(t_2)}{C(t = 0)} \qquad (4.18)$$

$$S(T) = \exp\left[\frac{-t_1}{\tau}\right] - \exp\left[\frac{-t_2}{\tau}\right] \qquad (4.19)$$

$S(T)$ in general depends on the temperature since τ is temperature dependent. When τ is of the same order as $t_2 - t_1$, $S(T)$ will be large. For lower temperatures, τ will be much larger than $t_2 - t_1$ and the slope will be neglible resulting in a neglible $S(T)$. For much higher temperatures τ will be much smaller than $t_2 - t_1$ and the transient will have already decayed back the to quiescent value at $t \leq t_1$. To find the maximum of $S(T)$, we take the derivative and set that equal to zero.

$$\frac{d}{d\tau}\left\{\exp\left[\frac{-t_1}{\tau}\right] - \exp\left[\frac{-t_2}{\tau}\right]\right\} = 0 \qquad (4.20)$$

$$t_1\tau^{-2}\exp\left[\frac{-t_1}{\tau}\right] - t_2\tau^{-2}\exp\left[\frac{-t_2}{\tau}\right] = 0 \qquad (4.21)$$

$$t_1\exp\left[\frac{-t_1}{\tau}\right] - t_2\exp\left[\frac{-t_2}{\tau}\right] = 0 \qquad (4.22)$$

$$\ln\left(t_1\exp\left[\frac{-t_1}{\tau}\right]\right) = \ln\left(t_2\exp\left[\frac{-t_2}{\tau}\right]\right) \qquad (4.23)$$

$$\ln t_1 + \frac{-t_1}{\tau} = \ln t_2 + \frac{-t_2}{\tau} \qquad (4.24)$$

$$\ln\left(\frac{t_1}{t_2}\right) = \frac{t_1 - t_2}{\tau} \qquad (4.25)$$

So if S(T) is maximum, the relation between τ and t_1 and t_2 is given by:

$$\tau_{max} = \frac{t_1 - t_2}{\ln\left(t_1 / t_2\right)} \qquad (4.26)$$

Thus the peak maximum produced in the DLTS signal will have a precisely defined emission rate (τ_{max}^{-1}) and a temperature (T_i) corresponding to the peak maximum. If the measurement is repeated using different ratewindows, you will obtain different values of τ_{max} and T_i, which can be used in determining the trap signature.

The set of τ_{max} and T_i generated from varying the ratewindows can be used to construct an Arrhenius plot to extract the activation energy and capture cross section. The emission rate can be manipulated to produce a linear curve on a semilog plot with the measured data. Equation 4.13 written as:

$$\frac{1}{\tau} = \gamma_n \sigma_n T^2 \exp\left(-\frac{\Delta E}{k_B T}\right) \qquad (4.27)$$

$$\frac{1}{\tau T^2} = \gamma_n \sigma_n \exp\left(-\frac{\Delta E}{k_B T}\right) \qquad (4.28)$$

$$-\ln\left(\tau T^2\right) = \ln\left(\gamma_n \sigma_n\right) - \frac{\Delta E}{k_B T} \qquad (4.29)$$

$$\ln\left(\tau T^2\right) = \frac{\Delta E}{k_B}\frac{1}{T} + \ln\left(\frac{1}{\gamma_n \sigma_n}\right) \qquad (4.30)$$

A semilog plot of τT^2 vs. $1/T$ will give a straight line with a slope of $\Delta E/k_B$ and a y-intercept of $\ln (1/\gamma\sigma)$. Since k_B and γ are known, the activation energy and capture cross section can be determined from the fit of the line. An example of the DLTS signal and resulting Arrhenius plot can be seen in figure 4.10. As commonly seen in literature, the x-variable of the data is plotted as $1000/T$ as opposed to $1/T$.
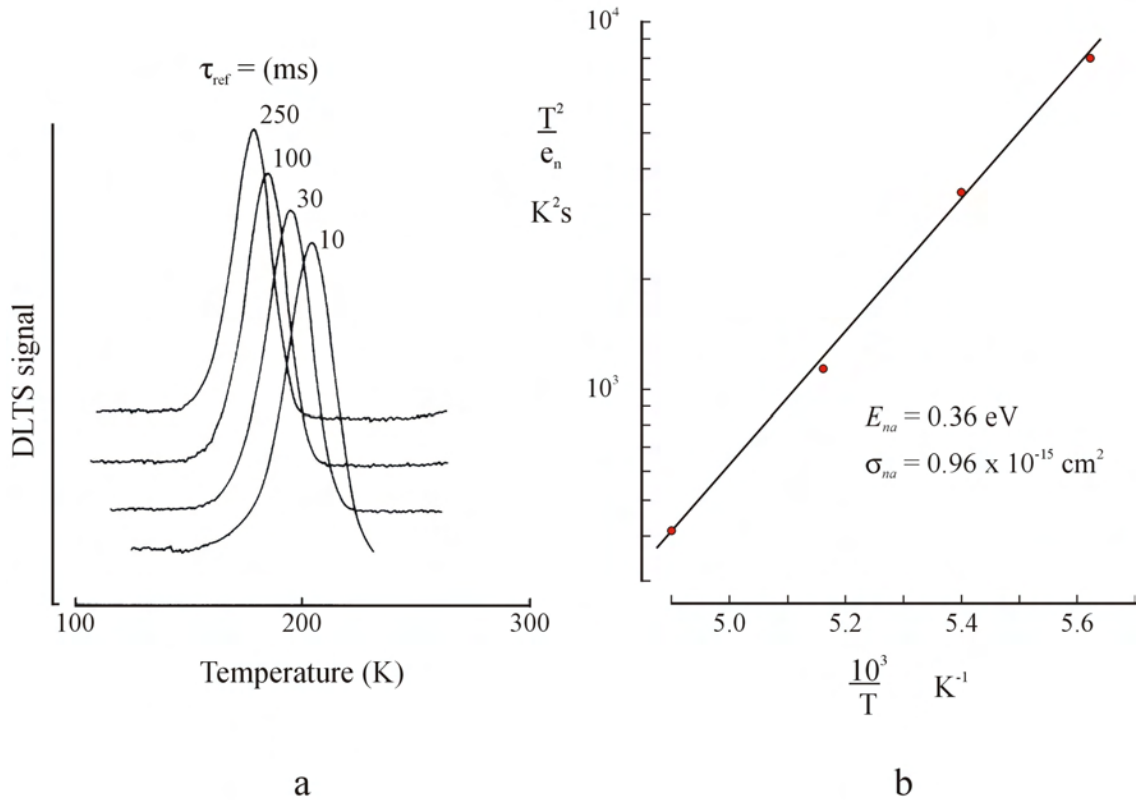
Figure 4.10
DLTS Signal and Arrhenius Plot: a) DLTS spectra for a sample of vapor phase epitaxial
n-type GaAs recorded with reference time constants indicated. (The zeros are displaced
to separate the curves.); b) An Arrhenius plot of this data giving a trap signature
characterized by the parameters E_{na} and σ_{na}[19]

4.6   Deep Level Transient Spectroscopy (Computer DLTS)

Over time, variations of Lang's original DLTS technique have come about as

computer processing power has improved. In contrast to the double boxcar DLTS, which

measures the capacitance transient at two specific times, the new techniques, referred to

as computer DLTS, will capture the entire capacitance transient waveform and digitize

the data for storage and analysis. Typically, the capacitance transient will be measured at

several different temperatures with several hundred data points per transient.

Mathematical algorithms can then be used on the waveform to fit the measured data and

extract the trap parameters. The advantage of computer DLTS over its predecessor is that it is faster, more accurate and has better resolution capabilities. In a computer DLTS measurement, only one temperature scan is necessary, whereas several temperature scans with varying ratewindows are required for conventional DLTS. Second, since computer DLTS captures the entire waveform, it is easy to establish whether or not the transient displays the exponential form associated with a trap. That is to say, it allows the user to distinguish between traps, noise variation or other phenomena, which may affect the capacitance transient. Computer DLTS also offers greater resolution and is able to separate two closely spaced deep level traps where conventional DLTS fails, as seen in figure 4.11. In the figure, two closely spaced traps (exponentials) are displayed as dotted lines. Since conventional DLTS only samples the capacitance at two points along the transient, this may lead to erroneous results in assuming that the transient is due to a single exponent.
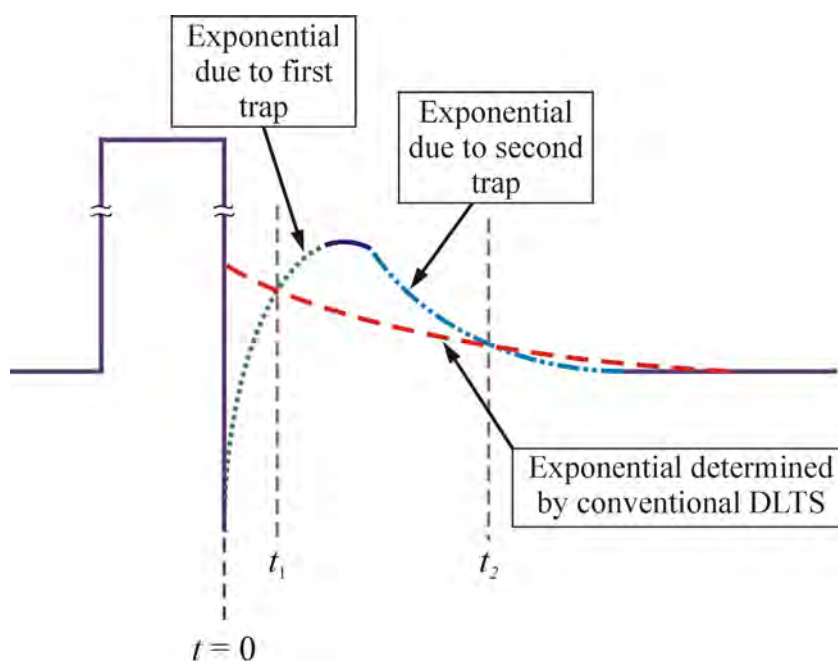

Figure 4.11
Comparison of Computer DLTS and Conventional DLTS

CHAPTER 5

SEMETROL DLTS SYSTEM

5.1   Comparison of Sula DLTS System and Semetrol DLTS System

The most significant modification to the original DLTS system was the new

control software (Semetrol). Two modifications were made to the hardware; a new

National Instruments interface card was installed and a Keithley 6487 Picoammeter/

Voltage Source was connected to the GPIB interface. The latter being only necessary for

the IVT portion of the Semetrol control software. The original DLTS measurement

system used the Sula module and accompanying Sula software (written in National

Instruments Labview). The Sula measurement technique follows Lang's conventional

DLTS measurement, where the capacitance is sampled at times t_1 and t_2 following the

filling pulse. A diagram of the Sula module is seen below in figure 5.1. The rotary dials

(potientiometer) of the pulse generator panel are used to set the filling pulse and the

capacitance meter panel measures the resulting capacitance. The correlator panel is used

to set the ratewindow and samples the capacitance at t_1 and t_2 and sends the signal to the

digitizer (DAQ card). The digitizer performs the analog to digital conversion, allowing

the computer (software) to process the measurement results. The pulse

generator/correlator panel is used for depth profiling in performing a Double correlation

technique DLTS (DDLTS) measurement or can be used to measure another ratewindow

during a DLTS measurement. During the DDLTS measurement, the pulse

generator/correlator is used to set the second filling pulse (differing from the first pulse

set by pulse generator panel) to provide depth profiling and to sample the capacitance
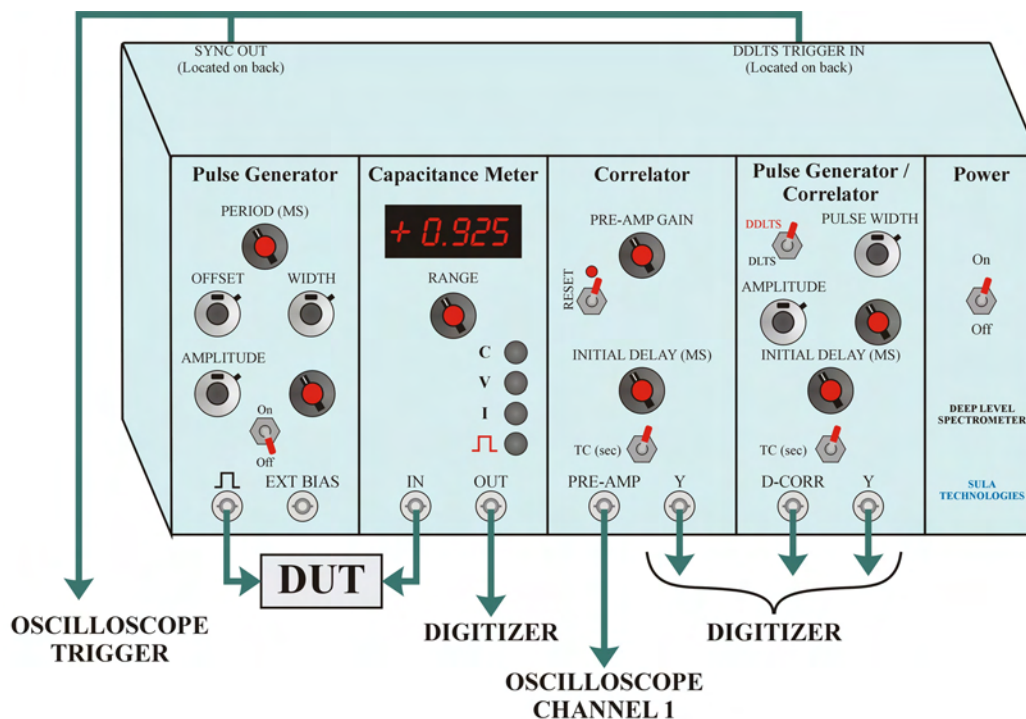
following the second pulse.

Figure 5.1
Sula Module

The use of the Semetrol software (written in National Instruments Labview)

eliminates the need for the entire Sula module, except the capacitance meter panel and

the EXT BIAS connection and the pulse connection on the pulse generator panel. The

Semetrol software uses the computer DLTS measurement technique and digitizes and

stores the capacitance transient waveform following the filling pulse. The transient can

then be fit to one or two exponentials to determine the trap(s) characteristics. In addition,

the Semetrol software can also be used to generate the conventional ratewindow DLTS

signal. Using this data, the user can do traditional ratewindow analysis to generate the

Arrhenius plot to determine the trap characteristics. The parameters of the filling pulse

and device bias are set in the software as compared to the use of the rotary knobs as in the

Sula hardware. The DC bias of the device is sent from a digital to analog converter on

the National Instruments DAQ card and through the National Instruments BNC-2090

terminal block to the Sula pulse generator panel connectors. The resulting transient is

measured by the Sula capacitance meter and sent through the NI BNC-2090 to an analog

to digital converter on the NI DAQ card. A block diagram of the DLTS system can be

seen in figure 5.2 (additional information can be found in Appendix B).
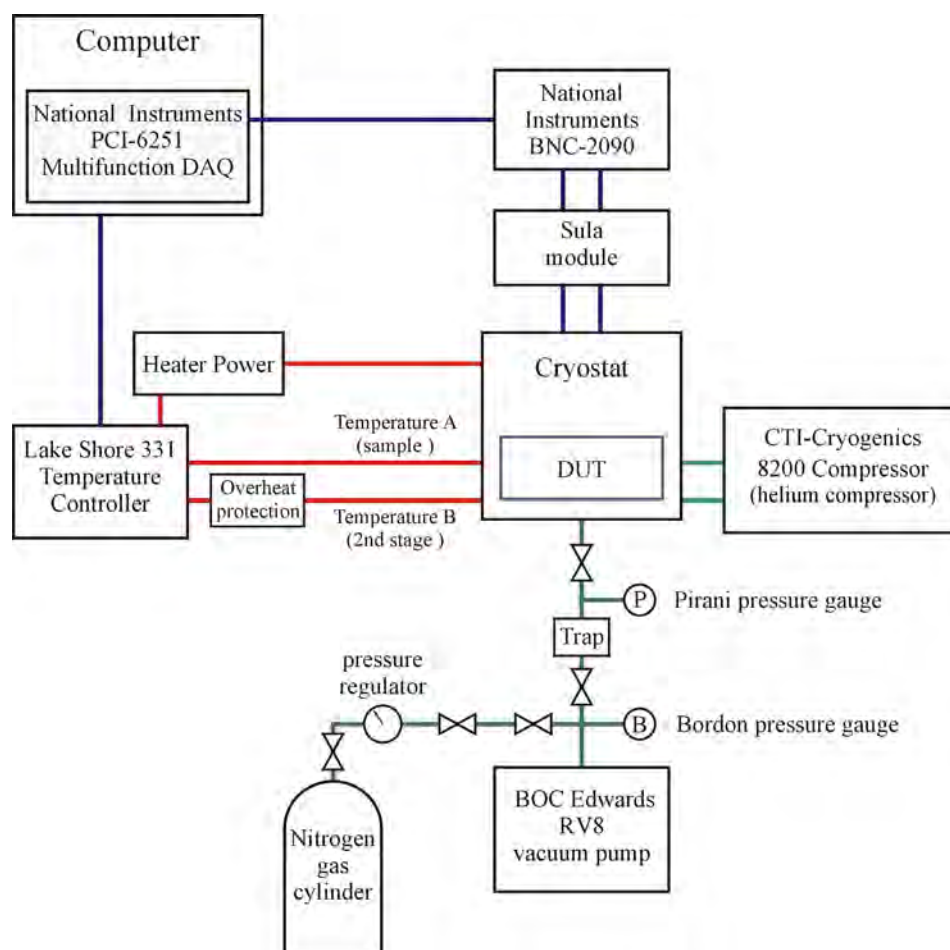

Figure 5.2
DLTS System Block Diagram

The Semetrol software offers several advantages over the Sula software and original hardware. As discussed in the previous chapter, the use of computer DLTS is more favorable compared to conventional DLTS. The Semetrol method is faster since only one temperature scan is required to measure all transients. Furthermore, the results are more accurate, and offer better resolution of closely spaced traps is obtained (simulated data and comparison of the two methods can be found in Appendix D).

The use of the Semetrol software allows the user to accurately set the filling pulse parameters and measurement voltage via windows in the software compared to the use of rotary knobs and relying on the reading of the scale. Another drawback of the Sula system is that the user must perform calculations to determine various settings as opposed to setting the values or reading them from the screen. For example, to determine the rate window from the initial delay settings of the correlator panel, you would use the following: RW (ms) = τ = 4.3 x INITIAL DELAY. Although the Sula software comes with approximately 40 pages of documentation and the Semetrol software offers a few pop up screens with abbreviated instructions, neither product gives a good detailed instruction and overview of the software and its capabilities. The lack of Semetrol documentation has been augmented by tutorials given by the Semetrol software creator. Despite the Sula hardware/software documentation, the Semetrol software seems more intuitive and easier to learn. Although both software packages offer DLTS and DDLTS programs, the Semetrol software offers more measurement and analysis capabilities. The following is a brief description of the capabilities of the Semetrol software:

1. CV profiling – measures CV curve, determines doping profile and depletion width.

2. Capacitance calculator – determines capacitance based on material properties, device dimensions, measurement conditions, series resistance and system capacitance (simulation).

3. IVT – measurement, analysis and simulation.

4. DLTS/ODLTS – DLTS and optical DLTS measurement.

5. DLTS Data Fitting and Analysis – Analyzes and extracts trap parameters using ratewindow technique and fits measured transients.

6. DDLTS – measurement and analysis.

7. DDLTS (Field Dependence).

8. Filling Pulse Width Dependence – used to determine if trap is a simple trap, has a potential barrier, or is a trap along a dislocation.

9. Arrhenius Plot Select Points – used in extracting trap parameters from data points used to generate Arrhenius plot.

10. Multiple Arrhenius Set Plotter – used to compare multiple Arrhenius plots.

11. Capture Process Simulation.

12. DLTS Data Simulation – used to simulate DLTS signal from user defined trap parameters.

5.2   Semetrol Software Modifications

In the course of working with the software, various issues have been found that resulted in modifying the software. Most of the modifications involved improving the existing features and one case of fixing an error in a calculation.

5.2.1   Algorithm for Finding τ_{MAX}

The Semetrol software generates a DLTS signal based on the transients measured. Ratewindow analysis is then performed on the DLTS signal and an Arrhenius plot is created from the τ_{MAX} (peak maximum or valley minimum) and the corresponding temperature, T. The original algorithm for determining T, τ_{MAX} used the user defined

settings (poly order, ½ width points and minimum width) to determine the existence of a peak or valley in the DLTS signal. The value of T, τ_{MAX} used in the Arrhenius plot was determined by assigning the measurement data closest to the maxima or minima (peak or valley). The new algorithm interpolates the measurement data and calculates T, τ_{MAX} from all measured data, giving more accurate values. In addition, since the T, τ_{MAX} points are interpolated values instead of measured data points, more data points not lying on top of each other are generated in the Arrhenius plot, resulting in a more linear curve. A pictorial representation of the original T, τ_{MAX} algorithm and the new T, τ_{MAX} algorithm can be seen in figure 5.3.
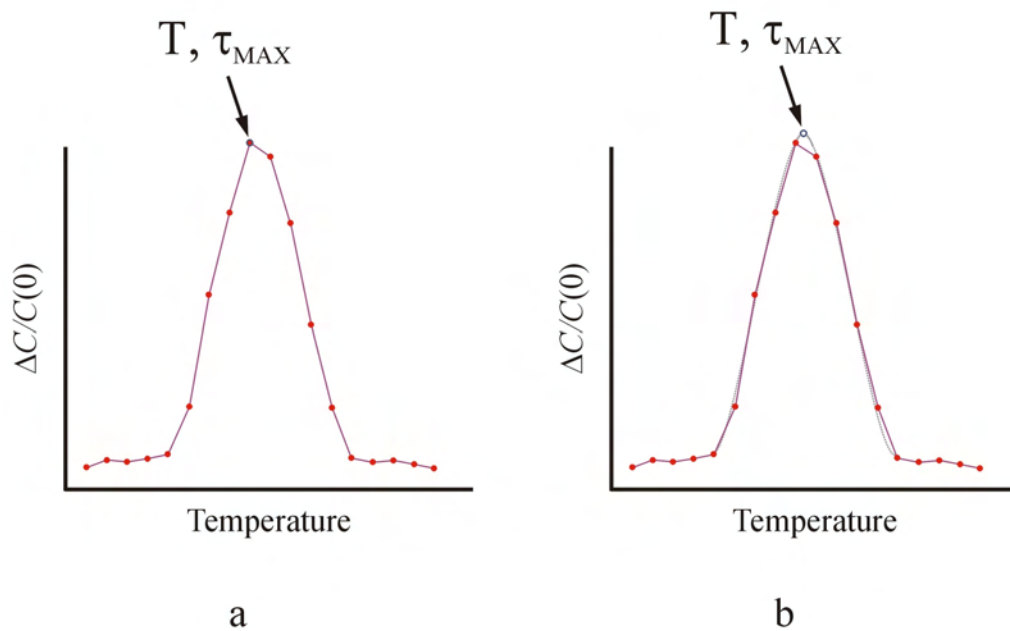

Figure 5.3
Algorithm for Finding τ_{MAX}: a) Original algorithm;
b) New algorithm – extrapolation of τ_{MAX}

5.2.2 Temperature Controller Settings

The sample (DUT) temperature is affected by the heating due to the Lakeshore 331 Temperature Controller and the cooling of the second stage from the helium

compressor, which constantly runs, driving the second stage temperature to approximately 8K. If the sample temperature is below the setpoint, the Lakeshore controller will supply power to the sample heater to drive the temperature toward the setpoint. If the sample temperature is above the setpoint, thermal energy is pulled away from the sample due to the second stage until the sample temperature is below the stepoint, at which time the temperature controller will supply power to the heater to maintain the sample temperature within the setpoint tolerance.

The Lakeshore 331 Temperature Controller is a proportional-integral-derivative (PID) controller. A PID controller attempts to correct for the error between the measured value and setpoint via a feedback loop by calculating a corrective action to the process. The calculated correction consists of three terms: the proportional value, the integral value and the derivative value. The proportional value determines the magnitude of the corrective action based on the magnitude of the error. The integral value determines the magnitude of the corrective action based on the duration of the error. So if the error exists for a larger period of time, the controller will more aggressively try to correct for this error. The derivative term will try to correct for sudden changes. For the Lakeshore 331 Temperature Controller, the heater power depends as on the error as follows:

$$Heater\ Ouput = P\left[e + I\int(e)dt + D\frac{de}{dt}\right] \tag{5.1}$$

where P, I, and D are the parameters of the PID controller and the error (e) is defined as e = setpoint – feedback reading.

It is not necessary that the PID controller use all three parameters in determining the corrective action. Often the controller may drive the process to the setpoint and achieves a stable process by using only the P parameter (with I = 0 and D = 0) or only the

P and I parameter (with D = 0). An example of a controller using only the P parameter,

the P and I parameters and P, I and D parameters can be seen in figure 5.4. The effect of

varying the parameters is summarized in table 5.1 and a representation of a process with a

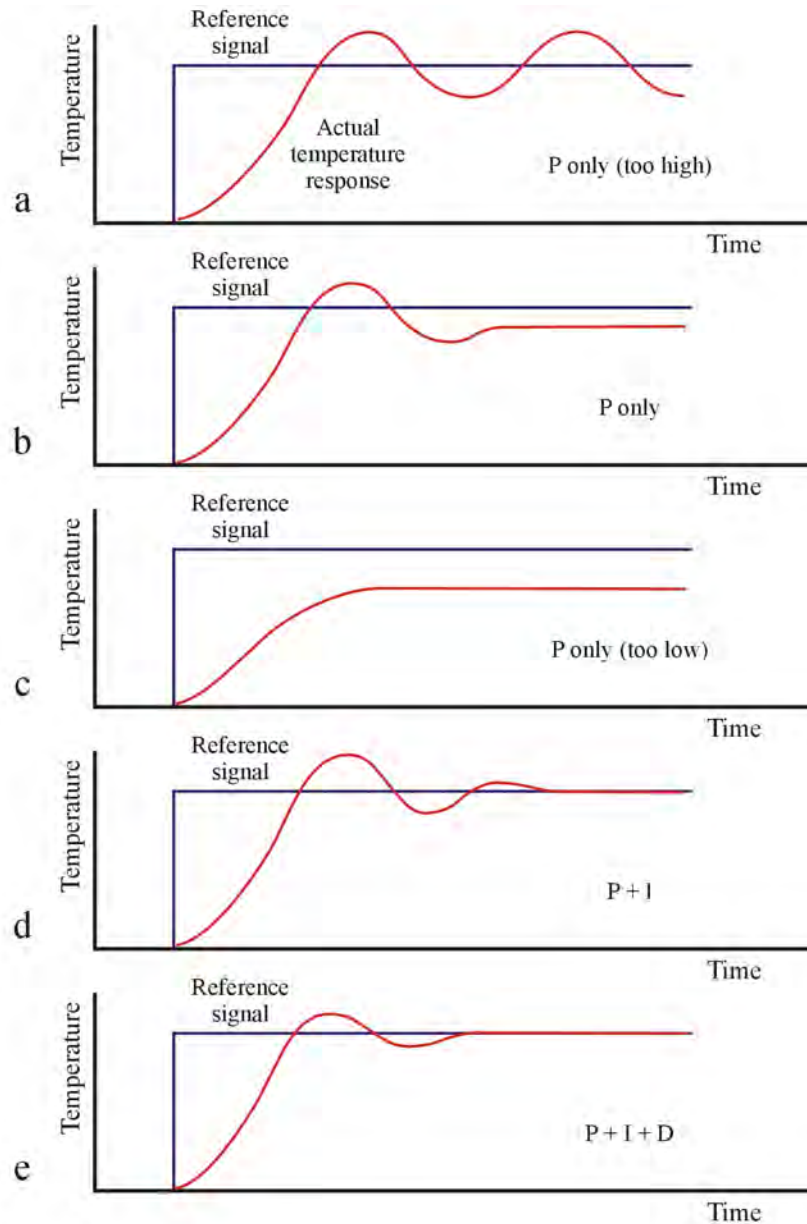PID controller using all three parameters is shown in figure 5.5.

Figure 5.4
Effect of PID Parameters:
a) P only (too high); b) P only; c) P only (too low); d) P and I; e) P, I and D[23]

Table 5.1
Effect of Varying PID Parameters[24]

Effect of *Increasing* Parameter Value				
Parameter	Rise Time	Overshoot	Settling Time	Steady State Error
P	Decrease	Increase	Small Change	Decrease
I	Decrease	Increase	Increase	Eliminate
D	Small Change	Decrease	Decrease	None
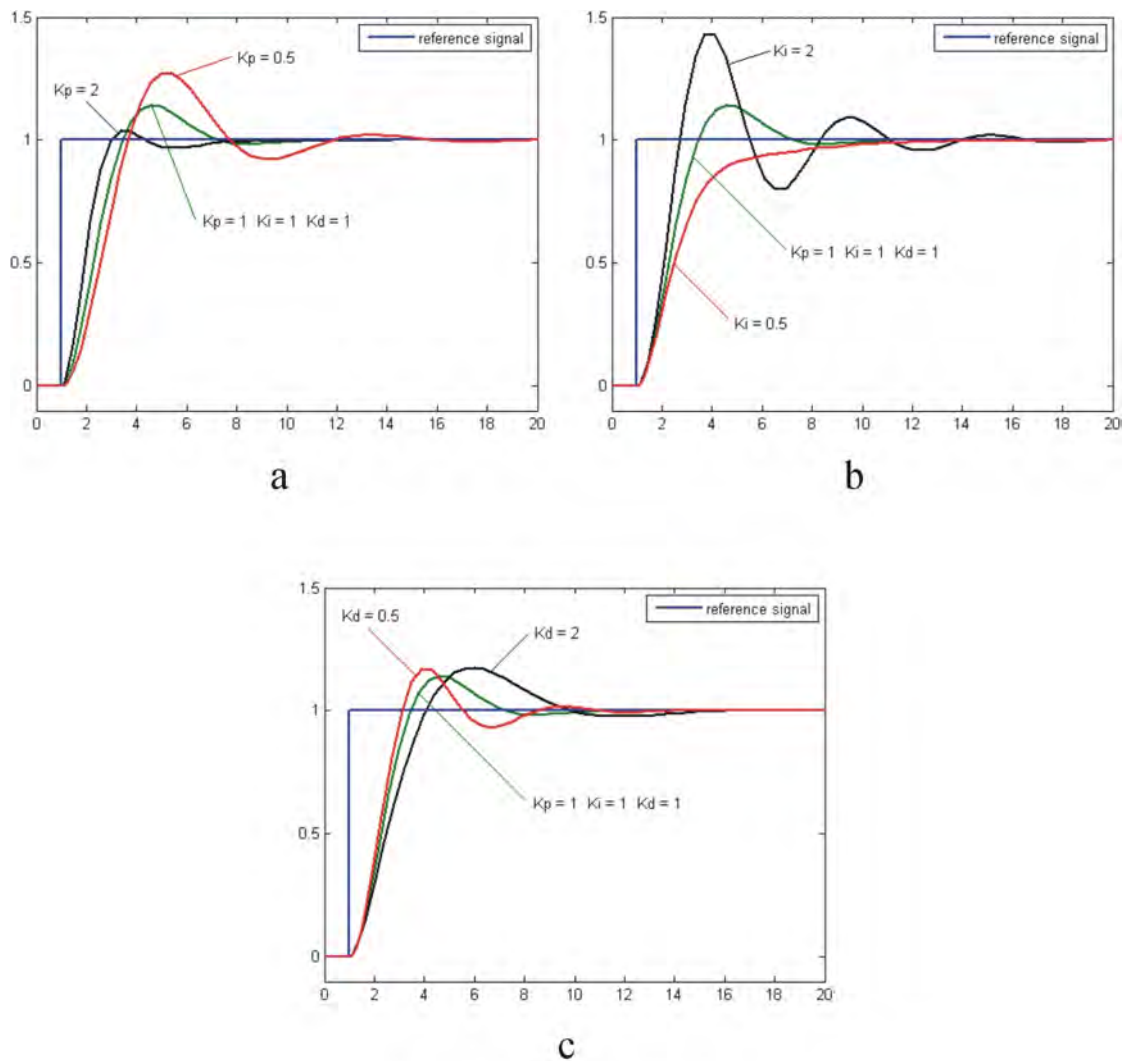
Figure 5.5
Effect of Varying PID Parameters (using all three parameters):
a) Varying P; b) Varying I; c) Varying D[25]

The original version of the Semetrol software allowed the user to set the proportional value (gain) of the temperature controller for a specified temperature range in the temperature stability settings table of the DLTS/ODLTS Data Acquisition window (discussed in Appendix C) while the integral and derivative values were set to zero. The software has been modified to allow the user to specify the integral (reset) and derivative (rate) values, in addition to the proportional value. After the modification to the software, the P and I values were optimized so the system achieved the setpoint tolerance within the shortest amount of time. The derivative value was set to zero for all temperature ranges. The addition of the integral parameter decreased the settling time and eliminated the steady state error. The stability count was adjusted so that the fluctuations of the temperature stayed within tolerance during the duration of the measurement. A table with the optimized default PID values is provided in Appendix C.

5.2.3   Logfile Creation

The measurement conditions can be saved and recalled using the data logging function of the National Instruments Labview software. This provides a record of the measurement conditions and eliminates the need for the user to re-enter all the values to repeat a measurement (discussed in Appendix C). However, if the user forgets to log the measurement conditions or the computer or software crashes this information may be lost. The Semetrol software has been modified to create a logfile while the measurement is in progress. The logfile saves the measurement conditions, sample temperature, date and time to a file and is updated following the measurement of the last transient at each temperature setpoint. This allows the users to review the history of the measurement to

identify possible issues (ie. power glitches, poor PID settings, poor vacuum in cryostat, etc.).

5.2.4   Capture Cross Section Calculation

As a result of the analysis of the simulations performed in Appendix D, an error in the software's calculation of the capture cross section was identified. The calculation of the capture cross section gave comparable values to the user defined value when the ratewindow analysis was performed on the simulated data. However, when the transient analysis was performed on the same simulated data, the calculated capture cross section differed by as much as an order of magnitude. It was determined that the error in the transient analysis calculation was due to using non-temperature dependent values (thermal velocity and density of states). The software is being modified by the supplier to correct for this error. At the time of this writing, the software currently being used for the system has not been corrected.

5.3   Replacement of DAQ Card

The hardware of the DLTS system also required modification in the replacement of the interface card. Originally the DLTS system used a National Instruments PCI 6035E multifunction DAQ interface card. As a result of the memory size on the NI PCI 6035E card, the system would experience buffer overflow errors and would halt the software and measurement. The limitations in card memory prevented the computer from simultaneously running any other application or other program in the Semetrol software while a measurement was in progress. In order to reduce the occurrence of this problem, the Semetrol software was set to the highest priority in the Microsoft Windows

Task Manager window and the screen resolution was reduced using the Display icon in the MS Windows Control Panel window.

The output of the NI PCI 6035E multifunction DAQ card was also measured with an oscilloscope at the pulse output on the Sula module. When the measurement and pulse bias were set to the same voltage (-2 V), a random jitter in the signal output was noticed, producing a 2V pulse with a width of 200 μs. Furthermore, the sampling rate of the card, 200 kS/s, limited the DLTS sample period to 5.0×10^{-4} s.

The original interface card was replaced with a National Instruments PCI 6251 multifunction DAQ, which has resolved the memory issues and allows the user to open multiple applications while a measurement is in progress. The new card has a sampling rate of 1.25 MS/s, which allows the DLTS sample period to set in the microsecond range. However, the card has increased the noise and a periodically sinusoidal interference effect is observed. For comparison, the DLTS signal of a 1N4007 diode measured with the original interface card is seen in figure 5.6 with the measurement conditions in table 5.2. The fit transient analysis was reviewed for the transient occurring at 300K since this area seemed relatively flat in the DLTS signal, indicating that no trap was present. A

Table 5.2
Measurement Conditions - 1N4007 Diode

Sample Description: 1N4007 Diode

Bias Parameters		**Measurement Parameters**	
Measure bias (V):	-7.00	Sample period:	3.00E-04
Pulse bias (V):	-2.00	Points:	1000
Pulse width:	1.00E-03	C-meter range:	10
LED quiescent:	0	No. Tx. Avg.:	256
LED pulse:	0		

noise level of less than 1fF can be approximated from the transient at 300K as seen in figure 5.7. The signal was estimated to be 6.935 pF and the noise level was estimated to be 7.57 x 10^{-5} pF resulting in a signal-to-noise ratio of 91611 (99 dB).

Using the new interface card, a measurement was performed on a 1N4002 diode. The measurement conditions were set the same as the 1N4007 diode, except that the measurement and pulse bias were set to 0V, which should give a flat transient response. Figure 5.8 shows the sinusoidal response occurring in a single transient during the measurement at 300K and figure 5.9 shows the same response in the average of the 256 transients. In figure 5.9, the signal was estimated to be 20.658 pF and the noise level was estimated to be 0.001 pF resulting in a signal-to-noise ratio of 20658 (86.3 dB).
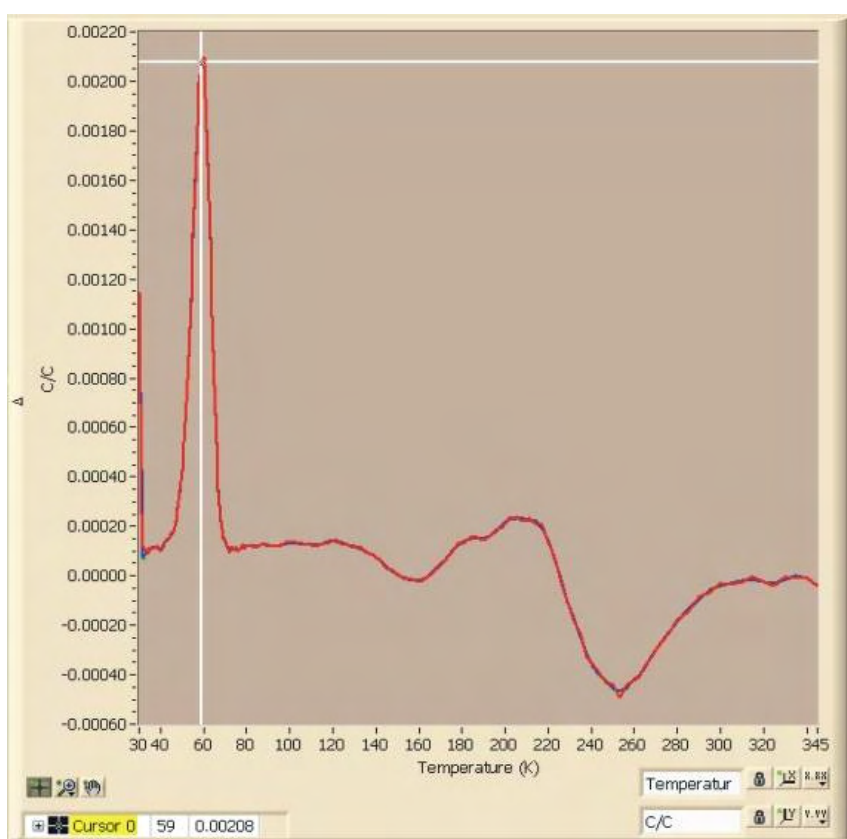
Figure 5.6
DLTS Signal – 1N4007 Diode
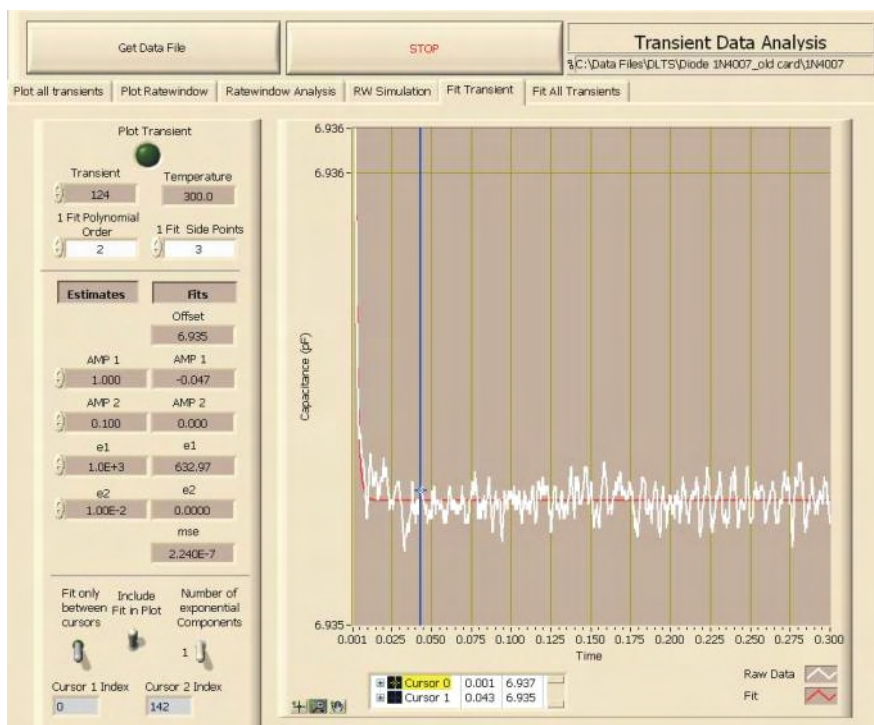
Figure 5.7
Fit Transient - 1N4007 Diode – 300K
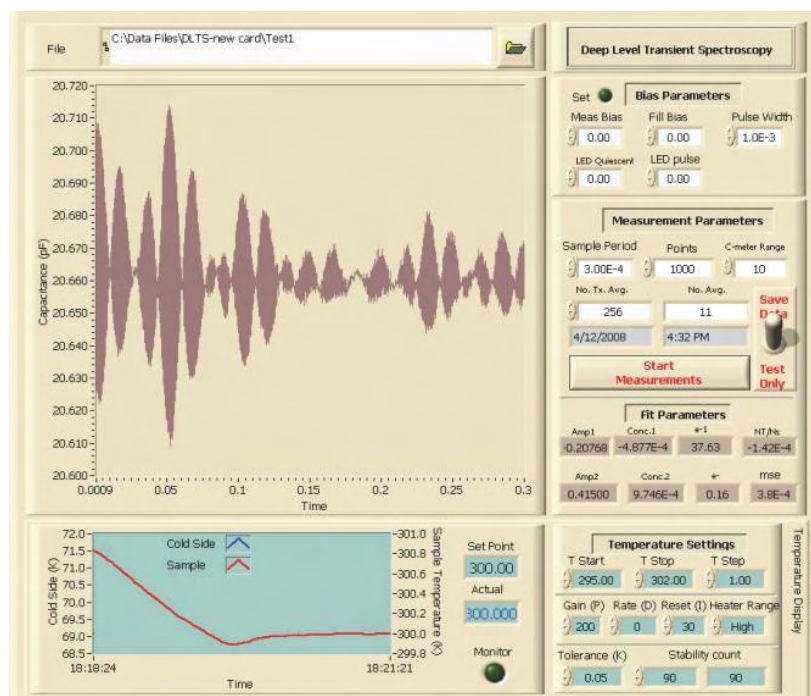
Figure 5.8
Transient Measurement - 1N4002 Diode – 300K
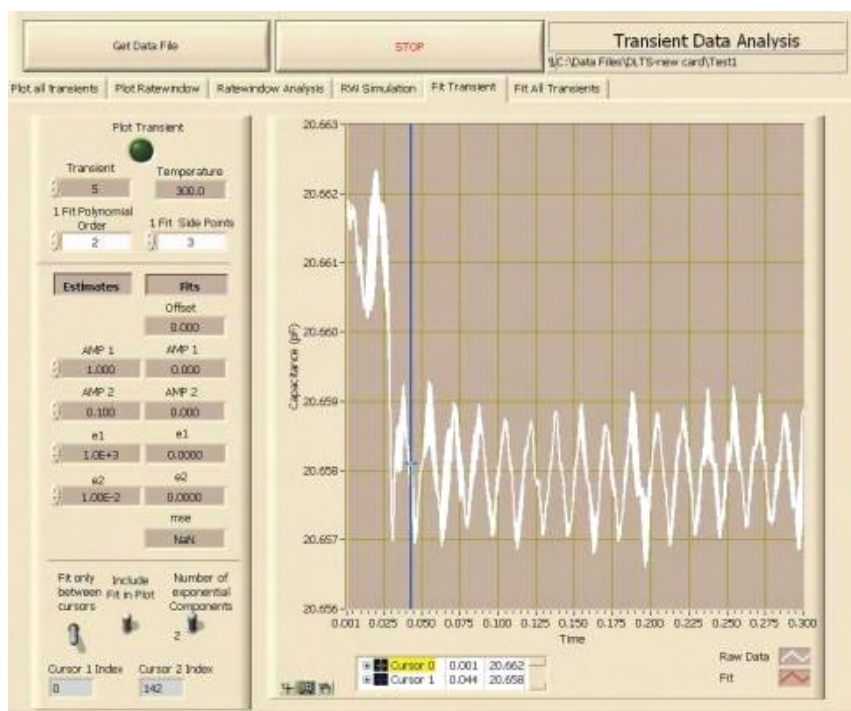
Figure 5.9
Fit Transient - 1N4002 Diode – 300K

CHAPTER 6

MEASUREMENT RESULTS

6.1   Device Selection

The first measurements using the DLTS system were performed on discrete

packaged diodes since they were readily available, would easily fit within the cryostat

and could be electrically connected to the measurement system without bonding. The

1N4001 – 1N4007 diffused junction rectifiers were selected because the junction

capacitance was within the range of the capacitance meter. The IV characteristics were

measured at room temperature for a 1N4007 device using a Hewlett-Packard 4145, which

showed that the device was suitable for the DLTS measurement since the reverse bias

leakage current was within the range of the capacitance meter ($< 100\ \mu A$). A CV curve

of the device at room temperature was also measured using a Hewlett-Packard 4192A,

indicating that '10' was an appropriate range for the capacitance meter.
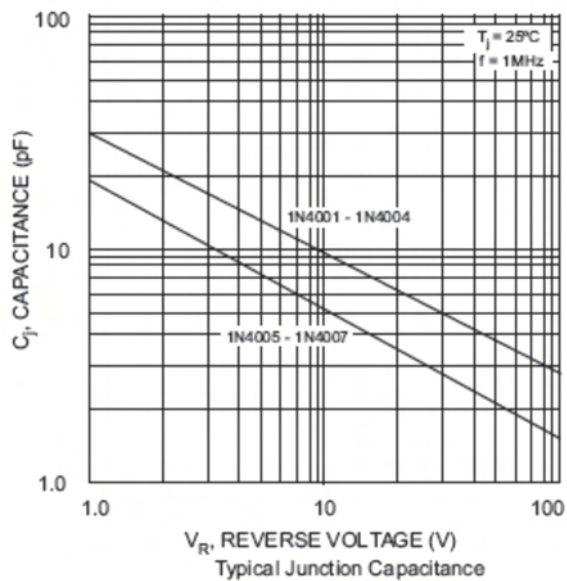
Figure 6.1
Manufacturer Datasheet Capacitance[26]
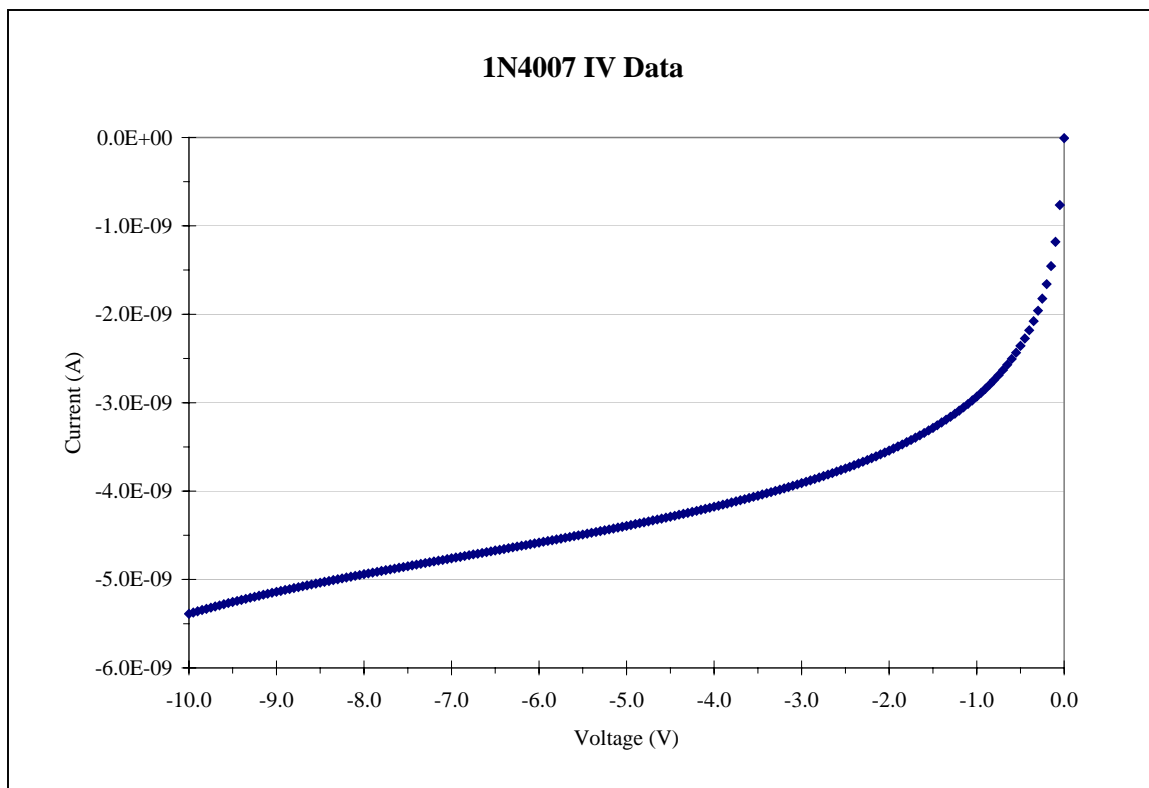
Figure 6.2
Reverse Bias Leakage Current, Room Temperature
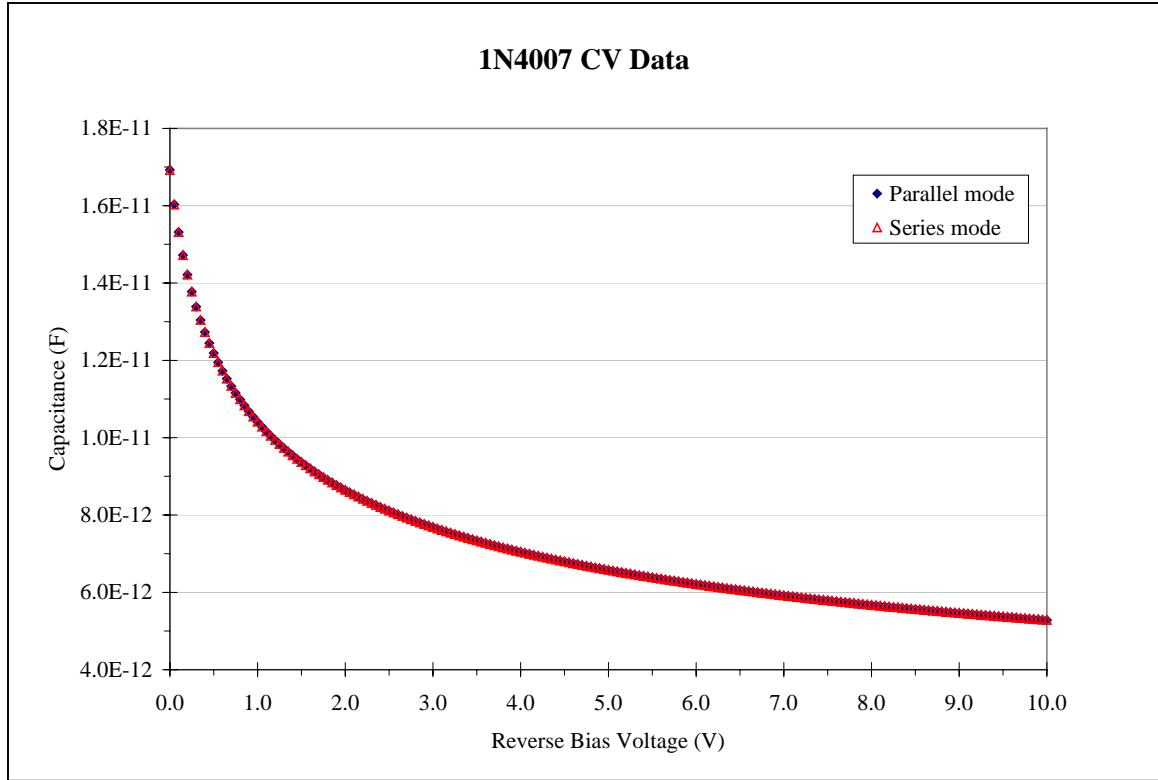
Figure 6.3
CV Measurement@1 MHz, Room Temperature

6.2 Measurement and Analysis with NI PCI 6035E Interface Card

6.2.1 1N4007 Diode DLTS Run1 (30 – 350K)

The measurement parameters were set to maximize the signal from the traps and

to keep the capacitance readings below the 10 pF range. The measurement settings can

be found in table 6.1. Measurements performed using the original interface card (NI PCI

6035E) were done prior to the software modifications of the temperature controller

settings discussed in section 5.2.2 and the optimization of the temperature controller

settings.

Table 6.1
Measurement Settings for 1N4007 DLTS Run1 (PCI 6035E)

Bias Parameters

Measure bias (V):	-7.00
Pulse bias (V):	-2.00
Pulse width:	1.00E-03
LED quiescent:	0
LED pulse:	0

Measurement Parameters

Sample period:	3.00E-04
Points:	1000
C-meter range:	10
No. Tx. Avg.:	256

Temperature Settings

T start:	30
T stop:	350

Temperature Stability Settings

Temp >	Step size	Gain (P)	Heater range	Tolerance	Stability Count
0	1	300	High	0.05	90
40	1	300	High	0.05	90
80	2	300	High	0.05	90
100	3	150	High	0.05	90
280	5	150	High	0.05	90
375	5	150	High	0.05	90
500	5	150	High	0.05	90
600	5	0	Off	0	0
700	5	0	Off	0	0
800	0	0	Off	0	0

A review of the *C-T* curve shown in figure 6.4 indicated that no shorts, opens or catastrophic device failure occurred during the measurement. The points of interest, indicating the presence of a trap level, in the DLTS spectra are in indicated by the arrows in figure 6.5. These areas of the DLTS spectra were analyzed using the ratewindow analysis and transient analysis of the Semetrol software. Ratewindow analysis was performed on the peaks at 60, 170 and 210K and the valley at 250K. The trap parameters determined by ratewindow analysis are shown in figures 6.6 to 6.9.
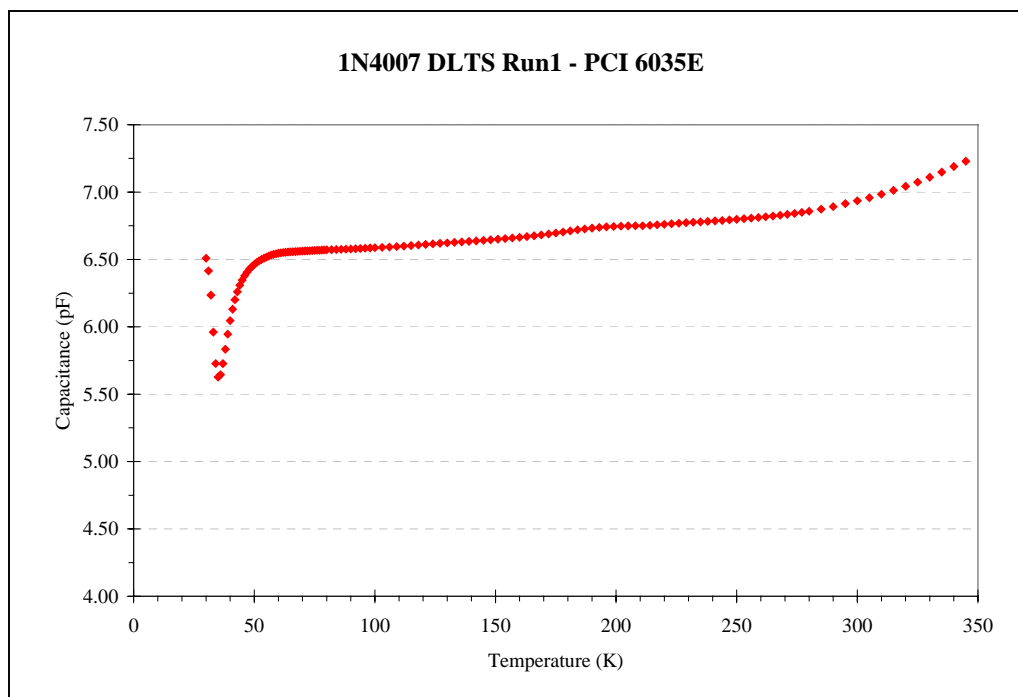
Figure 6.4
CT Data of 1N4007 DLTS Run1 (PCI 6035E)
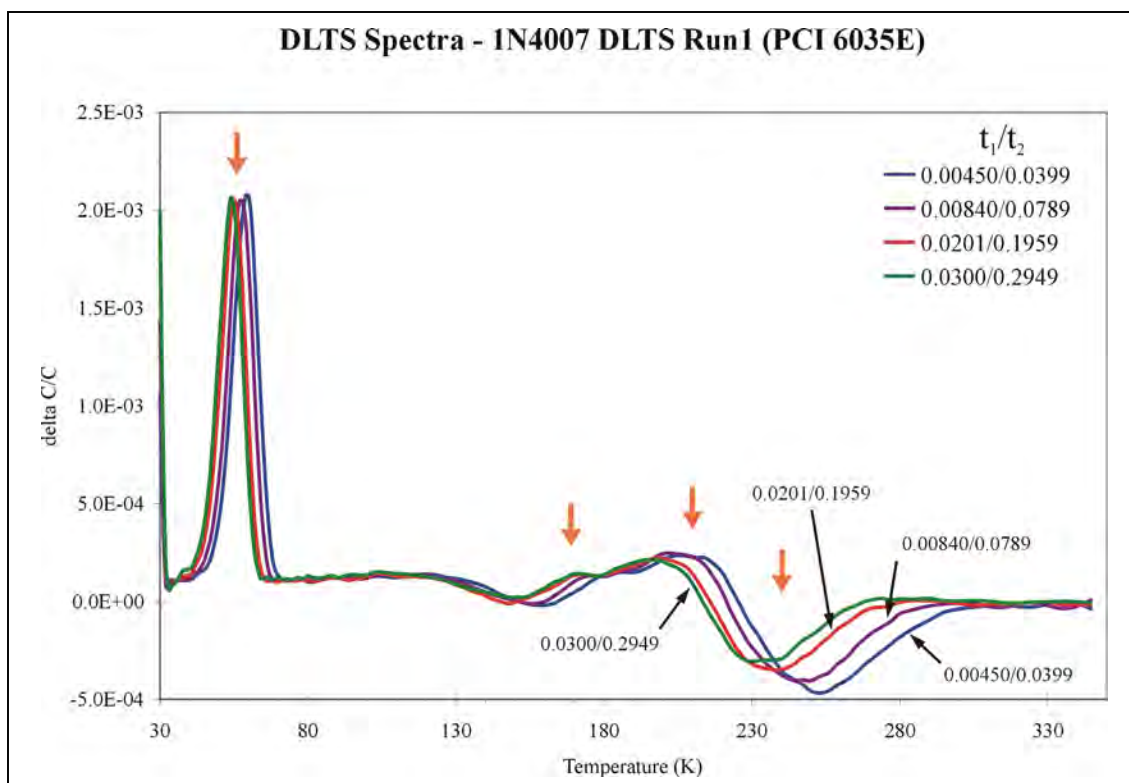
Figure 6.5
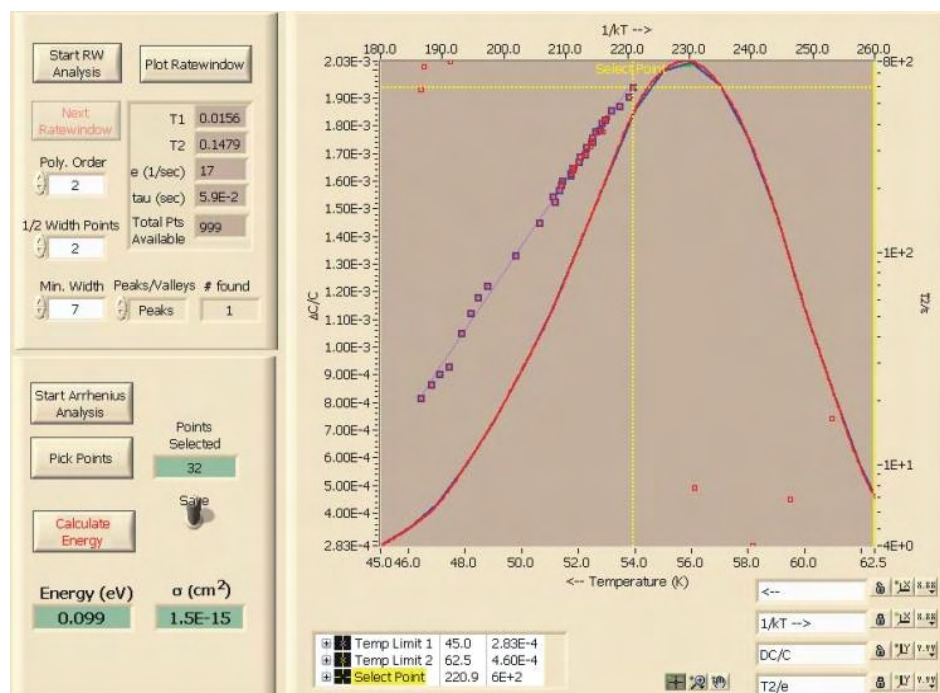*DLTS Spectra – 1N4007 DLTS Run1 (PCI 6035E)*

Figure 6.6
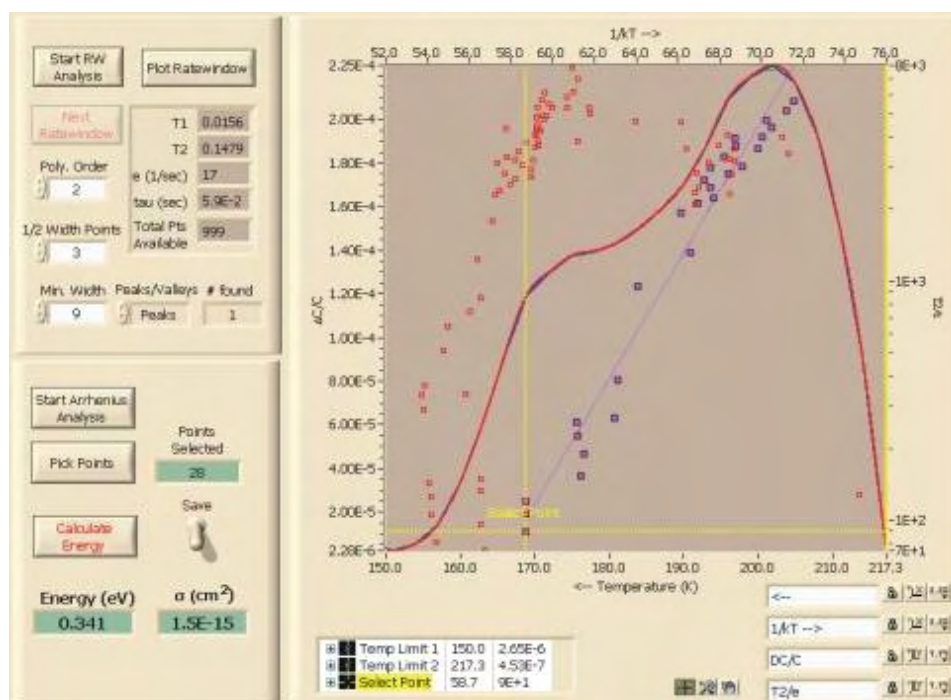*1N4007 DLTS Run1 (PCI 6035E) - Ratewindow Analysis of Peak at 60K*

Figure 6.7
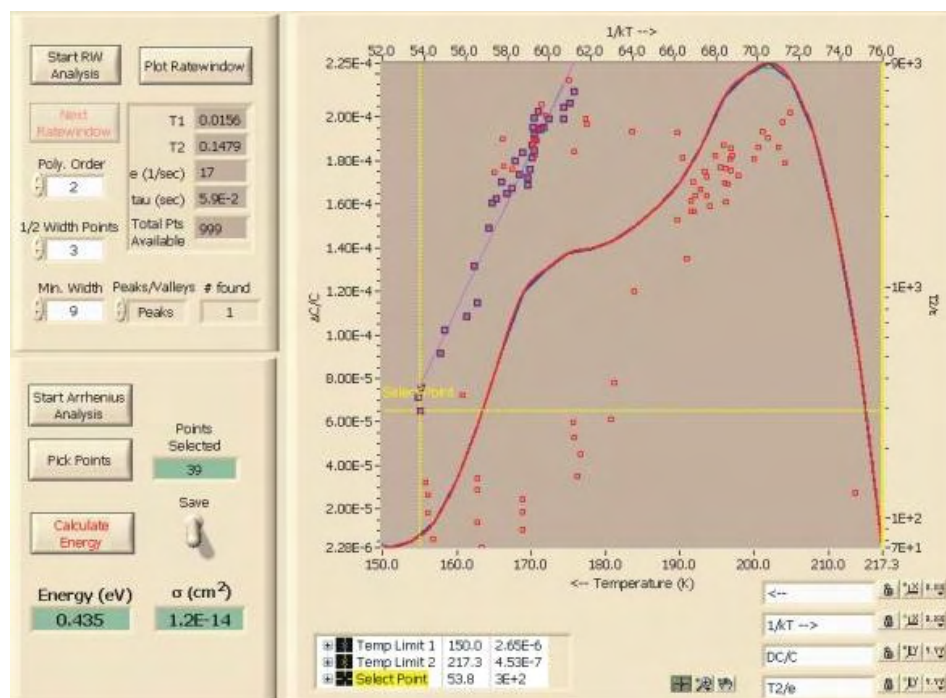*1N4007 DLTS Run1 (PCI 6035E) - Ratewindow Analysis of Peak at 170K*

Figure 6.8
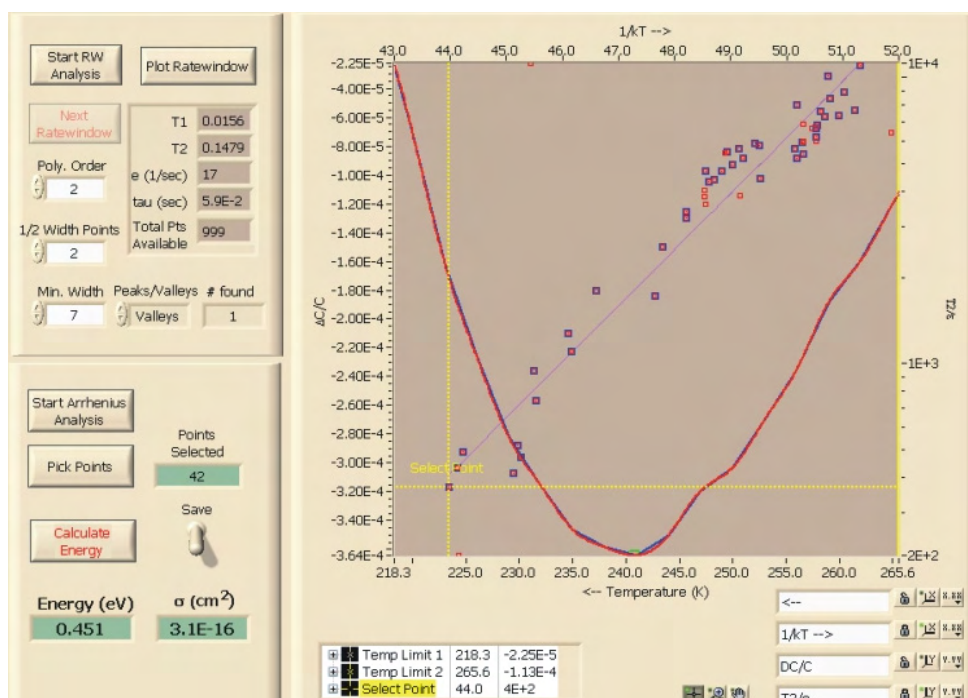*1N4007 DLTS Run1 (PCI 6035E) - Ratewindow Analysis of Peak at 210K*

Figure 6.9
1N4007 DLTS Run1 (PCI 6035E) - Ratewindow Analysis of Valley at 250K

Transient analysis was also performed on the same data and the Arrhenius plot
generated from the transient fits is shown in figure 6.10. In the figure, the trap
corresponding to the peak at 60K in the DLTS spectra (figure 6.5) is denoted by A. A
zoomed in view of the traps denoted by B (peak at 170K), C and D (valley at 250K) is
shown in figure 6.11. The resulting fits of the Arrhenius plot are shown in figures 6.12 to
6.16.
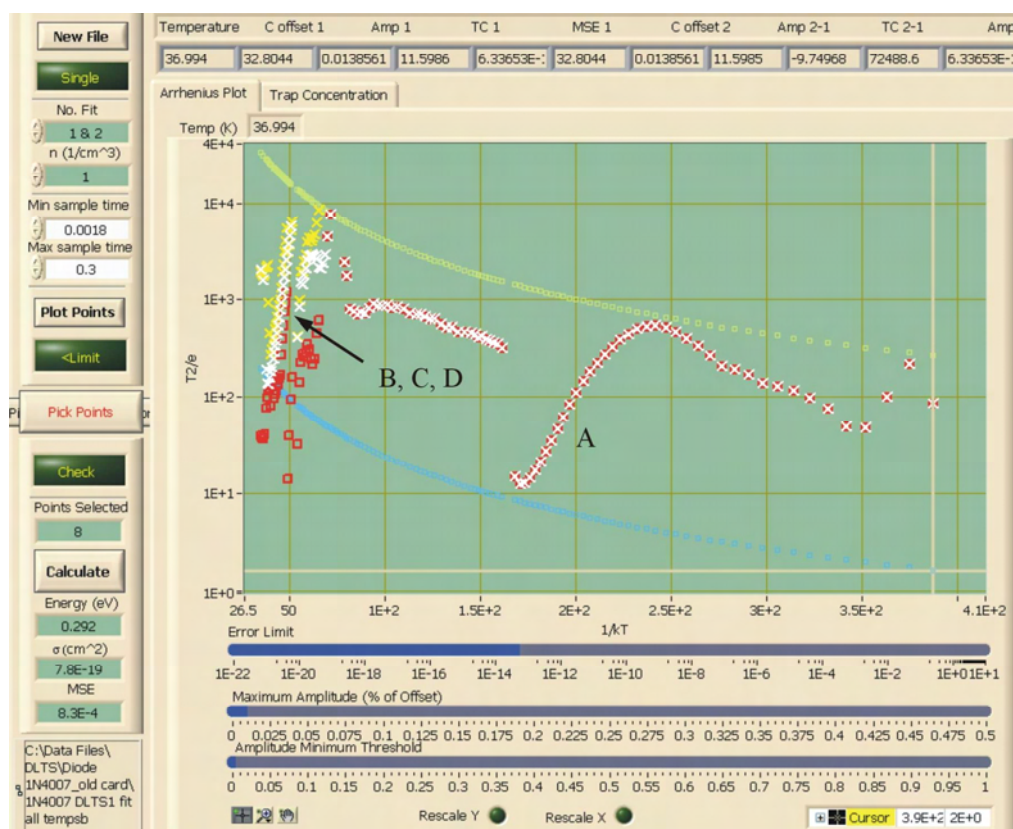
Figure 6.10
1N4007 DLTS Run1 (PCI 6035E) – Transient Analysis (30 – 350K)
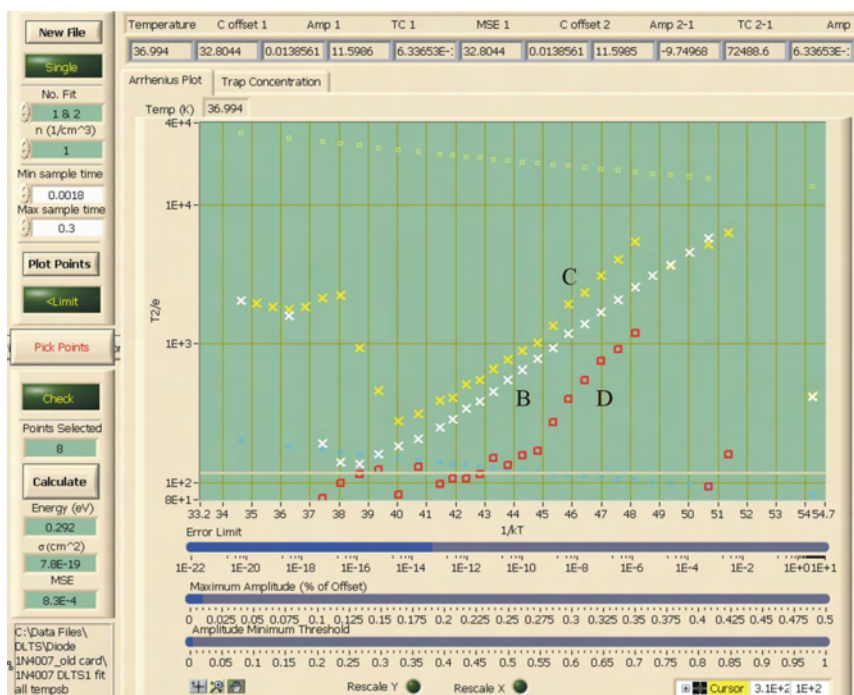
Figure 6.11
1N4007 DLTS Run1 (PCI 6035E) – Transient Analysis - Figure 6.10-B, C, D
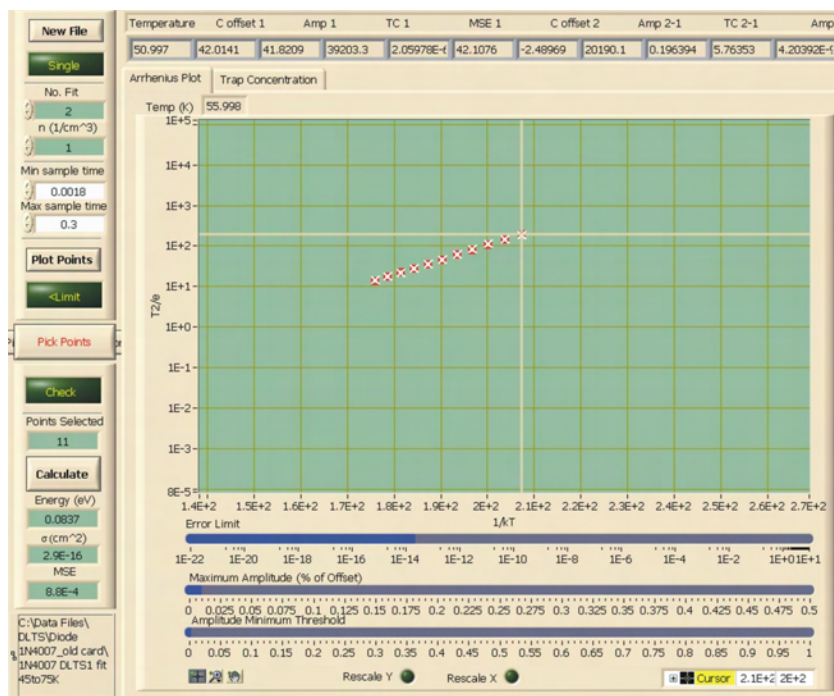
Figure 6.12
1N4007 DLTS Run1 (PCI 6035E) – Transient Analysis Fit of Figure 6.10-A
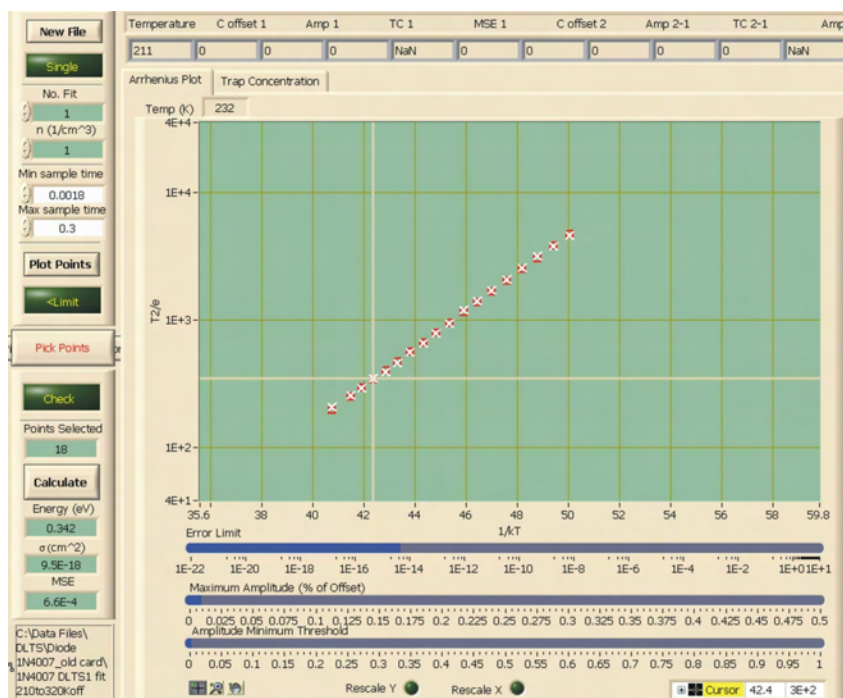
Figure 6.13
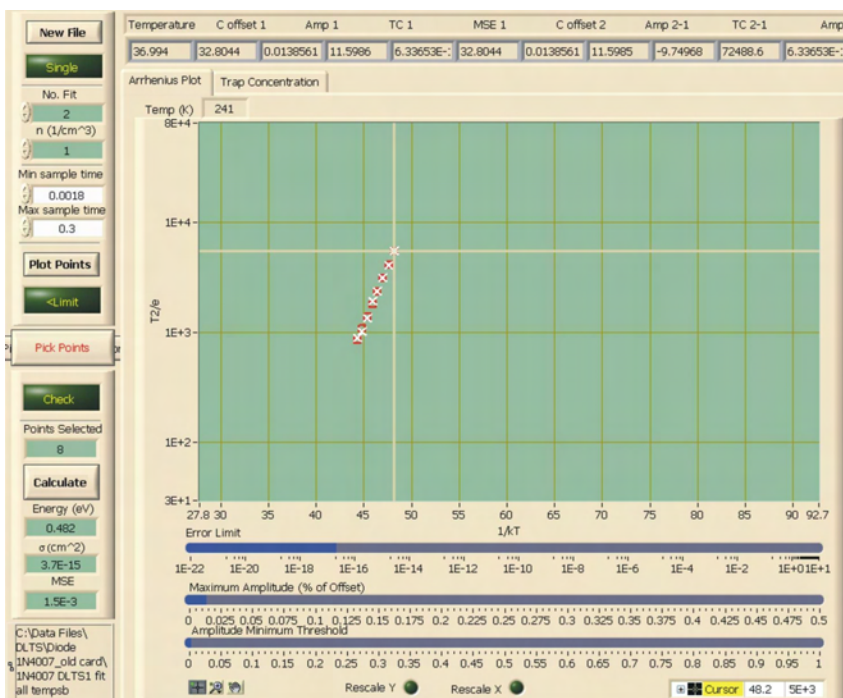*1N4007 DLTS Run1 (PCI 6035E) – Transient Analysis Fit of Figure 6.10-B*

Figure 6.14
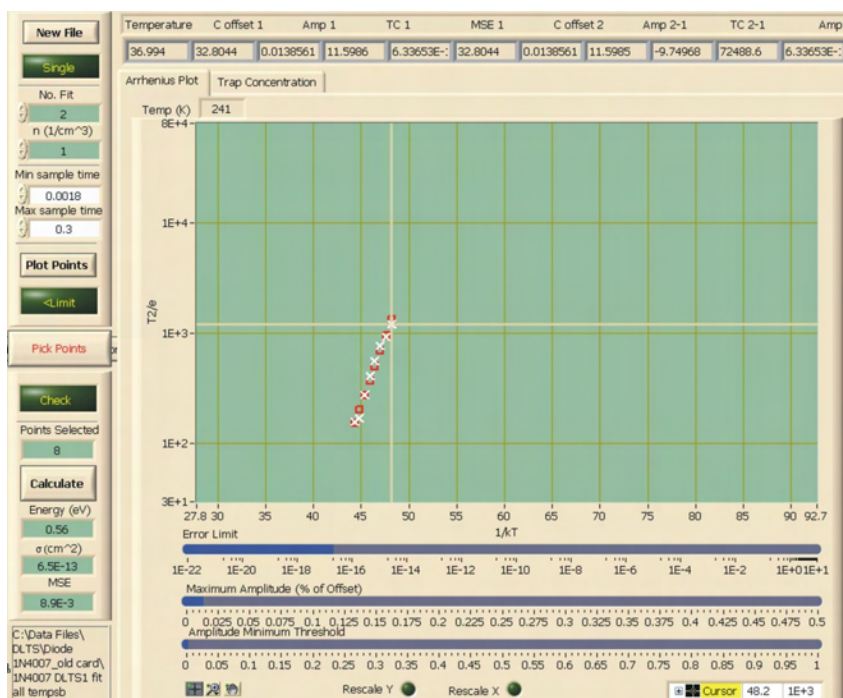*1N4007 DLTS Run1 (PCI 6035E) – Transient Analysis Fit of Figure 6.10-C*

Figure 6.15
1N4007 DLTS Run1 (PCI 6035E) – Transient Analysis Fit of Figure 6.10-D

The transient analysis of the 1N4007 diode proved to be difficult to perform in selecting linear curves on the Arrhenius plot. The large peak at 60K was easily identifiable and gave comparable values for each technique. It was difficult to conclusively identify the transients due to the peak at 210K and therefore it is not included. The transient analysis also revealed that the valley at 250K may be due to two separate trap levels, where the ratewindow analysis showed only one trap level. A summary of the results can be seen in table 6.2.

Table 6.2
Measurement Results - 1N4007 DLTS Run1 (PCI 6035E)

	Calculated - RW Analysis		Calculated - Transient Analysis			
	Energy (eV)	Sigma (cm^2)	Curve	Energy (eV)	Sigma (cm^2)	MSE
Peak at 60K	0.099	1.5E-15	A	0.0837	2.9E-16	8.8E-04
Peak at 170K	0.341	1.5E-15	B	0.342	9.5E-18	6.6E-04
Peak at 210K	0.435	1.2E-14		NA	NA	NA
Valley at 250K	0.451	3.1E-16	C	0.482	3.7E-15	1.5E-03
			D	0.560	6.5E-13	8.9E-03

6.2.2 1N4007 Diode DLTS Run3 (350 – 30K)

The 1N4007 diode was left in the cryostat and a second measurement (Run3) of

the device was performed. The measurement settings are identical to Run1, with the

exception that the temperature scan ran from the high temperature to the low temperature.

The measurement settings for Run3 are shown in table 6.3 with a starting temperature of

350K and a final temperature of 30K. A similar analysis was performed on the

measurement data as detailed in the following figures. The ratewindow analysis appears

in figures 6.18 to 6.20. The ratewindow analysis of the valley at 250K is omitted because

an easily identifiable linear curve did not appear on the Arrhenius plot. In performing the

fit of the transients, the software did not allow smaller temperature ranges (ie. peak in the

30 to 80K range) to be selected and would only allow the data for the entire temperature

range (350 – 30K) to be fit. The results of the transient fits are shown in figure 6.21 with

three regions of interest indicated. The linear region marked A appears to be the peak at

50K and the linear regions marked B and C are the peaks at 160K and 210K,

respectively. The fits of Arrhenius plot produced form the transient analysis are shown in

figures 6.22 to 6.24. A summary of the results for the ratewindow analysis and transient

analysis each is included in table 6.4.

Table 6.3
Measurement Settings for 1N4007 DLTS Run3 (PCI 6035E)

Bias Parameters

Measure bias (V):	-7.00
Pulse bias (V):	-2.00
Pulse width:	1.00E-03
LED quiescent:	0
LED pulse:	0

Measurement Parameters

Sample period:	3.00E-04
Points:	1000
C-meter range:	10
No. Tx. Avg.:	256

Temperature Settings

T start:	350
T stop:	30

Temperature Stability Settings

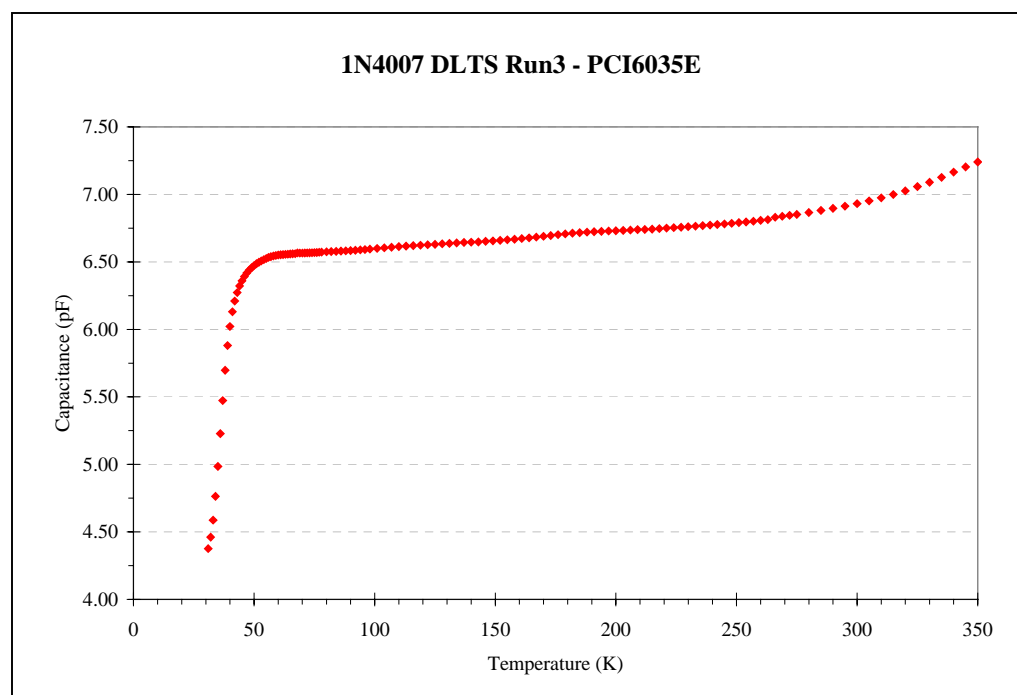| Temp >	Step size	Gain (P)	Heater range	Tolerance	Stability Count
0	1	300	High	0.05	90
40	1	300	High	0.05	90
80	2	300	High	0.05	90
100	3	150	High	0.05	90
280	5	150	High	0.05	90
375	5	150	High	0.05	90
500	5	150	High	0.05	90
600	5	0	Off	0	0
700	5	0	Off	0	0
800	0	0	Off	0	0

Figure 6.16
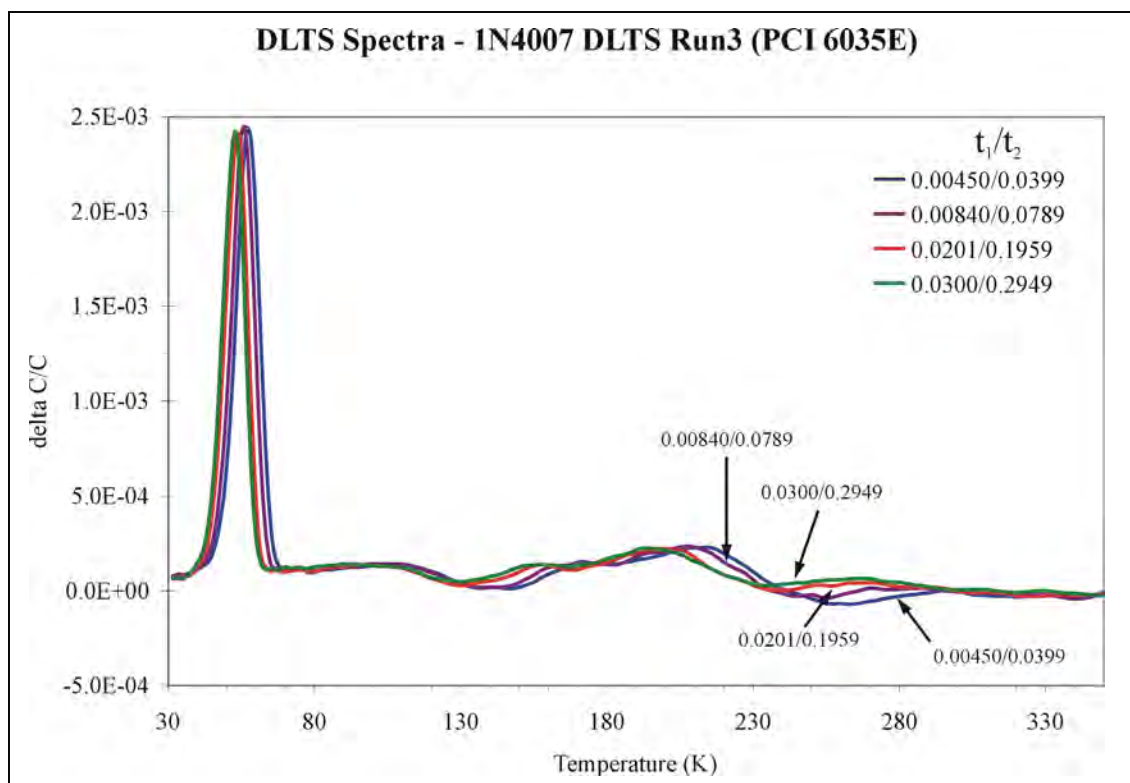*CT Data of 1N4007 DLTS Run3 (PCI 6035E)*

Figure 6.17
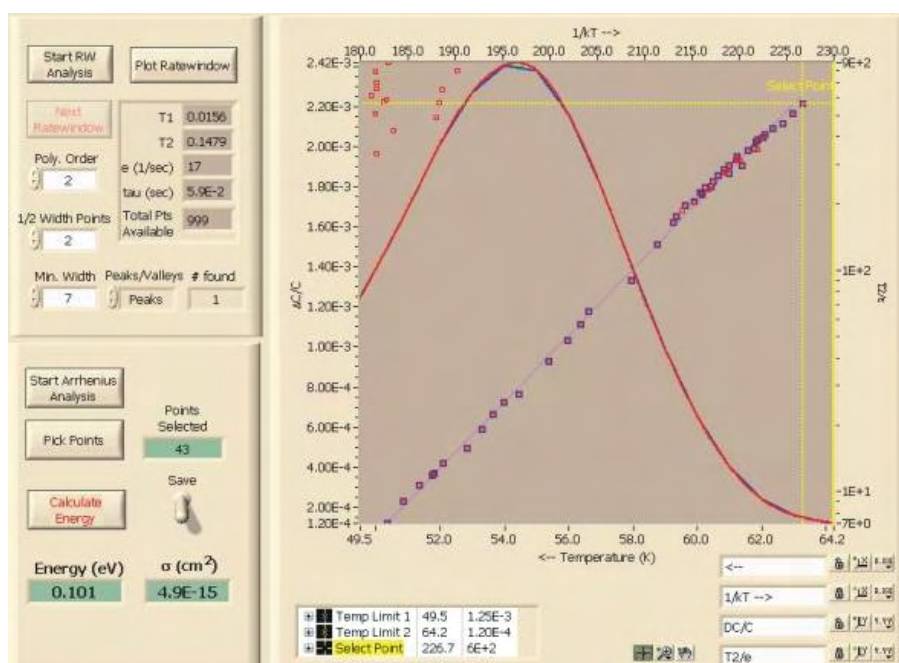*DLTS Spectra – 1N4007 DLTS Run3 (PCI 6035E)*

Figure 6.18
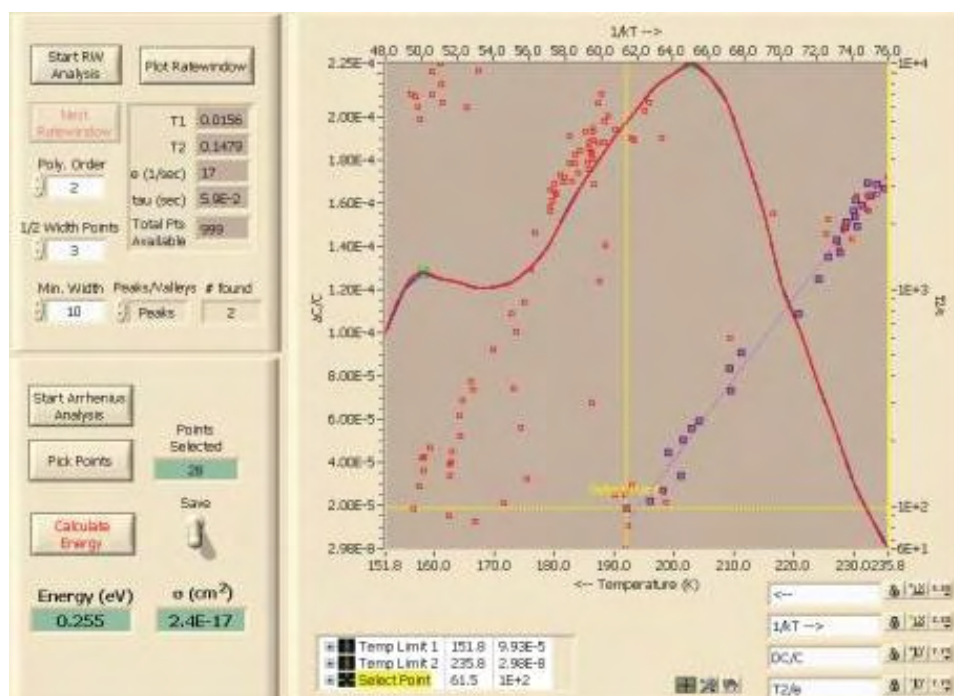*1N4007 DLTS Run3 (PCI 6035E) - Ratewindow Analysis of Peak at 50K*

Figure 6.19
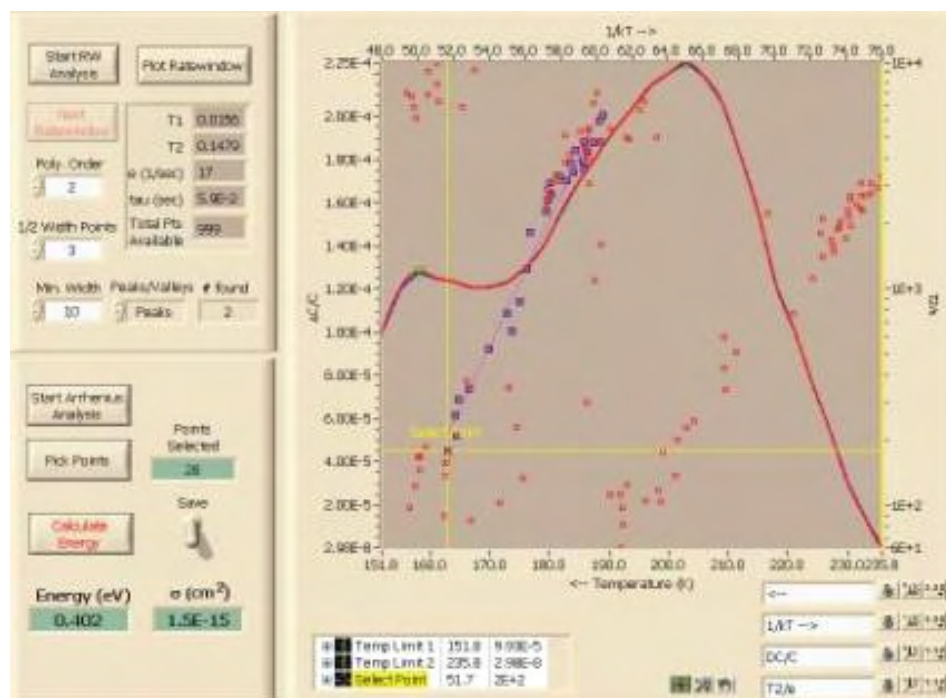*1N4007 DLTS Run3 (PCI 6035E) - Ratewindow Analysis of Peak at 160K*

Figure 6.20
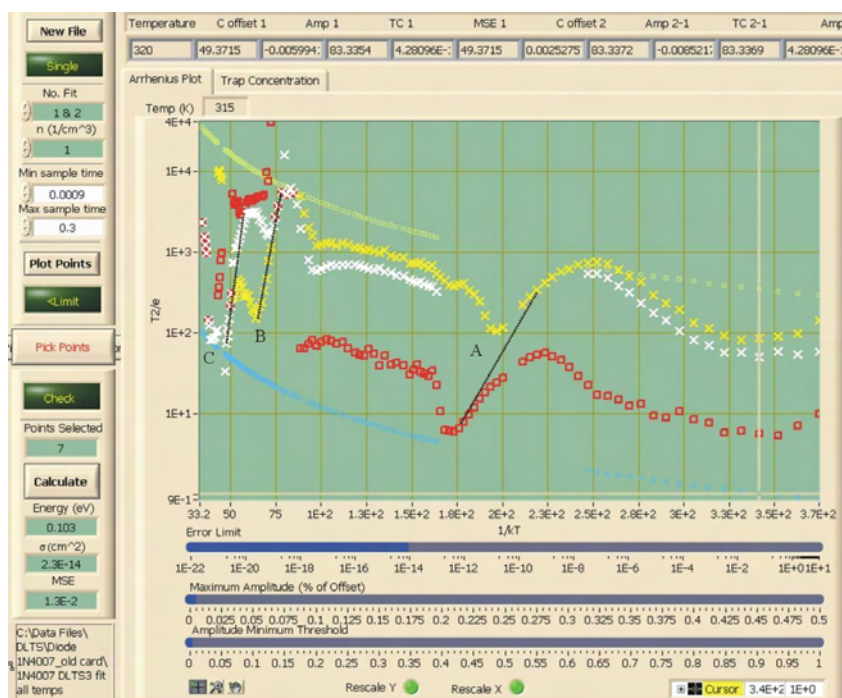*1N4007 DLTS Run3 (PCI 6035E) - Ratewindow Analysis of Peak at 210K*

Figure 6.21
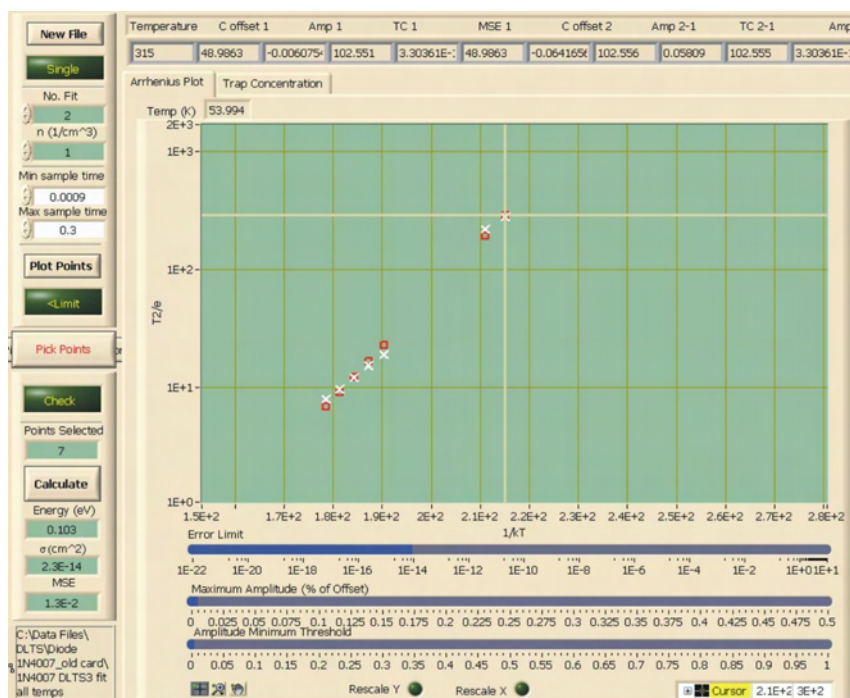*1N4007 DLTS Run3 (PCI 6035E) – Transient Analysis (30 – 350K)*

Figure 6.22
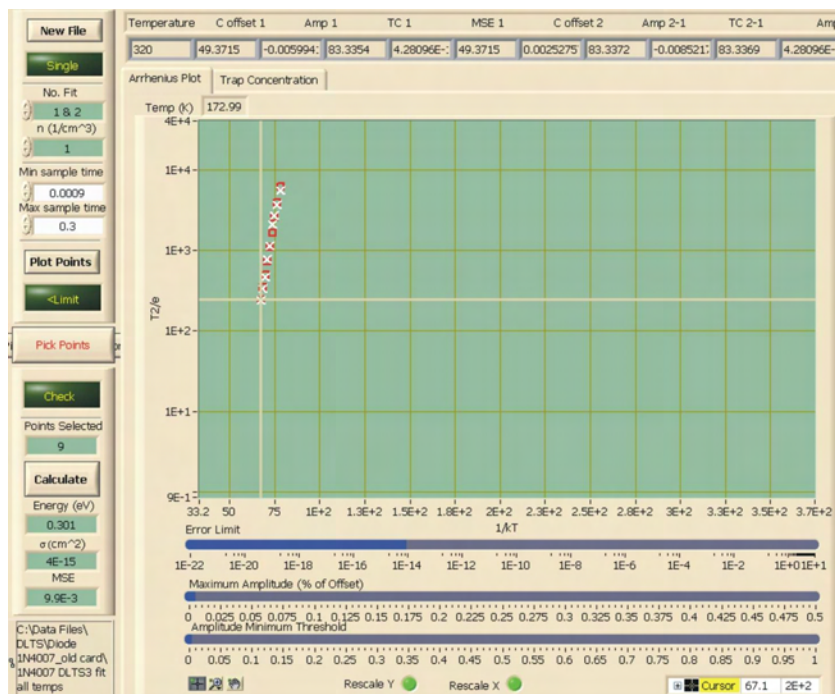*1N4007 DLTS Run3 (PCI 6035E) – Transient Analysis Fit of Figure 6.21-A*

Figure 6.23
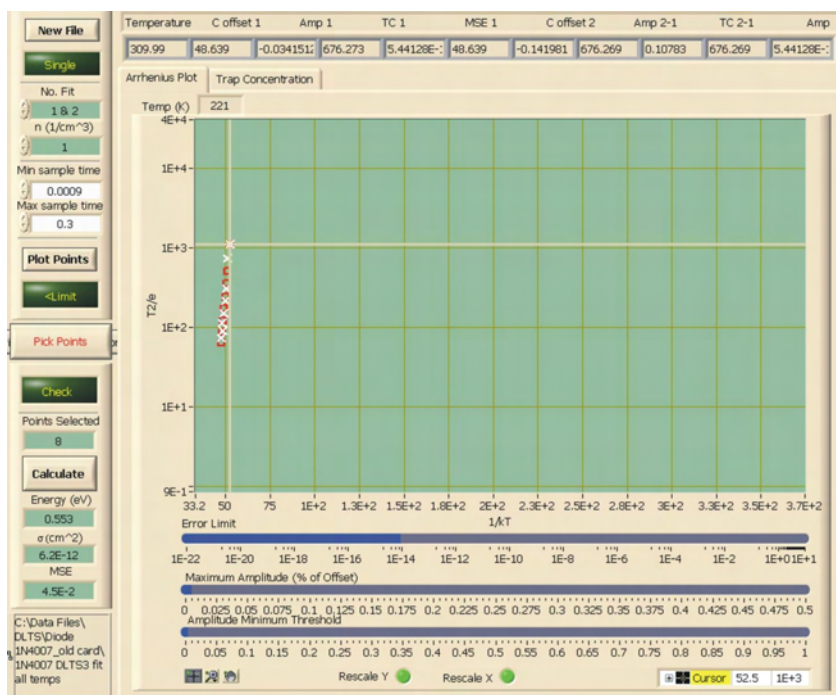*1N4007 DLTS Run3 (PCI 6035E) – Transient Analysis Fit of Figure 6.21-B*

Figure 6.24
1N4007 DLTS Run3 (PCI 6035E) – Transient Analysis Fit of Figure 6.21-C

Table 6.4
Measurement Results for 1N4007 DLTS Run3 (PCI 6035E)

	Calculated - RW Analysis		Calculated - Transient Analysis			
	Energy (eV)	Sigma (cm^2)	Curve	Energy (eV)	Sigma (cm^2)	MSE
Peak at 50K	0.101	4.9E-15	A	0.103	2.3E-14	1.3E-02
Peak at 160K	0.255	2.4E-17	B	0.301	4.0E-15	9.9E-03
Peak at 210K	0.402	1.5E-15		NA	NA	NA
Valley at 250K	NA	NA	C	0.553	6.2E-12	4.5E-02

The DLTS signal and resulting Arrhenius plot should show no difference between a measurement that is taken from a low temperature to a high temperature and one that is taken from a high temperature to a low temperature.[22] A comparison of the results listed in tables 6.2 and 6.4 indicate some discrepancies between the two measurements,

particularly at the higher temperatures. This may indicate that the high temperatures

from the first measurement permanently affects the device or more likely that the device

temperature has not stabilized and that the temperature sensor is not reading the true

device temperature.

6.3   Measurement and Analysis with NI PCI 6251 Interface Card

The measurements described in this section were done using the new interface

card (NI PCI 6251) and after the software modifications discussed in section 5.2 had been

implemented. The device measured is a 1N4007 diode as used in the measurements

described in section 6.2. However, it is should be noted that the 1N4007 diode measured

in section 6.3 is of the same type, but not the identical device as used in section 6.2.

6.3.1   1N4007 Diode DLTS Run1 (28 – 330K)

After further understanding of the capacitance meter limits, it was determined that

only the measurement bias had to be considered for determining the appropriate range of

the capacitance meter and that during the filling pulse the capacitance meter could go out

of range provided the current was below 30 mA. The measurement bias was set to –4.00

V so that the capacitance meter would be close to unity for the 10 pF range and the pulse

bias was set to 0.00 V. In comparison to the measurements described in section 6.2, the

time period for recording the transient was increased from 0.3 s to 1.2 s and the pulse

duration was increased by a factor of 3 to maximize the signal from the traps. The

measurement settings for 1N4007 DLTS Run1 (NI PCI 6251) are shown in table 6.5.

Review of the C-T data showed no abnormalities occurring during the

measurement. The resulting DLTS spectra is shown in figure 6.26. Ratewindow analysis

was performed on the peaks at 50K and 160K and the valley at 245K as shown in figures

6.27 to 6.29. The Arrhenius plot resulting from the transient analysis can be seen in figures 6.30 to 6.32. An optimized fit of the transients resulting from the peak at 50K (figure 6.30-A) was performed resulting in figure 6.31. Figure 6.32 is a zoomed in view of the figure 6.30-B, C, D. The fits of the Arrhenius plot are shown in figures 6.33 to 6.36. A summary of the results in included in table 6.6.

Table 6.5
Measurement Settings for 1N4007 DLTS Run1 (PCI 6251)

Bias Parameters

Measure bias (V):	-4.00
Pulse bias (V):	0.00
Pulse width:	3.00E-03
LED quiescent:	0
LED pulse:	0

Measurement Parameters

Sample period:	6.00E-04
Points:	2000
C-meter range:	10
No. Tx. Avg.:	100

Temperature Settings

T start:	28
T stop:	330

Temperature Stability Settings

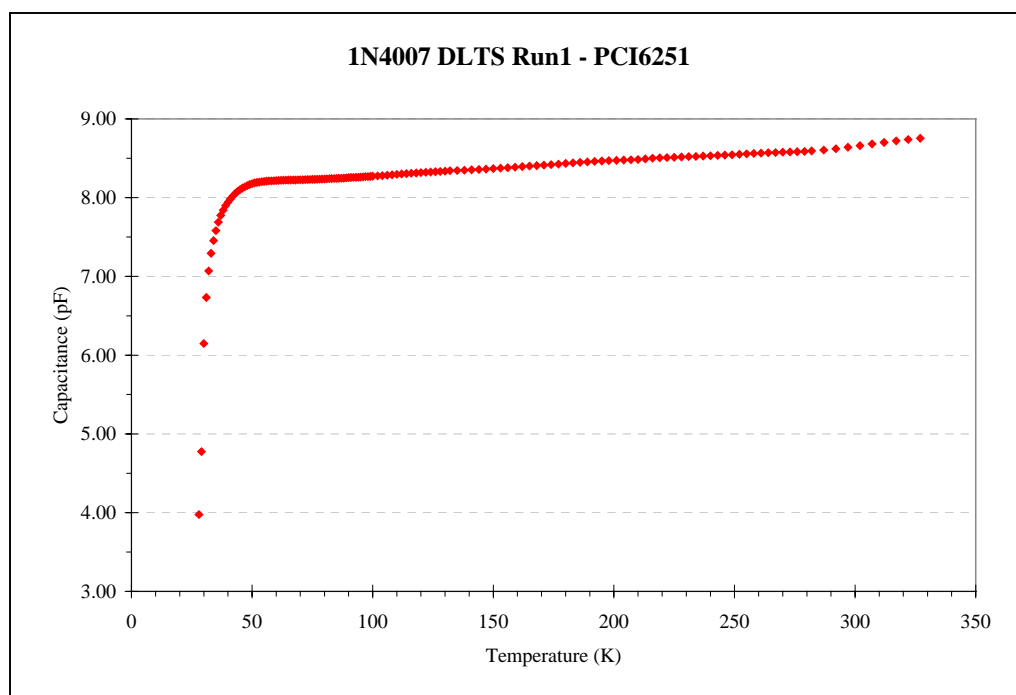| Temp >	Step size	Gain (P)	Heater range	Tolerance	Stability Count	Reset (I)	Rate (D)
0	0.5	1000	High	0.05	1	10	0
20	1	450	High	0.05	70	8	0
45	1	450	High	0.05	70	12	0
70	1	100	High	0.05	30	15	0
100	2	150	High	0.05	25	15	0
132	3	150	High	0.05	25	15	0
188	3	200	High	0.05	25	30	0
230	3	200	High	0.05	25	30	0
280	5	200	High	0.05	25	30	0
375	5	150	High	0.1	15	50	0
500	10	150	High	0.1	15	50	0
600	10	150	High	0.1	15	50	0
700	0	0	Off	0	0	0	0

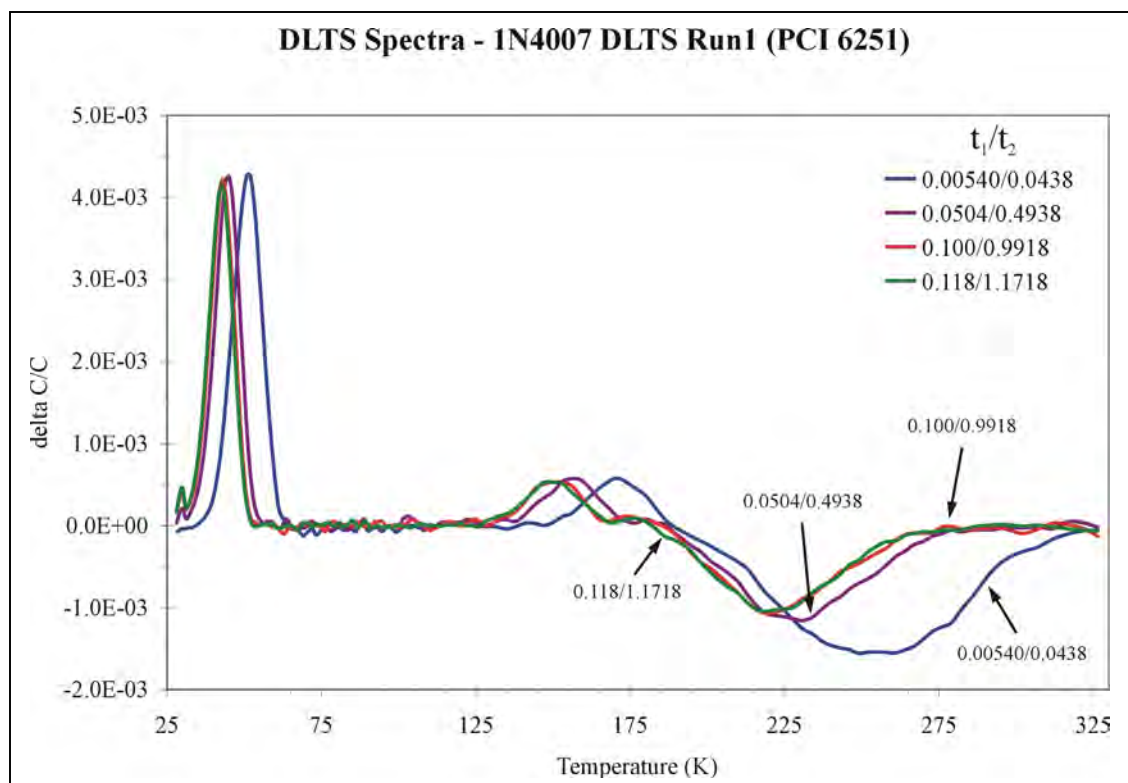*Figure 6.25*
CT Data of 1N4007 DLTS Run1 (PCI 6251)

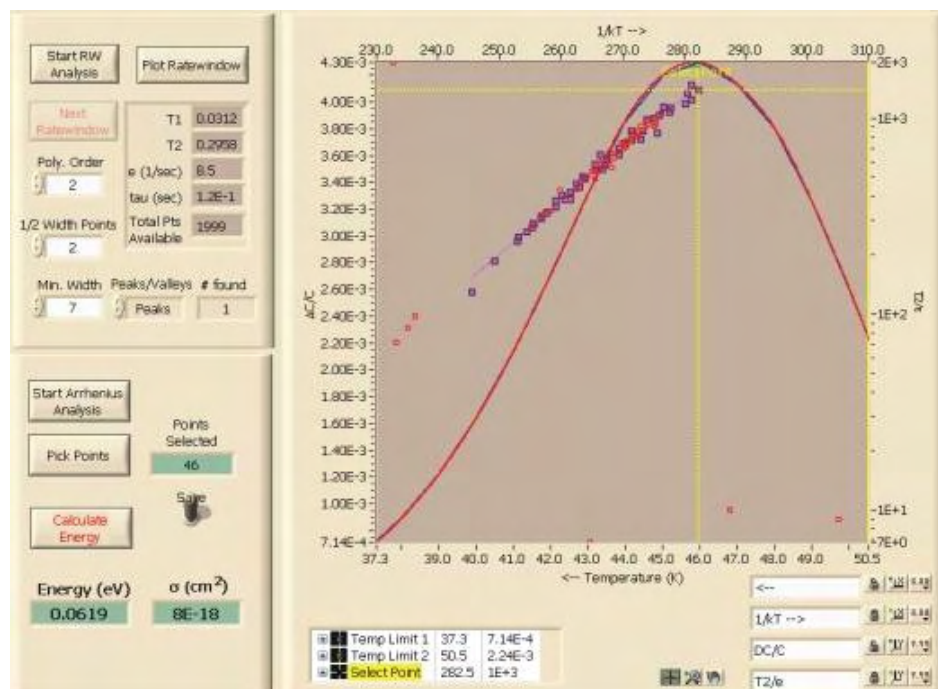*Figure 6.26*
DLTS Spectra – 1N4007 DLTS Run1 (PCI 6251)

Figure 6.27
1N4007 DLTS Run1 (PCI 6251) - Ratewindow Analysis of Peak at 50K
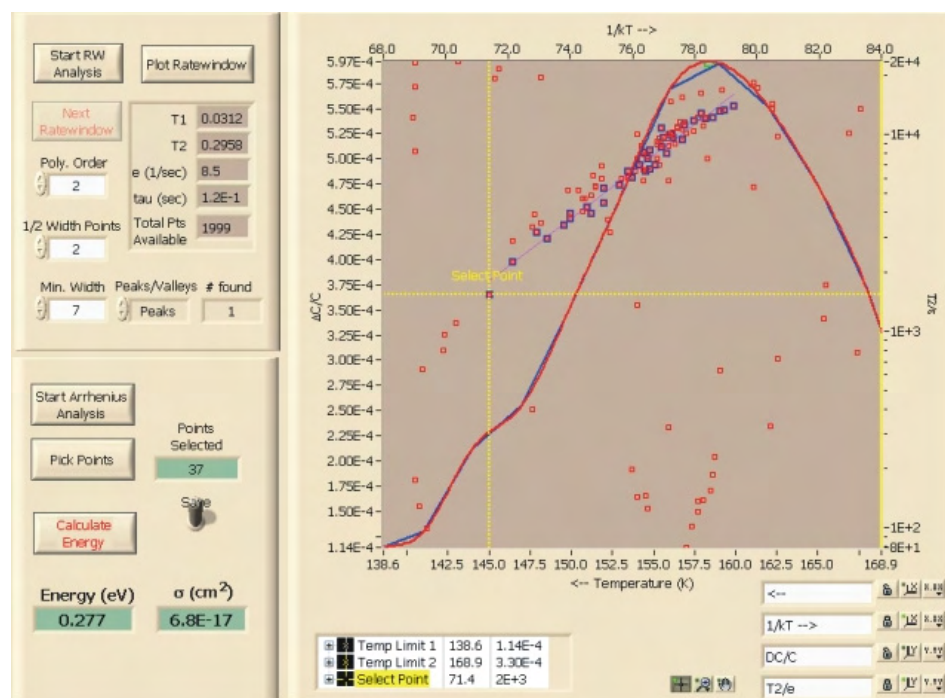

Figure 6.28
1N4007 DLTS Run1 (PCI 6251) - Ratewindow Analysis of Peak at 160K
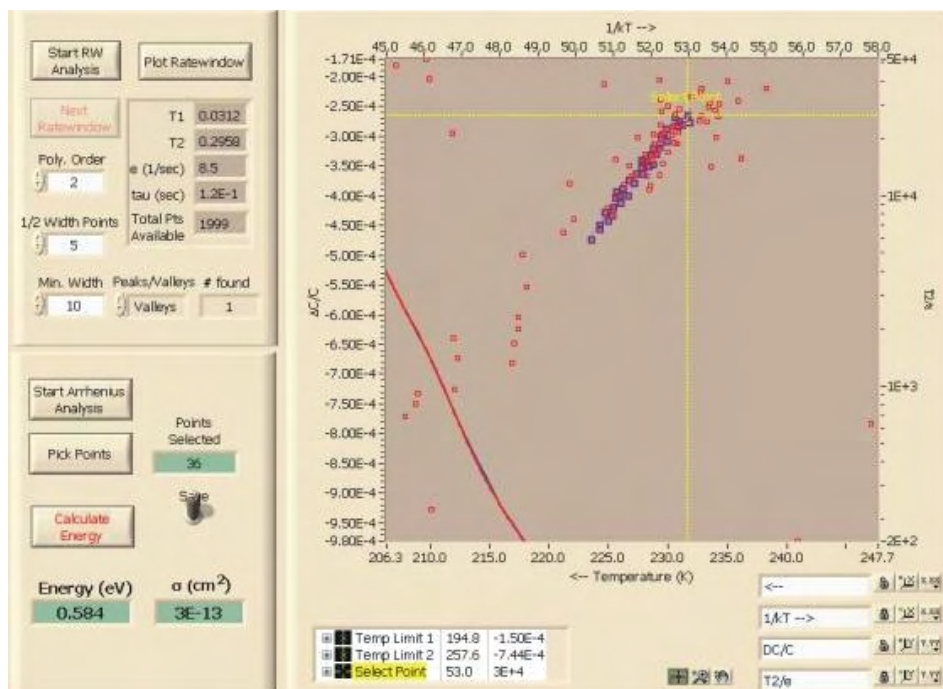
Figure 6.29
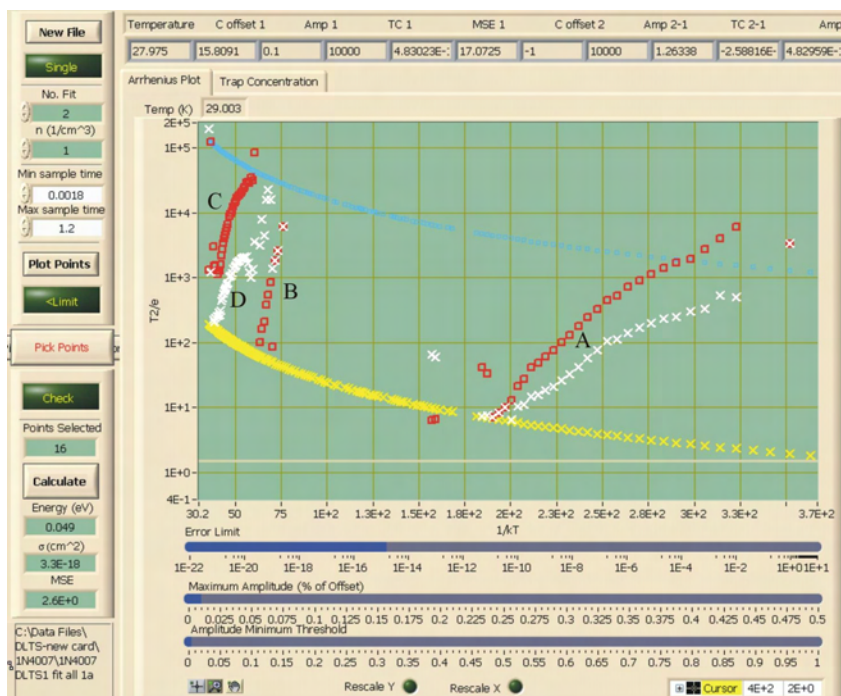*1N4007 DLTS Run1 (PCI 6251) - Ratewindow Analysis of Valley at 245K*

Figure 6.30
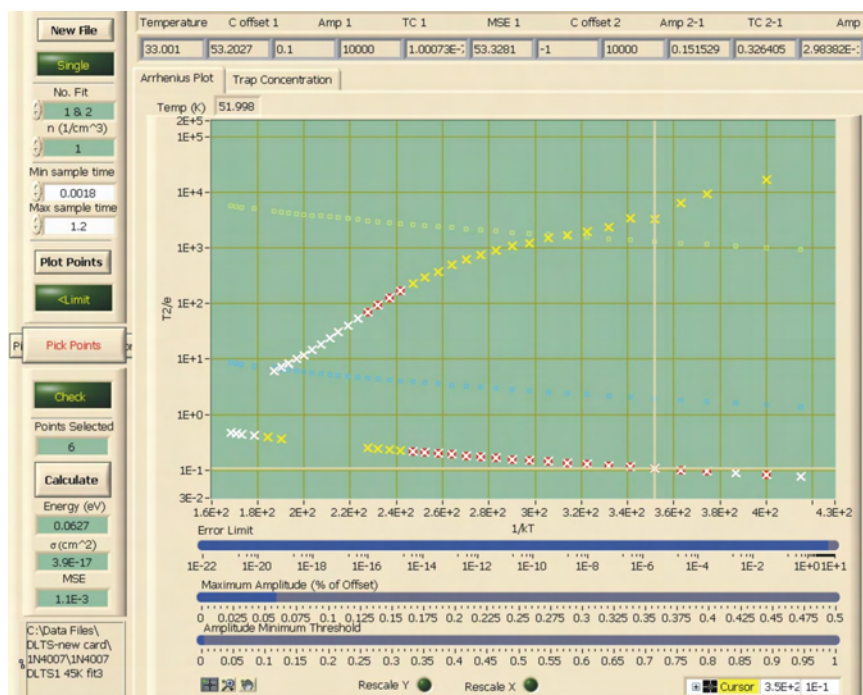*1N4007 DLTS Run1 (PCI 6251) – Transient Analysis (28 – 330K)*

Figure 6.31
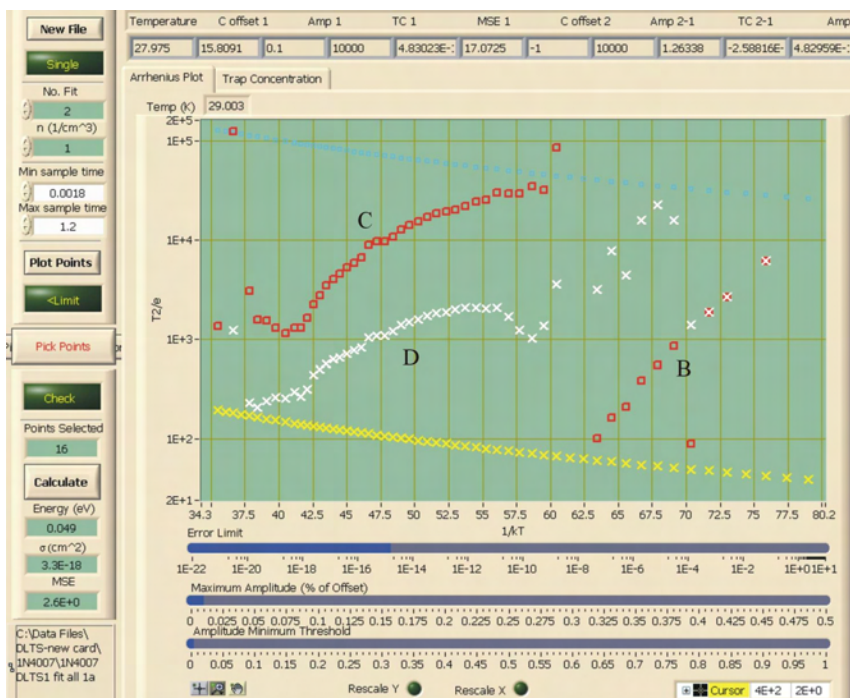*1N4007 DLTS Run1 (PCI 6251) – Transient Analysis – Figure 6.30-A Optimized*

Figure 6.32
1N4007 DLTS Run1 (PCI 6251) – Transient Analysis – Figure 6.30-B, C, D

Figure 6.33
1N4007 DLTS Run1 (PCI 6251) – Transient Analysis Fit of Figure 6.31

Figure 6.34
1N4007 DLTS Run1 (PCI 6251) – Transient Analysis Fit of Figure 6.30-B

Figure 6.35
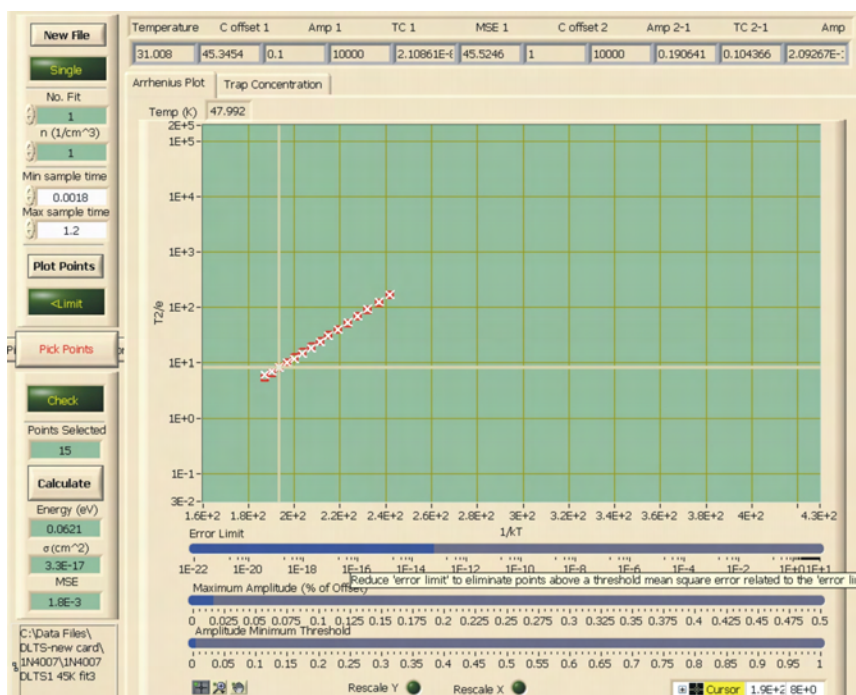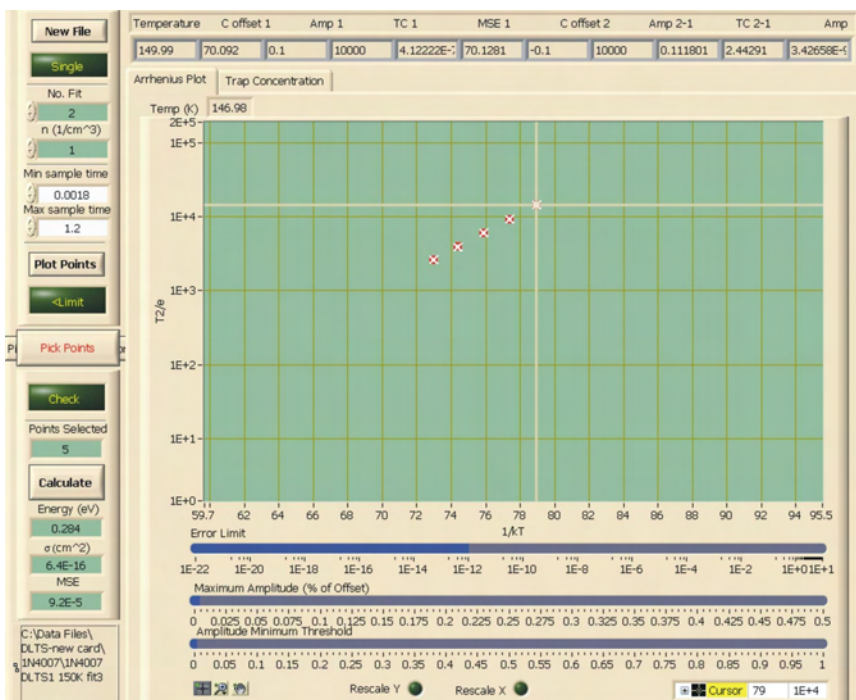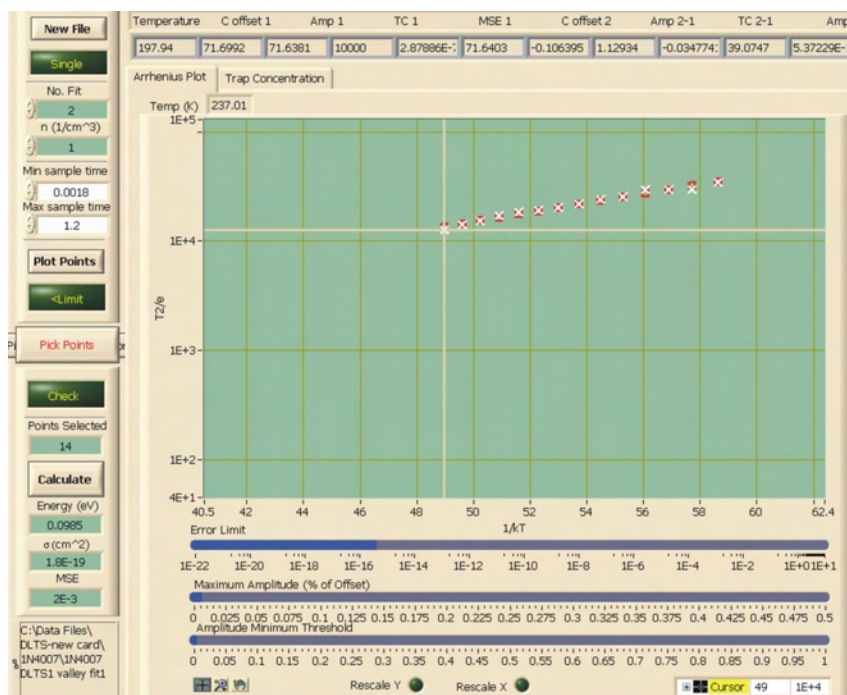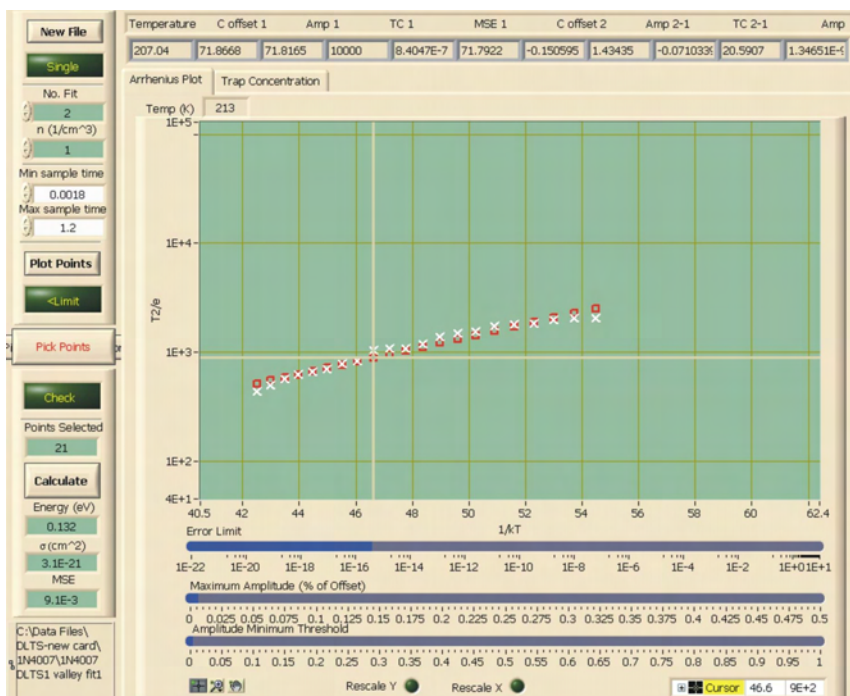*1N4007 DLTS Run1 (PCI 6251) – Transient Analysis Fit of Figure 6.30-C*

Figure 6.36
1N4007 DLTS Run1 (PCI 6251) – Transient Analysis Fit of Figure 6.30-D

Table 6.6
Measurement Results - 1N4007 DLTS Run1 (PCI 6251)

	Calculated - RW Analysis		Calculated - Transient Analysis			
	Energy (eV)	Sigma (cm^2)	Curve	Energy (eV)	Sigma (cm^2)	MSE
Peak at 50K	0.0619	8.0E-18	A	0.0621	3.3E-17	1.8E-03
Peak at 160K	0.277	6.8E-17	B	0.284	6.4E-16	9.2E-05
Valley at 245K	0.584	3.0E-13		NA	NA	NA
			C	0.0985	1.8E-19	2.0E-03
			D	0.132	3.1E-21	9.1E-03

6.3.2   1N4007 Diode DLTS Run3 (330 – 28K)

The 1N4007 diode was left in the cryostat and a second measurement (Run3) of

the device was performed. The measurement settings are identical to Run1, with the

exception that the temperature scan ran from 330K to 28K. A similar analysis was

performed on the measurement data as detailed in the following figures. The ratewindow

analysis was performed on the peaks at 50 and 160K and the valley at 245K as shown in

figures 6.39 to 6.41. The transient analysis follows, as shown in figures 6.42 to 6.47.

Table 6.7
Measurement Settings for 1N4007 DLTS Run3 (PCI 6251)

Bias Parameters

Measure bias (V):	-4.00
Pulse bias (V):	0.00
Pulse width:	3.00E-03
LED quiescent:	0
LED pulse:	0

Measurement Parameters

Sample period:	6.00E-04
Points:	2000
C-meter range:	10
No. Tx. Avg.:	100

Temperature Settings

T start:	330
T stop:	28

Temperature Stability Settings

Temp >	Step size	Gain (P)	Heater range	Tolerance	Stability Count	Reset (I)	Rate (D)
0	0.5	1000	High	0.05	1	10	0
20	1	450	High	0.05	70	8	0
45	1	450	High	0.05	70	12	0
70	1	100	High	0.05	30	15	0
100	2	150	High	0.05	25	15	0
132	3	150	High	0.05	25	15	0
188	3	200	High	0.05	25	30	0
230	3	200	High	0.05	25	30	0
280	5	200	High	0.05	25	30	0
375	5	150	High	0.1	15	50	0
500	10	150	High	0.1	15	50	0
600	10	150	High	0.1	15	50	0
700	0	0	Off	0	0	0	0

Figure 6.37
CT Data of 1N4007 DLTS Run3 (PCI 6251)
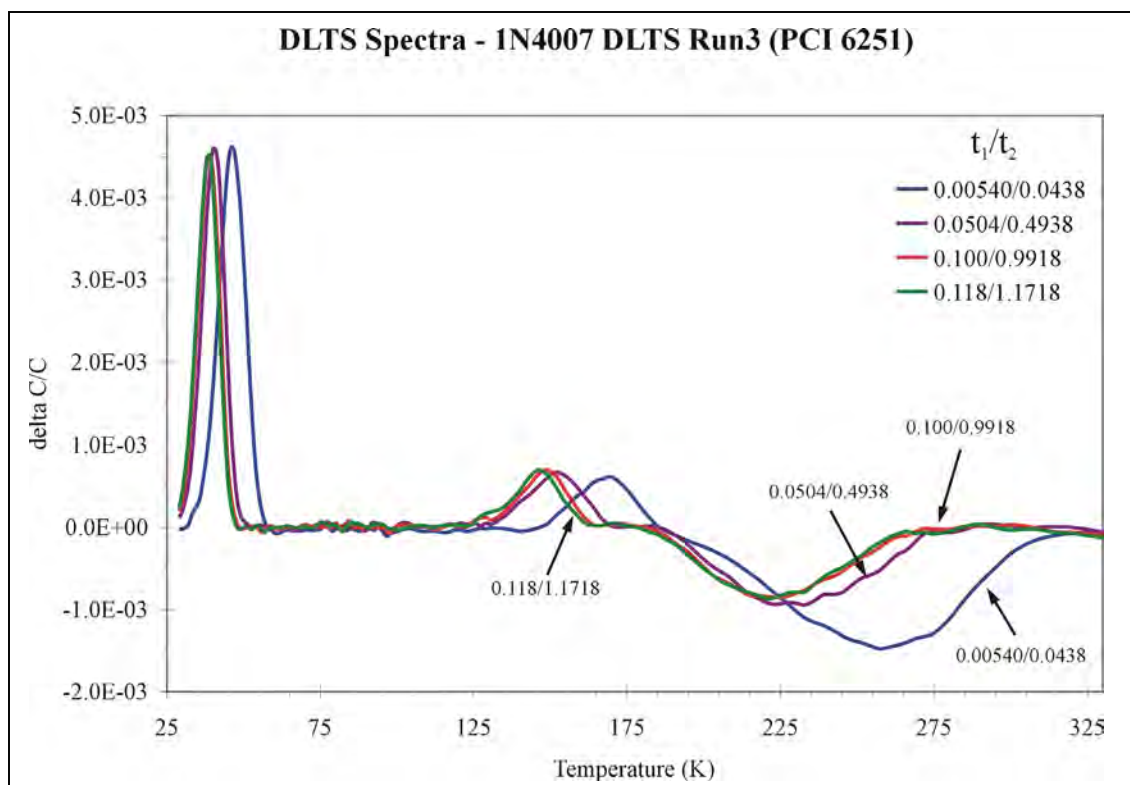
Figure 6.38
DLTS Spectra – 1N4007 DLTS Run3 (PCI 6251)
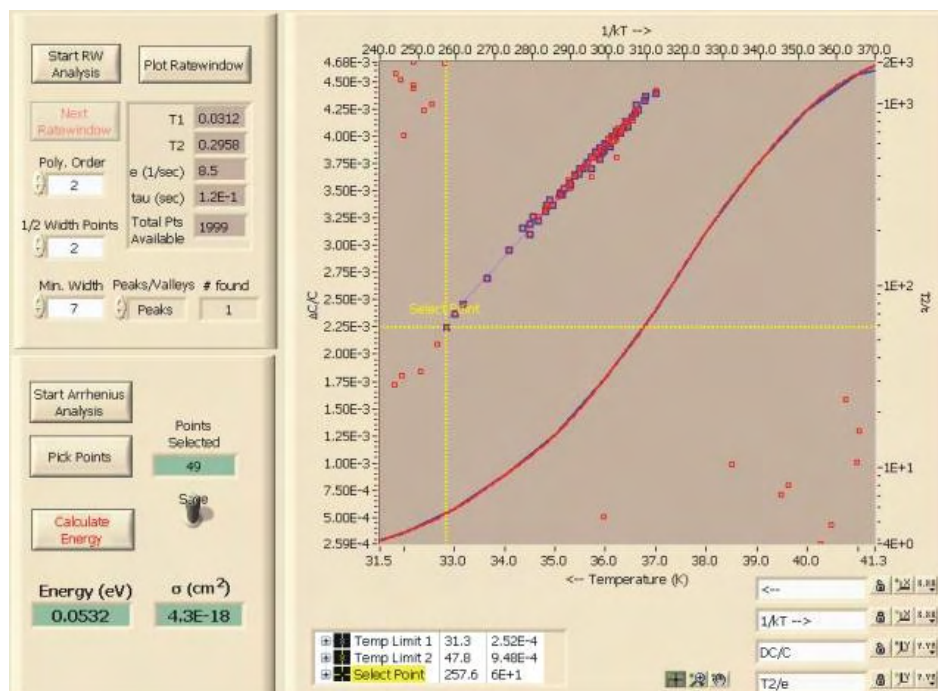
Figure 6.39
1N4007 DLTS Run3 (PCI 6251) - Ratewindow Analysis of Peak at 50K
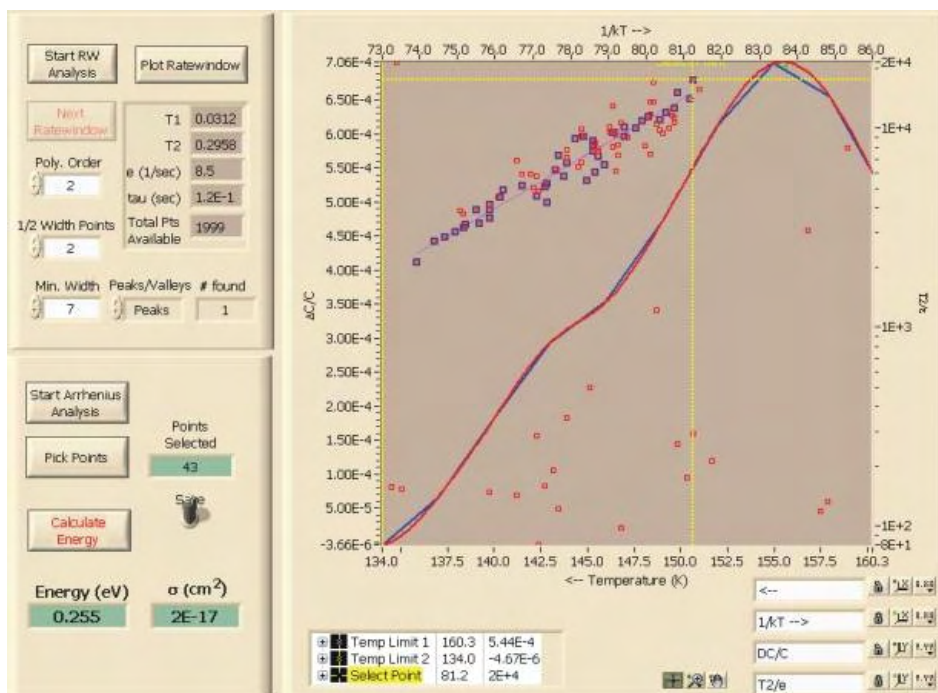
Figure 6.40
1N4007 DLTS Run3 (PCI 6251) - Ratewindow Analysis of Peak at 160K
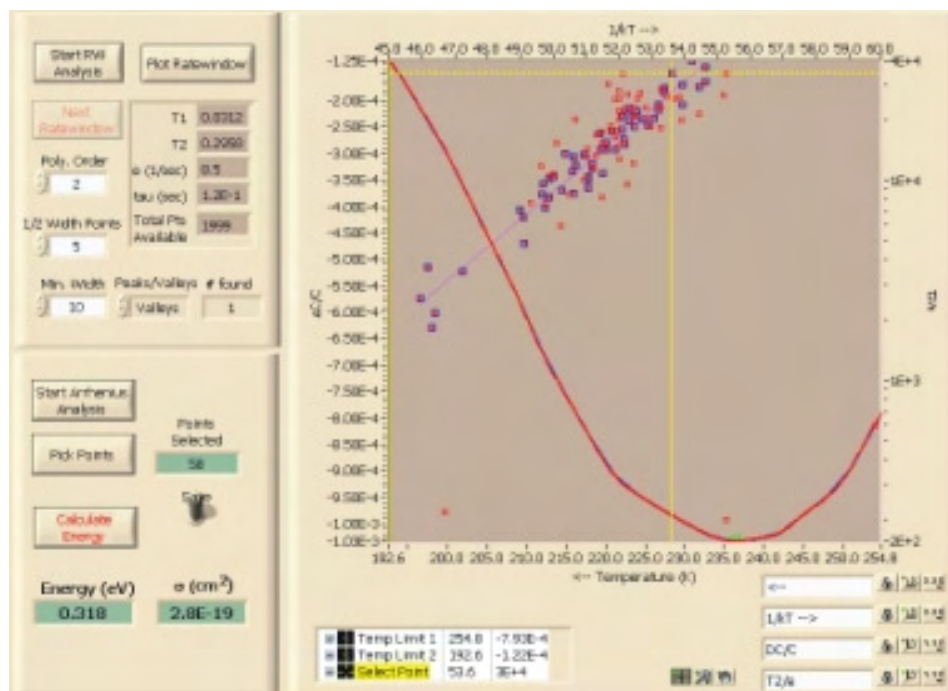
Figure 6.41
1N4007 DLTS Run3 (PCI 6251) - Ratewindow Analysis of Valley at 245K
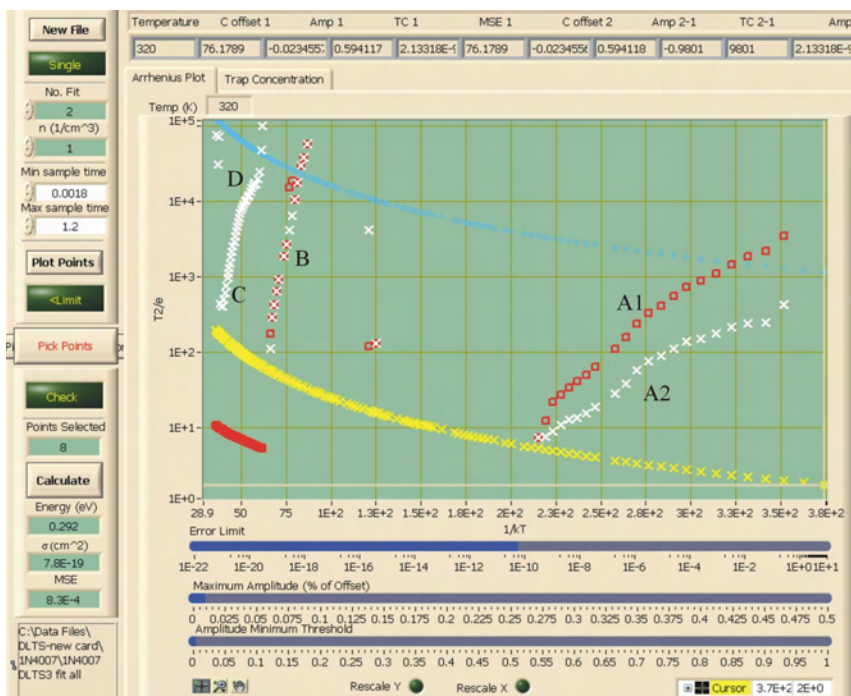
Figure 6.42
1N4007 DLTS Run3 (PCI 6251) – Transient Analysis (28 – 330K)

Figure 6.43
1N4007 DLTS Run3 (PCI 6251) – Transient Analysis Fit of Figure 6.42-A1
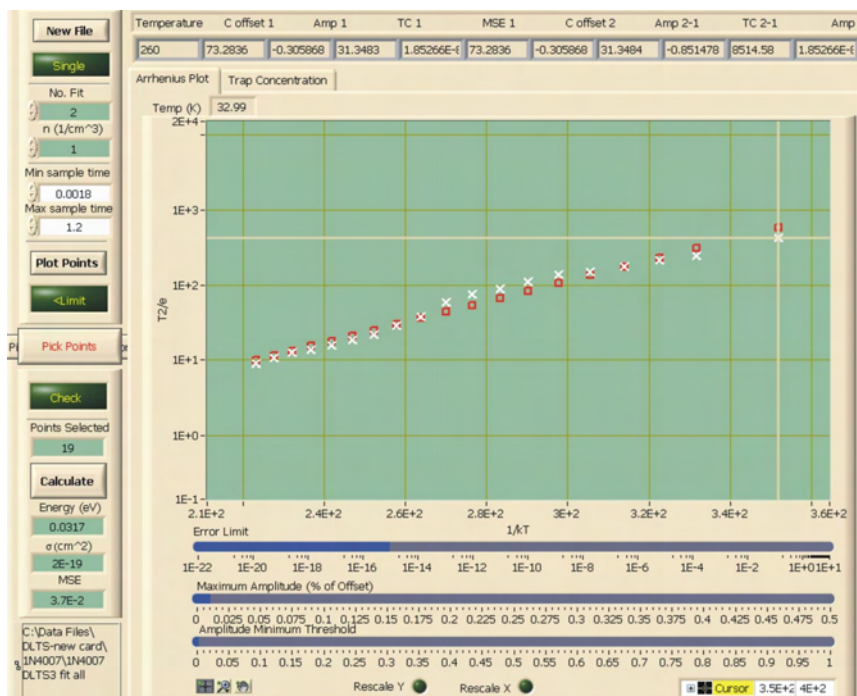
Figure 6.44
1N4007 DLTS Run3 (PCI 6251) – Transient Analysis Fit of Figure 6.42-A2
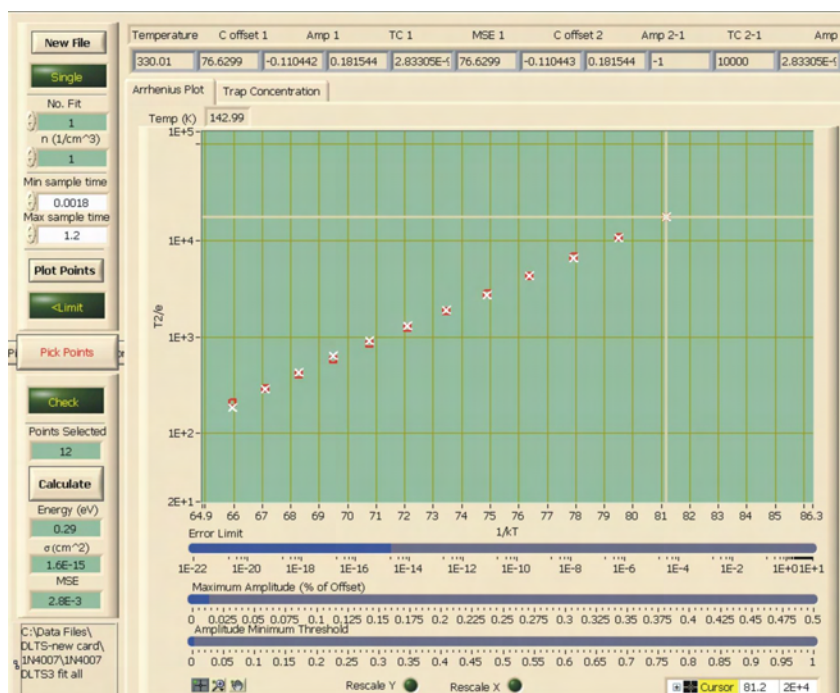
Figure 6.45
1N4007 DLTS Run3 (PCI 6251) – Transient Analysis Fit of Figure 6.42-B

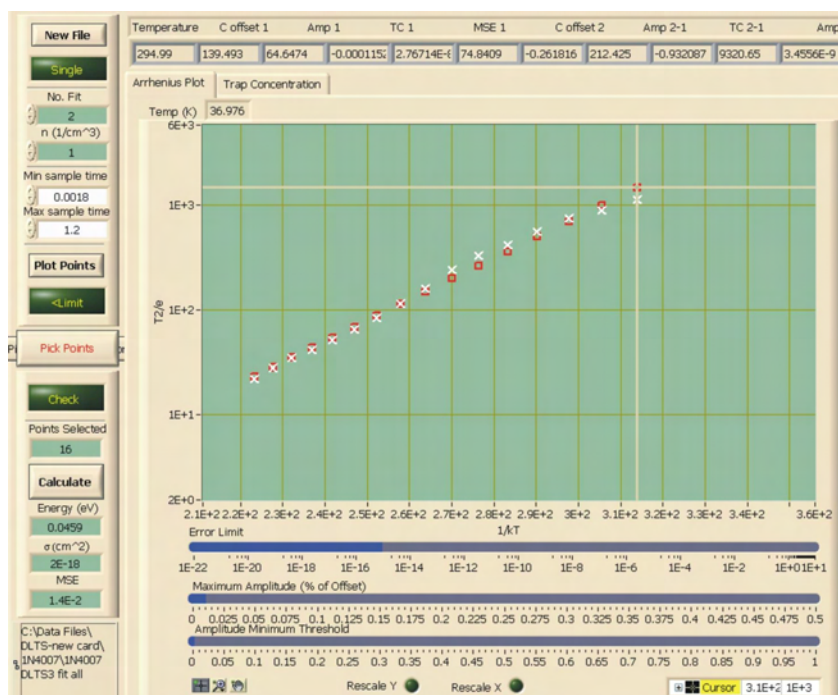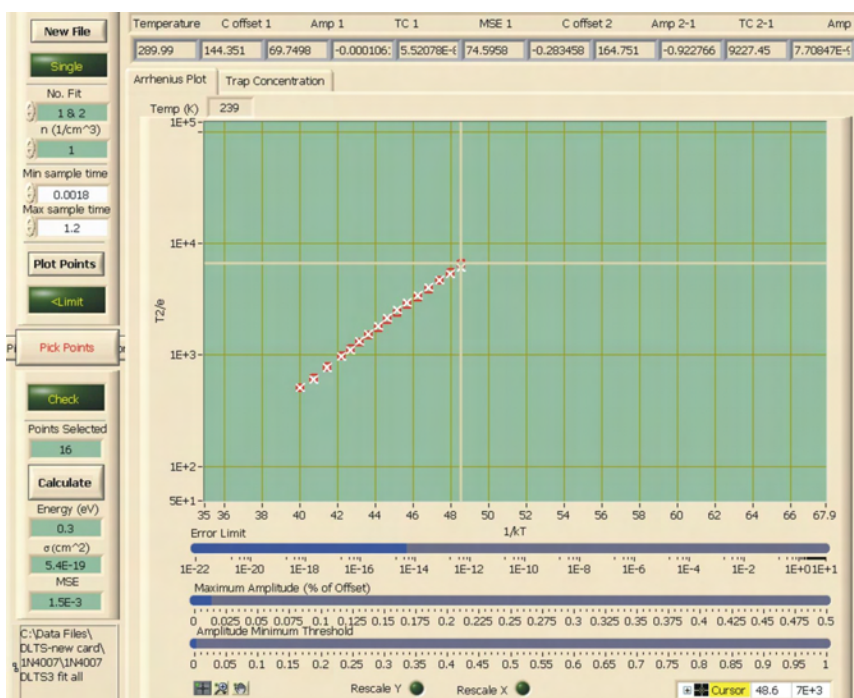*Figure 6.46*
1N4007 DLTS Run3 (PCI 6251) – Transient Analysis Fit of Figure 6.42-C
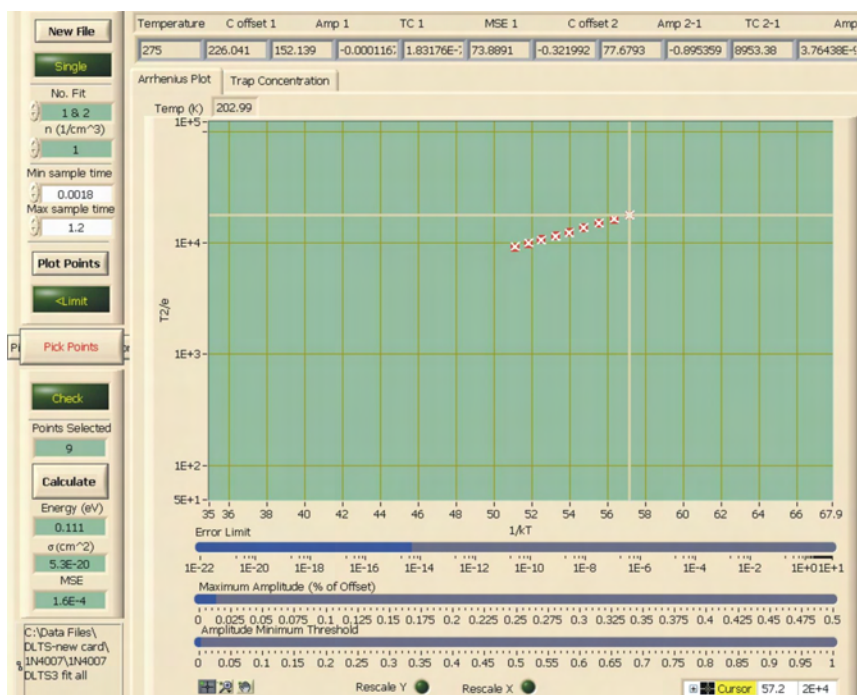
Figure 6.47
1N4007 DLTS Run3 (PCI 6251) – Transient Analysis Fit of Figure 6.42-D

Table 6.8
Measurement Results - 1N4007 DLTS Run3 (PCI 6251)

	Calculated - RW Analysis		Calculated - Transient Analysis			
	Energy (eV)	Sigma (cm^2)	Curve	Energy (eV)	Sigma (cm^2)	MSE
Peak at 50K	0.0532	4.3E-18	A1	0.0459	2.0E-18	1.4E-02
			A2	0.0317	2.0E-19	3.7E-02
Peak at 160K	0.255	2.0E-17	B	0.290	1.6E-15	2.8E-03
Valley at 245K	0.318	2.8E-19	C	0.300	5.4E-19	1.5E-03
			D	0.111	5.3E-20	1.6E-04

A comparison of the results listed in tables 6.6 and 6.8 show a better agreement in

energy values between the two measurement runs detailed in section 6.3 than the two

measurement runs in section 6.2, with exception of the valley feature in the DLTS

spectra. In section 6.3, the close agreement of the energy values obtained for the peak at

160K utilizing the new card and optimized temperature controller indicate that the sensor temperature is closer to the actual temperature of the device. However, the optimized temperature controller settings have resulted in a longer measurement time. Furthermore, the energy values obtained for the peak at 50K closely match the ionization energies of boron and phosphorus in silicon, which are 0.0445 and 0.0455 eV. Since the 1N4007 device is made of silicon with a diffused junction, it would be logical to assume the presence of boron and phosphorus in the device and that the measurement results are valid. The discrepancy in the values obtained for the valley at 245K may be due to poor selection of points in the Arrhenius plot, particularly in figure 6.41.

CHAPTER 7

CONCLUSIONS

As a result of this study, improvements to the original DLTS system have been made and a foundation for future students established. The implementation of the Semetrol software has resulted in more powerful analysis capabilities, better resolution and a faster measurement and analysis procedure. Evaluation of the software, feedback to Semetrol and the resulting software modifications have yielded improvements to the product. Preliminary measurements on devices have been performed which demonstrate progress has been made in establishing DLTS analysis capabilities at Texas State University-San Marcos. Operational procedures of the DLTS system have been outlined so that others may continue the development.

Future work includes resolving the issues of the capture cross section calculation during the transient analysis and correcting the noise and interference effects which has surfaced due to the new interface card. For high resistance materials and minority trap filling, the optical DLTS options needs to be installed. In addition, a method of establishing electrical connectivity to thin film samples must be implemented so that the materials currently being researched can be analyzed.

APPENDIX A

LIST OF SYMBOLS

β		heating rate
χ	(eV)	electron affinity
γ	(cm^{-2}s^{-1}K^{-2})	substitutional variable for emission rate, $\gamma = \dfrac{4\sqrt{6\pi^3}\, m^* k_B^2}{h^2}$
ε_o	(F/m)	permittivity of free space (8.8542 x 10^{-12} *F/m)*
λ	(m)	wavelength
μ	(cm^2/V·s)	mobility
μ_p	(cm^2/V·s)	hole mobility
μ_n	(cm^2/V·s)	electron mobility
Φ	(eV)	work function
Φ_m	(eV)	metal work function
Φ_s	(eV)	semiconductor work function
σ_n	(cm^2)	electron capture cross section
σ_p	(cm^2)	hole capture cross section
τ	(s)	time constant ($\tau = 1/e_n$)
$<v_n>$		electron thermal velocity
$<v_p>$		hole thermal velocity
v	(s^{-1})	frequency
A	(m^2)	area
c_n	(s^{-1})	electron capture rate
c_p	(s^{-1})	hole capture rate
C	(F)	capacitance
C_j	(F)	junction capacitance
D	(m^2/s)	diffusion constant

ΔE	(eV)	energy difference between the trap level and the band edge to which the charge carrier is emitted
E	(V/m)	electric field
E_C	(eV)	conduction band energy level
E_F	(eV)	Fermi energy level
E_{Fm}	(eV)	Fermi energy level of metal
E_{Fs}	(eV)	Fermi energy level of semiconductor
E_g	(eV)	bandgap
e_n	(s^{-1})	electron emission rate
e_p	(s^{-1})	hole emission rate
E_V	(eV)	valence band energy level
g		degeneracy
h		Planck's constant (4.14×10^{-15} $eV{\cdot}s$, 6.63×10^{-34} $J{\cdot}s$)
$\hbar$		$h/2\pi$
J	(C/m$^2{\cdot}$s)	current density
k_B		Boltzman constant (8.6174×10^{-5} eV/K, 1.3087×10^{-5} J/K)
K_s		relative permittivity
l		orbital angular momentum quantum number, $l = 0, 1, 2, \ldots(n-1)$
m^*_n	(kg)	electron effective mass
m^*_p	(kg)	hole effective mass
m_l		magnetic quantum number, $m_l = 0, \pm1, \pm2, \ldots, \pm l$
m_s		spin angular momentum quantum number, $m_s = \pm\frac{1}{2}$
n		principal quantum number, $n = 1, 2, 3, 4, \ldots$
n	(cm^{-3})	electron density
N_A	(cm^{-3})	acceptor doping density
N_C	(cm^{-3})	effective density of states at the edge of the conduction band
N_D	(cm^{-3})	donor doping density
n_n	(cm^{-3})	electron density in n-type material
n_p	(cm^{-3})	electron density in p-type material
n_T	(cm^{-3})	occupied trap density
N_T	(cm^{-3})	trap density

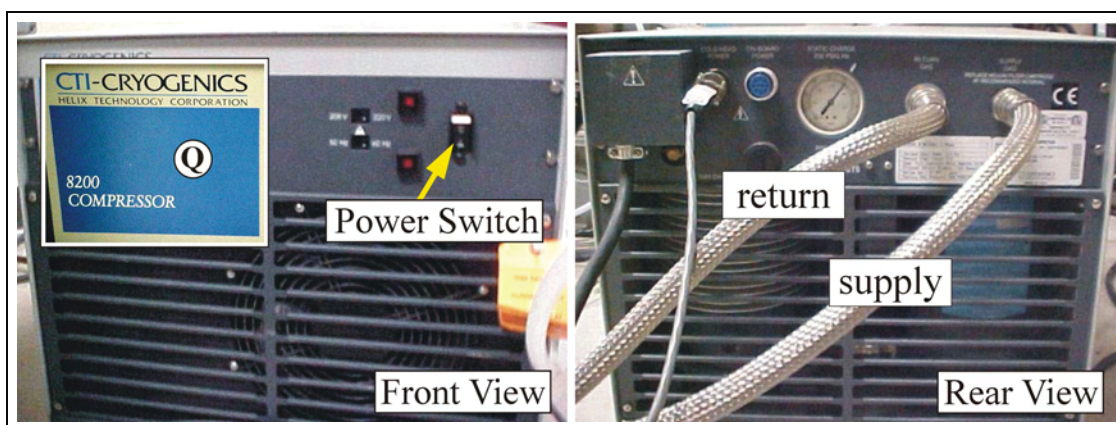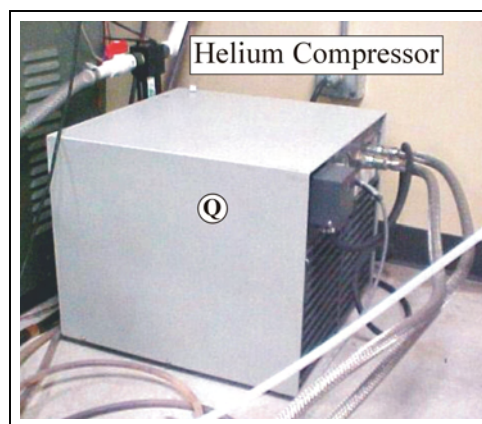| N_V	(cm^{-3})	effective density of states at the edge of the valence band
p	(cm^{-3})	hole density
p_n	(cm^{-3})	hole density in n-type material
p_p	(cm^{-3})	hole density in p-type material
q	(C)	elementary charge, $q = 1.6022 \times 10^{-19}\, C$
Q	(C)	total charge
Q_n	(C)	total charge in n-type material
Q_p	(C)	total charge in p-type material
t	(s)	time
T	(K)	temperature
V	(V)	voltage
V_A	(V)	applied voltage
V_{BR}	(V)	breakdown voltage
V_n	(V)	voltage at the depletion region and n-type region interface
V_o	(V)	built-in potential or contact potential
V_p	(V)	voltage at the depletion region and p-type region interface
W	(m)	depletion width or space charge width
x_p	(m)	depletion width or space charge width into p-type material
x_n	(m)	depletion width or space charge width into n-type material

APPENDIX B

DLTS-IVT-HALL EFFECT SYSTEM

The DLTS-IVT-Hall effect system is able to perform DLTS (Deep Level Transient Spectroscopy), IVT or Hall effect measurements using a shared cryostat.

I. Overview of System Components:

A. Keithley 2182A Nanovoltmeter
B. Keithley 6221 DC/AC Current Source
C. Keithley 7001 Switch System
     Keithley 7065 Hall Effect Card
D. Lake Shore 331 Temperature Controller
E. Keithley 6487 Picoammeter/ Voltage Source
F. National Instruments BNC-2090
G. Sula DLTS Module
H. HP 4275A Multi-Frequency LCR Meter
I. BK Precision DC Power Supply 1630 (for Pirani pressure gauge)
J. HP 3488A Switch/Control Unit
K. Switching Unit (polarity of magnet)
L. HP 6681A DC Power Supply (magnet power supply B)
M. HP 6681A DC Power Supply (magnet power supply A)
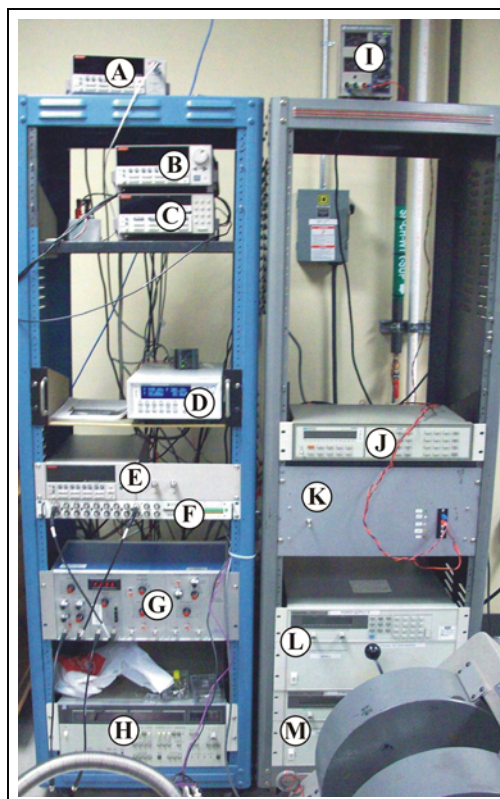
N. Water Supply Line (electromagnet)

O. Water Return Line (electromagnet)

P. Vacuum Pump Exhaust Line

Q. CTI-Cryogenics 8200 Compressor

    (helium compressor)

R. BOC Edwards RV8 Vacuum Pump

S. Vacuum Pump Foreline

Back view of electromagnet

Power Switch

Vacuum Pump

Helium Compressor

CTI-CRYOGENICS
HELIX TECHNOLOGY CORPORATION

8200 COMPRESSOR

Power Switch

Front View

return

supply

Rear View
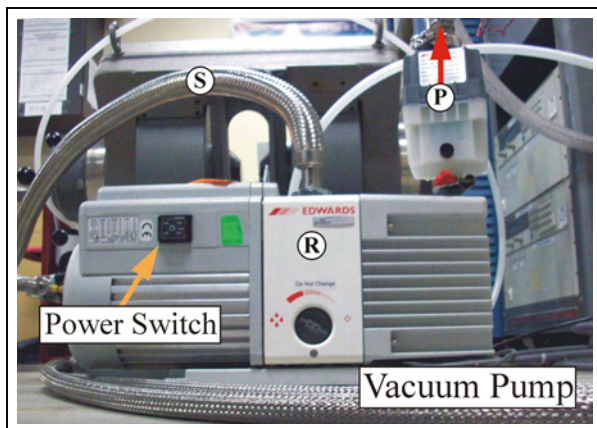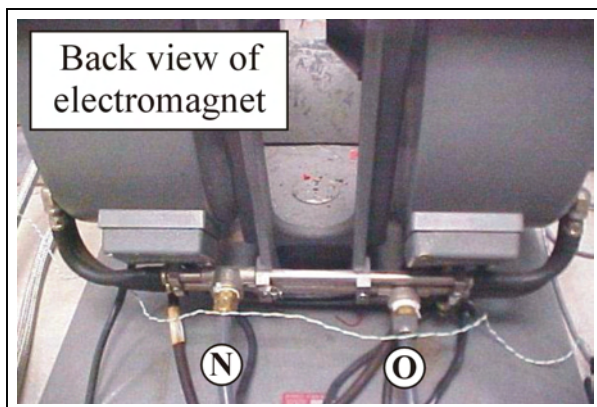
T. Vacuum Line Valve A

U. Foreline Trap

V. Pirani Pressure Gauge

W. Nitrogen Gas Inlet Valve

X. Nitrogen Gas Line

Y. Foreline Pressure Gauge (Bordon Pressure Gauge)
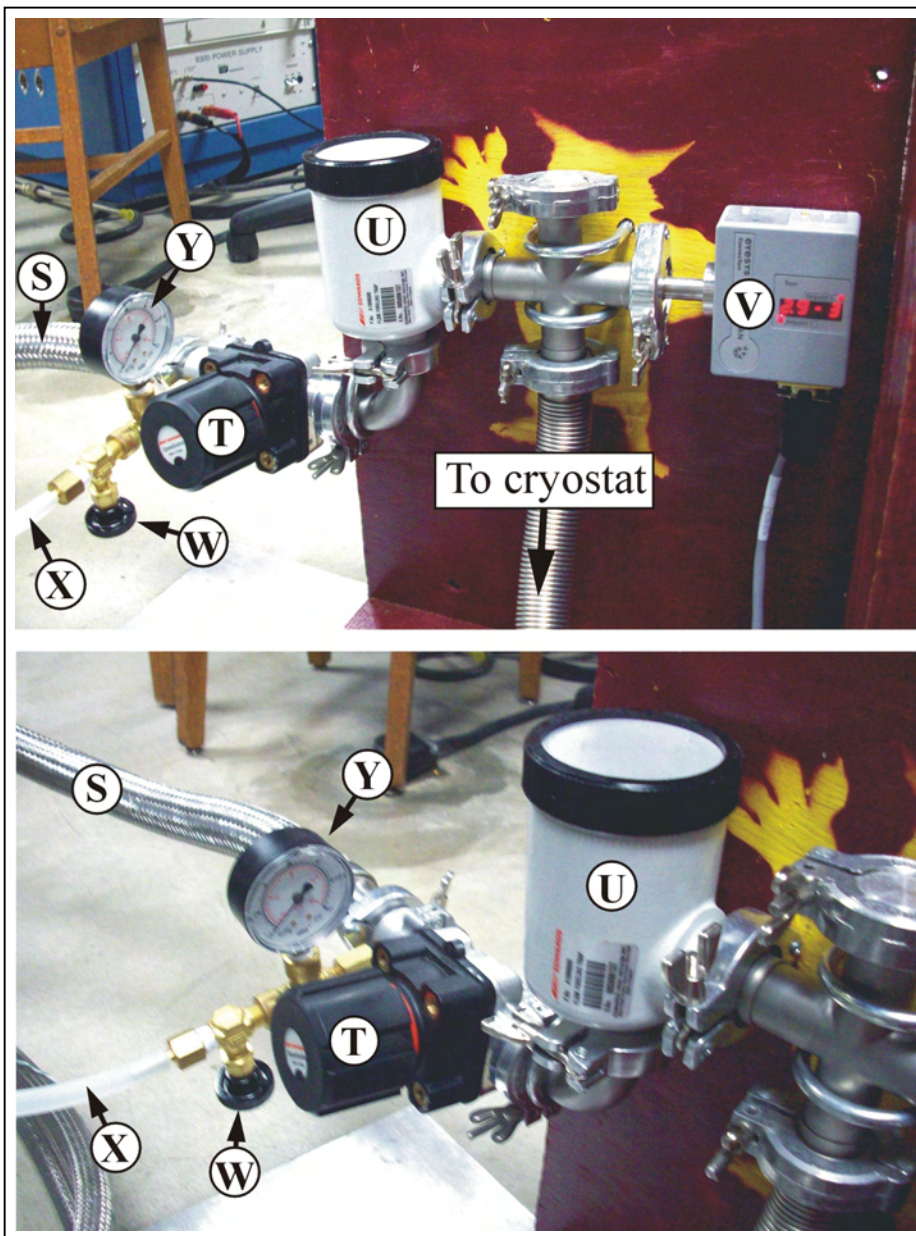
Z.   Vacuum Line Valve B

AA. Electrical Connection to
     Temperature A (Sample)

AB. Electrical Connection to
     Temperature B (Cold head)

AC. Cold head Power Supply

AD. Heater Power Supply

AE. Electrical Connection to
     DUT

AF. Clasp for Cryostat Shroud
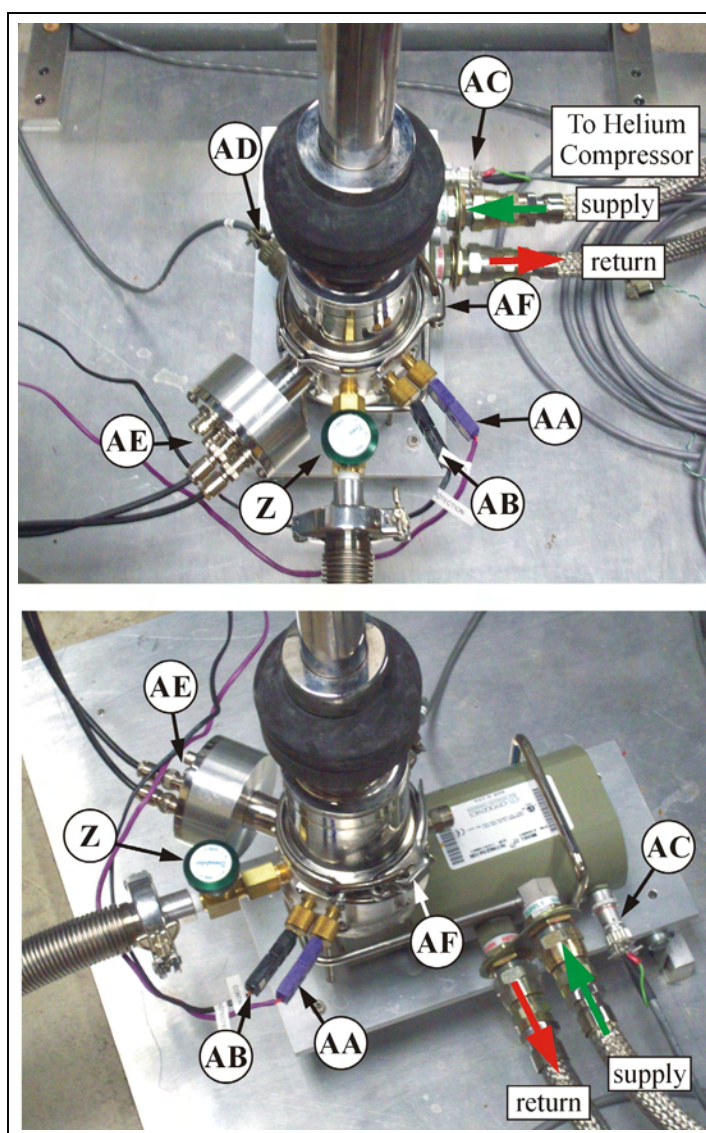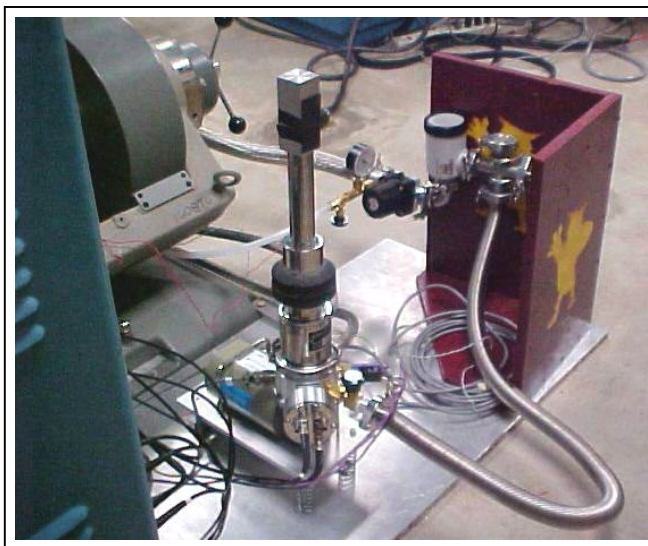
AG. Nitrogen Gas Valve

AH. Nitrogen Gas Cylinder Valve

AI. Varian model #V3703-1
Electromagnet

Cryostat rotated into Electromagnet

Window in Cryostat to DUT
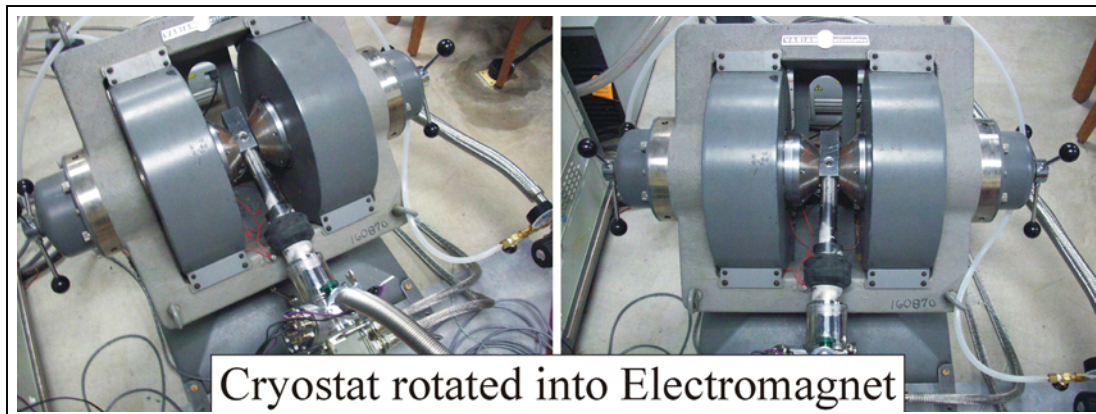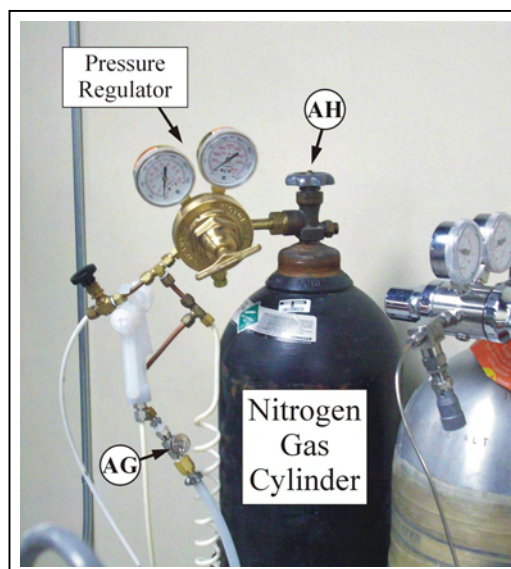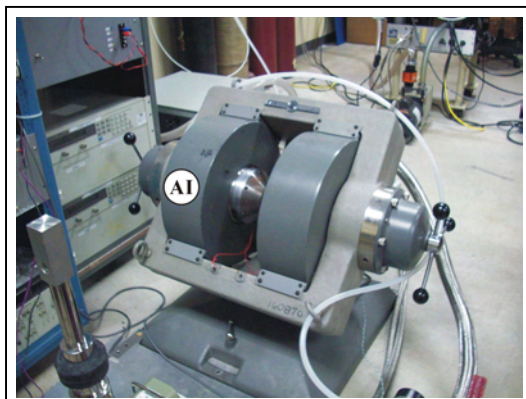
II. Lake Shore 331 Temperature Controller
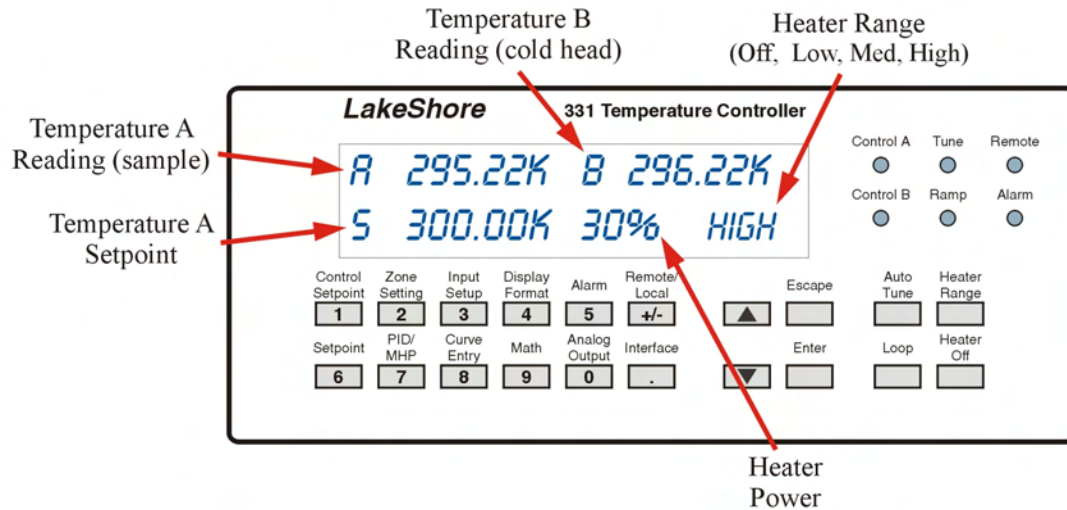
To turn heater off – Press the "Heater Off" button in the lower right hand corner of the module. The heater range on the display should change to "Off"

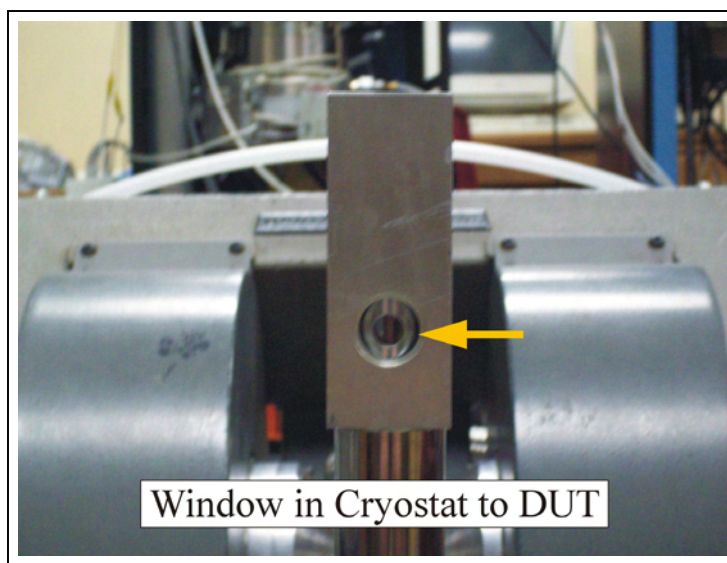To turn heater on - Press the "Heater Range" button four times until the display reads "Heater Range High" and then press "Enter".

To change the heater setpoint (Temperature A setpoint) – Press the "Setpoint" button. Enter the temperature value using the numeric keys and then press the "Enter" button. The new value should appear on the display. If the heater is on (heater range is not "Off"), the heater will begin to work if the setpoint temperature is above temperature A. **DO NOT EXCEED 700K FOR THE SETPOINT AS THIS MAY DAMAGE THE EQUIPMENT. DAMAGE TO THE DUT MAY OCCUR AT A LOWER TEMPERATURE.**

Additional information regarding the operation of the Lake Shore 331 Temperature Controller can be found in the user manual.

III. Electrical Connections for DLTS
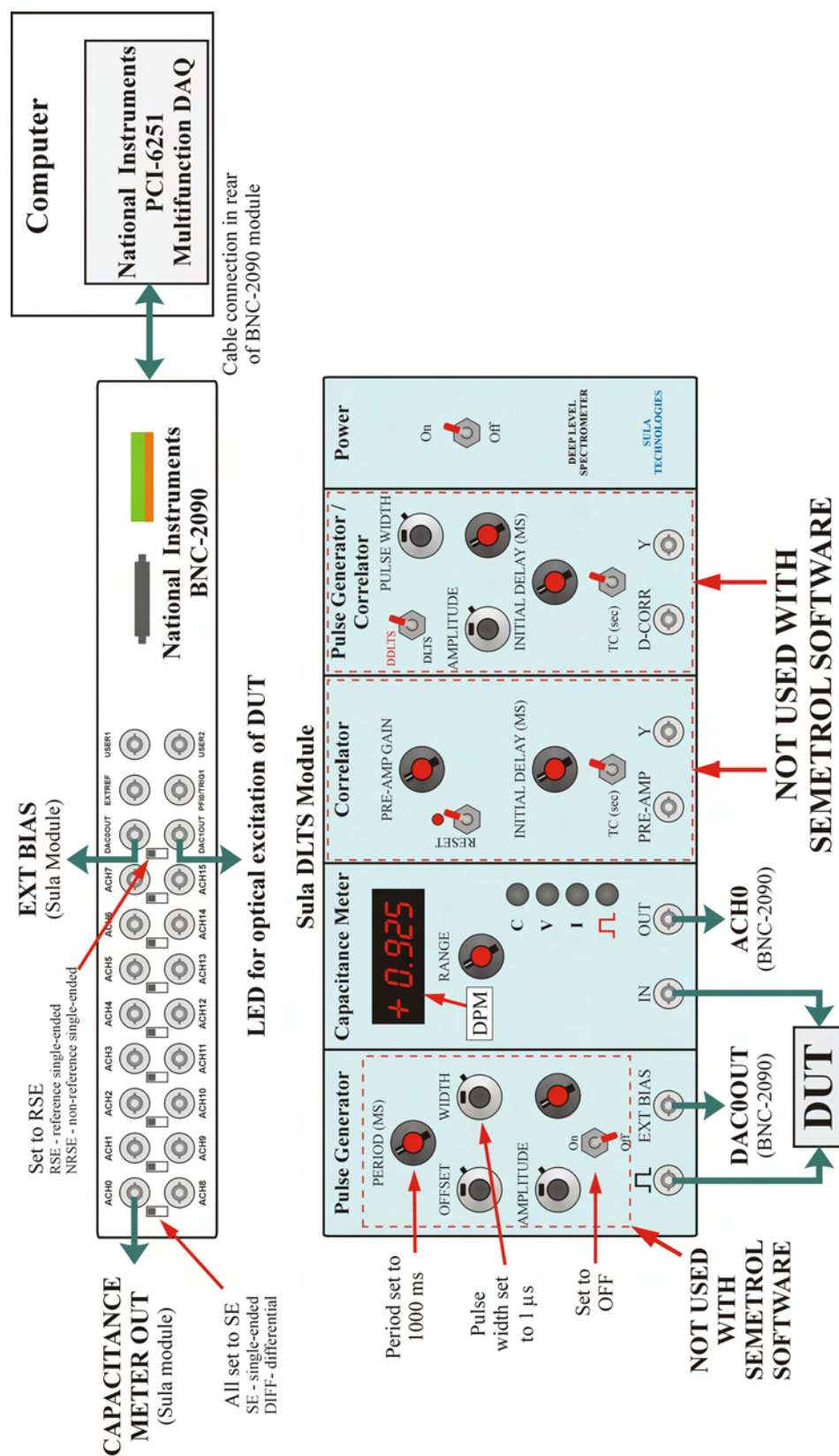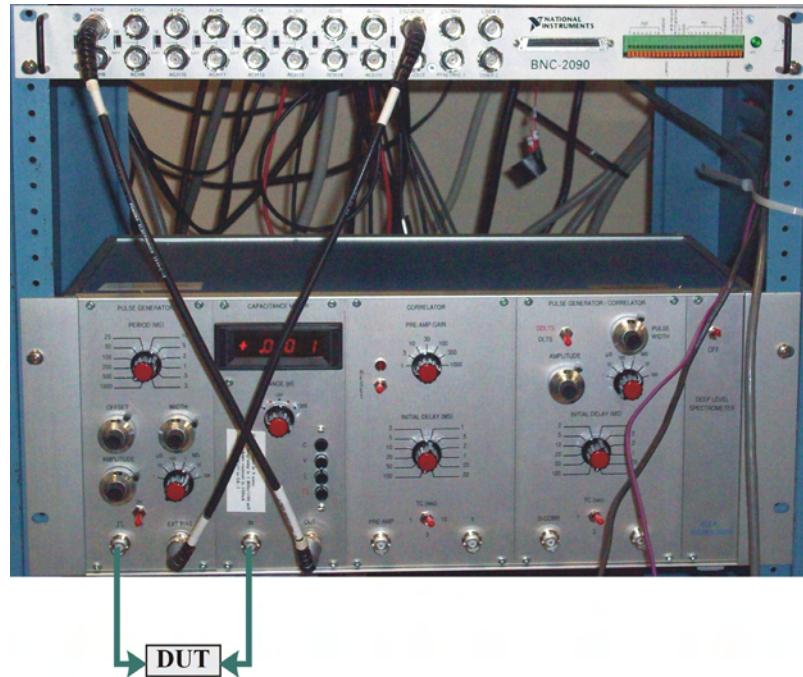
As shown on the diagram on the previous page, only the Capacitance Meter panel, the coaxial connections on the Pulse generator and Capacitance Meter panels and the power switch on the Sula module function with the Semetrol software.

IV. Capacitance Meter operation

The capacitance of the DUT can be measured by selecting the "C" button on the Capacitance Meter panel. The capacitance can be determined from the following:

C (pF) = Range x DPM value

The range is determined by adjusting the rotary selector knob to the appropriate value (10, 30, 100, 300, 1000 pF) for maximum sensitivity. The range selector knob is only used with the capacitance measurement and will not work with the voltage and current measurement features of the panel. The range selector knob must be in the correct position to match the value used in the DLTS/ODLTS Data Acquisition window in the Semetrol software when performing DLTS measurements. The DPM (Digital Panel Meter) value is displayed in the window.

For best sensitivity the DPM value should be close to unity and not exceeding 1.2. The signal-to-noise ratio is inversely proportional to the DPM value and non-linearity sets in above 1.2. The maximum DPM value is 1.9. If this value is exceeded, this may overload the DPM, which is indicated by blanking the display. In the case of strong overloads, this may lead to negative DPM values or a decreasing DPM value as the range is also decreased.

Selecting the "V" button on the Capacitance meter will monitor the steady state or continuous bias.

Selecting the "i" button measures the current through the DUT in microamperes with the full scale range being 150 µA. When performing a DLTS measurement, the leakage current should not exceed 100 µA during the steady state capacitance measurement, because this overloads the capacitance meter circuit. The meter can tolerate large current overloads (< 30 mA) during the pulse interval.

The square wave button monitors the pulse level in volts.

Unless the user is verifying the voltage or leakage current, the meter should be left with the measurement selection set to capacitance meter.

V. Cooling the System Down

Cooling down the system requires approximately 4 hours. It is recommended that you verify your sample is electrically connected and perform a short measurement prior to closing the cryostat and cooling the system down.

1. Verify the heater is off. Verify the nitrogen inlet valve and vacuum line valve A are closed.

2. Turn on the vacuum pump, allowing it to run for ~ 3 minutes and evacuate the foreline. The Bordon pressure gauge should show a vacuum in the foreline.

3. Open vacuum line valve A and vacuum line valve B.

4. When the pressure on the Pirani gauge reaches the millitorr range (-3), turn on the helium compressor. The vacuum pump should remain running until you are finished working with the system.

5. Allow the compressor to run until the sample temperature (Temperature A) reaches approximately 8K (minimum temperature). The helium compressor will stay on until you are finished working with the system and want the system to return to room temperature.

If the system has difficulty going below 150K, then the system does not have a good vacuum seal or the inner shield is touching the cryostat shroud. Turn off the compressor and vacuum pump and allow the system to return to room temperature. Check the seal at the base of the cryostat shroud (this is the most probable source of the problem) and whether the inner shield is flush in the pedestal.

Cryostat Cooldown Time

Temperature A [sample]

Temperature B [second stage]

Time (minutes)

Temperature (K)
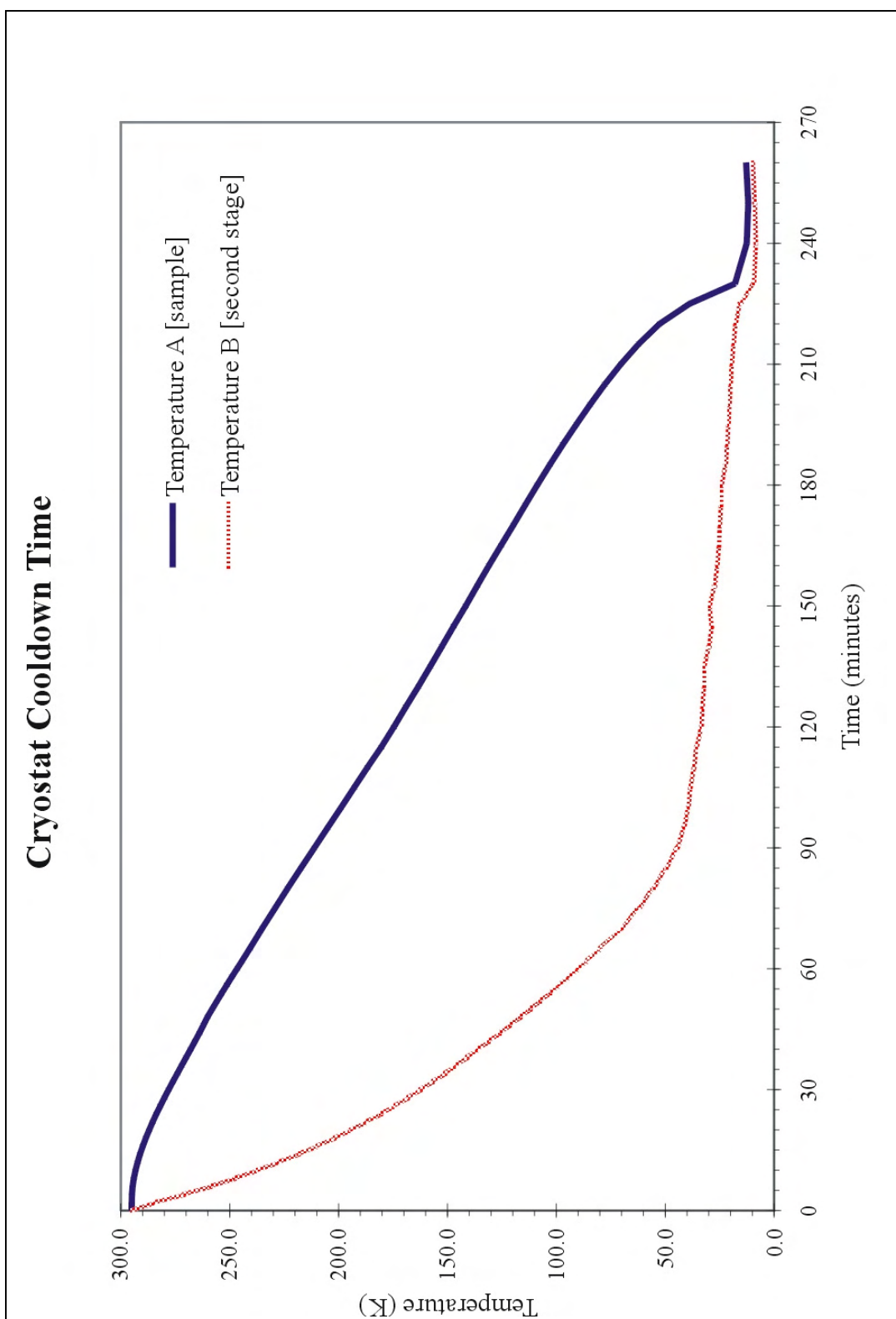
Cryostat Cooldown Time

Time (minutes)	Temp A (K) [sample]	Temp B (K) [second stage]	Pressure (Torr)	Time (minutes)	Temp A (K) [sample]	Temp B (K) [second stage]	Pressure (Torr)
0	295.05	294.67	5.00E-03	80	223.33	55.54	4.00E-03
2	295.02	284.03	4.80E-03	85	217.27	49.64	4.00E-03
4	294.91	270.84	4.70E-03	90	211.12	44.48	4.30E-03
6	294.58	258.57	4.60E-03	95	204.98	41.41	4.00E-03
8	294.02	247.40	4.50E-03	100	198.85	39.34	4.00E-03
10	293.25	237.00	4.50E-03	105	192.78	38.44	4.00E-03
12	292.30	227.32	4.40E-03	110	186.73	36.71	4.00E-03
14	291.18	218.23	4.40E-03	115	180.37	35.69	4.00E-03
16	289.90	209.73	4.30E-03	120	174.61	33.27	4.00E-03
18	288.51	201.70	4.30E-03	125	169.07	32.87	3.90E-03
20	286.98	194.18	4.20E-03	130	163.36	32.20	3.90E-03
22	285.38	187.07	4.20E-03	135	157.87	32.20	3.90E-03
24	283.66	180.47	4.20E-03	140	152.52	29.85	3.90E-03
26	281.84	173.96	4.20E-03	145	147.15	28.55	3.90E-03
28	279.99	168.06	4.10E-03	150	141.62	29.77	3.90E-03
30	278.04	162.29	4.10E-03	155	136.34	27.25	3.90E-03
32	276.07	156.61	4.10E-03	160	131.01	26.07	3.80E-03
34	274.06	151.03	4.10E-03	165	125.40	25.32	3.80E-03
36	272.01	145.84	4.10E-03	170	119.85	24.95	3.80E-03
38	270.02	140.91	4.10E-03	175	114.33	24.36	3.80E-03
40	267.94	135.85	4.10E-03	180	108.78	24.23	3.80E-03
42	265.95	130.89	4.10E-03	185	103.05	22.17	3.80E-03
44	263.93	125.97	4.10E-03	190	97.10	21.51	3.80E-03
46	262.08	121.30	4.10E-03	195	90.87	20.96	3.80E-03
48	260.21	116.55	4.00E-03	200	84.50	20.50	3.80E-03
50	258.08	111.92	4.00E-03	205	77.70	19.96	3.80E-03
52	255.80	107.31	4.00E-03	210	70.39	19.43	3.80E-03
54	253.58	102.84	4.00E-03	215	62.22	18.63	3.80E-03
56	251.30	98.53	4.00E-03	220	52.56	17.71	3.80E-03
58	249.01	94.19	4.00E-03	225	38.73	15.67	3.80E-03
60	246.64	89.97	4.00E-03	230	17.91	9.26	3.80E-03
62	244.25	85.76	4.00E-03	240	12.53	8.34	3.80E-03
65	240.78	79.78	4.00E-03	250	11.84	8.88	3.80E-03
70	235.08	70.47	4.00E-03	260	12.83	9.80	3.80E-03
75	229.18	62.29	4.00E-03				

VI. When measurements are completed – backfill system with nitrogen

Allow system to return to room temperature before returning the chamber to atmospheric pressure. If the chamber is vented while still at low temperatures, moisture will condense on the inside of the system.

1. While waiting for the system to return to room temperature, the vacuum pump can be returned to atmospheric pressure by filling the foreline with nitrogen gas.

2. Close vacuum line valve A and vacuum line valve B.

3. Turn the vacuum pump off. The foreline should still be under vacuum.

4. Open the nitrogen gas cylinder valve on top of the nitrogen gas cylinder (the gauges on the pressure regulator attached to the gas cylinder should now have a reading). Open the nitrogen gas valve connected to the plastic tubing and allow nitrogen to flow to the nitrogen inlet valve. You should be able to hear nitrogen gas flowing through the plastic tubing since the tubing is loosely place over the nitrogen inlet.

5. Open the nitrogen inlet valve. The vacuum in the foreline will pull the nitrogen into the vacuum pump/foreline until the pressure is at atmosphere.

6. Close the nitrogen inlet valve when the Bordon pressure gauge reaches atmospheric pressure.

7. Close the nitrogen gas cylinder valve on the nitrogen bottle and then the nitrogen gas valve.

After the system has returned to room temperature, the vacuum pump and cryostat can be backfilled with nitrogen gas.

1. Turn on the vacuum pump and allow it to run for five minutes to evacuate the foreline.

2. Open vacuum line valve A and vacuum line valve B. The chamber and vacuum foreline should now be under vacuum.

3. Turn off the vacuum pump.

4. Open the nitrogen gas cylinder valve on top of the nitrogen gas cylinder (the gauges on the pressure regulator attached to the gas cylinder should now have a reading). Open the nitrogen gas valve connected to the plastic tubing and allow nitrogen to flow to the nitrogen inlet valve. You should be able to hear nitrogen gas flowing through the plastic tubing since the tubing is loosely place over the nitrogen inlet.

5. Open the nitrogen inlet valve. The vacuum in the foreline and cryostat will pull the nitrogen into the vacuum pump/foreline and cryostat until the pressure is at atmosphere.

6. Close the nitrogen inlet valve.

7. Close the nitrogen gas cylinder valve on the nitrogen bottle and then the nitrogen gas valve

APPENDIX C

LOADING THE DUT AND DATA ACQUISITION

I. Loading the DUT

1. Verify the system is at room temperature and atmospheric pressure before opening the clasp for the cryostat shroud at the base of the cryostat.

2. Put on gloves to protect the inside of the chamber from becoming contaminated.

3. Open the clasp for the cryostat shroud at the base of the cryostat and lift the cryostat shroud straight up. Set the shroud aside so that the gasket and vacuum grease on the bottom of the shroud is not disturbed and will not become dirty.
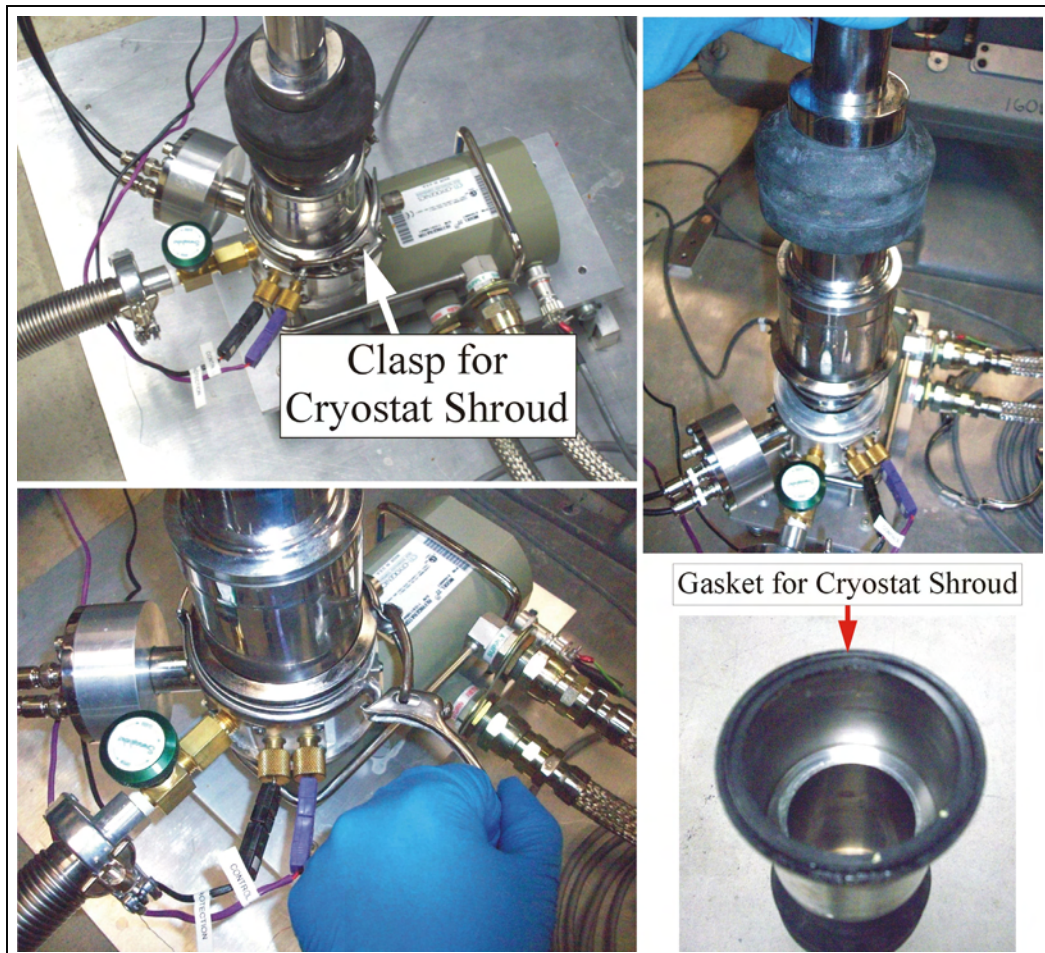
4. Using a hex wrench (3.5 mm), unscrew the four hex bolts securing the inner shield to the base and gently lift the shield straight upward. Remove the four hexbolts and set them aside. Do not turn the shield upside down and lose the four hexbolts.
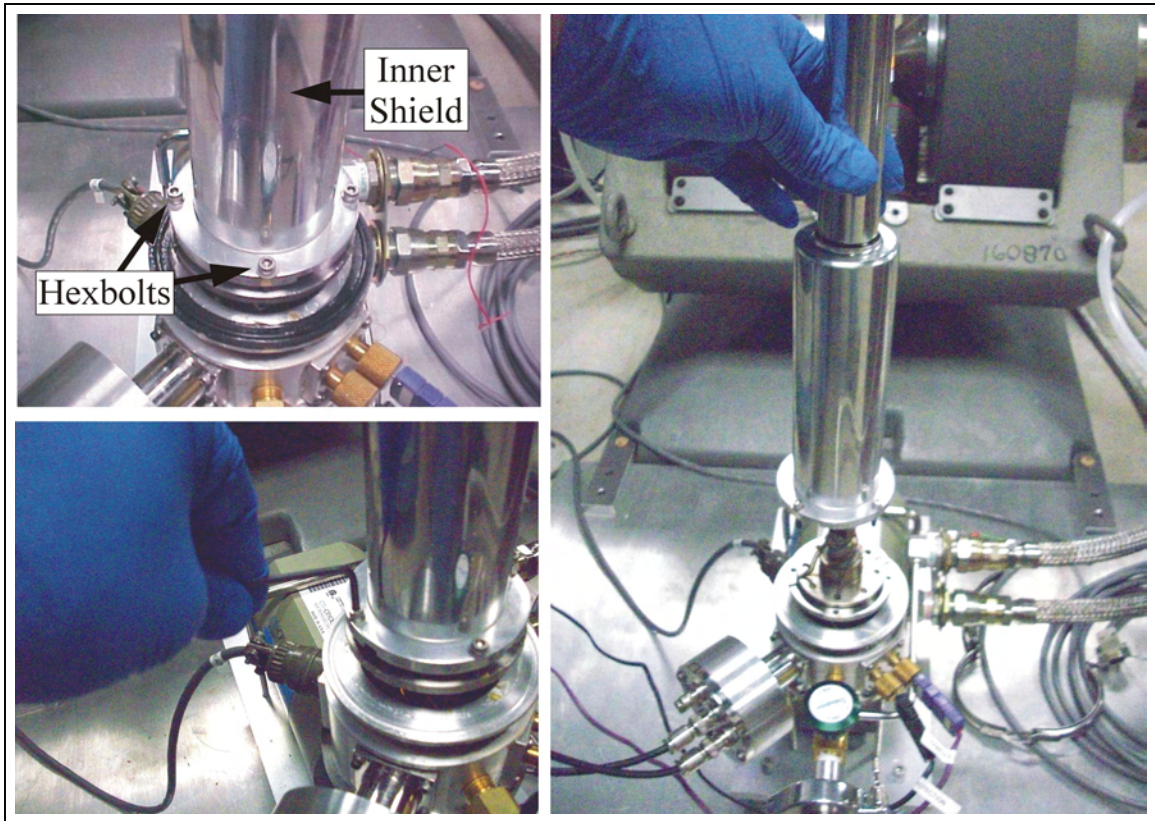
5. Mount DUT on the cold finger and make the appropriate electrical connections. **It is recommended that you test the electrical connections before closing the system up**. ** Refer to the section on mounting the DUT.

6. Gently slide the inner shield down on to the base, making sure it is in the groves and not on any wires, and screw in the four hexbolts.

7. Put the cryostat shroud back on the pedestal and secure the clasp.

II. Mounting the DUT - Discrete component

1. Remove the previously measured DUT if attached. Remove the top screw of the mounting bracket holding the DUT against the cold finger. Remove the DUT and disconnect from the wires. The wires are very fine and break easily. If the wires break, it may be necessary to remove insulation from the ends of the wire to ensure an electrical connection to the new DUT. Use sandpaper to gently remove the insulation.
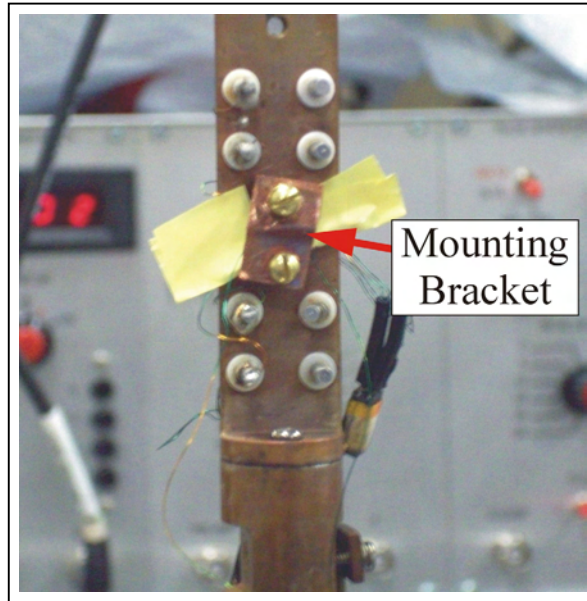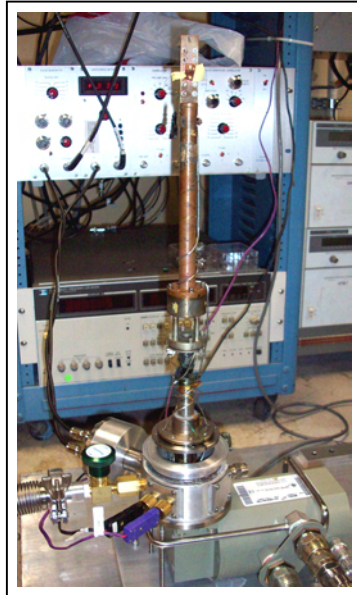
2. Place the edge of the new DUT on sandpaper and gently sand away the cover to create a flat surface for better thermal conduction. Do not sand away too much material and expose the device inside the packaging.

3. Trim the leads on the DUT to approximately ½ inch in length. Verify the trimmed leads will fit in the center hole of the wire wrap tool. It may be necessary to remove any burrs from the ends of the leads. Remove the DUT from the wire wrap tool.

Wire Wrap Tool
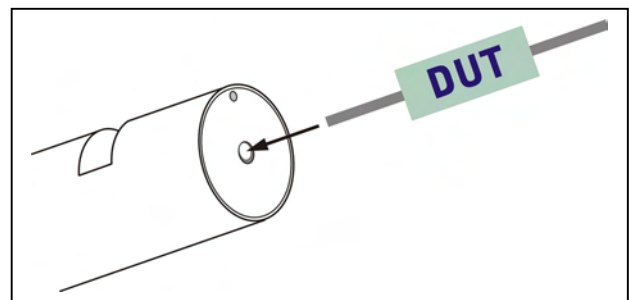
4. Cut two pieces of heavier gauge wire approximately 3 inches in length. Due to the small gauge of the measurement wires, it is necessary to secure the measurement wire to the leads of the DUT using the heavier gauge wire. The heavier gauge wire is only used to physically hold the measurement wires and does not aid in electrical conduction.

5. Gently wrap a measurement wire around a piece of the heavier gauge wire. This will aid in inserting the wires into the wire wrap tool.

6. Insert the wires into the top hole of the wire wrap tool and feed them through until they come out of the notch on the top of the wire wrap tool.
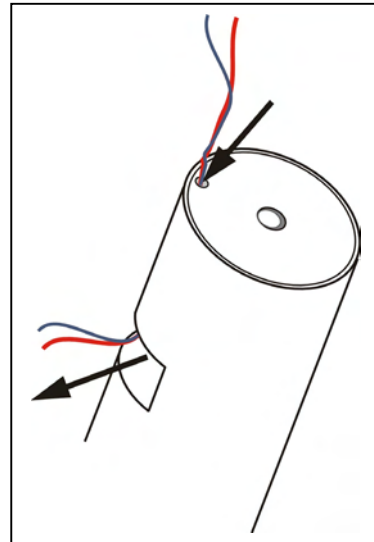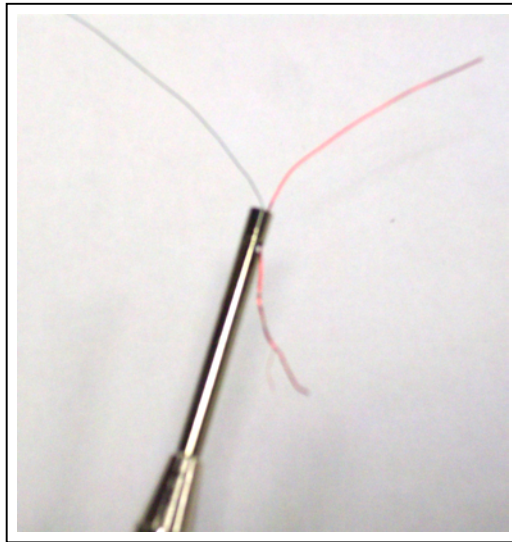
7. Insert the leads of the DUT into the center hole on the wire wrap tool. Firmly hold the wires at the end of the tool and slowly rotate the tool around the DUT lead. The wires fed through the notch at the top of the tool will slowly feed into the tool as it wraps around the leads.
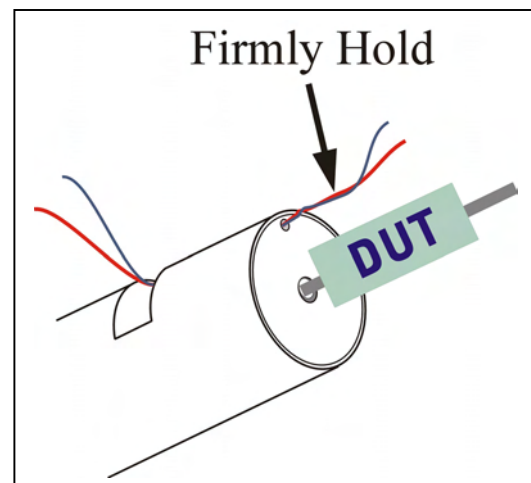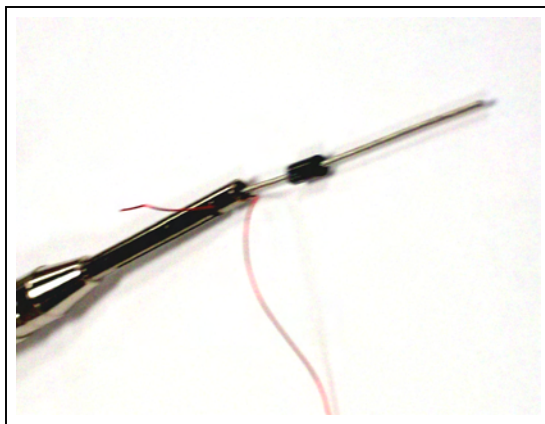
8. Trim the excess heavy gauge wire and DUT leads if necessary. Repeat the wrapping procedure for the second DUT lead.
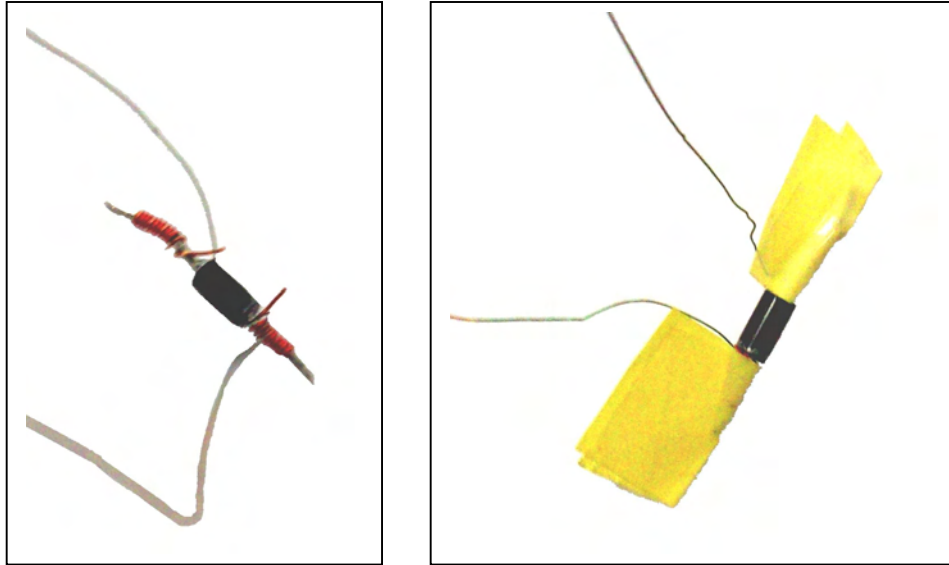

9. Fold a small piece of cryostat tape over the wrapped wire on each side to prevent shorts. Trim any excess tape.

10. Place the DUT in the mounting bracket with the sanded flat against the cold finger. Replace the screws to secure the bracket and device.

11. Test the electrical connection to the device using the Semetrol CV Profile described in the next section.

III. CV Profile – Testing Electrical Connection to DUT

It is recommended that you test the electrical connection to the device after attaching the measurement wires to the DUT leads and after replacing the inner shield.

Open the Semetrol software by clicking on the shortcut on the desktop and click the run button (arrow) on the top left of the toolbar to run the software. The subprograms are positioned on the main menu with data acquisition (measurement) programs on the left side of the menu and data analysis programs on the right side. The simulation programs, IVT and DLTS, are on left and right side respectively.
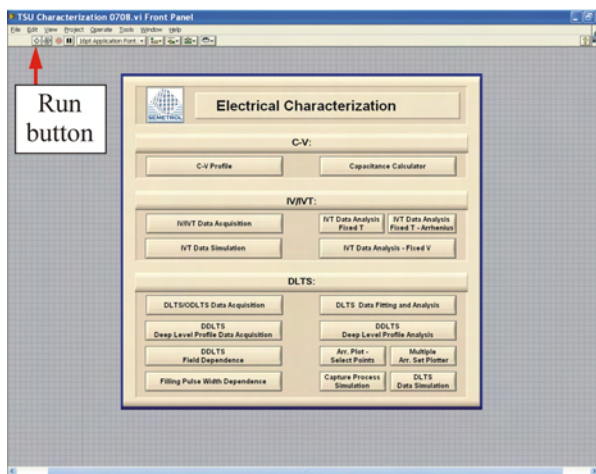
Semetrol software main menu window

Select the "C-V Profile" button on the Semetrol software main menu.
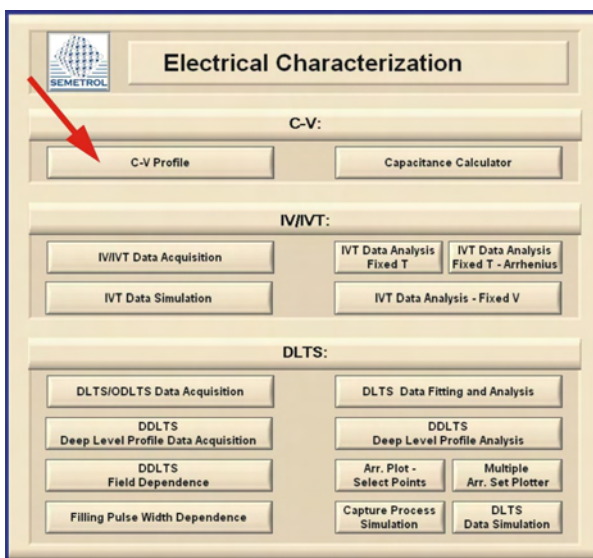
Semetrol software main menu window

The CV Profile window should open. Further analysis of the device can be done using the other tabs in the CV Profile window. However, you can test the electrical connection and correct biasing of the device using the CV Data Acquisition tab.
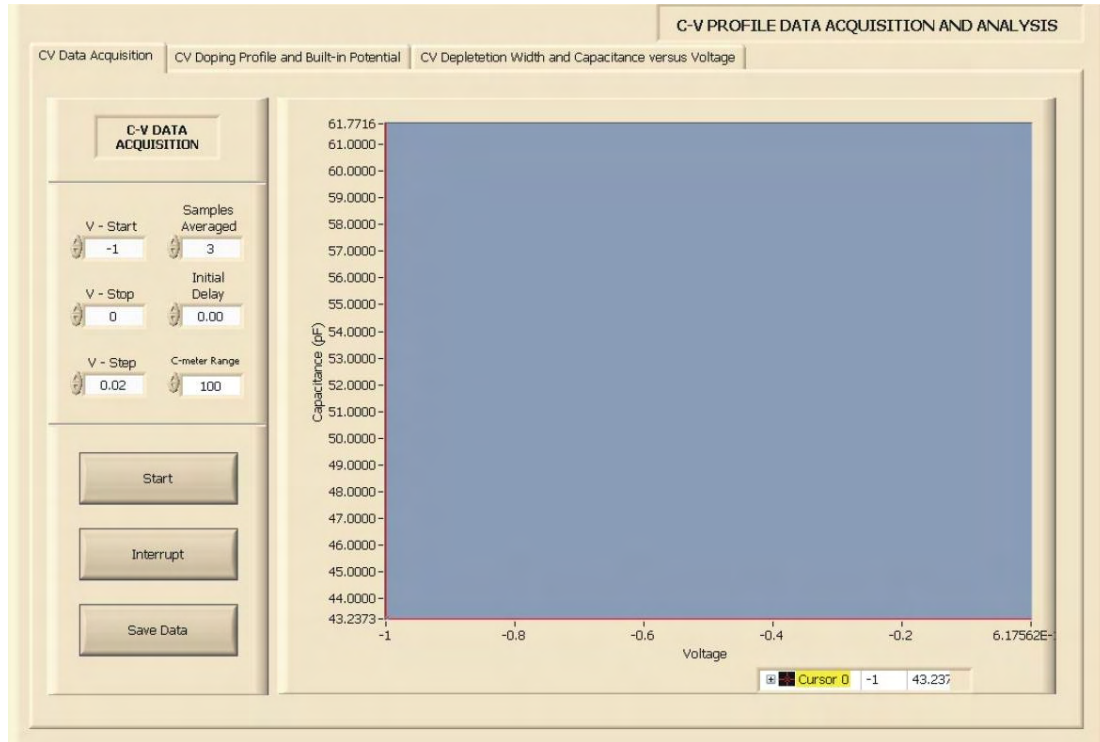

CV Profile window

Input the starting voltage (V-Start), final voltage (V-Stop) and the voltage step (V-step). Input the number of samples to be averaged together (Samples Averaged) and the initial delay time (Initial Delay). Set the C-meter Range to the appropriate setting so that the Digital Panel Meter on the Sula module does not go out of range (> 1.9). The C-meter Range value on the Semetrol software should be set to the same value as the range rotary knob on the Sula capacitance meter panel.

Press the "Start" button on the CV Profile window to begin the CV measurement.

As the bias is increased, a typical CV curve will show a decreasing capacitance corresponding to a widening of the depletion region. The CV curve of the device used in these examples is shown below measured at 1 MHz using the HP4192.
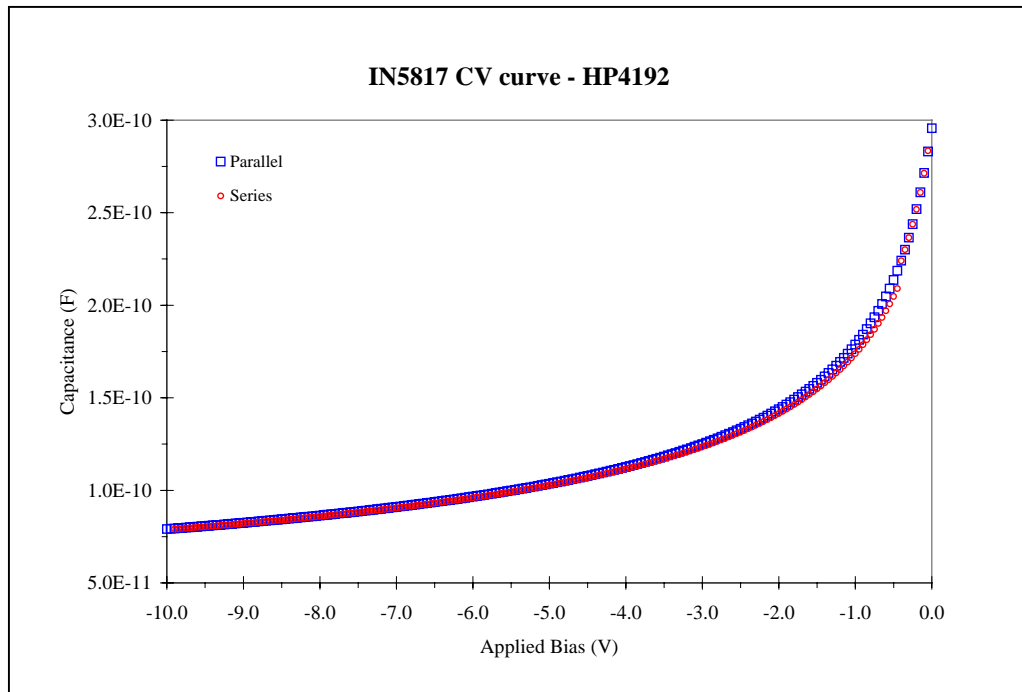
In the CV measurement below, a typical curve is not shown, indicating that the bias may be applied to the wrong side of the device. Flip the connectors to place the diode in reverse bias, if the capacitance increases a function of the bias voltage. This can easily be corrected by switching the cables attached to the square wave pulse on the pulse generator and the "capacitance meter IN" on the Sula module.
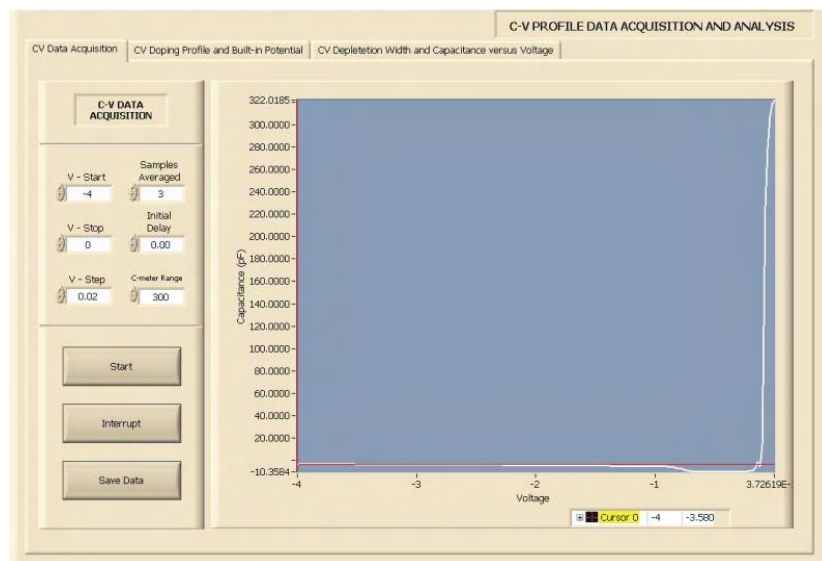
CV measurement – Incorrect bias

After the cables are switched and the CV curve is measured, we obtain the following plot, indicating correct bias of the device.
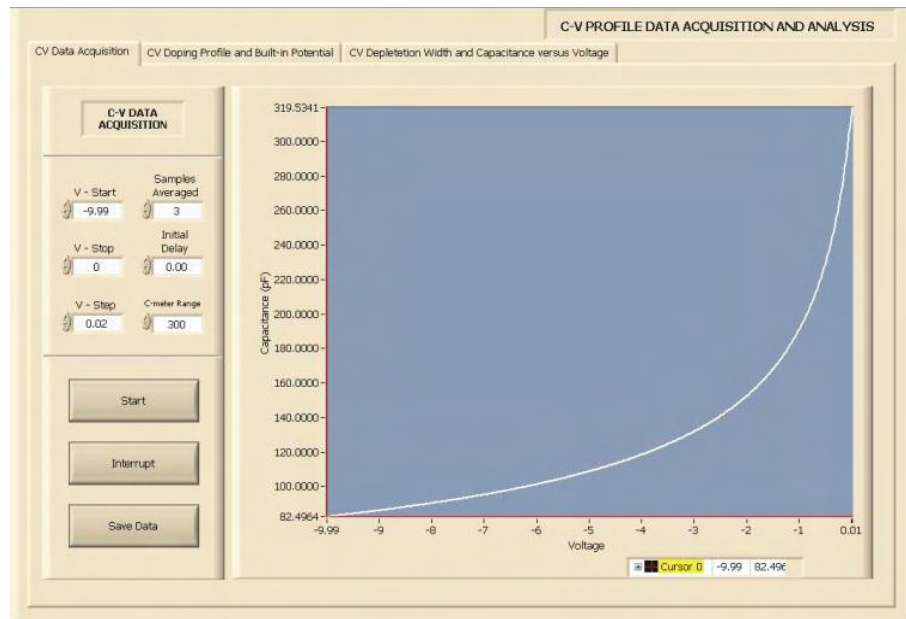
CV measurement – Correct bias (C-meter Range = 300 pF)

As mentioned previously, care should be taken when setting the C-meter Range on the software and Sula module. Below is the CV curve with the range set to 100 pF. Since the Sula module has a maximum DPM value of 1.9, capacitance values exceeding 190 pF causes the meter to overload.
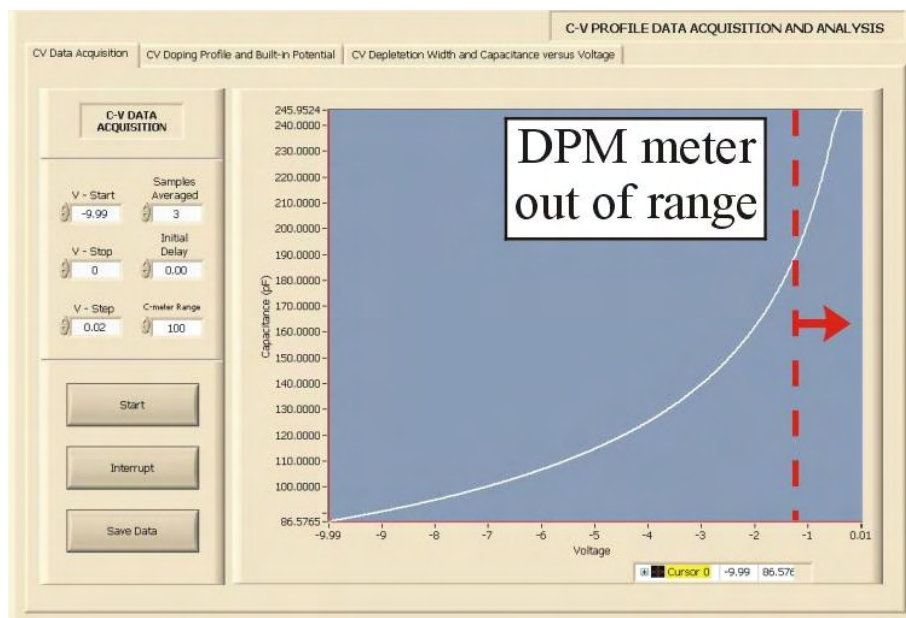
CV measurement – Correct bias (C-meter Range = 100 pF)

It is also possible to have the DPM meter in range, but still get erroneous values if the Semetrol software C-meter range is not set to the same value as the Sula module. In the measurement below the Sula module is set to a range of 300 pF and the software is set to 100 pF. The software records the DPM value x software range setting.
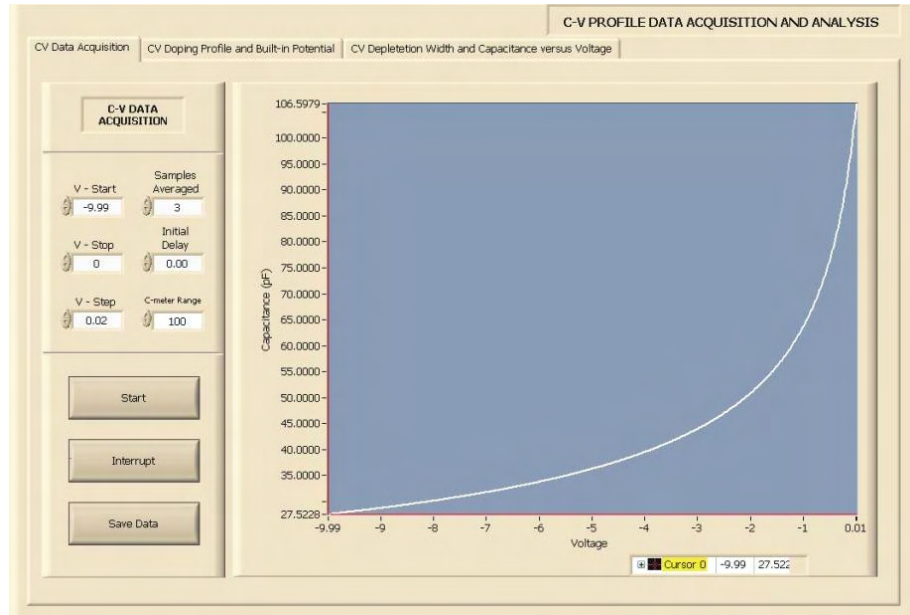
CV measurement – Correct bias
(Sula C-meter Range = 300 pF, Semetrol C-meter Range = 100 pF)

IV. DLTS/ODLTS Data Acquisition

The DLTS/ODLTS Data Acquisition window is used to set up the parameters of a DLTS or optical DLTS (ODLTS) measurement. At the bottom of the window, when the temperature display tab is selected, the temperature of the sample (DUT) and the second stage of the cryostat can be monitored. The second tab at the bottom of the window, control settings, allows the user to vary the parameters (P, I, and D) of the temperature controller and adjust the temperature tolerance and stability count for different temperature intervals.

Select the "DLTS/ODLTS Data Acquisition" button on the Semetrol software main menu.
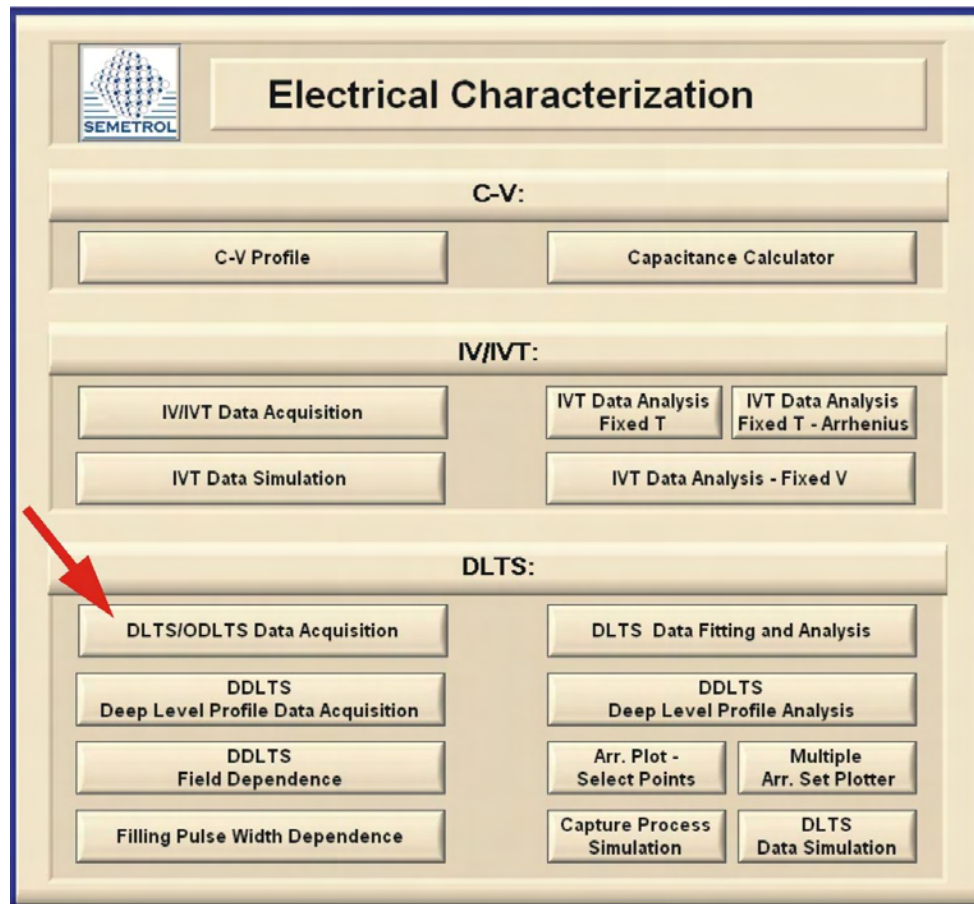
Semetrol software main menu window

The DLTS/ODLTS Data Acquisition window will open up.

DLTS/ODLTS Data Acquisition window

DLTS/ODLTS Data Acquisition window – Control Settings tab

A. The measurement file can be saved by clicking on the file folder icon at the top of the window.   After clicking on the icon, a directory menu will pop up to allow you to specify the location where the measurement file will be saved and to enter the filename. After entering the information, the directory and filename will appear in the small window named "file", to the left of the file folder icon.

B. Bias Parameters: The bias parameters section located at the top right of the window will allow you to set up the voltage parameters of the measurement. If you are performing a DLTS measurement (electrical filling pulse), you will leave the "LED Quiescent" and "LED Pulse" values set to zero. The measurement bias is the voltage at which the capacitance measurement will take place following the filling pulse. The fill bias determines the height of the pulse and should not forward bias the device such that the maximum current (30 mA) is exceeded. Precaution should be taken in selecting the fill bias and measurement bias as not to exceed the maximum value of the DPM (see Appendix B) and to keep leakage current below 100 µA during the measurement bias to prevent overloading the circuit. The meter can tolerate large currents (< 30 mA) during the filling pulse. The pulse width is the duration of the filling pulse in seconds. Following the filling pulse, the capacitance transient will be measured based upon the settings supplied in section C. The traps in the DUT may also be filled by optical stimulation of carriers (ODLTS). The LED Quiescent value is the voltage applied to the LED during the measurement following the filling pulse and the LED pulse value is the voltage applied to the LED during the filling pulse. The duration of the pulse is set by the pulse width value.
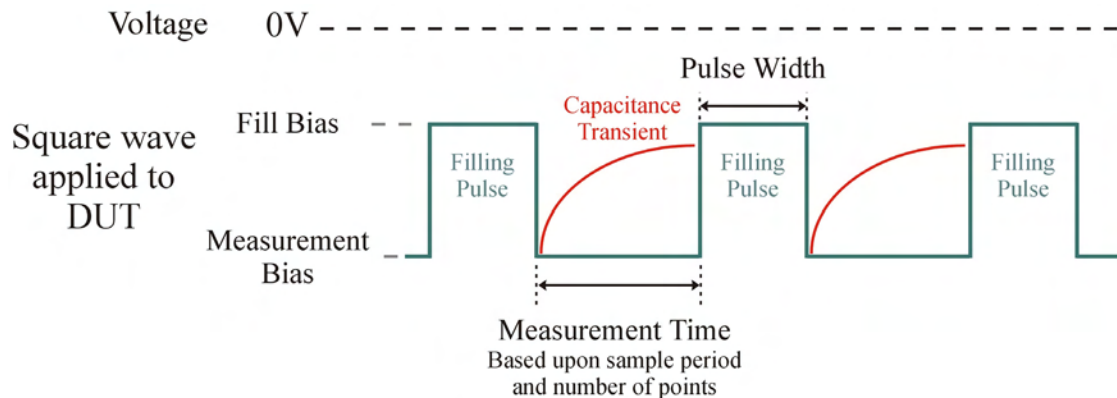
C. Measurement Parameters: The sample period is the time in seconds between each capacitance measurement as the transient decays. The first capacitance measurement is taken at time (3 x sample period) following the filling pulse. The number of points is the number of data points recorded as the transient decays. The duration of the transient that is measured is from (3 x sample period) until (number of points x sample period). The C-meter Range is set to the same value as the rotary selector knob on the Sula module. The No. Tx. Avg. value is number of transients that are averaged together to give the final average transient that is recorded in the measurement file. Increase the No. Tx. Avg. value to minimize the effect of noise on the measurement. The No. Avg. is the counter of the number of transients measured

for computing the average and is determined by the software. This window will flash red as the measurements are in progress and will increment the value after each transient is measured. The value will increase as the measurement progresses until it reaches the value set in the No. Tx. Avg. window, at which time the software will then change the setpoint of the temperature controller and proceed to the next measurement temperature setpoint. The "Start Measurement" button will initiate the measurement conditions determined by the position of the toggle switch to the right, provided the monitor button in the temperature display is off. The toggle switch can be put to "Save Data" or "Test Only". When put in the "Save Data" position, the software will begin the measurement at the initial temperature and continue until the final temperature (specified in section E), saving the measurement data under the filename specified in the file window at the top of the DLTS/ODLTS Data Acquisition window. When the switch is put in the "Test Only" position it will initiate the measurement at the current temperature without changing the parameters of the Lakeshore temperature controller. The measurement will measure the number of transients specified by the No. Tx. Avg. value and then stop.

*After filling pulse*
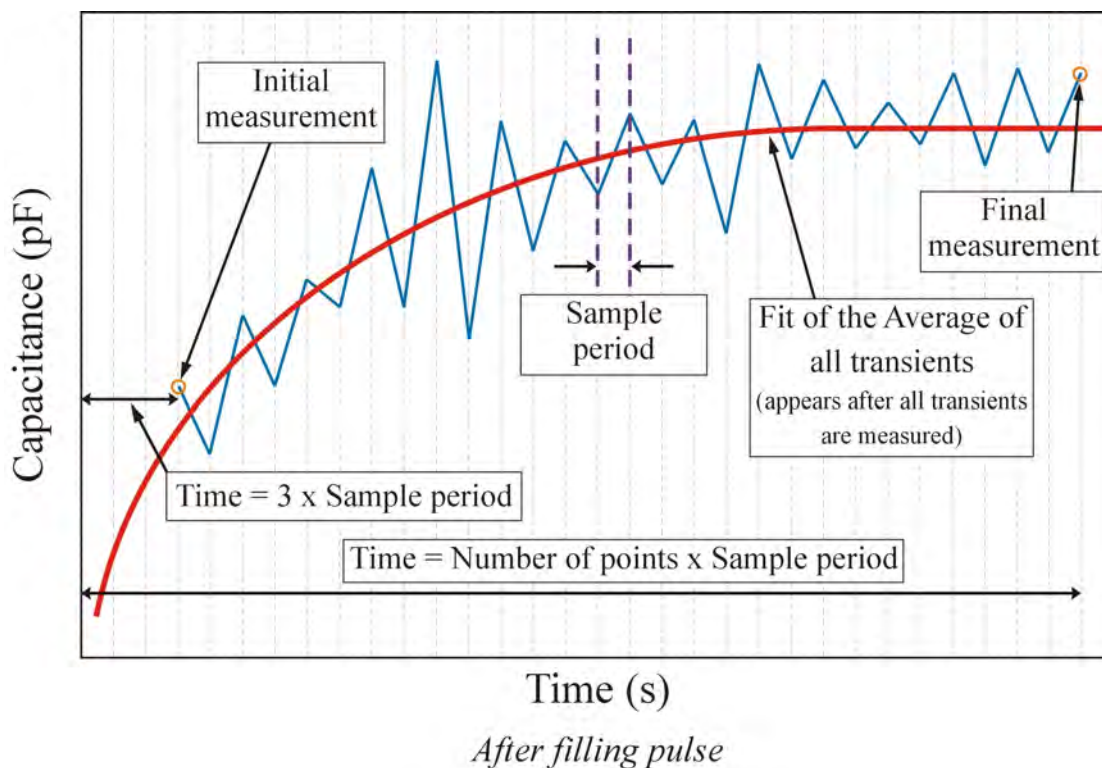
D. Fit Parameters: After all the transients are measured, the fit of the average will appear on the screen as a thin line. The parameters for the fit will appear in the section of the window. When optimizing the measurement settings (pulse width, measurement bias, fill bias, etc.), you want to maximize the NT/Ns value, which is the ratio of the trap density (NT) to background (Ns).

E. Temperature Settings: The only values that you can change in this section are the initial temperature (T Start) and the final temperature of the measurement (T Stop). These two values specify the temperature range over which the measurement will be performed. The remaining values are specified by the table in the temperature controller settings tab (see section G). Under stability count, the left side value is given by the temperature controller settings table and the rights side value is a counter determined by the software. This right side value will increase for each second the sample temperature is within tolerance, until the stability count is reached, at which time the measurement will begin. The right side box will flash red when the temperature is out of tolerance.

Below is an example of the temperature settling on the setpoint. The stability count is incremented when the temperature is within tolerance, as indicated by the circles. For this plot, the count will increment to 20. If the stability count is set to 20, the measurement will begin following the last circle and the temperature controller will continue to try to settle on the temperature setpoint while the measurement is in progress.
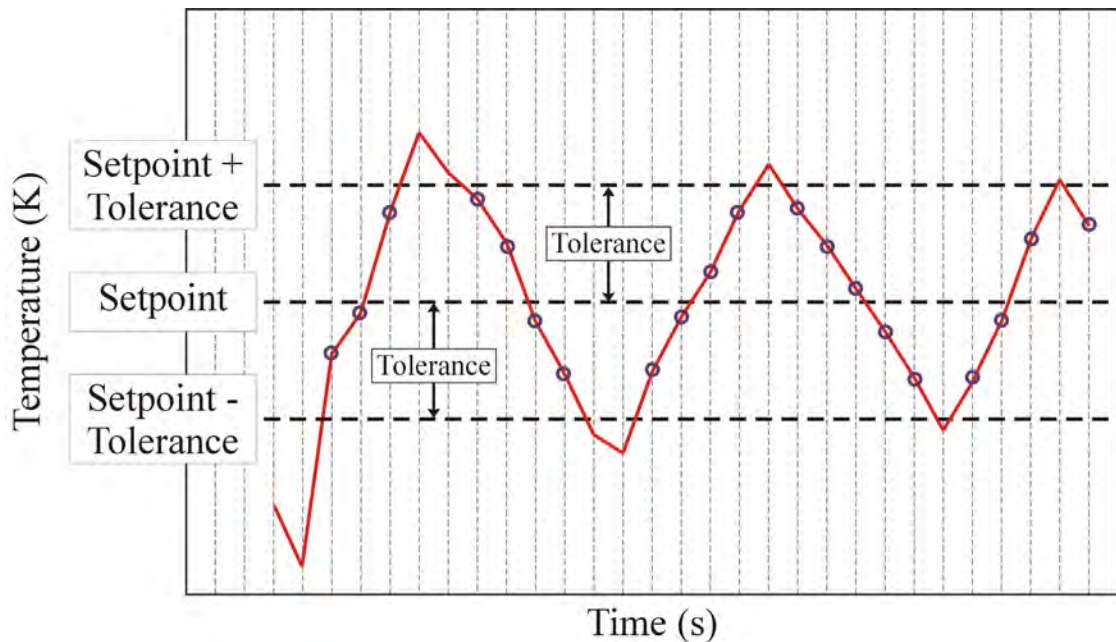
In order to have a stable temperature throughout the measurement, you can increase the stability count. However, this does not guarantee that the temperature is stable. The stability of the temperature is also dependent on the PID settings of the temperature controller. As seen in the following plot, poor PID settings can cause the temperature to oscillate, exceeding the tolerance. In the following plot the stability count will increment to 27 in the same time span as previous plot, but give a less stable temperature.
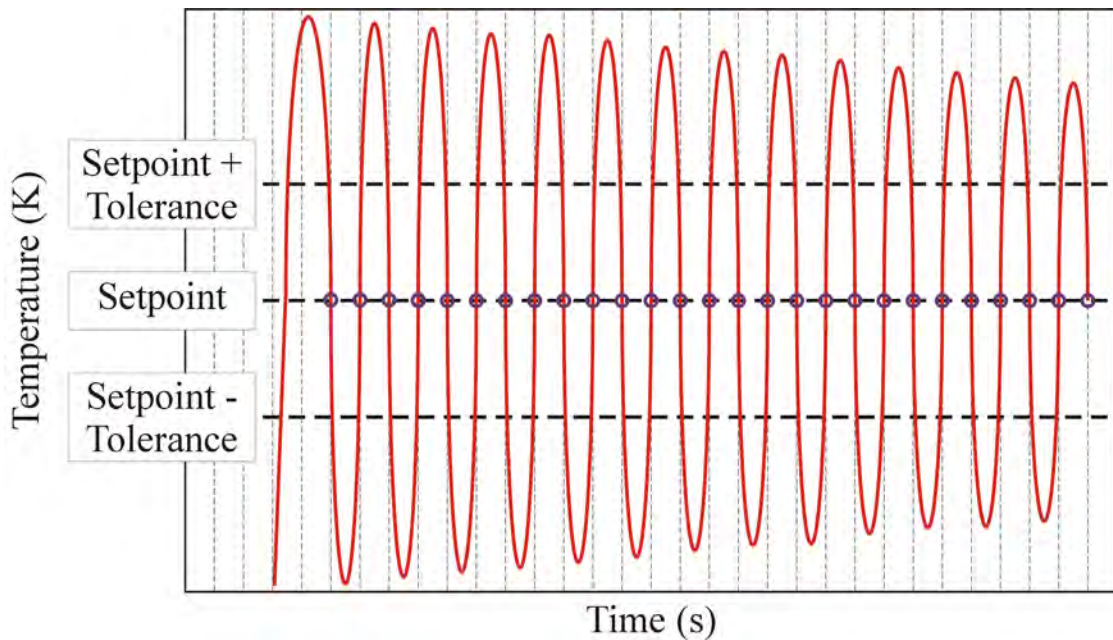
F. Temperature Monitor: In the temperature monitor window, the user can turn the monitor on by clicking the monitor button in the lower right on the section. A scrolling plot of the sample temperature and second stage temperature ("Cold Side") will appear in the window. The temperature scale can by adjusted by right-clicking on the scale and taking it off autoscale. You can then type in new values for the upper or lower limit and the plot will resize itself. The same can be done on the horizontal time axis by highlighting the value of the limits and entering in a new value. When the sample temperature is below the setpoint and the monitor button and heater are on, the heater power will pulse off and on trying to reach the setpoint. Under the same conditions, when the monitor button is off, the heater power will remain on and not pulse. *The monitor button must be off to start a measurement and remain off during the measurement.* During a measurement, the window will only display the sample temperature in the same scrolling fashion as when the monitor button is on. When the stability count is reached on the counter and the measurement of the transients begins, the window stops scrolling and will begin recording the temperature again after all of the transients at that temperature setpoint have been measured. This may appear as small sudden drop or increase in the temperature on the plot. *Although both the sample temperature and cold side temperature curves will appear during the measurement, each curve is a record of the sample temperature.* The numerical values of the setpoint and actual value will appear in the boxes to the right of the plot. The scaling of the axis can be adjusted in the manner previously described.

The two graphs below illustrate the temperature monitoring function. As seen below in the first image, the monitor button is on and both temperatures are displayed as the cryostat cools down to the 0K setpoint.
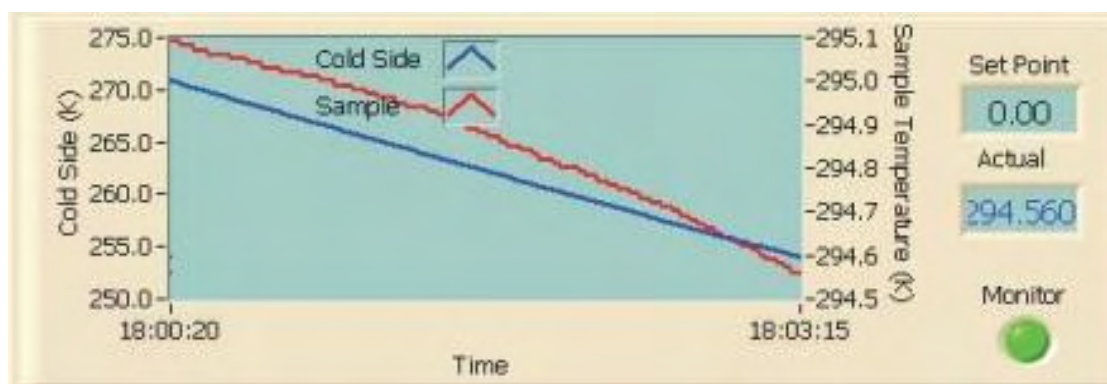

Monitor button - On

During the measurement, only the sample temperature is recorded. In the picture below both curves are displayed, however since the scales are the same (autoscale – on), the two curves fall on top of each other. The two drops in the temperature readings indicate that the transients were measured at 263 and 260K.

Measurement in progress – Monitor button - Off

G. Temperature Controller Settings: The temperature controller settings, tolerance, and stability count can be changed by clicking on the control settings tab at the bottom of the window. The stability settings table should appear. The first column specifies the temperature range in which the setting will be applied. In the table shown, the first row of settings is for temperature range 0 to 20K. Once the temperature exceeds 20K, the second row of settings will be applied. The second column specifies the temperature step size within the range. If the temperature range for the scan was set from 70 to 150K (T Start = 70K, T Stop = 150K), then for the temperature range of 70 to 100K, the transients are measured every 1K. After the transients are measured

at the 100K setpoint, the new setpoint will become 102K and the transients are measured every 2K until the temperature exceeds 132K, at which time step size will become 3K. The PID settings for Lakeshore Temperature controller for each temperature range are taken from the Gain (P), Reset (I) and Rate (D) columns. These values have been optimized for the system and should not be changed. The Heater Range column specifies the range of the current applied the sample heater. This may be set to "Low", "Med" or "High". The temperature controller will apply a percentage (0 to 100%) of the current at the specified range to the heater based upon the temperature setpoint, current temperature and PID settings. The current version of the software will only activate the heater when this is set to "High". When the heater range is set to "High", the Lakeshore temperature controller is sensitive enough to achieve stable temperatures at low temperature setpoints (> 20K). When the heater range is set to "Low" or "Med", there is insufficient power to increase the sample temperature in the higher temperature ranges (ie. > 200K). The temperature tolerance (in Kelvin) and stability count described in section E can be set in columns 5 and 6. The small box to the right of the table ("End Temp") sets the final temperature setpoint after the last measurement is completed. For the picture below, the temperature setpoint will change to 10K after the last measurement is completed. After the measurement is completed, the system will attempt to stabilize the sample temperature at the setpoint and remain at that temperature until attended by the user.
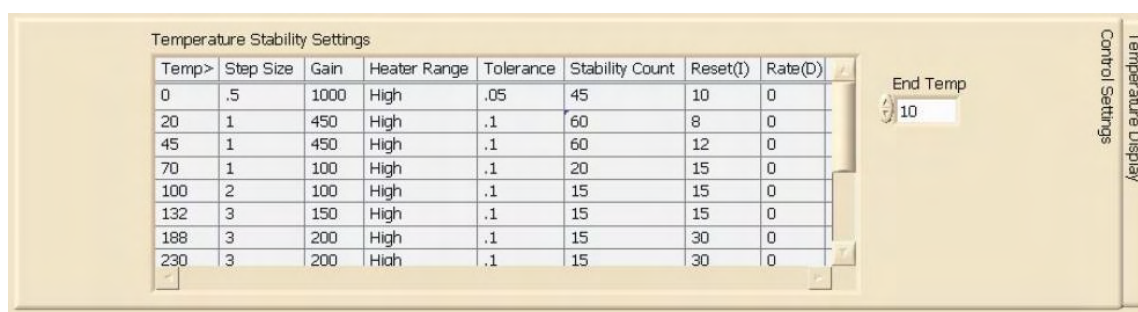
Default Temperature Stability Settings

Temp >	Step size	Gain (P)	Heater Range	Tolerance	Stability Count	Reset (I)	Rate (D)
20	1	450	High	0.05	60	8	0
45	1	450	High	0.05	60	12	0
70	1	100	High	0.05	20	15	0
100	2	150	High	0.05	15	15	0
132	3	150	High	0.05	15	15	0
188	3	200	High	0.05	15	30	0
230	3	200	High	0.05	15	30	0
280	5	200	High	0.05	15	30	0
375	5	150	High	0.05	15	50	0
500	10	150	High	0.05	15	50	0
600	10	150	High	0.05	15	50	0
700	0	0	Off	0	0	0	0

Two examples of the data acquisition screen as a measurement is in progress (325 to 25K) can be seen below. In the first screen, the 27th transient of 50 is shown at the temperature setpoint 257K. The No. Avg box will flash red as the counter increases until after the 50th transient is measured. In the second screen, the final transient (50th) was measured at temperature setpoint 254K. The fit of the average appears as a thin line in the center and the fit parameters of the line appear on the right side of the window. The setpoint has changed to 251K causing the "Actual" temperature box and stability count box to flash red since the current temperature is outside of the tolerance.
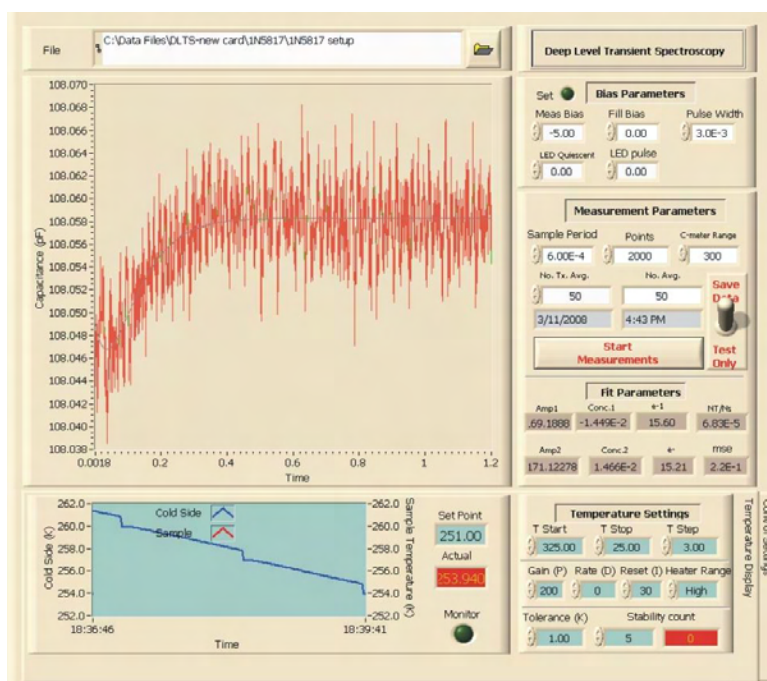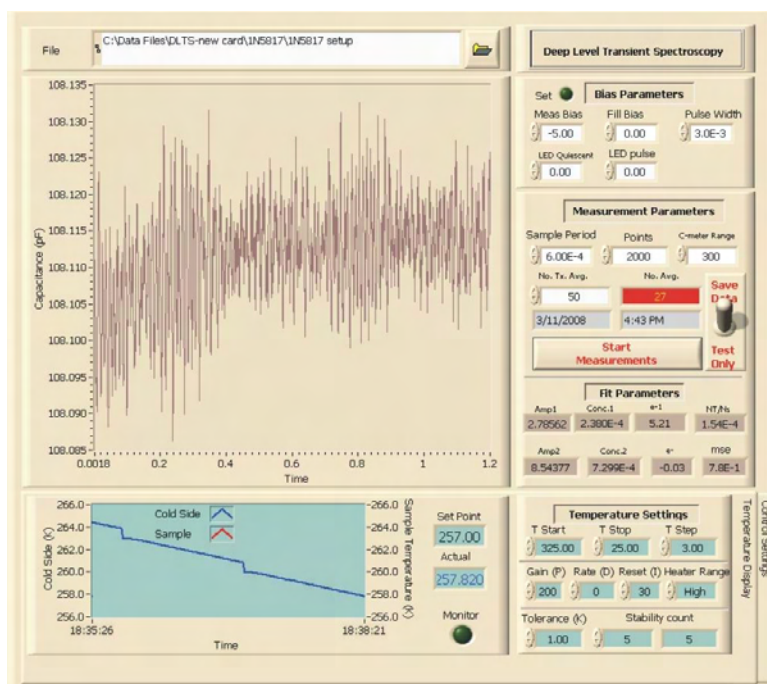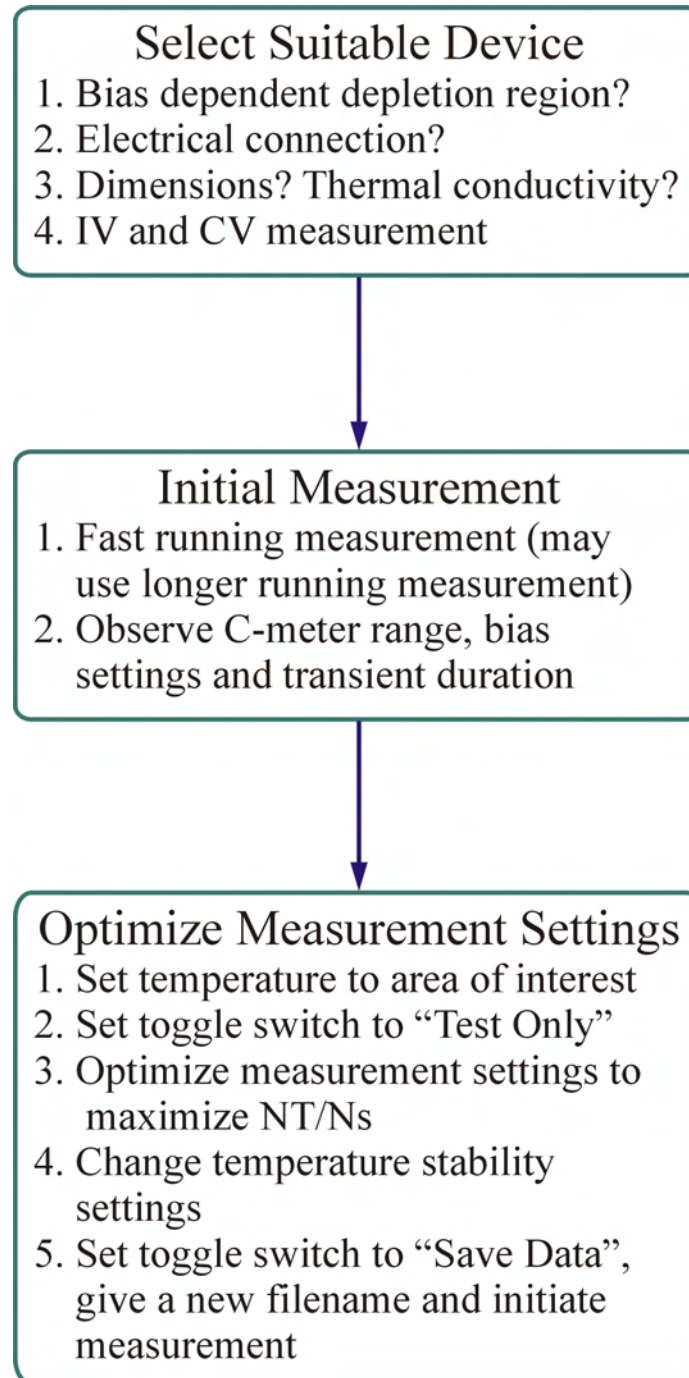
V. DLTS – Measurement Strategy

The following is an outline of the steps used in measuring a device in the DLTS system.

1. Selecting a suitable device:

    A. The device must be able to be biased in such a manner to form a depletion region with a measurable capacitance.

    B. The device must have electrical connections that can easily connect to the measurement wires in the DLTS system and withstand the variation in temperature it will be subjected to in the cryostat. For example, a processed wafer with test structures and 100x100 μm bonding pads is not considered a suitable device, unless the pads are bonded out to larger leads, which may be attached to the measurement wires.

    C. The dimensions of the device must be small enough to fit inside the cryostat inner shield and make good thermal contact with the cold finger.

    D. Electrical measurements (CV and IV) should be performed on the device to ensure the capacitance and leakage current are within acceptable limits for the temperature range of interest. Generally, as the temperature increases, so does the capacitance and leakage current. Measurements performed at room temperature will be valid for lower temperature ranges. The capacitance meter of the Sula module performs the capacitance measurement using a 1MHz signal. The C-meter range can be varied from 10 to 1000 pF, which limits the capacitance from approximately 8 pF to 1900 pF. Smaller capacitances can be measured, but the noise in the measurement will be significant. The maximum acceptable leakage current is limited to 100 μA.

2. Initial measurement: A fast running scan (ie, large tolerance, low stability count, low No. Tx. Avg. value) can be performed to looks for trap signatures in the scan that will later be used to optimize the measurement settings. This will also give you an opportunity to observe the transient measurement and make any necessary corrections to the C-meter range, bias settings and the duration of the transient measurement.

3. Optimize measurement settings: Once the initial measurement is completed, review the measurement data in the ratewindow plot to look for areas of interest (peaks or valleys caused by traps). Set the Lakeshore temperature controller setpoint to the corresponding temperature seen in the ratewindow plot and allow the DUT to stabilize at that temperature. Set the toggle switch in the DLTS/ODLTS Data Acquisition window to "Test Only". Click the "Start Measurement" button to perform the measurement at the current temperature. Adjust the bias and measurement parameters and repeat the measurement to maximize the value in the NT/Ns box. The pulse width (minimum = 0.3 ms) should be increased until all traps are saturated as indicated by no further increase in the Nt/Ns value. Once the settings

are optimized, set the No. Tx. Avg. to an appropriate value. This value can be increased to reduce the influence of noise in the measurement. Set the tolerance and stability count to an appropriate value. Set the initial (T Start) and final (T Stop) temperatures in the temperature settings to the range of interest. Give the file a new name, set the toggle switch to "Save Data" and click the "Start Measurement" button.

Select Suitable Device
1. Bias dependent depletion region?
2. Electrical connection?
3. Dimensions? Thermal conductivity?
4. IV and CV measurement

Initial Measurement
1. Fast running measurement (may use longer running measurement)
2. Observe C-meter range, bias settings and transient duration

Optimize Measurement Settings
1. Set temperature to area of interest
2. Set toggle switch to "Test Only"
3. Optimize measurement settings to maximize NT/Ns
4. Change temperature stability settings
5. Set toggle switch to "Save Data", give a new filename and initiate measurement

VI. Measurement Records

A. Data Logging

The measurement settings can be saved and recalled later in a log file, providing a record of the measurement settings and eliminating the need to re-enter the values.

Saving the data log file

1. Stop the software from running by clicking the stop button in the top left of the window.

2. From the menu bar, select Operate → Data Logging → Log… to save the measurement settings under filename given in the file window.
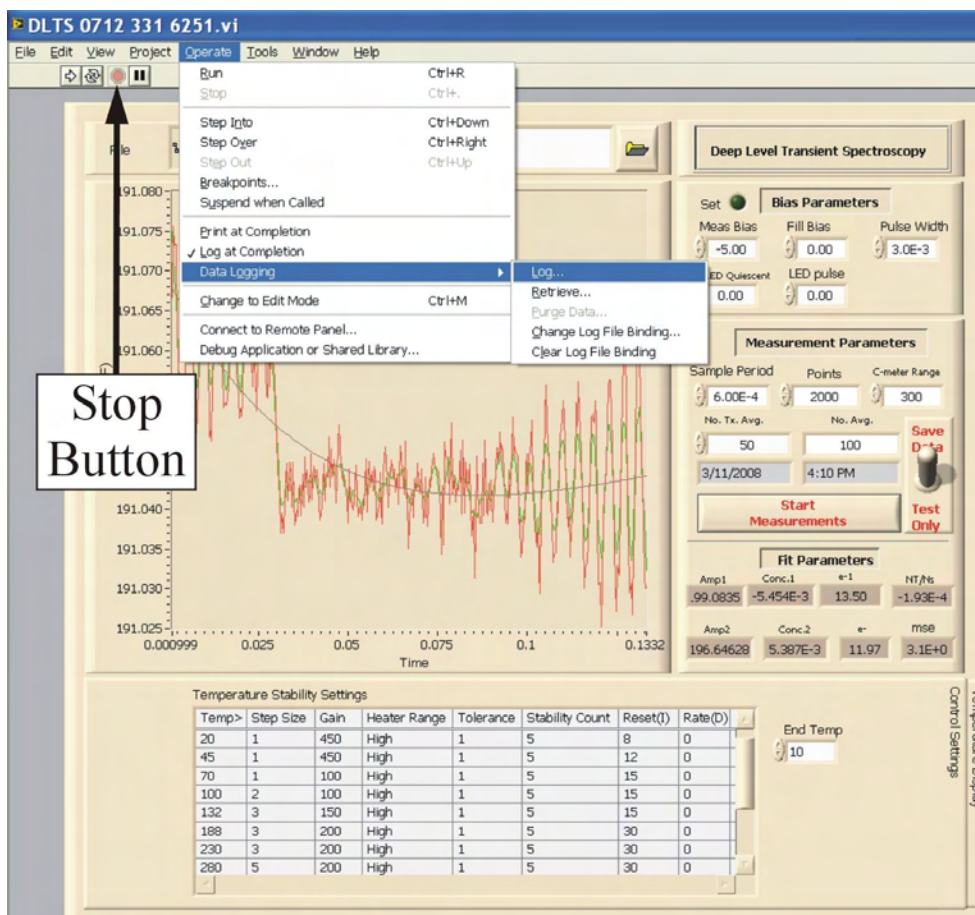
Recalling the data log file

1. Stop the software from running by clicking the stop button in the top left of the window.

2. From the menu bar, select Operate → Data Logging → Retrieve… and a toolbar at the top of the window will appear. Toggle though the saved log files using the arrow keys on the toolbar. Once the appropriate log file is found, it can be loaded by clicking the check mark. Log files may also be deleted clicking the trash can.
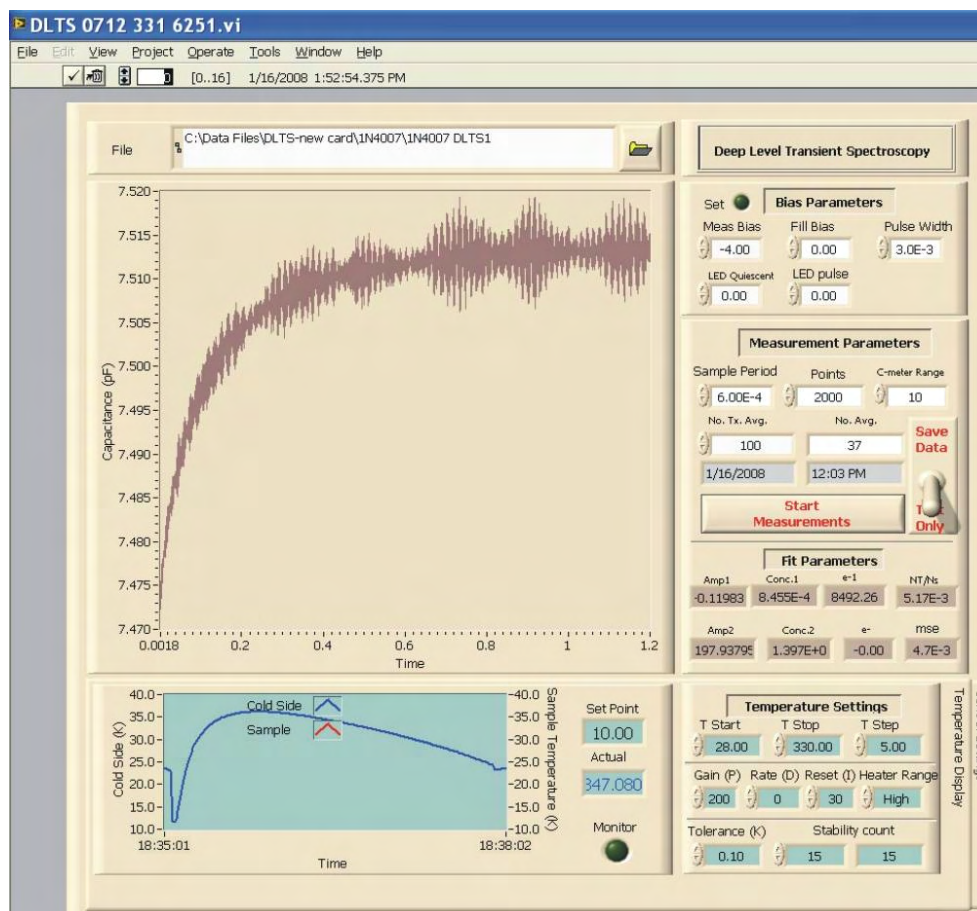
B. Logfile

As the measurement runs, a file of the date, time and measurement parameters is recorded in a file under the name "logXXXX" and is saved in the same directory as the measurement file. For example if the measurement file is saved under the following, "C:\Data Files-DLTS-new card\1N5817\1N5817 measurement", given in the file window at the top of the data acquisition screen, the logfile will be saved in the "C:\Data Files-DLTS-new card\1N5817" directory under the name "log1N5817 measurement". The file is updated and saved following the measurement of the last transient at each temperature setpoint. The date and time (to the minute) recorded in the logfile are the local date and time set in the computer operating system and corresponds to time after the last transient at each temperature setpoint is measured. The logfile can be opened and reviewed using Microsoft Excel and appears as table of values without column headings. An example of a few rows of the logfile is given on the following page with the column headings added.

Date	Time	Measure Bias	Fill Bias	Pulse Width	Led Quiescent	LED Pulse	Sample Period	Points	C-meter Range	No. Tx. Avg.	Sample Temperature	Gain (P)	Reset (I)	Rate (D)	Heater Range	Tolerance	Stability Count
3/12/2008	5:57 PM	-5	-1	3.00E-03	0	0	0.0006	2000	2	250	324.980011	200	30	0	3	0.05	25
3/12/2008	6:05 PM	-5	-1	3.00E-03	0	0	0.0006	2000	2	250	319.970001	200	30	0	3	0.05	25
3/12/2008	6:14 PM	-5	-1	3.00E-03	0	0	0.0006	2000	2	250	314.970001	200	30	0	3	0.05	25
3/12/2008	6:23 PM	-5	-1	3.00E-03	0	0	0.0006	2000	2	250	309.970001	200	30	0	3	0.05	25
3/12/2008	6:31 PM	-5	-1	3.00E-03	0	0	0.0006	2000	2	250	304.959991	200	30	0	3	0.05	25
3/12/2008	6:40 PM	-5	-1	3.00E-03	0	0	0.0006	2000	2	250	299.970001	200	30	0	3	0.05	25
3/12/2008	6:49 PM	-5	-1	3.00E-03	0	0	0.0006	2000	2	250	294.970001	200	30	0	3	0.05	25

C-meter Range

0 = 10 pF
1 = 30 pF
2 = 100 pF
3 = 300 pF
4 = 1000 pF

Heater Range

1 = Low
2 = Medium
3 = High

APPENDIX D

SIMULATION AND DATA ANALYSIS

The simulation portion of the software will generate a data set based on the parameters you give it. This will enable you to work with a data set with known values to become more familiar with the software. You can then open the data set using the DLTS Data Fitting and Analysis and extract the known values (energy, capture cross section, etc.) or see how the various parameters will affect the data. You are limited to simulating two exponentials (two traps) and peaks only.

Open the Semetrol software by clicking on the shortcut on the desktop and click the run button (arrow) on the top left of the toolbar to run the software. The subprograms are positioned on the main menu with data acquisition (measurement) programs on the left side of the menu and data analysis programs on the right side. The simulation programs, IVT and DLTS, are on left and right side respectively.
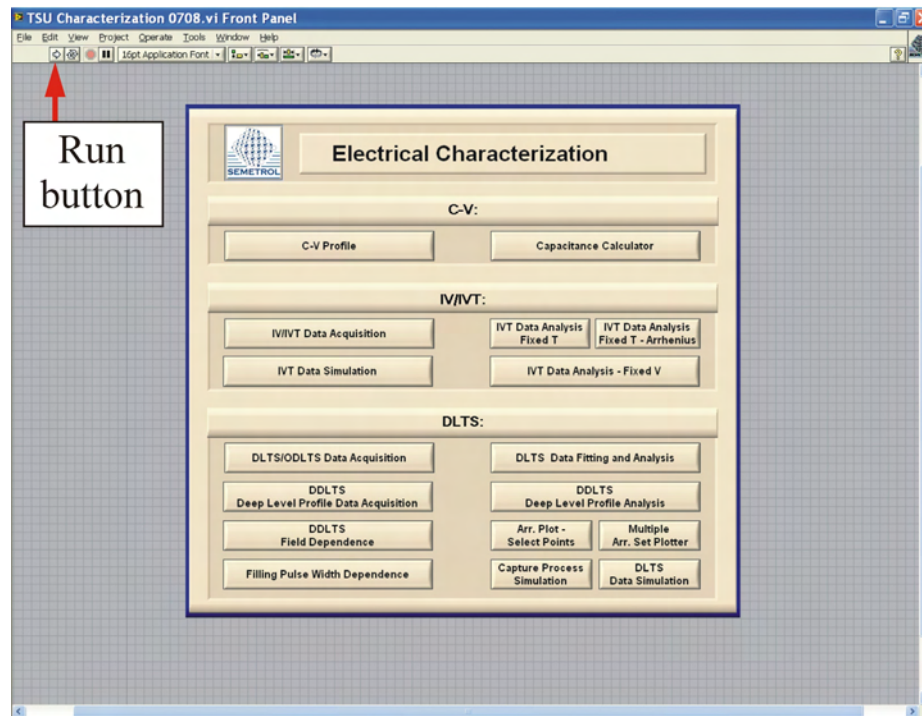
Semetrol software main menu window

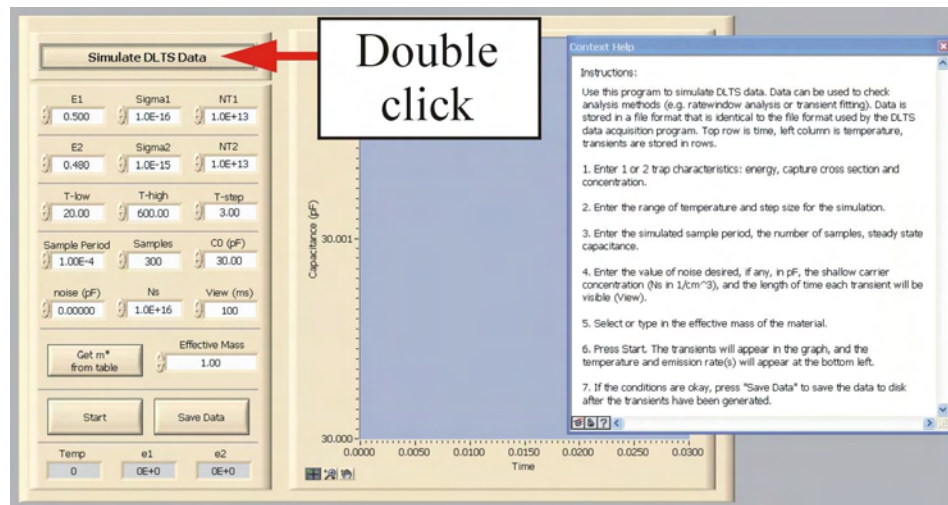## I. DLTS Data Simulation

A. Introduction to the Data Simulation Window

Select the "DLTS Data Simulation" button on the Semetrol software main menu.
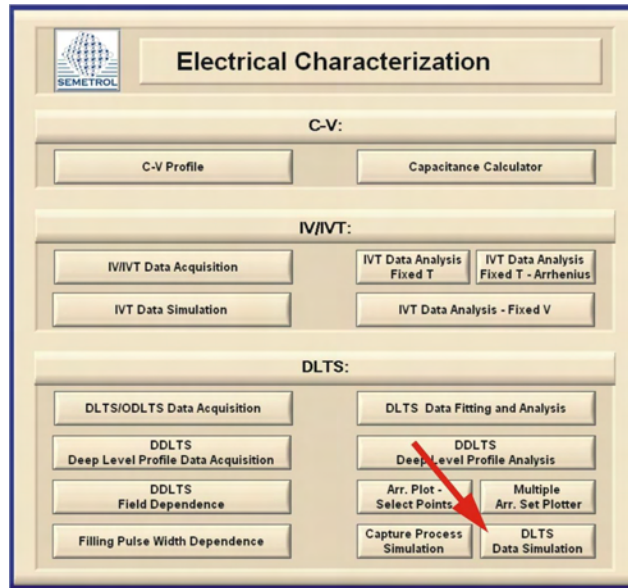
Semetrol software main menu window

The DLTS Data Simulation window should open. The instructions can be opened by clicking the "Simulate DLTS Data" bar.
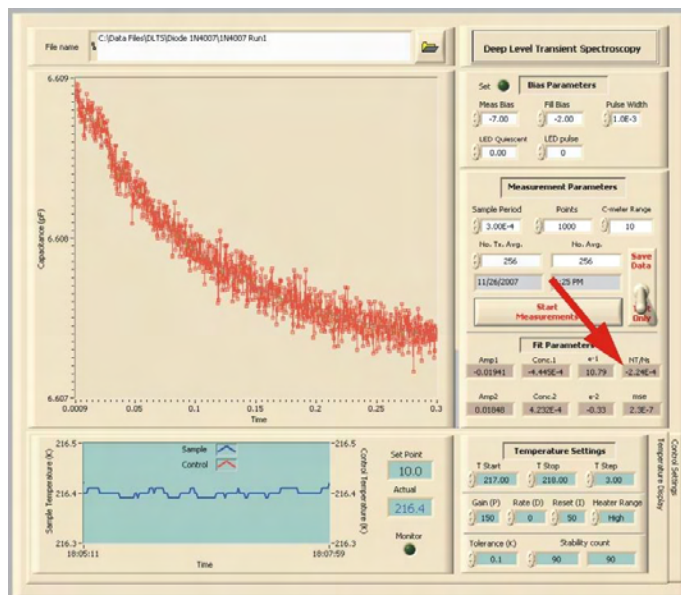

DLTS Data Simulation window

Enter the information for the trap(s) in the spaces provided under the "Simulate DLTS Data" bar.

Input the trap information (energy [eV] (E1)), capture cross section [cm^2] (Sigma1), and trap density [cm^{-3}] (NT1)). If you wish to simulate two traps then add the information for the second trap (E2, Sigma2, NT2).

Input the temperature range for the scan and the step information.

Input the sample period, number of samples, and the steady state capacitance (C0(pF)) in picofarads.

Input the noise level if any. *It is recommended that you begin working with the noise level set to zero.* Set the shallow level carrier concentration (Ns) and the length that each transient is visible (view (ms)). To estimate the shallow level carrier concentration, the ratio of the shallow level carrier concentration (Ns) and the trap density (NT) can be determined from the DLTS/ODLTS Data Acquisition window (NT/Ns) for the various traps.

NT/Ns from the DLTS/ODLTS Data Acquisition window

Input the effective mass.

Press the "Start" button on the DLTS Data Simulation window to begin the simulation. If you are satisfied with the results, you can then click the "Save Data" button and give the filename to save the data under. This file can later be opened using the DLTS Data Fitting and Analysis window.
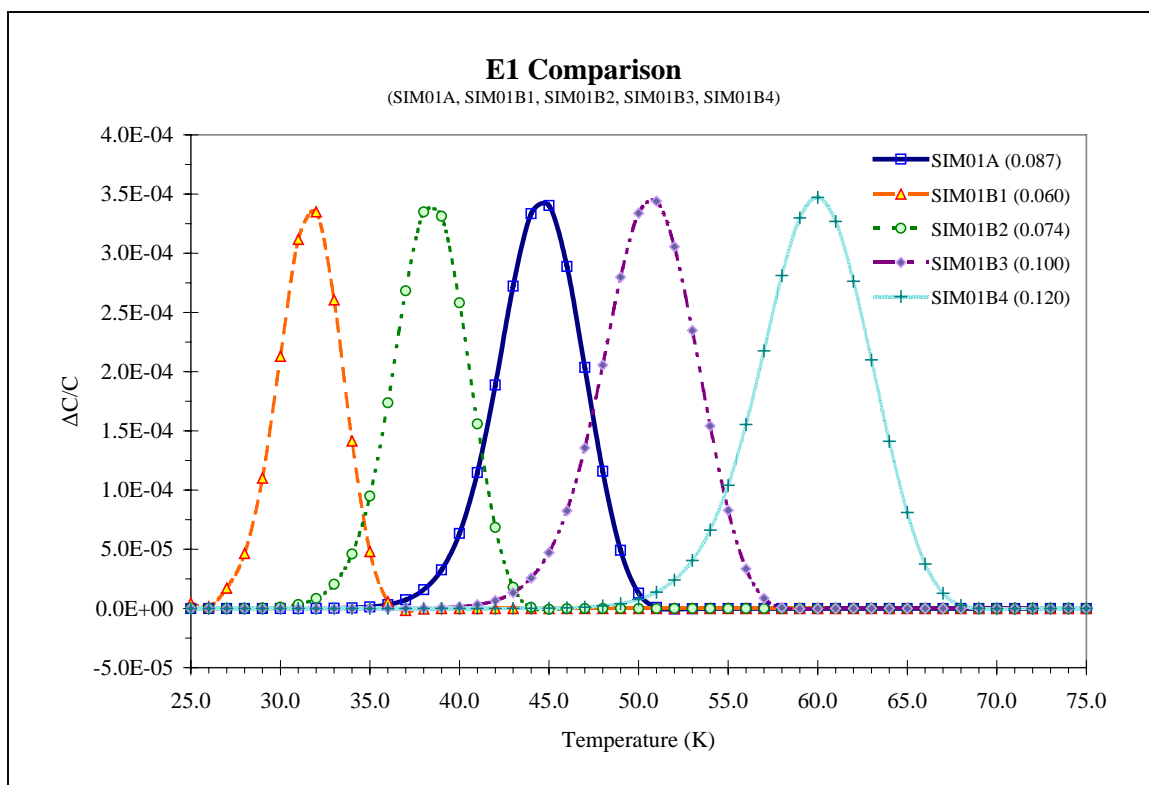
B. Comparison of resulting rate window plots for varying parameters – One trap

The following simulations show the resulting ratewindow generated by the DLTS Data Fitting and Analysis for one trap (E2 = 0, Sigma2 = 0, NT2 = 0). Simulations with a varying parameter are plotted together for comparison. The parameters of each simulation are listed in the table accompanying each plot. The variation in the parameters may be identified by the comment in the table. The varying parameter is on the plot title and the values are listed in the legend for each plot. Each simulation uses the same ratewindow (t_1 = 0.100 / t_2 = 1.0026).

1. E1 Comparison

2. Sigma1 Comparison

3. NT1 Comparison

4. Effective Mass Comparison

5. Noise Level Comparison for C0 = 10 pF

6. Noise Level Comparison for C0 = 100 pF

7. Noise Level Comparison for C0 = 1000 pF

8. C0 Comparison without noise, C0 = 10, 100, 1000 pF

1. E1 Comparison

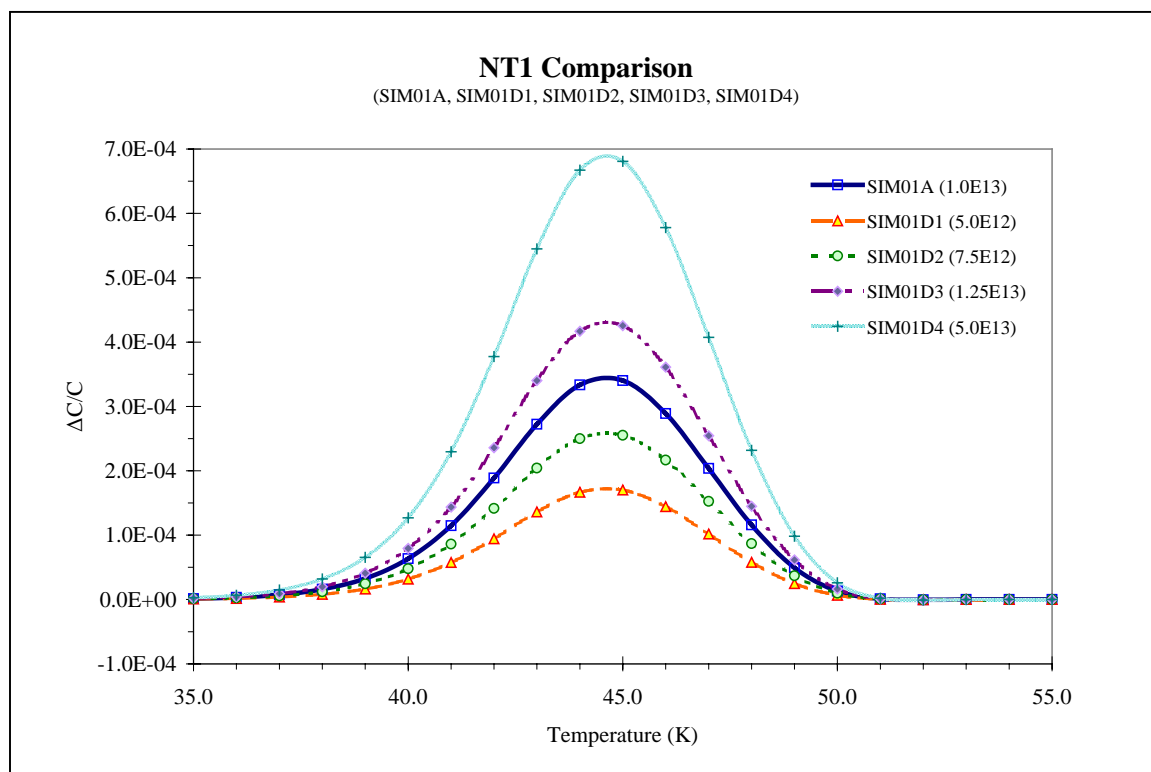| Filename:	SIM01A	SIM01B1	SIM01B2	SIM01B3	SIM01B4
Comments:	Standard - 10 pF	E1 = 0.060	E1 = 0.074	E1 = .100	E1 = .120
Parameter					
E1 (eV)	0.087	0.06	0.074	0.100	0.120
Sigma1 (cm^2)	2.50E-15	2.50E-15	2.50E-15	2.50E-15	2.50E-15
NT1 (cm^{-3})	1.00E+13	1.00E+13	1.00E+13	1.00E+13	1.00E+13
E2 (eV)	0.00	0.00	0.00	0.00	0.00
Sigma2 (cm^2)	0.00	0.00	0.00	0.00	0.00
NT2 (cm^{-3})	0.00	0.00	0.00	0.00	0.00
T-low (K)	25.00	25.00	25.00	25.00	25.00
T-high (K)	121.00	121.00	121.00	121.00	121.00
T-step (K)	1.00	1.00	1.00	1.00	1.00
Sample Period (s)	6.00E-04	6.00E-04	6.00E-04	6.00E-04	6.00E-04
Samples	2000	2000	2000	2000	2000
C0(pF)	10.00	10.00	10.00	10.00	10.00
Noise (pF)	0.00	0.00	0.00	0.00	0.00
Ns	1.00E+16	1.00E+16	1.00E+16	1.00E+16	1.00E+16
View (ms)	1200	1200	1200	1200	1200
Effective Mass	1.07	1.07	1.07	1.07	1.07

E1 Comparison
(SIM01A, SIM01B1, SIM01B2, SIM01B3, SIM01B4)

As seen on the graph as the energy of the trap increases, the peak position corresponds to a higher temperature.

2. Sigma1 Comparison

Filename:	SIM01C1	SIM01C2	SIM01C3	SIM01C4	SIM01C5
Comments:	Sigma1 = 1.0E-14	Sigma1 = 5.0E-14	Sigma1 = 7.5E-14	Sigma1 = 1.0E-15	Sigma1 = 4.0E-15
Parameter					
E1 (eV)	0.087	0.087	0.087	0.087	0.087
Sigma1 (cm^2)	1.00E-14	5.00E-14	7.50E-14	1.00E-15	4.00E-15
NT1 (cm^{-3})	1.00E+13	1.00E+13	1.00E+13	1.00E+13	1.00E+13
E2 (eV)	0.00	0.00	0.00	0.00	0.00
Sigma2 (cm^2)	0.00	0.00	0.00	0.00	0.00
NT2 (cm^{-3})	0.00	0.00	0.00	0.00	0.00
T-low (K)	25.00	25.00	25.00	25.00	25.00
T-high (K)	121.00	121.00	121.00	121.00	121.00
T-step (K)	1.00	1.00	1.00	1.00	1.00
Sample Period (s)	6.00E-04	6.00E-04	6.00E-04	6.00E-04	6.00E-04
Samples	2000	2000	2000	2000	2000
C0(pF)	10.00	10.00	10.00	10.00	10.00
Noise (pF)	0.00	0.00	0.00	0.00	0.00
Ns	1.00E+16	1.00E+16	1.00E+16	1.00E+16	1.00E+16
View (ms)	1200	1200	1200	1200	1200
Effective Mass	1.07	1.07	1.07	1.07	1.07

Filename:	SIM01C6	SIM01C7	SIM01C8	SIM01C9
Comments:	Sigma1 = 5.0E-15	Sigma1 = 7.5E-15	Sigma1 = 1.0E-16	Sigma1 = 1.5E-16
Parameter				
E1 (eV)	0.087	0.087	0.087	0.087
Sigma1 (cm^2)	5.00E-15	7.50E-15	1.00E-16	1.50E-16
NT1 (cm^{-3})	1.00E+13	1.00E+13	1.00E+13	1.00E+13
E2 (eV)	0.00	0.00	0.00	0.00
Sigma2 (cm^2)	0.00	0.00	0.00	0.00
NT2 (cm^{-3})	0.00	0.00	0.00	0.00
T-low (K)	25.00	25.00	25.00	25.00
T-high (K)	121.00	121.00	121.00	121.00
T-step (K)	1.00	1.00	1.00	1.00
Sample Period (s)	6.00E-04	6.00E-04	6.00E-04	6.00E-04
Samples	2000	2000	2000	2000
C0(pF)	10.00	10.00	10.00	10.00
Noise (pF)	0.00	0.00	0.00	0.00
Ns	1.00E+16	1.00E+16	1.00E+16	1.00E+16
View (ms)	1200	1200	1200	1200
Effective Mass	1.07	1.07	1.07	1.07

As the capture cross section (σ) decreases, the peak position shifts to a higher temperature and becomes slightly wider.

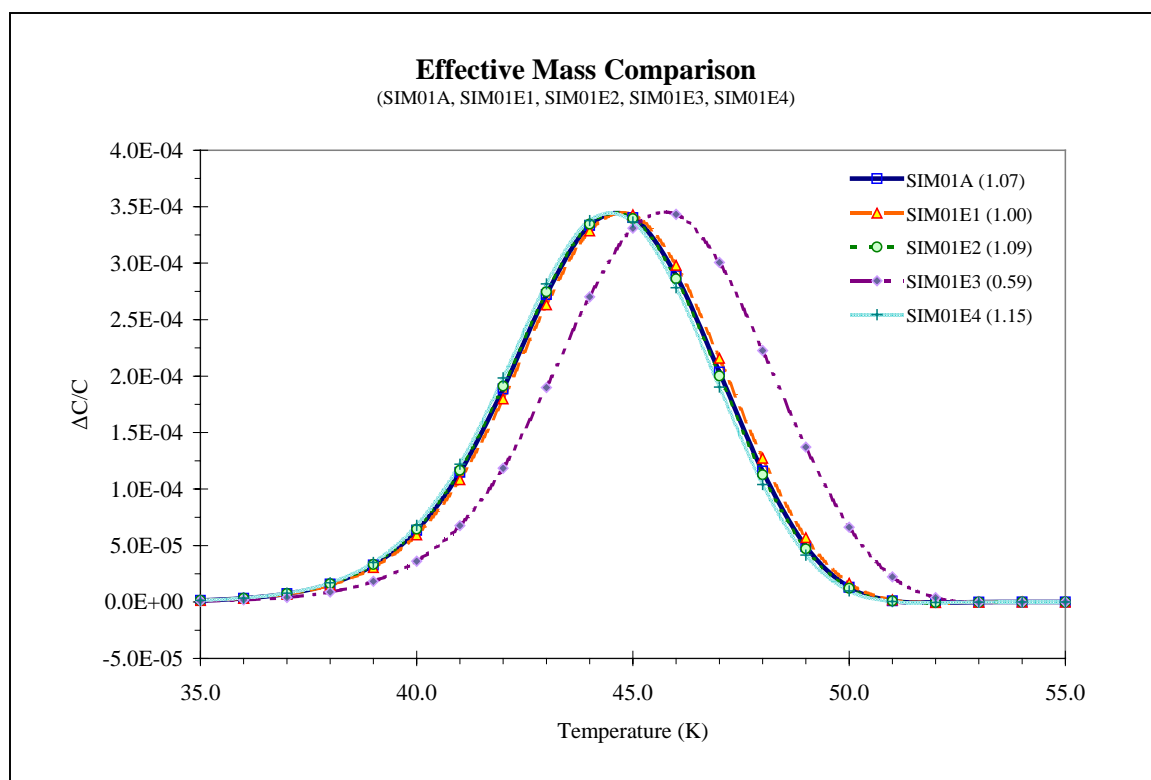**Sigma1 Comparison**
(SIM01A, SIM01C1, SIM01C2, SIM01C3, SIM01C4, SIM01C5, SIM01C6, SIM01C7, SIM01C8, SIM01C9)
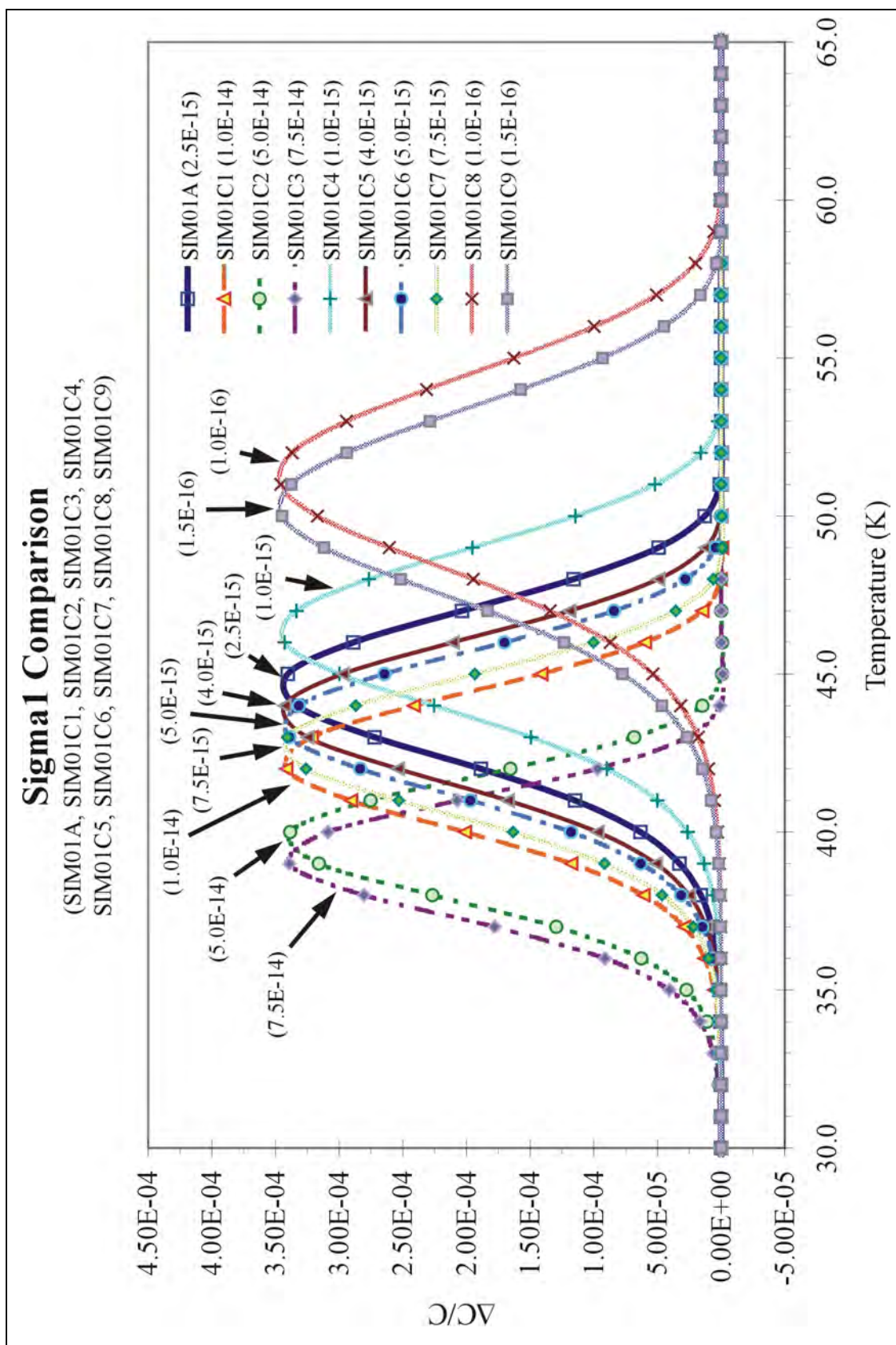
3. NT1 Comparison

| Filename:	**SIM01D1**	**SIM01D2**	**SIM01D3**	**SIM01D4**
Comments:	NT1 = 5.00E+12	NT1 = 7.50E+12	NT1 = 1.25E+13	NT1 = 5.00E+13
Parameter				
E1 (eV)	0.087	0.087	0.087	0.087
Sigma1 (cm^2)	2.50E-15	2.50E-15	2.50E-15	2.50E-15
NT1 (cm^{-3})	5.00E+12	7.50E+12	1.25E+13	5.00E+13
E2 (eV)	0.00	0.00	0.00	0.00
Sigma2 (cm^2)	0.00	0.00	0.00	0.00
NT2 (cm^{-3})	0.00	0.00	0.00	0.00
T-low (K)	25.00	25.00	25.00	25.00
T-high (K)	121.00	121.00	121.00	121.00
T-step (K)	1.00	1.00	1.00	1.00
Sample Period (s)	6.00E-04	6.00E-04	6.00E-04	6.00E-04
Samples	2000	2000	2000	2000
C0(pF)	10.00	10.00	10.00	10.00
Noise (pF)	0.00	0.00	0.00	0.00
Ns	1.00E+16	1.00E+16	1.00E+16	1.00E+16
View (ms)	1200	1200	1200	1200
Effective Mass	1.07	1.07	1.07	1.07

NT1 Comparison
(SIM01A, SIM01D1, SIM01D2, SIM01D3, SIM01D4)

The height of the peak increases with trap concentration.

4. Effective Mass Comparison

Filename:	SIM01E1	SIM01E2	SIM01E3	SIM01E4
Comments:	Eff Mass = 1.00	Eff Mass = 1.09	Eff Mass = 0.59	Eff Mass = 1.15
Parameter				
E1 (eV)	0.087	0.087	0.087	0.087
Sigma1 (cm^2)	2.50E-15	2.50E-15	2.50E-15	2.50E-15
NT1 (cm^{-3})	1.00E+13	1.00E+13	1.00E+13	1.00E+13
E2 (eV)	0.00	0.00	0.00	0.00
Sigma2 (cm^2)	0.00	0.00	0.00	0.00
NT2 (cm^{-3})	0.00	0.00	0.00	0.00
T-low (K)	25.00	25.00	25.00	25.00
T-high (K)	121.00	121.00	121.00	121.00
T-step (K)	1.00	1.00	1.00	1.00
Sample Period (s)	6.00E-04	6.00E-04	6.00E-04	6.00E-04
Samples	2000	2000	2000	2000
C0(pF)	10.00	10.00	10.00	10.00
Noise (pF)	0.00	0.00	0.00	0.00
Ns	1.00E+16	1.00E+16	1.00E+16	1.00E+16
View (ms)	1200	1200	1200	1200
Effective Mass	1.00	1.09	0.59	1.15

Effective Mass Comparison
(SIM01A, SIM01E1, SIM01E2, SIM01E3, SIM01E4)

5. Noise Level Comparison for C0 = 10 pF

| Filename:	SIM01F1	SIM01F2	SIM01F3	SIM01F4	SIM01F5
Comments:	Noise = 0.01 pF	Noise = 0.005 pF	Noise = 0.001 pF	Noise = 0.0005 pF	Noise = 0.0001 pF
Parameter					
E1 (eV)	0.087	0.087	0.087	0.087	0.087
Sigma1 (cm^2)	2.50E-15	2.50E-15	2.50E-15	2.50E-15	2.50E-15
NT1 (cm^{-3})	1.00E+13	1.00E+13	1.00E+13	1.00E+13	1.00E+13
E2 (eV)	0.00	0.00	0.00	0.00	0.00
Sigma2 (cm^2)	0.00	0.00	0.00	0.00	0.00
NT2 (cm^{-3})	0.00	0.00	0.00	0.00	0.00
T-low (K)	25.00	25.00	25.00	25.00	25.00
T-high (K)	121.00	121.00	121.00	121.00	121.00
T-step (K)	1.00	1.00	1.00	1.00	1.00
Sample Period (s)	6.00E-04	6.00E-04	6.00E-04	6.00E-04	6.00E-04
Samples	2000	2000	2000	2000	2000
C0(pF)	10.00	10.00	10.00	10.00	10.00
Noise (pF)	0.01	0.005	0.001	0.0005	0.0001
Ns	1.00E+16	1.00E+16	1.00E+16	1.00E+16	1.00E+16
View (ms)	1200	1200	1200	1200	1200
Effective Mass	1.07	1.07	1.07	1.07	1.07

Noise Level Comparison for C0 = 10 pF
(SIM01A, SIM01F1, SIM01F2, SIM01F3, SIM01F4)
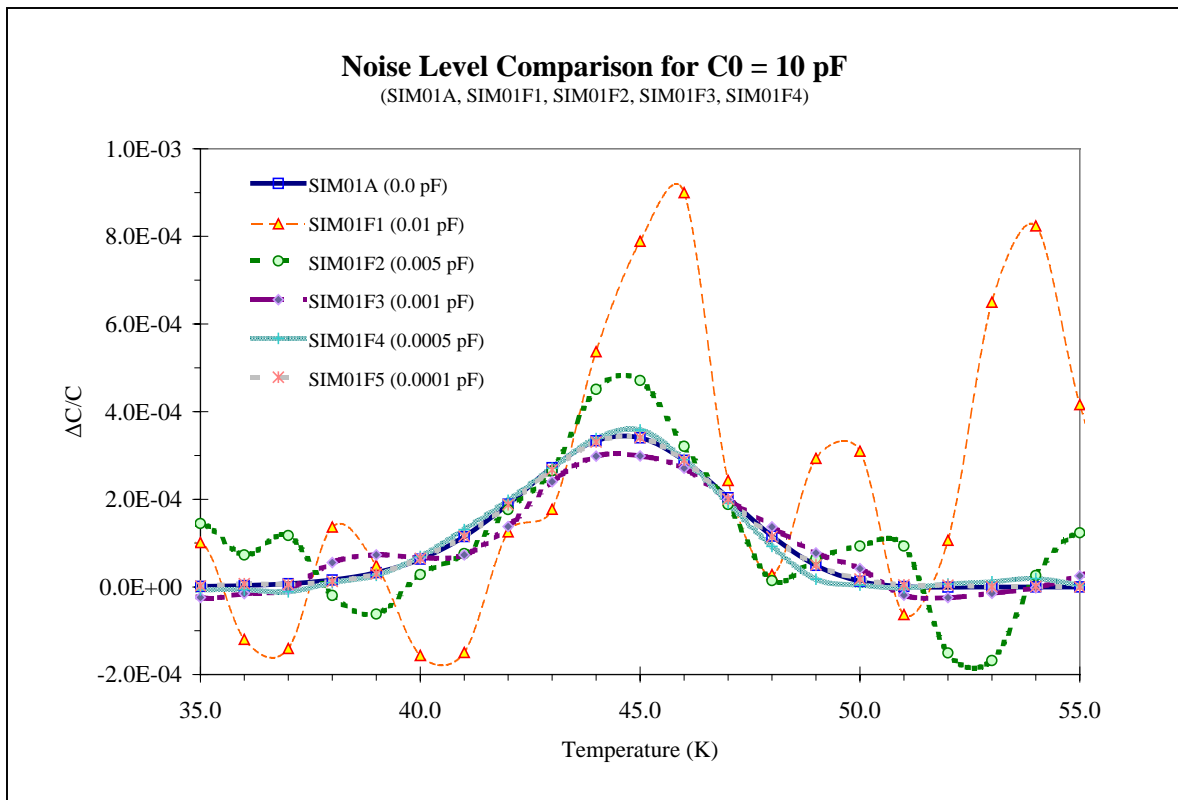
6. Noise Level Comparison for C0 = 100 pF

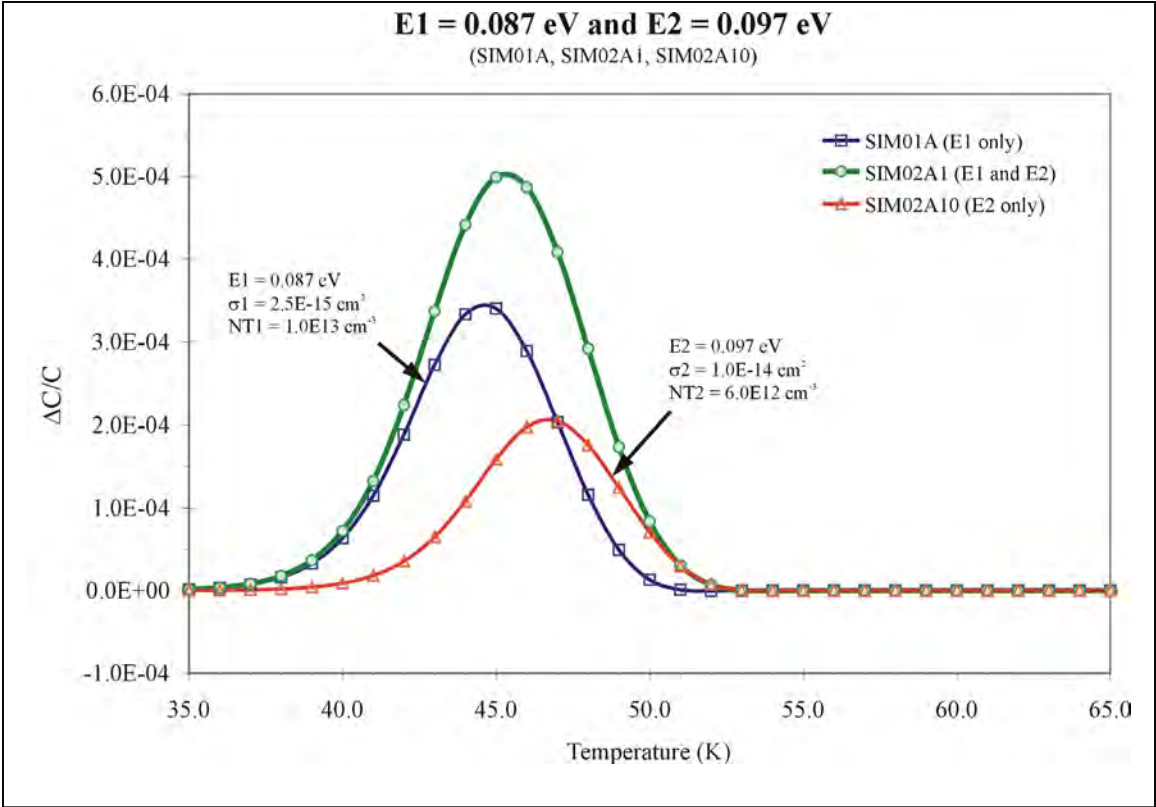| Filename:	SIM01G1	SIM01G2	SIM01G3	SIM01G4
Comments:	Standard - 100 pF	Standard - 100 pF	Standard - 100 pF	Standard - 100 pF
Parameter		Noise = 0.01 pF	Noise = 0.005 pF	Noise = 0.001 pF
E1 (eV)	0.087	0.087	0.087	0.087
Sigma1 (cm^2)	2.50E-15	2.50E-15	2.50E-15	2.50E-15
NT1 (cm^{-3})	1.00E+13	1.00E+13	1.00E+13	1.00E+13
E2 (eV)	0.00	0.00	0.00	0.00
Sigma2 (cm^2)	0.00	0.00	0.00	0.00
NT2 (cm^{-3})	0.00	0.00	0.00	0.00
T-low (K)	25.00	25.00	25.00	25.00
T-high (K)	121.00	121.00	121.00	121.00
T-step (K)	1.00	1.00	1.00	1.00
Sample Period (s)	6.00E-04	6.00E-04	6.00E-04	6.00E-04
Samples	2000	2000	2000	2000
C0(pF)	100.00	30.00	30.00	30.00
Noise (pF)	0.00	0.01	0.005	0.001
Ns	1.00E+16	1.00E+16	1.00E+16	1.00E+16
View (ms)	1200	1200	1200	1200
Effective Mass	1.07	1.07	1.07	1.07

Noise Level Comparison for C0 = 100 pF
(SIM01G1, SIM01G2, SIM01G3, SIM01G4)
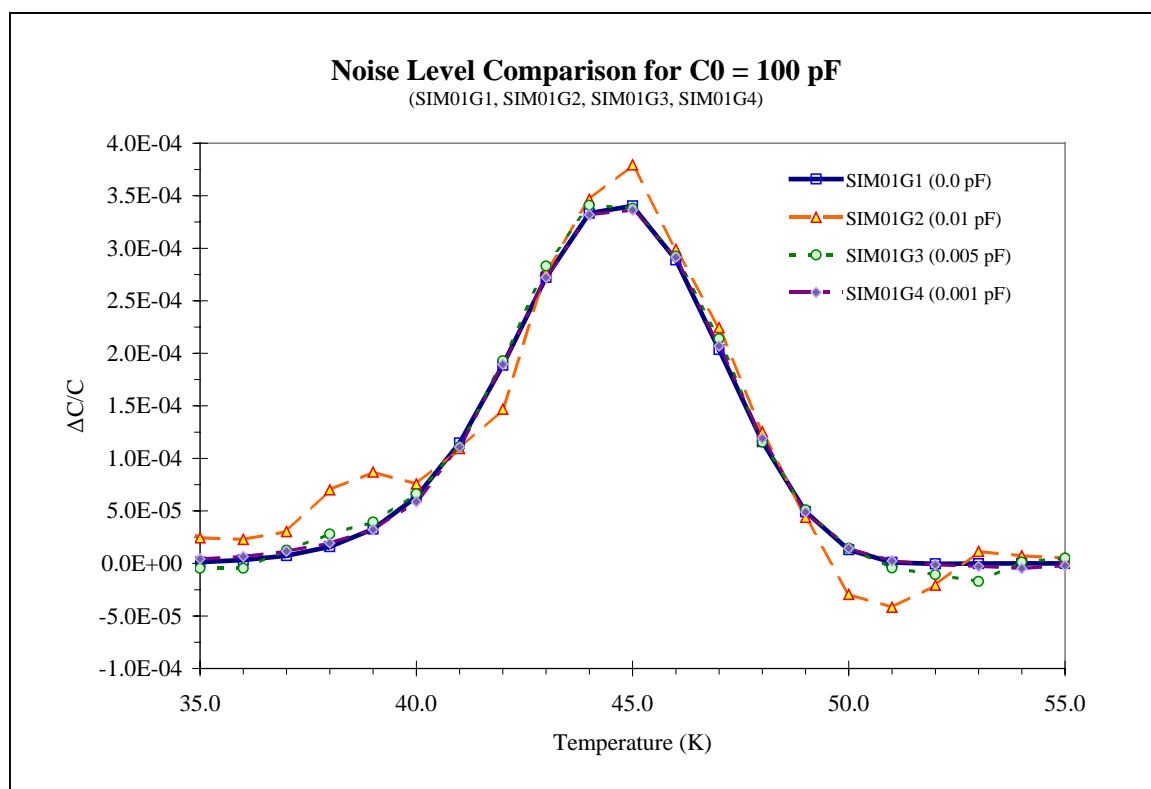
7. Noise Level Comparison for C0 = 1000 pF

Filename:	SIM01H1	SIM01H2	SIM01H3	SIM01H4
Comments:	Standard - 1000 pF	Standard - 1000 pF	Standard - 1000 pF	Standard - 1000 pF
Parameter		Noise = 0.1 pF	Noise = 0.05 pF	Noise = 0.01 pF
E1 (eV)	0.087	0.087	0.087	0.087
Sigma1 (cm^2)	2.50E-15	2.50E-15	2.50E-15	2.50E-15
NT1 (cm^{-3})	1.00E+13	1.00E+13	1.00E+13	1.00E+13
E2 (eV)	0.00	0.00	0.00	0.00
Sigma2 (cm^2)	0.00	0.00	0.00	0.00
NT2 (cm^{-3})	0.00	0.00	0.00	0.00
T-low (K)	25.00	25.00	25.00	25.00
T-high (K)	121.00	121.00	121.00	121.00
T-step (K)	1.00	1.00	1.00	1.00
Sample Period (s)	6.00E-04	6.00E-04	6.00E-04	6.00E-04
Samples	2000	2000	2000	2000
C0(pF)	1000.00	1000.00	1000.00	1000.00
Noise (pF)	0.00	0.10	0.05	0.01
Ns	1.00E+16	1.00E+16	1.00E+16	1.00E+16
View (ms)	1200	1200	1200	1200
Effective Mass	1.07	1.07	1.07	1.07

Noise Level Comparison for C0 = 1000 pF
(SIM01H1, SIM01H2, SIM01H3, SIM01H4)
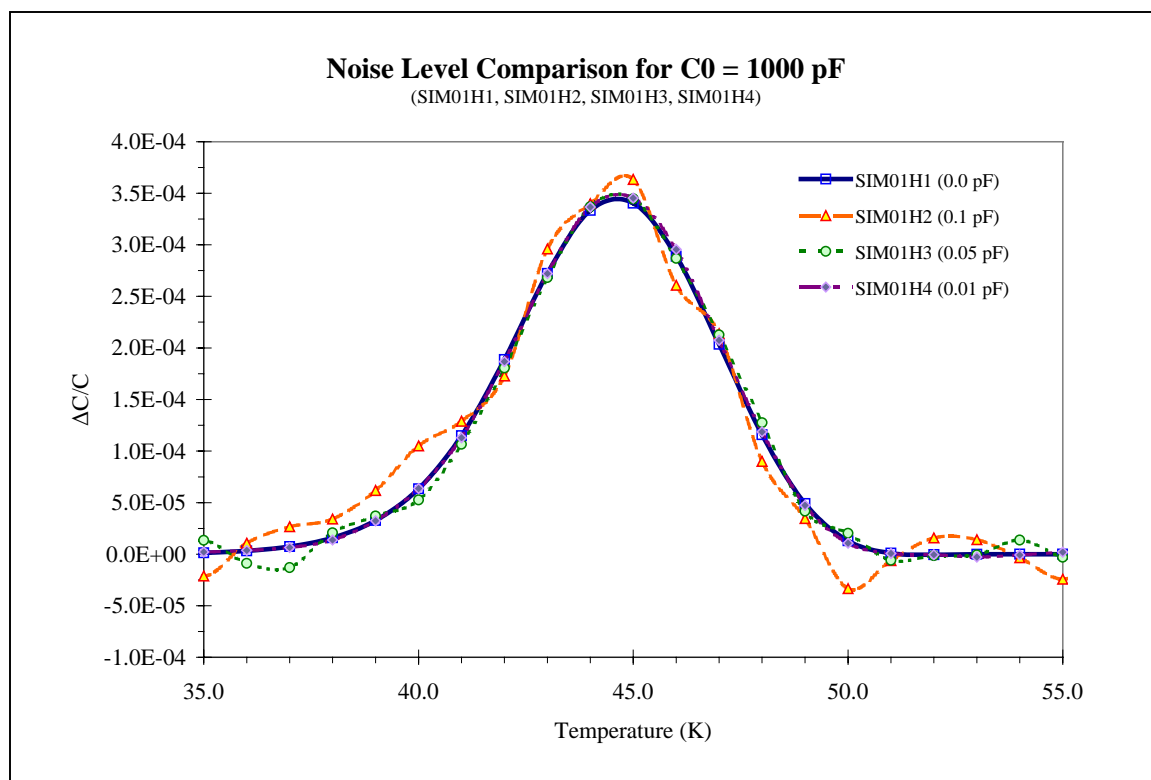
8. C0 Comparison without noise, C0 = 10, 100, 1000 pF

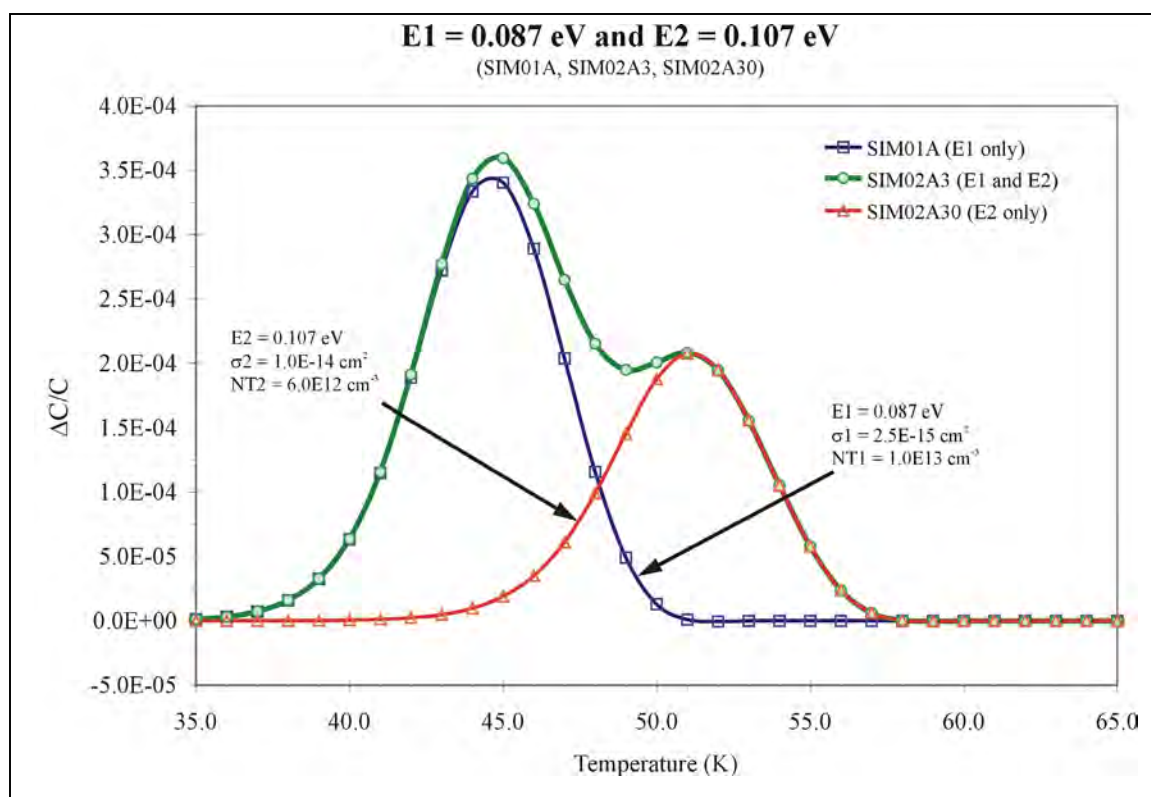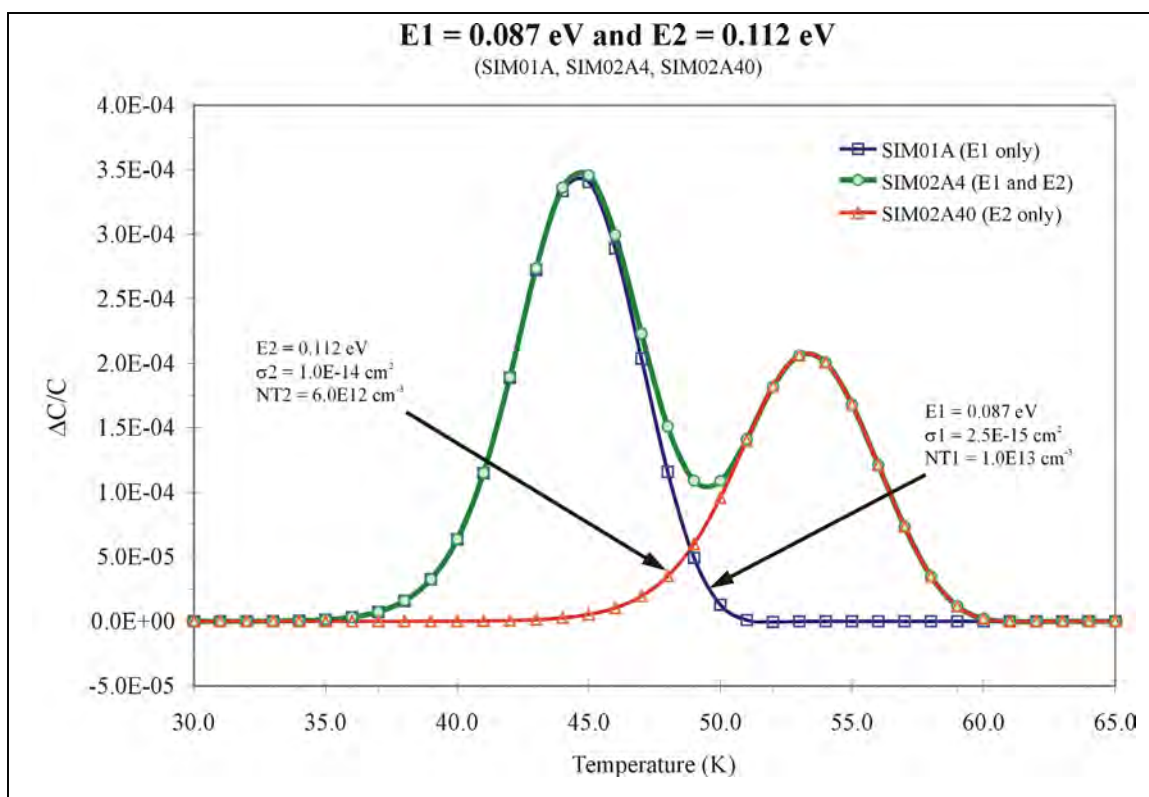| Filename:	SIM01A	SIM01G1	SIM01H1
Comments:	Standard - 10 pF	Standard - 100 pF	Standard - 1000 pF
Parameter			
E1 (eV)	0.087	0.087	0.087
Sigma1 (cm^2)	2.50E-15	2.50E-15	2.50E-15
NT1 (cm^{-3})	1.00E+13	1.00E+13	1.00E+13
E2 (eV)	0.00	0.00	0.00
Sigma2 (cm^2)	0.00	0.00	0.00
NT2 (cm^{-3})	0.00	0.00	0.00
T-low (K)	25.00	25.00	25.00
T-high (K)	121.00	121.00	121.00
T-step (K)	1.00	1.00	1.00
Sample Period (s)	6.00E-04	6.00E-04	6.00E-04
Samples	2000	2000	2000
C0(pF)	10.00	100.00	1000.00
Noise (pF)	0.00	0.00	0.00
Ns	1.00E+16	1.00E+16	1.00E+16
View (ms)	1200	1200	1200
Effective Mass	1.07	1.07	1.07

C0 Comparison
(SIM01A, SIM01G1, SIM01H1)
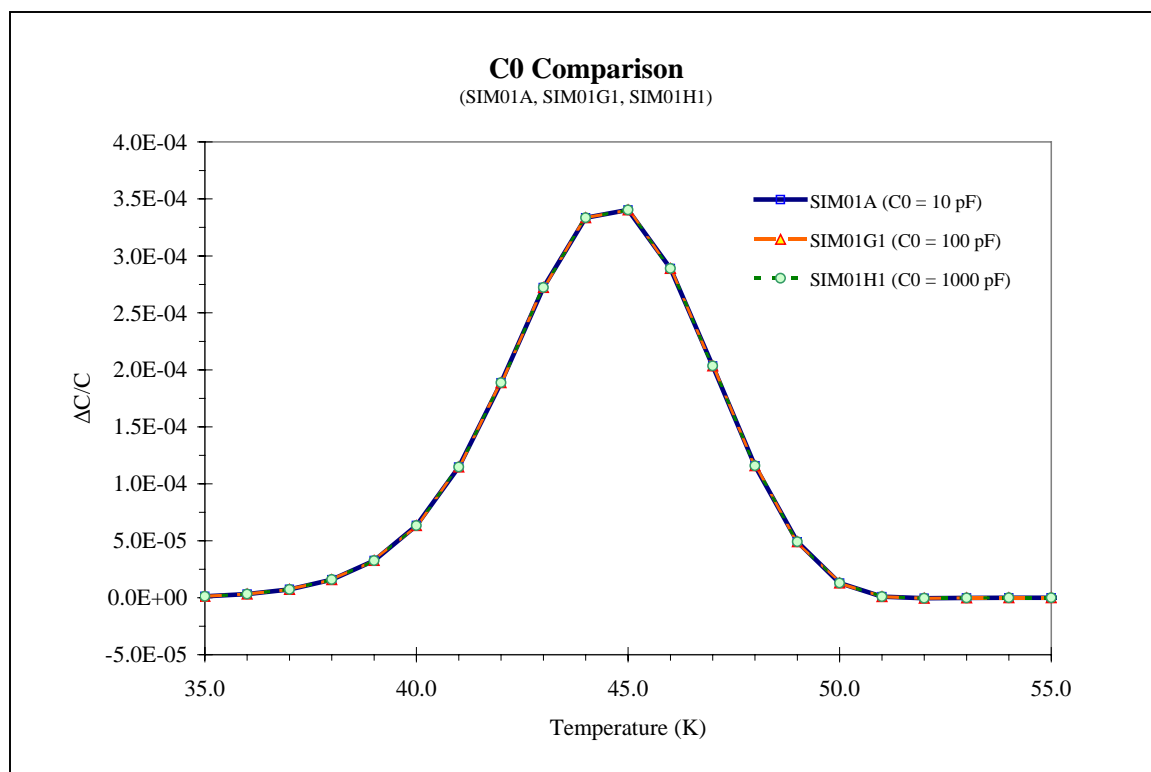
C. Comparison of resulting rate window plots for varying parameters – Two traps

The following simulations show the resulting ratewindow for two traps with close energy values. If the energy values of the two traps differ significantly, then they may be treated as individual traps. The ratewindow for each individual trap and the ratewindow of the combined traps is displayed for comparison. Each simulation uses the same ratewindow ($t_1 = 0.100 / t_2 = 1.0026$).

1. E1 fixed with varying E2 and NT1 > NT2

2. NT1 fixed with varying NT2 and E2 > E1

1a.

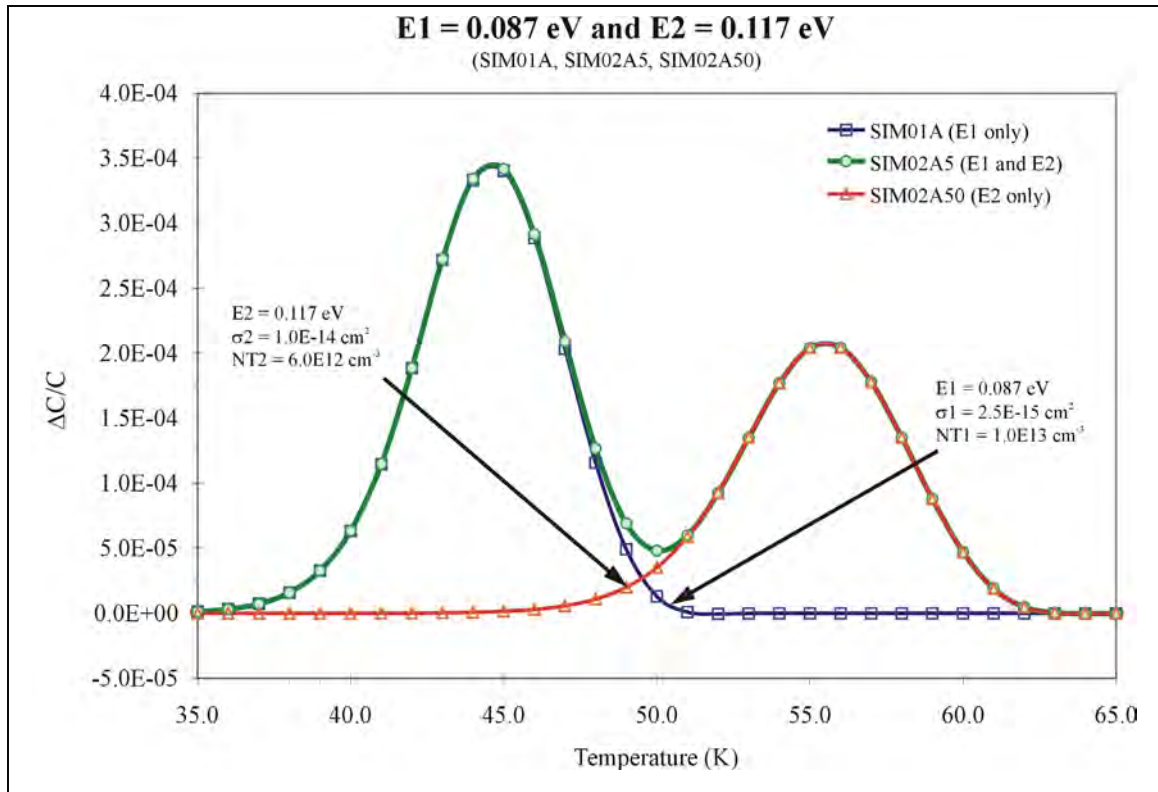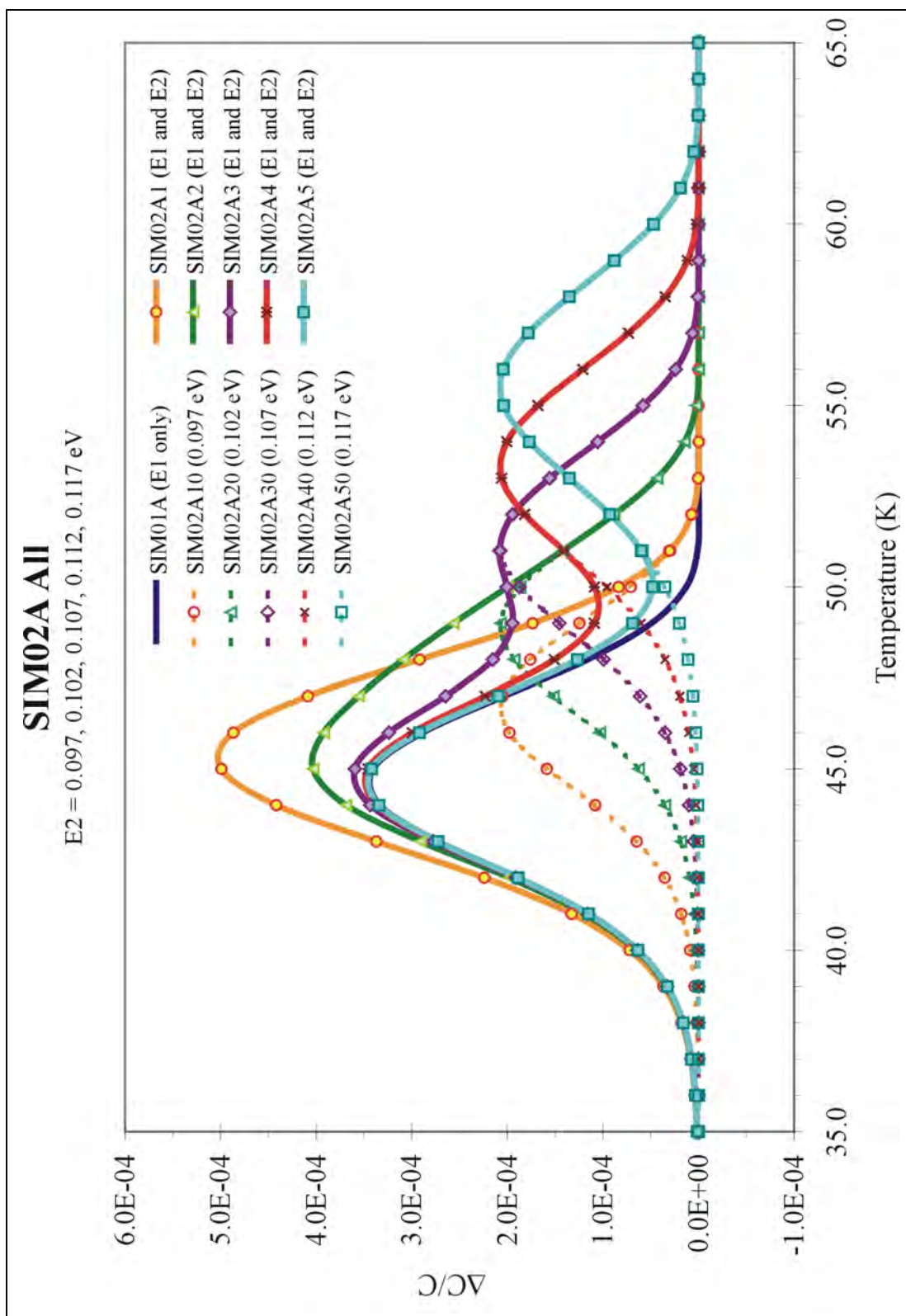| Filename:	SIM01A	SIM02A1	SIM02A10
Comments:	E1 = 0.087	E1 = 0.087	E1 = 0
	E2 = 0	E2 = 0.097	E2 = 0.097
Parameter			
E1 (eV)	0.087	0.087	0.00
Sigma1 (cm^2)	2.50E-15	2.50E-15	0.00
NT1 (cm^{-3})	1.00E+13	1.00E+13	0.00
E2 (eV)	0.00	0.097	0.097
Sigma2 (cm^2)	0.00	1.00E-14	1.00E-14
NT2 (cm^{-3})	0.00	6.00E+12	6.00E+12
T-low (K)	25.00	25.00	25.00
T-high (K)	121.00	101.00	101.00
T-step (K)	1.00	1.00	1.00
Sample Period (s)	6.00E-04	6.00E-04	6.00E-04
Samples	2000	2000	2000
C0(pF)	10.00	10.00	10.00
Noise (pF)	0.00	0.00	0.00
Ns	1.00E+16	1.00E+16	1.00E+16
View (ms)	1200	1200	1200
Effective Mass	1.07	1.07	1.07

E1 = 0.087 eV and E2 = 0.097 eV
(SIM01A, SIM02A1, SIM02A10)

1b.

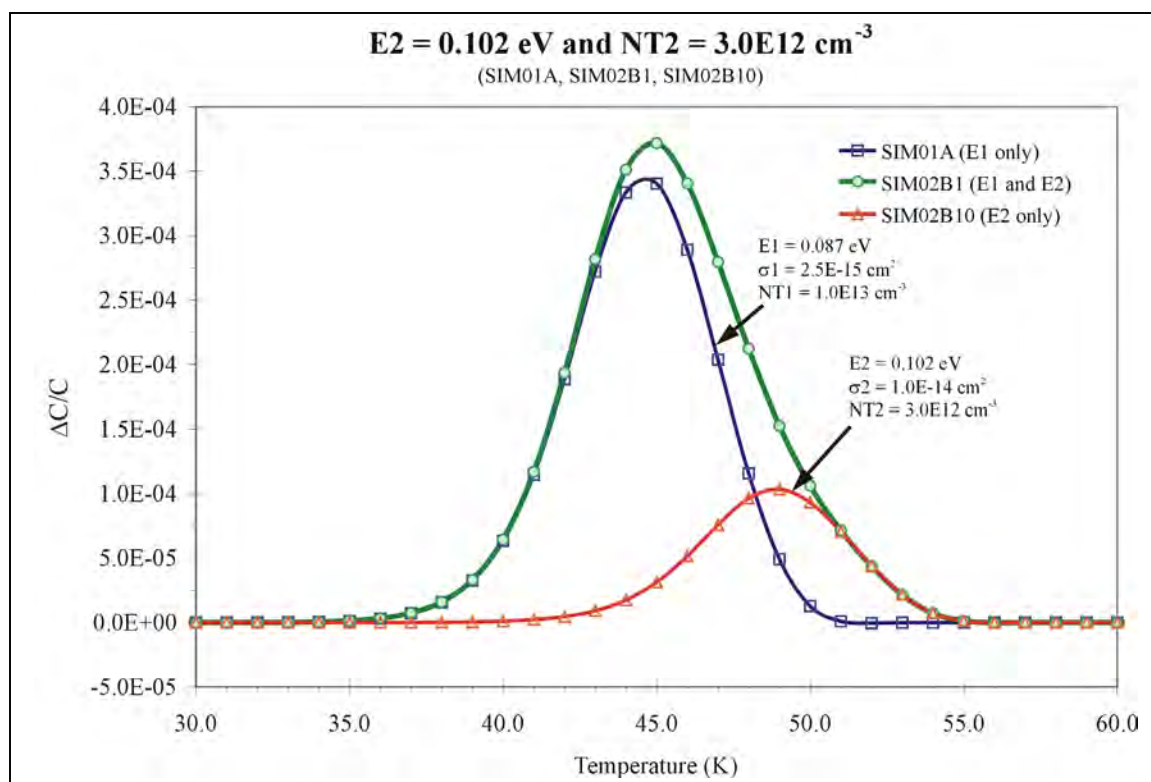| Filename:	SIM01A	SIM02A2	SIM02A20
Comments:	E1 = 0.087	E1 = 0.087	E1 = 0
	E2 = 0	E2 = 0.102	E2 = 0.102
Parameter			
E1 (eV)	0.087	0.087	0.00
Sigma1 (cm^2)	2.50E-15	2.50E-15	0.00
NT1 (cm^{-3})	1.00E+13	1.00E+13	0.00
E2 (eV)	0.00	0.102	0.102
Sigma2 (cm^2)	0.00	1.00E-14	1.00E-14
NT2 (cm^{-3})	0.00	6.00E+12	6.00E+12
T-low (K)	25.00	25.00	25.00
T-high (K)	121.00	101.00	101.00
T-step (K)	1.00	1.00	1.00
Sample Period (s)	6.00E-04	6.00E-04	6.00E-04
Samples	2000	2000	2000
C0(pF)	10.00	10.00	10.00
Noise (pF)	0.00	0.00	0.00
Ns	1.00E+16	1.00E+16	1.00E+16
View (ms)	1200	1200	1200
Effective Mass	1.07	1.07	1.07

E1 = 0.087 eV and E2 = 0.102 eV
(SIM01A, SIM02A2, SIM02A20)

1c.

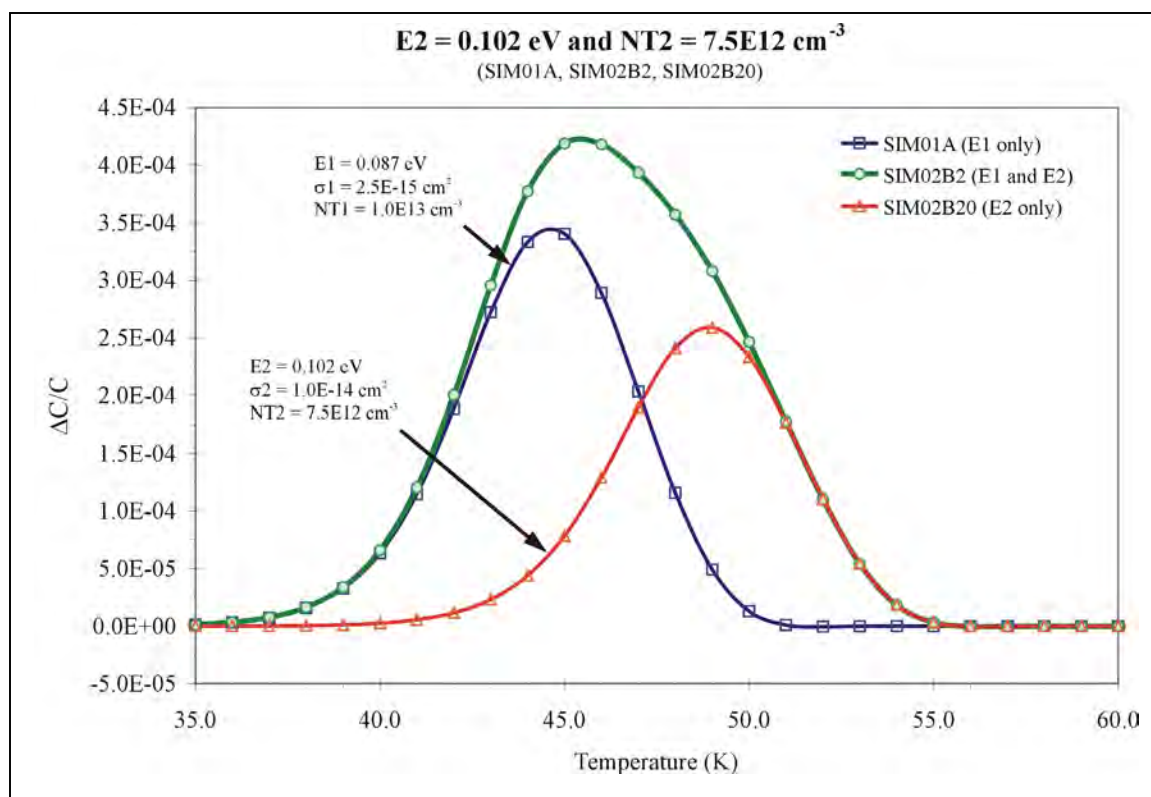| Filename:	SIM01A	SIM02A3	SIM02A30
Comments:	E1 = 0.087	E1 = 0.087	E1 = 0
	E2 = 0	E2 = 0.107	E2 = 0.107
Parameter			
E1 (eV)	0.087	0.087	0.00
Sigma1 (cm^2)	2.50E-15	2.50E-15	0.00
NT1 (cm^{-3})	1.00E+13	1.00E+13	0.00
E2 (eV)	0.00	0.107	0.107
Sigma2 (cm^2)	0.00	1.00E-14	1.00E-14
NT2 (cm^{-3})	0.00	6.00E+12	6.00E+12
T-low (K)	25.00	25.00	25.00
T-high (K)	121.00	101.00	101.00
T-step (K)	1.00	1.00	1.00
Sample Period (s)	6.00E-04	6.00E-04	6.00E-04
Samples	2000	2000	2000
C0(pF)	10.00	10.00	10.00
Noise (pF)	0.00	0.00	0.00
Ns	1.00E+16	1.00E+16	1.00E+16
View (ms)	1200	1200	1200
Effective Mass	1.07	1.07	1.07

E1 = 0.087 eV and E2 = 0.107 eV
(SIM01A, SIM02A3, SIM02A30)

1d.

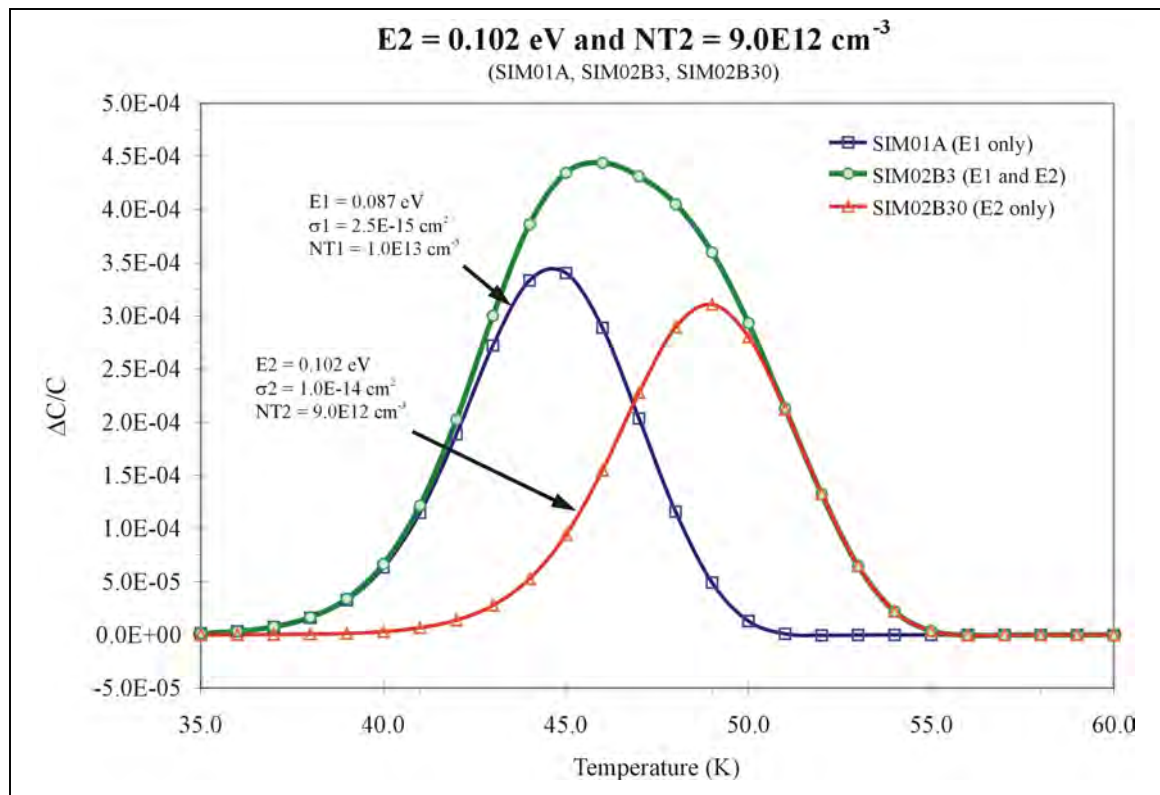| Filename:	SIM01A	SIM02A4	SIM02A40
Comments:	E1 = 0.087	E1 = 0.087	E1 = 0
	E2 = 0	E2 = 0.112	E2 = 0.112
Parameter			
E1 (eV)	0.087	0.087	0.00
Sigma1 (cm^2)	2.50E-15	2.50E-15	0.00
NT1 (cm^{-3})	1.00E+13	1.00E+13	0.00
E2 (eV)	0.00	0.112	0.112
Sigma2 (cm^2)	0.00	1.00E-14	1.00E-14
NT2 (cm^{-3})	0.00	6.00E+12	6.00E+12
T-low (K)	25.00	25.00	25.00
T-high (K)	121.00	101.00	101.00
T-step (K)	1.00	1.00	1.00
Sample Period (s)	6.00E-04	6.00E-04	6.00E-04
Samples	2000	2000	2000
C0(pF)	10.00	10.00	10.00
Noise (pF)	0.00	0.00	0.00
Ns	1.00E+16	1.00E+16	1.00E+16
View (ms)	1200	1200	1200
Effective Mass	1.07	1.07	1.07

E1 = 0.087 eV and E2 = 0.112 eV
(SIM01A, SIM02A4, SIM02A40)

1e.

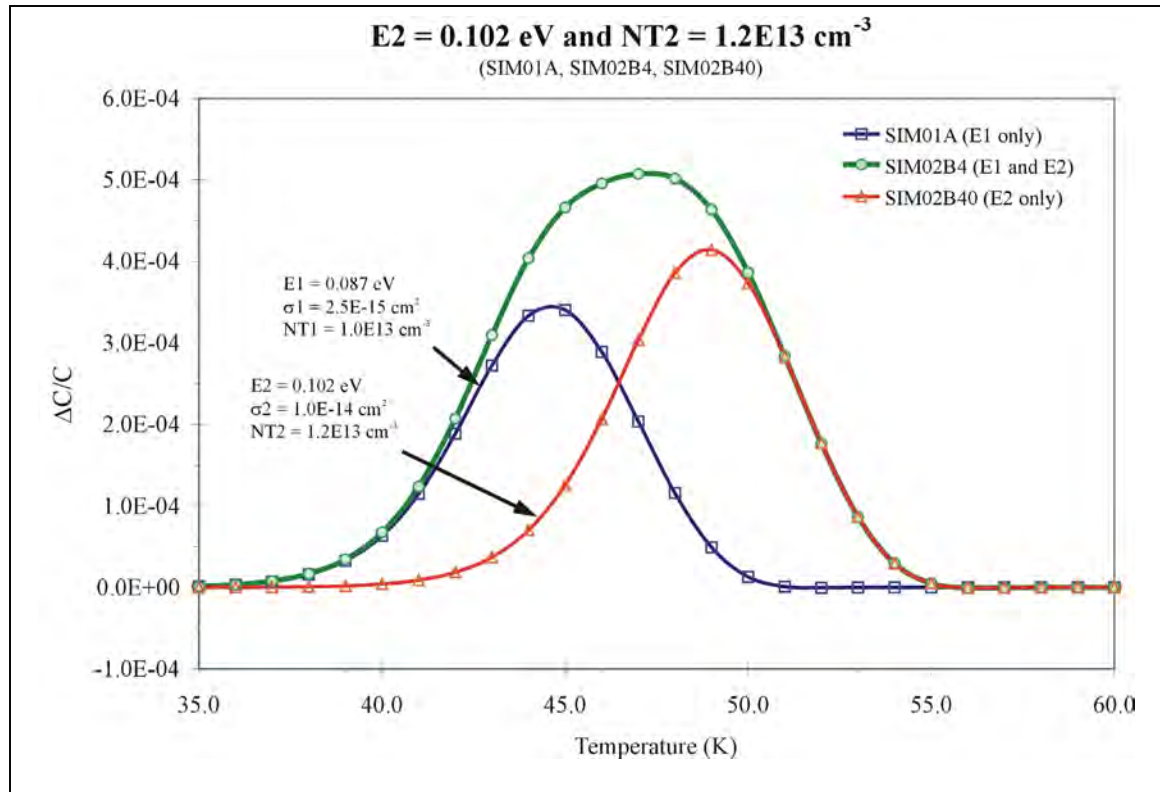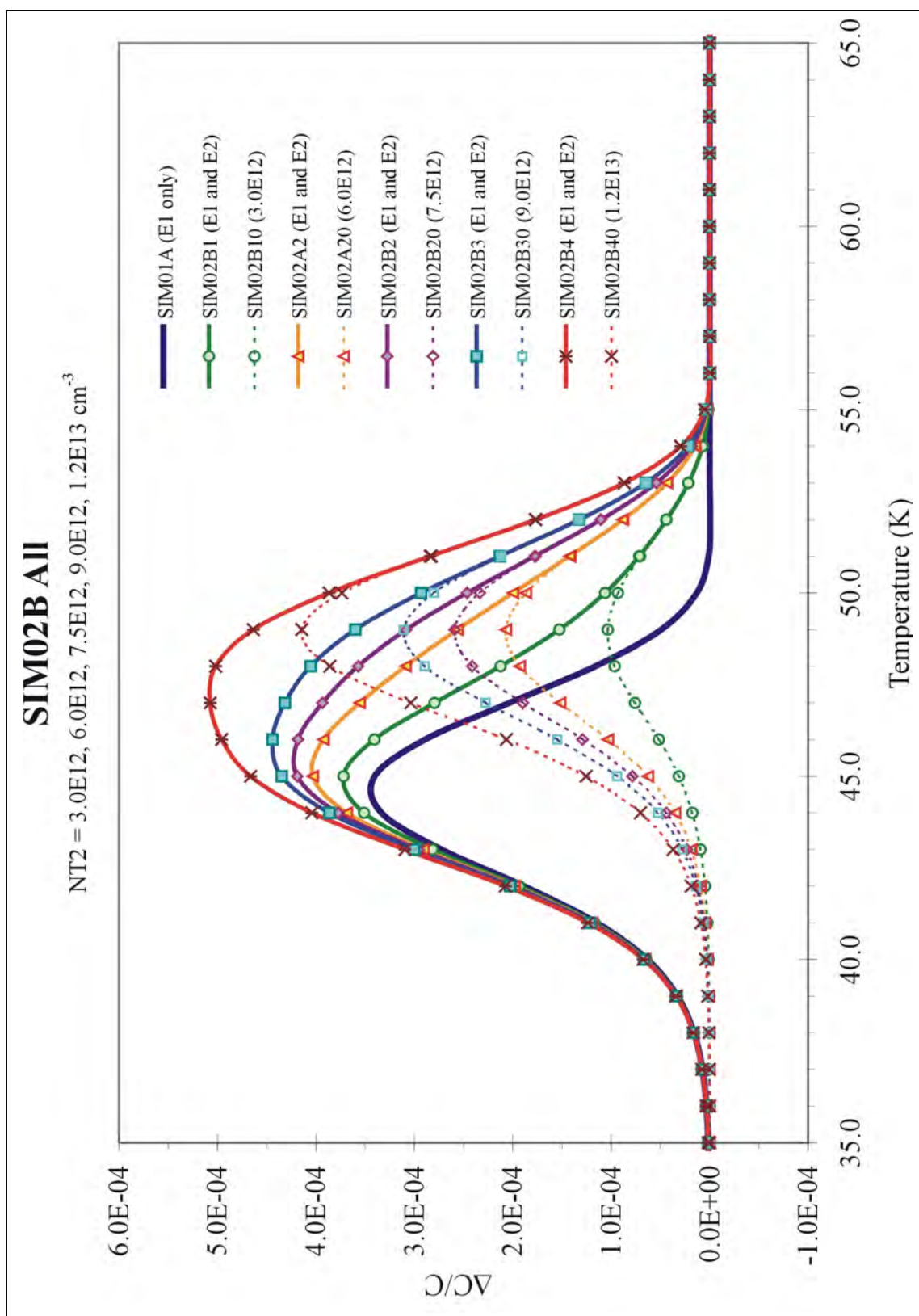| Filename:	SIM01A	SIM02A5	SIM02A50
Comments:	E1 = 0.087	E1 = 0.087	E1 = 0
	E2 = 0	E2 = 0.117	E2 = 0.117
Parameter			
E1 (eV)	0.087	0.087	0.00
Sigma1 (cm^2)	2.50E-15	2.50E-15	0.00
NT1 (cm^{-3})	1.00E+13	1.00E+13	0.00
E2 (eV)	0.00	0.117	0.117
Sigma2 (cm^2)	0.00	1.00E-14	1.00E-14
NT2 (cm^{-3})	0.00	6.00E+12	6.00E+12
T-low (K)	25.00	25.00	25.00
T-high (K)	121.00	101.00	101.00
T-step (K)	1.00	1.00	1.00
Sample Period (s)	6.00E-04	6.00E-04	6.00E-04
Samples	2000	2000	2000
C0(pF)	10.00	10.00	10.00
Noise (pF)	0.00	0.00	0.00
Ns	1.00E+16	1.00E+16	1.00E+16
View (ms)	1200	1200	1200
Effective Mass	1.07	1.07	1.07

E1 = 0.087 eV and E2 = 0.117 eV
(SIM01A, SIM02A5, SIM02A50)

SIM02A AII

E2 = 0.097, 0.102, 0.107, 0.112, 0.117 eV

2a.

Filename:	SIM01A	SIM02B1	SIM02B10
Comments:	E1 = 0.087	E2 = 0.102	E1 = 0
	E2 = 0	NT2 = 3.0E12	E2 = 0.102
Parameter			
E1 (eV)	0.087	0.087	0.00
Sigma1 (cm^2)	2.50E-15	2.50E-15	0.00
NT1 (cm^{-3})	1.00E+13	1.00E+13	0.00
E2 (eV)	0.00	0.102	0.102
Sigma2 (cm^2)	0.00	1.00E-14	1.00E-14
NT2 (cm^{-3})	0.00	3.00E+12	3.00E+12
T-low (K)	25.00	25.00	25.00
T-high (K)	121.00	101.00	101.00
T-step (K)	1.00	1.00	1.00
Sample Period (s)	6.00E-04	6.00E-04	6.00E-04
Samples	2000	2000	2000
C0(pF)	10.00	10.00	10.00
Noise (pF)	0.00	0.00	0.00
Ns	1.00E+16	1.00E+16	1.00E+16
View (ms)	1200	1200	1200
Effective Mass	1.07	1.07	1.07

$E2 = 0.102$ eV and $NT2 = 3.0E12$ cm^{-3}
(SIM01A, SIM02B1, SIM02B10)

2b.

| Filename:	SIM01A	SIM02B2	SIM02B20
Comments:	E1 = 0.087	E2 = 0.102	E1 = 0
	E2 = 0	NT2 = 7.5E12	E2 = 0.102
Parameter			
E1 (eV)	0.087	0.087	0.00
Sigma1 (cm^2)	2.50E-15	2.50E-15	0.00
NT1 (cm^{-3})	1.00E+13	1.00E+13	0.00
E2 (eV)	0.00	0.102	0.102
Sigma2 (cm^2)	0.00	1.00E-14	1.00E-14
NT2 (cm^{-3})	0.00	7.50E+12	7.50E+12
T-low (K)	25.00	25.00	25.00
T-high (K)	121.00	101.00	101.00
T-step (K)	1.00	1.00	1.00
Sample Period (s)	6.00E-04	6.00E-04	6.00E-04
Samples	2000	2000	2000
C0(pF)	10.00	10.00	10.00
Noise (pF)	0.00	0.00	0.00
Ns	1.00E+16	1.00E+16	1.00E+16
View (ms)	1200	1200	1200
Effective Mass	1.07	1.07	1.07

E2 = 0.102 eV and NT2 = 7.5E12 cm^{-3}
(SIM01A, SIM02B2, SIM02B20)

2c.

Filename:	SIM01A	SIM02B3	SIM02B30
Comments:	E1 = 0.087	E2 = 0.102	E1 = 0
	E2 = 0	NT2 = 9.0E12	E2 = 0.102
Parameter			
E1 (eV)	0.087	0.087	0.00
Sigma1 (cm^2)	2.50E-15	2.50E-15	0.00
NT1 (cm^{-3})	1.00E+13	1.00E+13	0.00
E2 (eV)	0.00	0.102	0.102
Sigma2 (cm^2)	0.00	1.00E-14	1.00E-14
NT2 (cm^{-3})	0.00	9.00E+12	9.00E+12
T-low (K)	25.00	25.00	25.00
T-high (K)	121.00	101.00	101.00
T-step (K)	1.00	1.00	1.00
Sample Period (s)	6.00E-04	6.00E-04	6.00E-04
Samples	2000	2000	2000
C0(pF)	10.00	10.00	10.00
Noise (pF)	0.00	0.00	0.00
Ns	1.00E+16	1.00E+16	1.00E+16
View (ms)	1200	1200	1200
Effective Mass	1.07	1.07	1.07

$E2 = 0.102$ eV and $NT2 = 9.0E12$ cm^{-3}
(SIM01A, SIM02B3, SIM02B30)

2d.

Filename:	SIM01A	SIM02B4	SIM02B40
Comments:	E1 = 0.087	E2 = 0.102	E1 = 0
	E2 = 0	NT2 = 1.2E13	E2 = 0.102
Parameter			
E1 (eV)	0.087	0.087	0.00
Sigma1 (cm^2)	2.50E-15	2.50E-15	0.00
NT1 (cm^{-3})	1.00E+13	1.00E+13	0.00
E2 (eV)	0.00	0.102	0.102
Sigma2 (cm^2)	0.00	1.00E-14	1.00E-14
NT2 (cm^{-3})	0.00	1.20E+13	1.20E+13
T-low (K)	25.00	25.00	25.00
T-high (K)	121.00	101.00	101.00
T-step (K)	1.00	1.00	1.00
Sample Period (s)	6.00E-04	6.00E-04	6.00E-04
Samples	2000	2000	2000
C0(pF)	10.00	10.00	10.00
Noise (pF)	0.00	0.00	0.00
Ns	1.00E+16	1.00E+16	1.00E+16
View (ms)	1200	1200	1200
Effective Mass	1.07	1.07	1.07

$E2 = 0.102$ eV and $NT2 = 1.2E13$ cm^{-3}
(SIM01A, SIM02B4, SIM02B40)

SIM02B All

NT2 = 3.0E12, 6.0E12, 7.5E12, 9.0E12, 1.2E13 cm^{-3}

Legend:
- SIM01A (E1 only)
- SIM02B1 (E1 and E2)
- SIM02B10 (3.0E12)
- SIM02A2 (E1 and E2)
- SIM02A20 (6.0E12)
- SIM02B2 (E1 and E2)
- SIM02B20 (7.5E12)
- SIM02B3 (E1 and E2)
- SIM02B30 (9.0E12)
- SIM02B4 (E1 and E2)
- SIM02B40 (1.2E13)

Temperature (K)

$\Delta C/C$

II. DLTS Data Fitting and Analysis

The simulated data was used with the analysis portion of the software to determine the trap parameters.

A. One Trap – without noise

1. Ratewindow Analysis

Select the "DLTS Data Fitting and Analysis" button on the Semetrol software main menu.
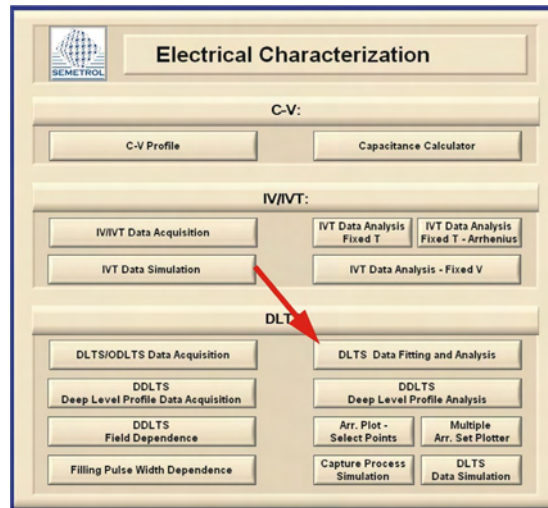
Semetrol software main menu window

The DLTS Data Fitting and Analysis window will open up to the "Plot Ratewindow" tab.
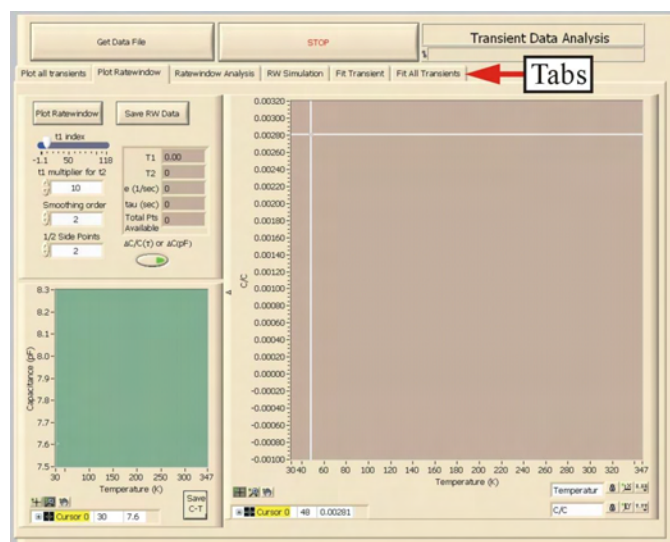
DLTS Data Fitting and Analysis window - Plot Ratewindow tab

Select the "Get Data File" button and then select the file that you want to open from the menu. Select the "Plot Ratewindow" button. The file should appear in the ratewindow plot. Once the file is loaded, it will work with all of the tabs in the DLTS Data Fitting and Analysis window. It is not necessary to use the "Get Data File" after switching to other tabs in the window.
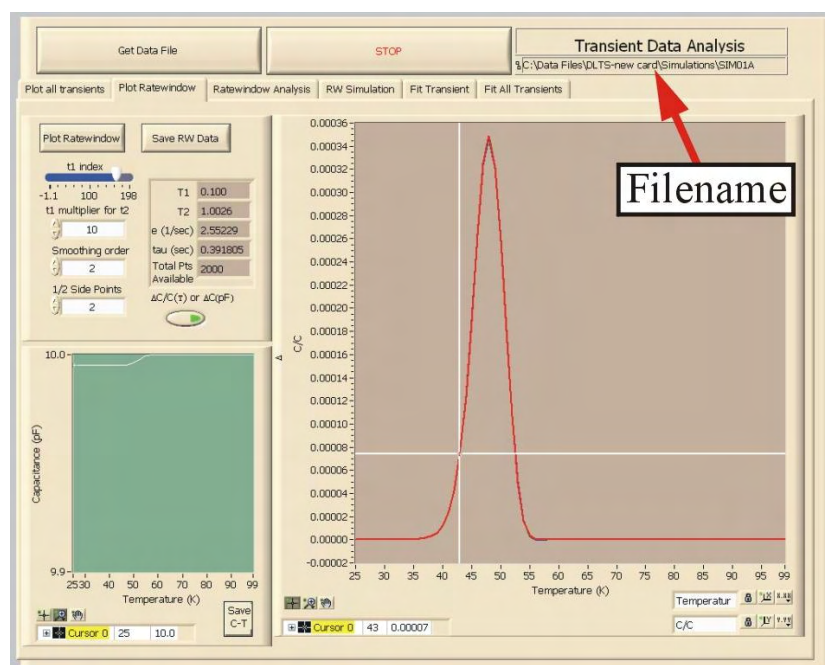
DLTS Data Fitting and Analysis window - Plot Ratewindow tab
Ratewindow of SIM01A simulation ($t_1 = 0.100/t_2 = 1.0026$)

Parameters for SIM01A

E1 (eV)	0.087	Sigma1 (cm^2)	2.50E-15	NT1 (cm^{-3})	1.00E+13
E2 (eV)	0.00	Sigma2 (cm^2)	0.00	NT2 (cm^{-3})	0.00
T-low (K)	25.00	T-high (K)	100.00	T-step (K)	1.00
Sample Period (s)	6.00E-04	Samples	2000	C0(pF)	10.00
Noise (pF)	0.00	Ns	1.00E+16	View (ms)	1200
Effective Mass	1.07				

The scale of the ratewindow plot and the capacitance vs. temperature plot can be change to give a better view of the data using the tool buttons located at the lower left of each plot. The red curve in the ratewindow is the raw data from the measurement (or simulation), the blue curve is the smoothed data and the green curve is used for finding the $\Delta C/C$ max points for the Arrhenius plot. The ratewindow and C-T data can be saved into a file and by pressing the "Save RW Data" and "Save C-T" buttons respectively. The files can later be opened in plotting software. Issues with the measurement or DUT may be indicated by sudden jumps in the C-T curve. The resulting C-T curve for SIM01A can be seen below.
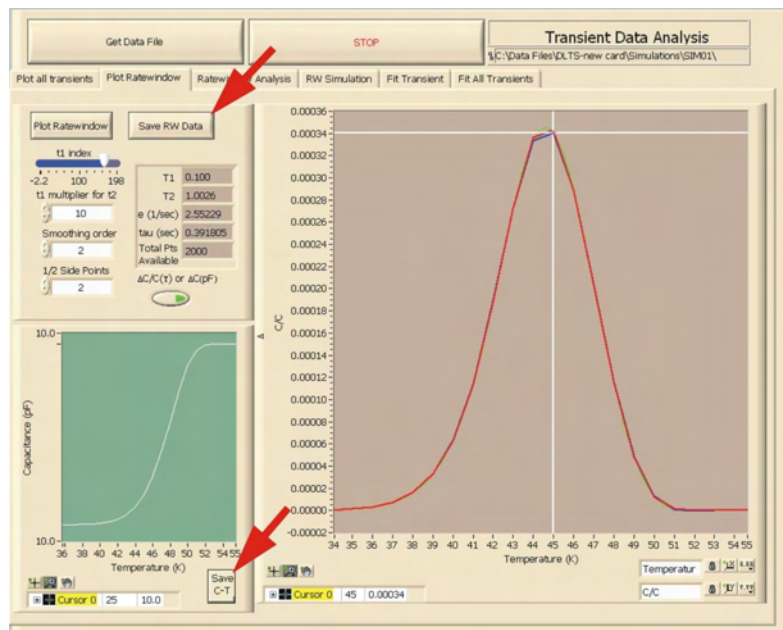
Plot Ratewindow – SIM01A zoomed in

C-T Data for SIM01A
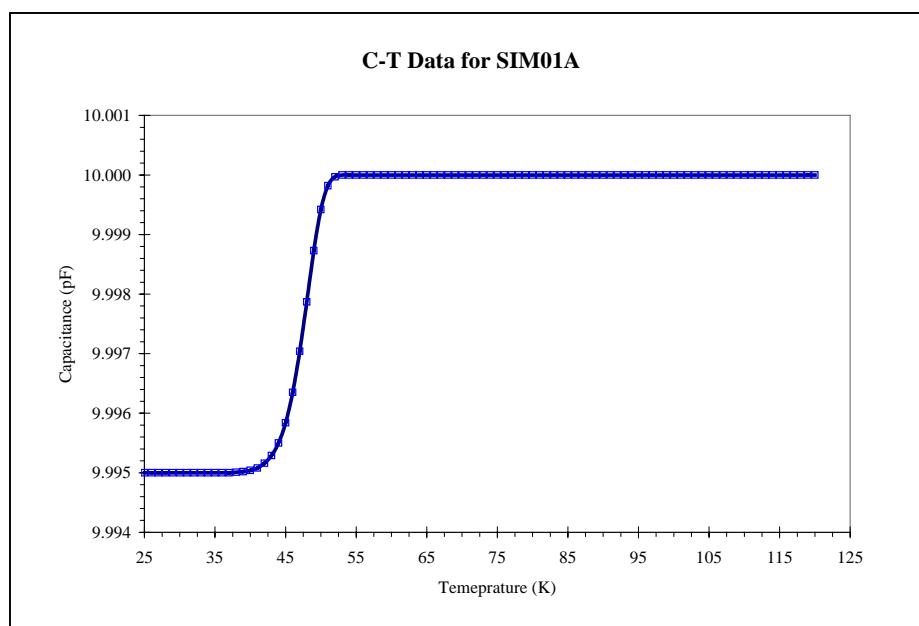
Different ratewindows (t_1/t_2) can be viewed by adjusting the slider ("t1 index") at the top left of the window and by varying the value of the "t1 multiplier for t2". As the ratewindow is varied the peak position will change along the temperature axis.
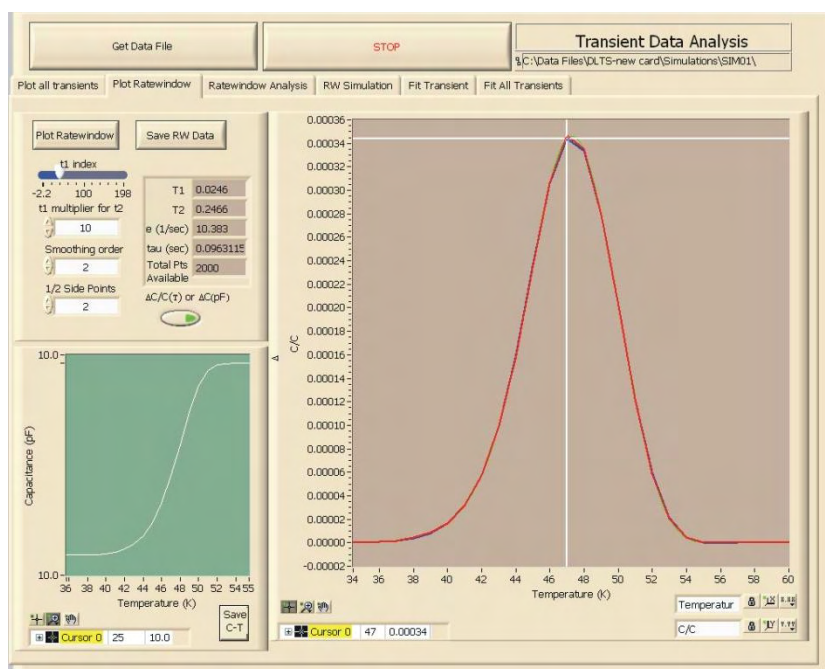
Ratewindow of SIM01A simulation ($t_1 = 0.0246/t_2 = 0.2466$)
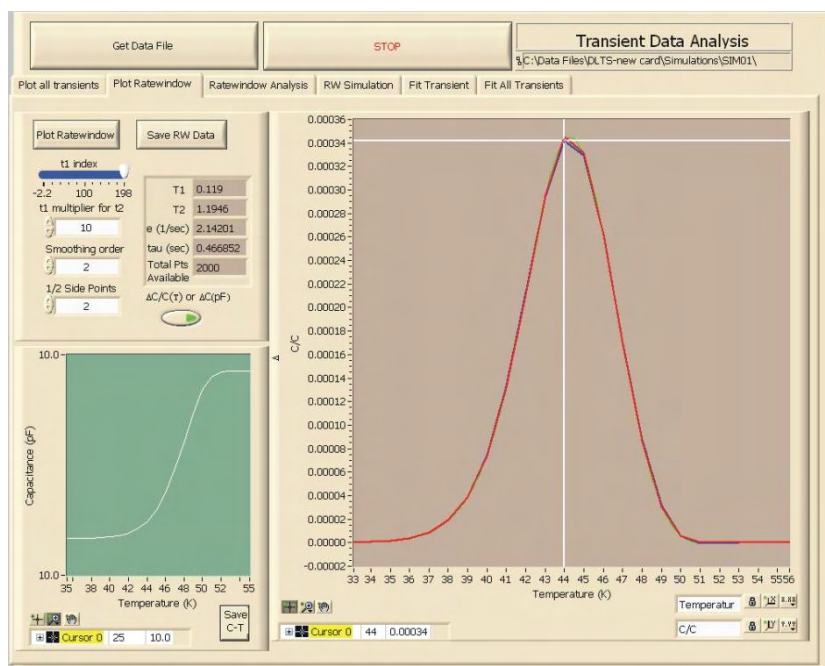
Ratewindow of SIM01A simulation ($t_1 = 0.119/t_2 = 1.1946$)

The ratewindow data can also be changed to display ΔC versus temperature by clicking the "ΔC/C(T) or ΔC(pF)" button. The ΔC plot of SIM01A can be seen below.

A rough estimate of the trap concentration can be obtained by multiplying the peak height by two times the shallow carrier concentration when displaying ΔC/C(T)
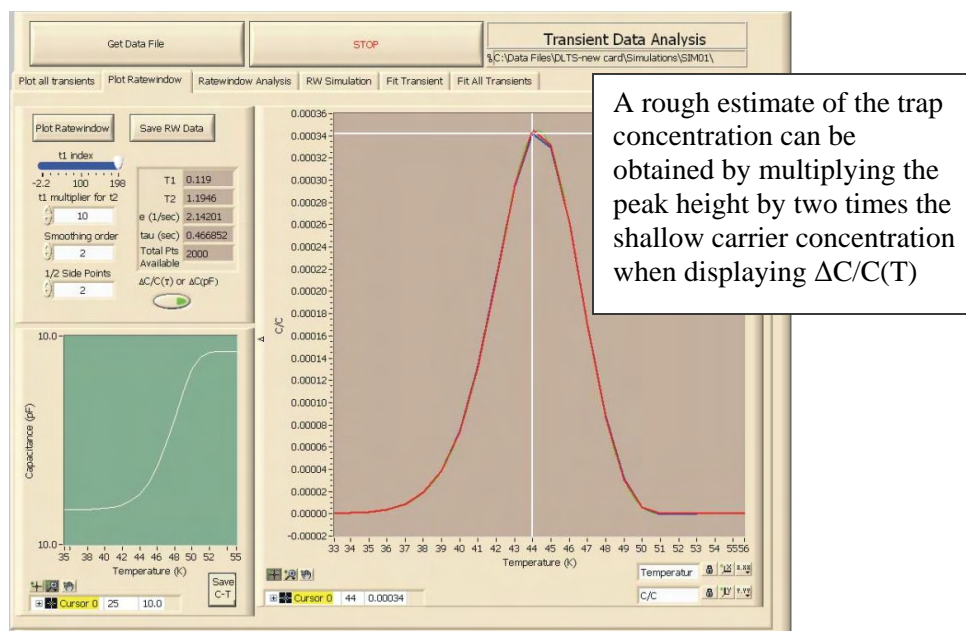
ΔC plot of SIM01A

The simulated data can also be viewed in a 3-D plot by selecting the "Plot all transients" tab and then selecting the "Plot" button.
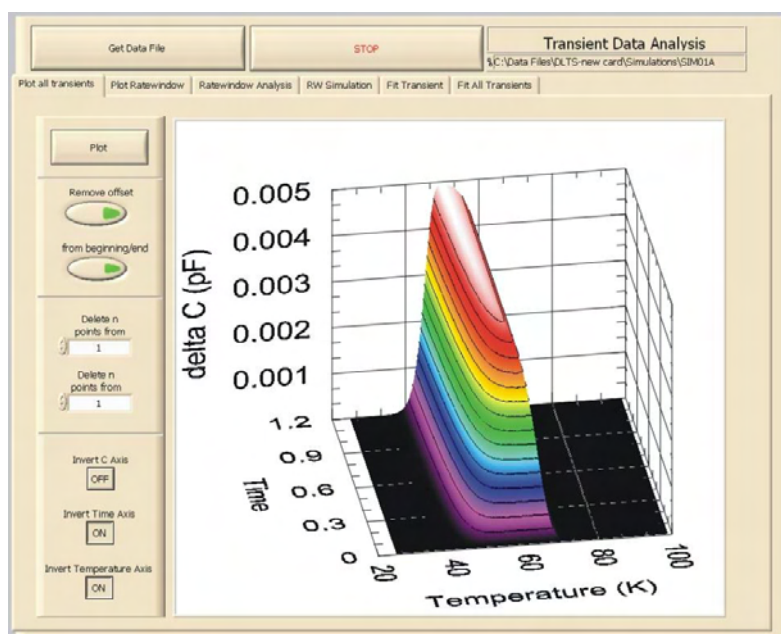
DLTS Data Fitting and Analysis window - Plot all transients
SIM01A simulation

The energy and capture cross section of the trap can be determined by using the ratewindows to produce an Arrhenius plot. Click on the "Ratewindow Analysis" tab and press the "Plot Ratewindow" button to display the ratewindow plot. The scale of the plot can be adjusted by using the three tool buttons below the plot. The temperature for analysis can be adjusted by using the crosshair tool button and moving the temperature limit bars in the plot. The tan colored bar sets the lower temperature limit (Temp Limit 1) and the yellow bar sets the upper temperature limit (Temp Limit 2). Set the poly order (usually set to 2), the ½ width points (usually set to ≥2) and the minimum width. The ratewindow analysis algorithm is limited to working with positive values, so the "peak/valley" selector must be changed to make the algorithm run correctly. Select the appropriate condition based on the data within the temperature limits.
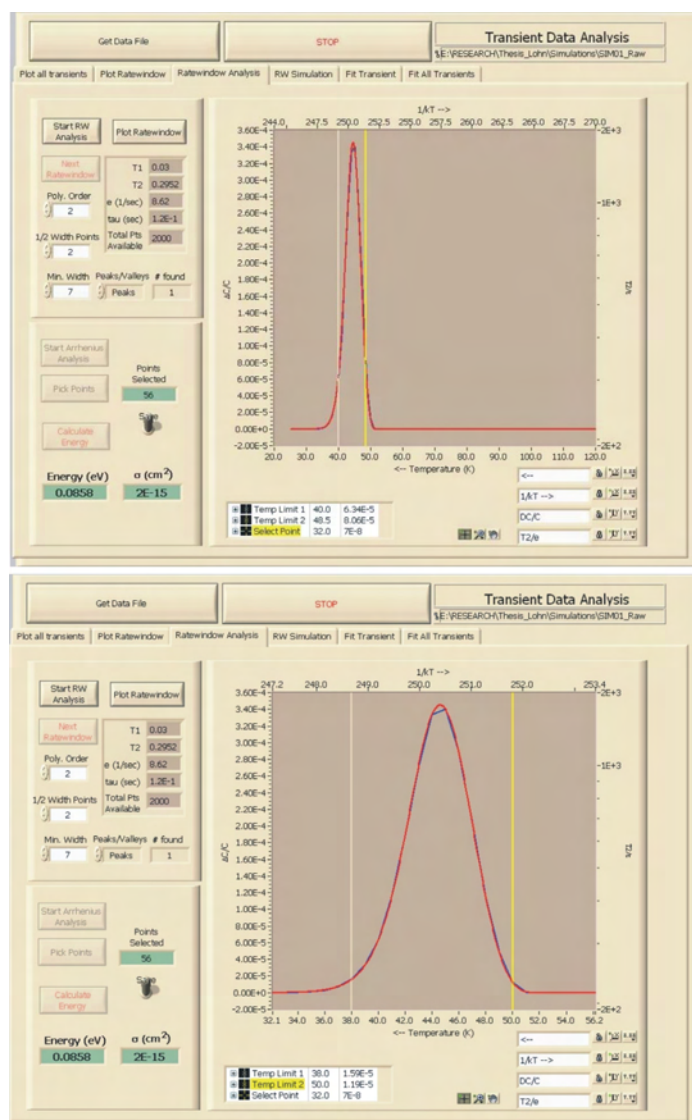
DLTS Data Fitting and Analysis window - Ratewindow Analysis
SIM01A

Click the "Start RW Analysis" button to begin searching for the peaks in the ratewindows. The algorithm will analyze the first ratewindow and search for a peak. If no point is found no data point will be recorded in the Arrhenius plot. If a data point is found, it will be indicated by the green square at the top of the peak in the ratewindow and a corresponding red square in the Arrhenius plot. Click the "Next Ratewindow" button and the algorithm will change the t_1 and t_2 values and analyze the resulting ratewindow. Continue clicking the "Next Ratewindow" button until all ratewindows have been analyzed ("Next Ratewindow" button will vanish).
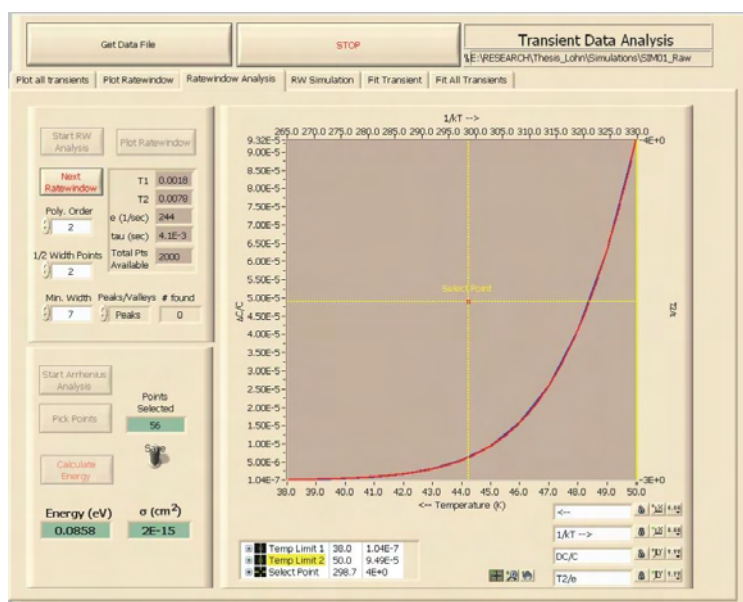
No point found in ratewindow
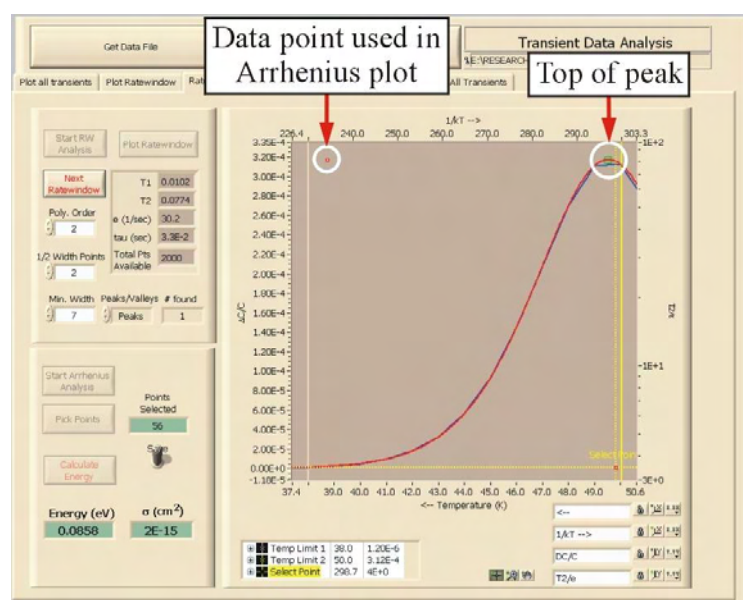
Point found in ratewindow

After all ratewindows have been analyzed, the screen will not change when the "Next Ratewindow" button is selected and the "Next Ratewindow" button will vanish.
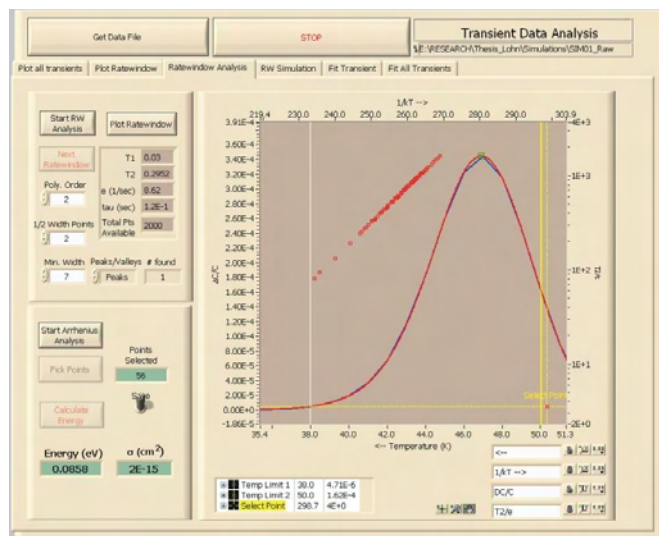
After all points have been found

You can then begin the Arrhenius analysis by clicking the "Start Arrhenius Analysis" button. The "Pick Points" button should become visible and the points selected value will become zero. Click the crosshairs tool button and drag the crosshairs to the point you wish to select. Press the enter key or click the "Pick Points" button to select that point. The window may be resized to make points easier to select by using the tool buttons at the bottom of the window. After all points have been selected, click the "Calculate Energy" button to calculate the energy and capture cross section. The selected points will become highlighted and the linear fit will appear. When the toggle switch is in the save position, a popup window will prompt you to save the data and give a filename.
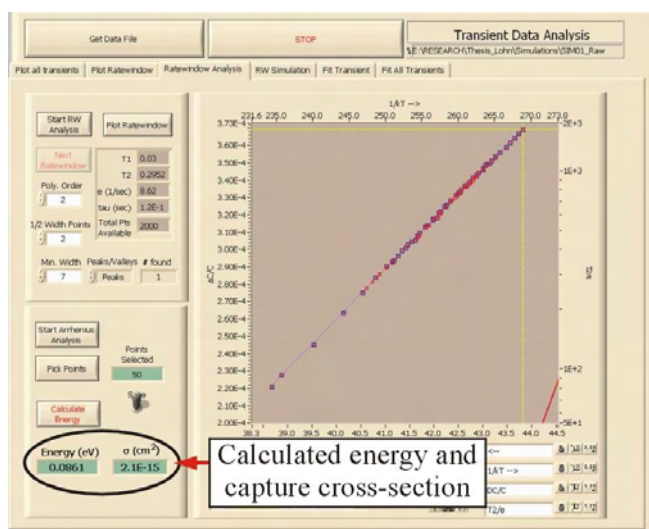
The ratewindow analysis and energy calculation was performed on the SIM01A data (E1 = 0.087 eV, sigma1 = 2.50E-15 cm^2) with varying temperature limits. The results of the analysis can be seen in the table below.

Temp Limit 1	Temp Limit 2	Number of point selected	Energy (eV)	Sigma (cm^2)
36	58	37	0.0869	2.6E-15
38	50	50	0.0861	2.2E-15
40	48.5	56	0.0858	2.0E-15
42	47	56	0.0854	1.8E-15
43	46	40	0.0848	1.5E-15

The values (energy and capture cross section) obtained from the Arrhenius plot can be compared with a simulated ratewindow by selecting the "RW Simulation" tab. The raw data appears as the red curve, the smoothed data appears as the blue curve and the simulated data is the green curve. Input the trap characteristics to simulate in the window using the sliders. The prefactor value is used as a multipler in adjusting the height of the simulated curve. The difference between the simulated and measured data can be seen by setting the toggle switch to subtract.
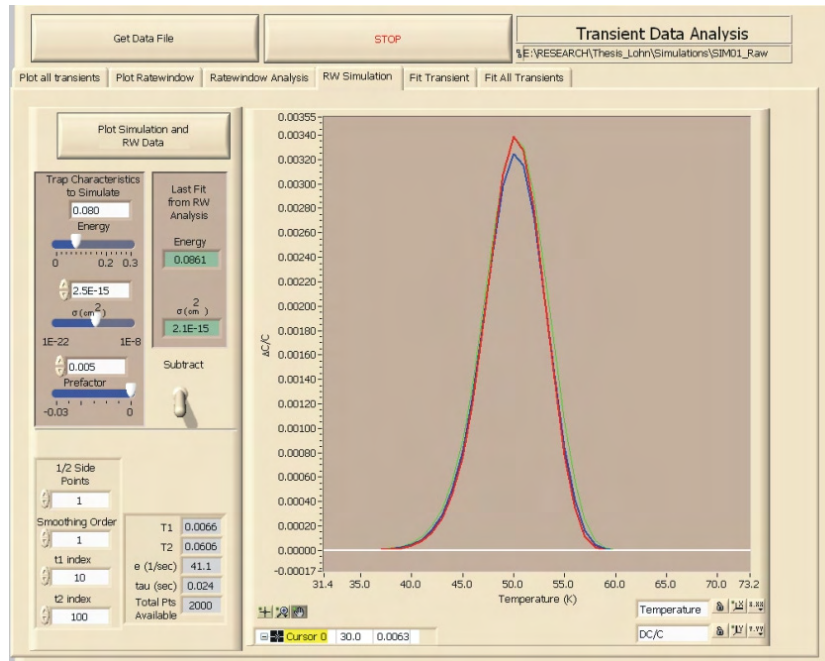
DLTS Data Fitting and Analysis window - RW simulation

2. Transient Analysis

The Semetrol software records the capacitance transient over the time period and determines the emission rate from this information. The software fits the transient to an exponential function involving one or two exponents. The fit parameters can be viewed and adjusted using the "Fit Transient" tab. Use the mean square error (mse) to gauge the goodness of fit. This information may be used for the following tab "Fit All Transients" as the "Initial Values" in performing the fit of the data. The software performs a maximum of 600 iterations to fit all of the data within the specified temperature range.
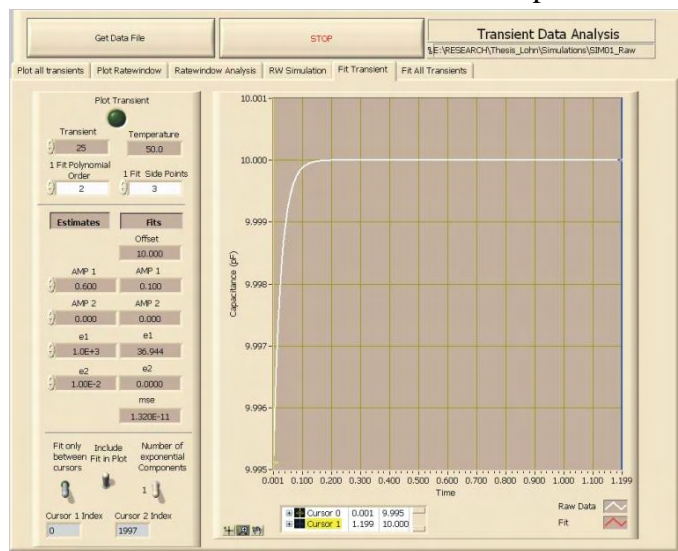
DLTS Data Fitting and Analysis window - Fit Transient
SIM01A fit using one exponent
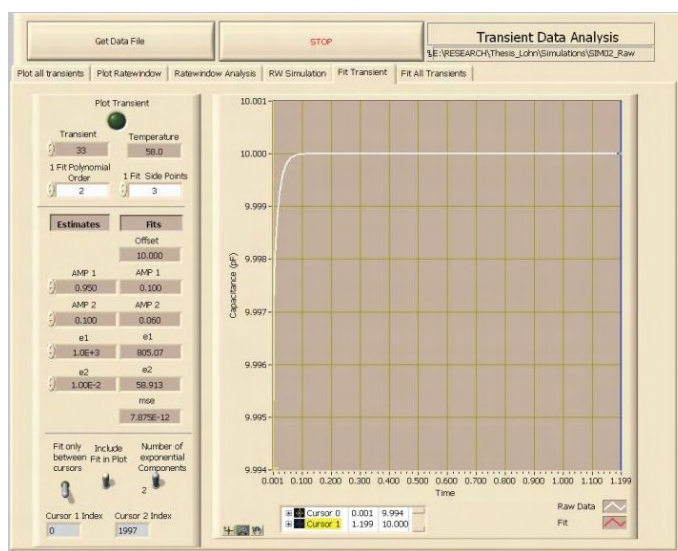
DLTS Data Fitting and Analysis window - Fit Transient
SIM02A3 fit using two exponents

A second method for determining the energy of the trap(s) and capture cross section is by fitting the individual transients to an exponential function and saving the information to a file, which can be opened in the Arrhenius Plot Select Points program.

Put in the number of data points (≤ Total points available) you wish to analyze in the "Number of points" block and the point number (≥ 1) that you wish to begin with in the "Start Index" block. This will allow you to filter out the beginning or the end of the transient

Click the "smooth" button (green light on) to work with the smoothed data or leave the off to work with the raw data.

Click the "All Temps?" button (green light on) to work with the data over the entire temperature range or turn off the button and fill in the start and end temperature to specify the temperature range.

Click the "Use initial value" button (green light on) to use the values determined from the "Fit Transient" tab window as the starting point for the iterations. Turn the button off to allow the software to perform the fits using the previous fit as the starting point for the iterations. The software performs a maximum of 600 iterations, for this reason it may become necessary to specify the initial values so the maximum is not reach before obtaining an acceptable fit.

After you have set the parameters of the fit, click the "Fit All" button and the software will perform the fits of the transients. You can monitor the results in the lower left hand corner of the window. After all transients are complete, you will be prompted to save the file.
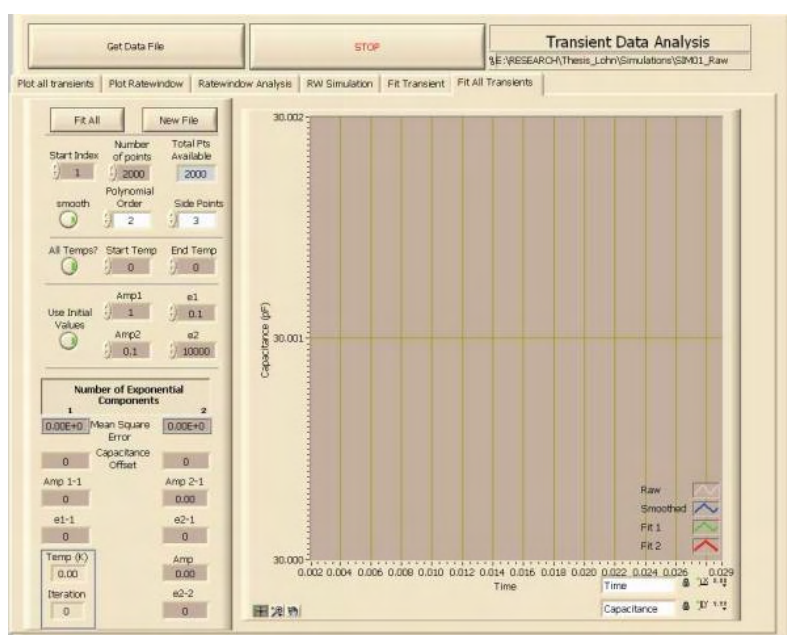
DLTS Data Fitting and Analysis window - Fit All Transients

The SIM01A data was fit using the Fit All Transients program using the following conditions:

All fits used
Start Index: 1   Number of points: 2000
Smooth: On   Polynomial Order: 2   Side points: 3

Fit1: All temps - On, Use initial values – On
        (Initial Values: Amp1 = 0.9, e1 = 0.1; Amp2 = 0, e2 = 0)

        *Since we know only one trap was used in generating the simulated data, Amp2
        and e2 were set to zero.*

Fit2: All temps - On, Use initial values – Off

Fit3: All temps - Off, Use initial values – On
        (Start Temp = 36K, End temp = 58K)
        (Initial Values: Amp1 = 0.9, e1 = 0.1; Amp2 = 0, e2 = 0)

Fit4: All temps - Off, Use initial values – Off
        (Start Temp = 36K, End temp = 58K)

The Fit All Transient files can be opened and analyzed using the Arrhenius Plot – Select Points program which can be opened from the main menu window.
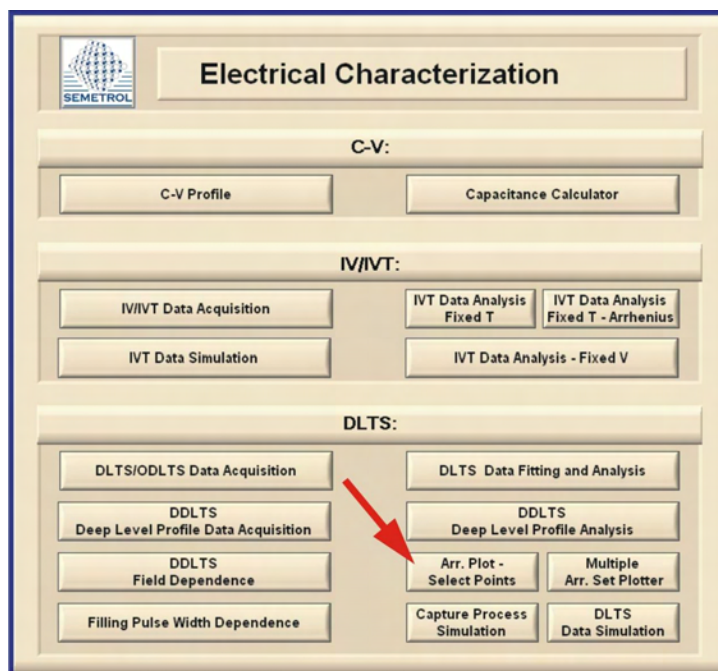
Semetrol software main menu window

The Fit All Transient file can be loaded by selecting the "New File" and then selecting the file from the pop up menu. The data will appear in the Arrhenius plot (T^2/e vs. $1/kT$).

The No. Fit value can be set to 1, 2, or 1&2 depending on whether you want to display the data fit to one exponent (1), two exponents (2) or see both at the same time (1&2). The n value is generally set to 1. The minimum and maximum sample time determine the limits of valid data. The minimum sample time should be set to the sampling period of the measurement and the maximum sampling time should be equal or less than the sampling period multiplied by the number of samples, which is equal to the duration of the transient.

The sampling period was 6.0E-4 seconds and the number of samples (or points) was 2000 for the SIM01A data. Therefore the minimum and maximum sampling period are:

Minimum sample period: 6.0E-4 seconds
Maximum sample period: 6.0E-4 seconds x 2000 samples = 1.2 seconds

Press the "Plot Points" button to plot the data on the graph.

When the data is displayed, points will appear or disappear based on the settings of the blue sliders at the bottom of the window. The top slider adjusts the error limit based on the mean square error. The middle slider is used to remove transients with unrealistically large amplitudes and the bottom slider removes transients with low amplitudes. The maximum amplitude is based on ΔC/C value and the amplitude minimum threshold is based on the ΔC value.

Arrhenius Plot – Select Points window
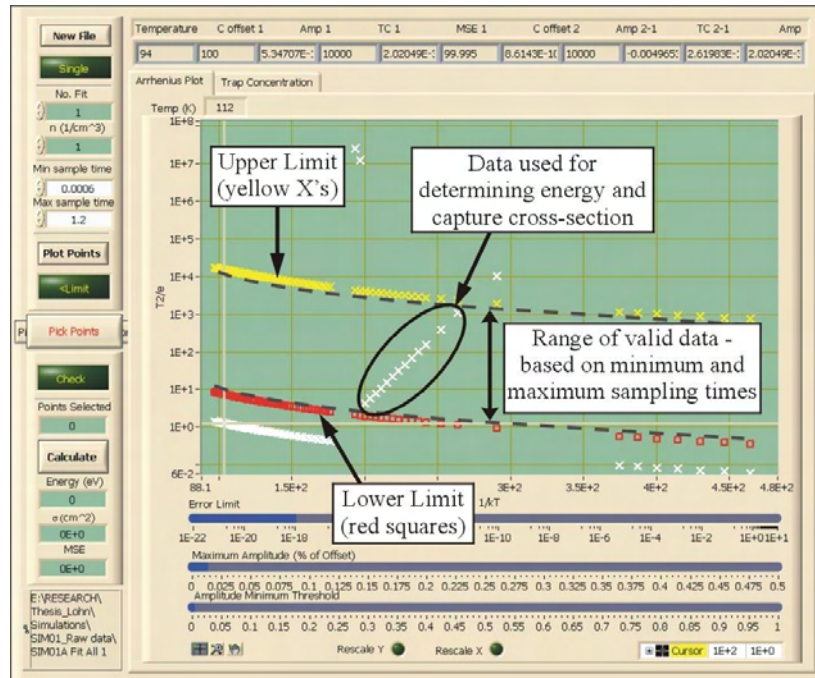
SIM01A Fit 1 – No. Fit = 1

Press the "Pick Points" button and use the crosshairs to select the points you wish to use in the Arrhenius plot. If the crosshairs are not visible, right-click the cursor legend in the bottom right of the window and select 'bring to center'. Drag the crosshairs to the point and press the enter key or use the "pick points under cursor" button that will appear under the "Pick Points" button to select the point. After all points are selected, press the "Calculate" button to calculate energy, capture cross section and mean square error.
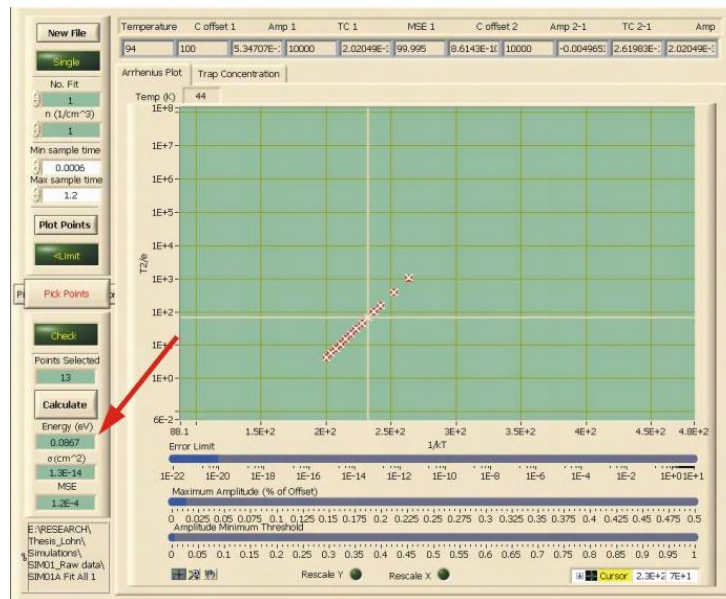
SIM01A Fit 1 – No. Fit = 1 calculation

The same data can also be seen resulting from the second exponent and both exponents. When changing the No. Fit between 1, 2 and 1&2, the markers on the plots will change. The 2nd exponent fit can be seen below. As expected, there is no data within the valid range since the simulated data has only one trap.
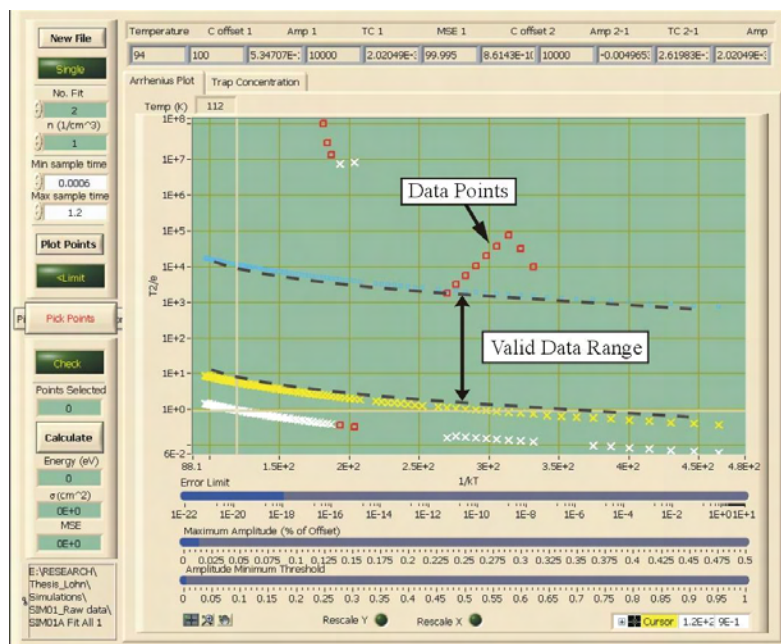
SIM01A Fit 1 – No. Fit = 2
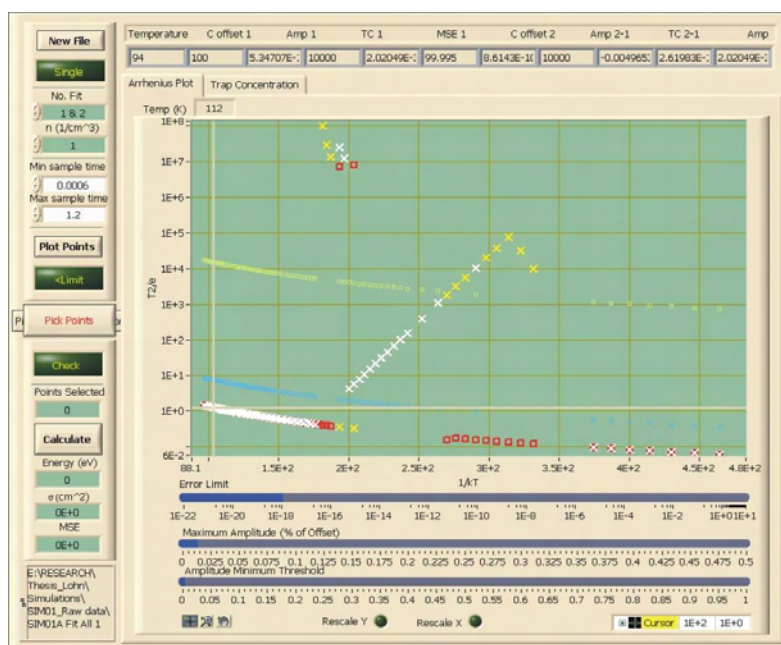
SIM01A Fit 1 – No. Fit = 1&2

The three remaining fits from the Fit All Transients (Fit2, Fit3 and Fit4) gave similar results. A table summarizing the results can be seen following Fit 4. The data was plotted setting the No. Fit to one exponent and the energy was calculated from the selected data points.
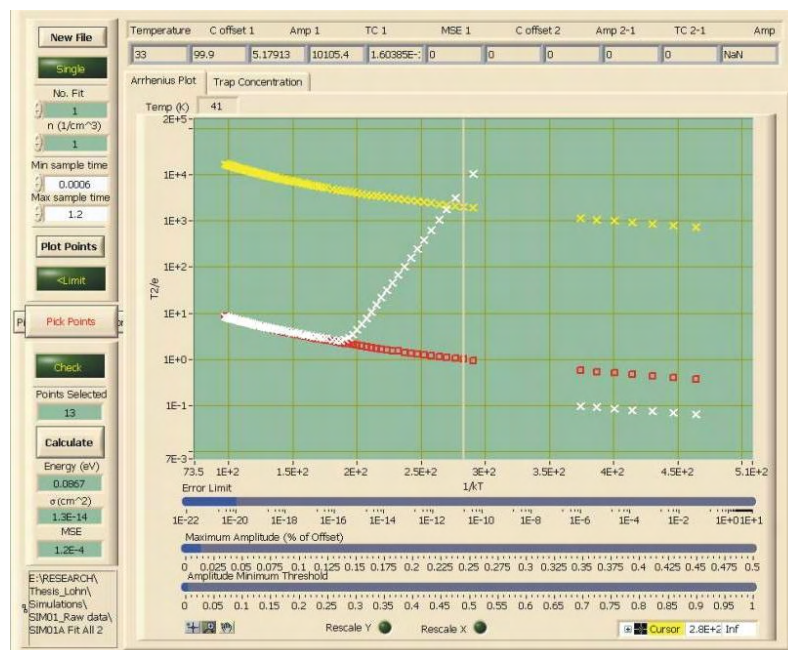
SIM01A Fit 2 – No. Fit = 1
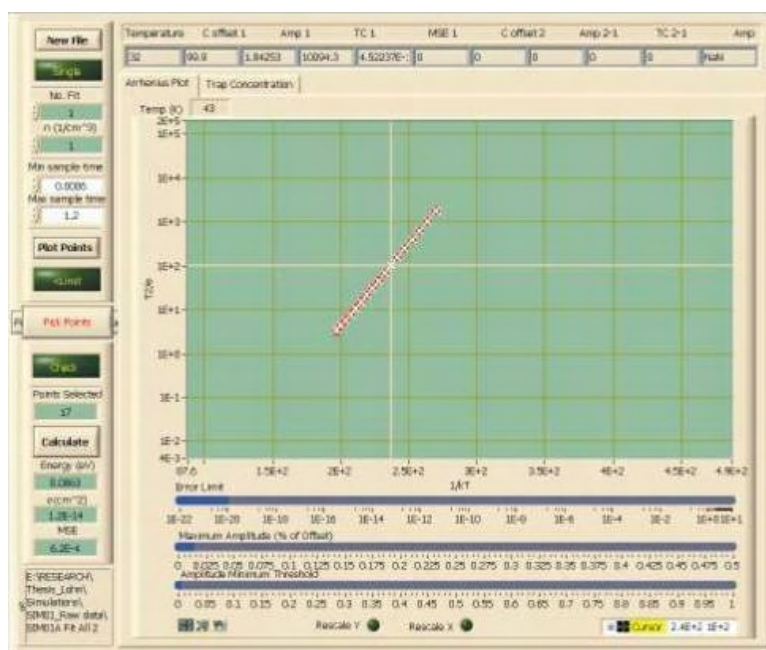
SIM01A Fit 2 – No. Fit = 1 calculation

For Fit 3 and Fit 4 the temperature range during the fit was 36 to 58K. When the user sets All Temps? To off and defines the temperature range there are fewer data points on the plots
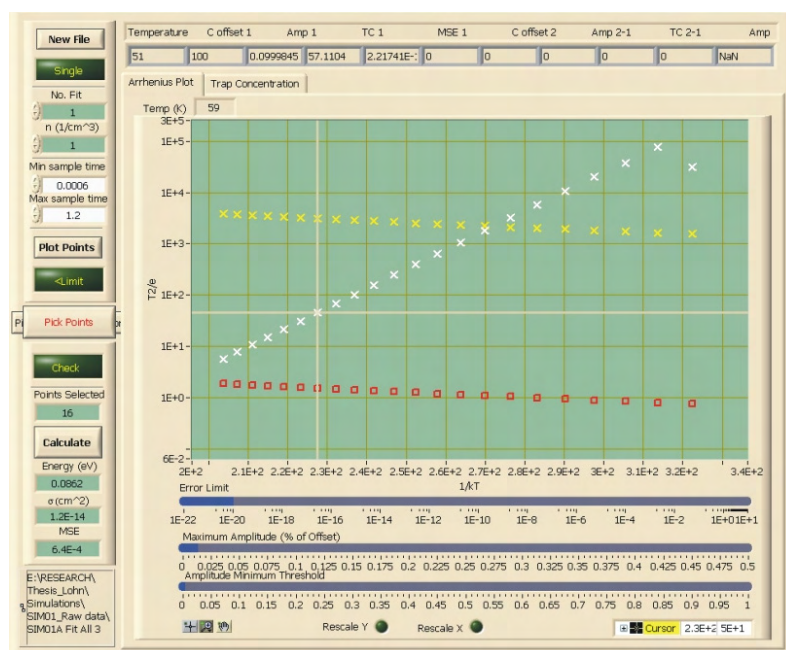
SIM01A Fit 3 – No. Fit = 1
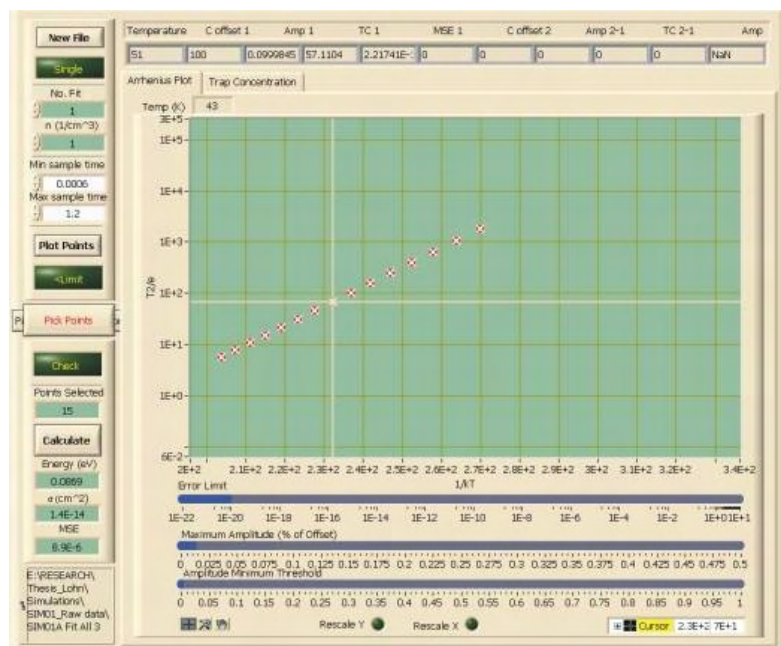
SIM01A Fit 3 – No. Fit = 1 calculation
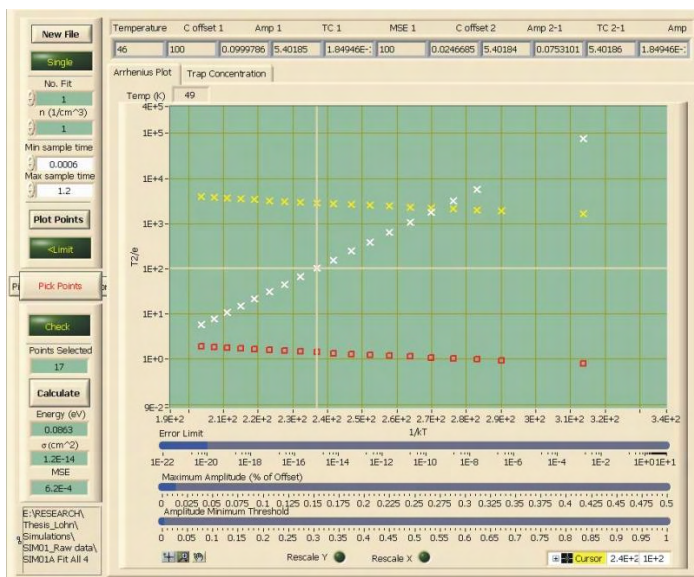
SIM01A Fit 4 – No. Fit = 1
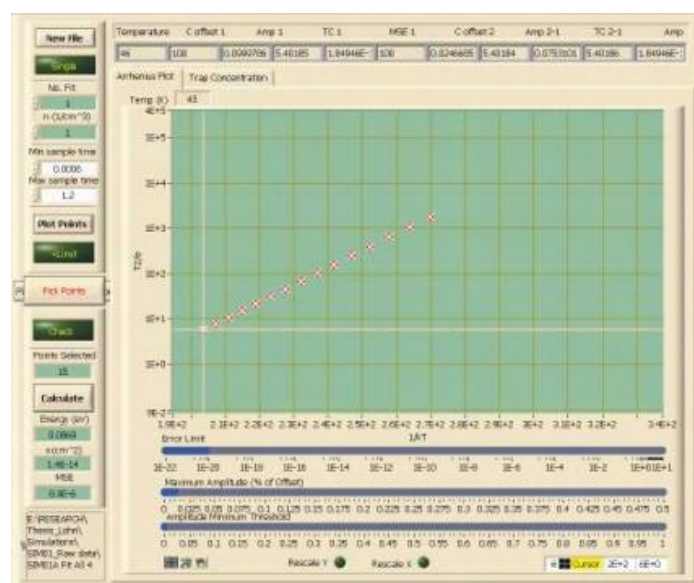
SIM01A Fit 4 – No. Fit = 1 calculation

The resulting energy values matched the simulated value, but the capture cross section was off by an order of magnitude (simulated values: E1 = 0.087 eV, sigma1 = 2.50E-15 cm^2).

	All Temps?	Start Temp	End Temp	Use initial values	Amp1	e1	Amp2	e2	Energy (eV)	Sigma (cm^2)	MSE
Fit 1	On	NA	NA	On	0.9	0.1	0	0	0.0867	1.3E-14	1.2E-04
Fit 2	On	NA	NA	Off	NA	NA	NA	NA	0.0863	1.2E-14	6.2E-04
Fit 3	Off	36	58	On	0.9	0.1	0	0	0.0869	1.4E-14	8.9E-06
Fit 4	Off	36	58	Off	NA	NA	NA	NA	0.0869	1.4E-14	8.9E-06

B. One Trap – with noise

1. Ratewindow Analysis

For comparison, the ratewindow analysis and fit all transient analysis was performed on the SIM01F5 data. The SIM01F5 data has the same parameters as the SIM01A data (noise = 0 pF), but has a noise level of 0.0001 pF (approximately 3% of ΔC). All parameters except temperature limits of the SIM01F5 ratewindow analysis had the same settings as were done on the SIM01A ratewindow analysis.
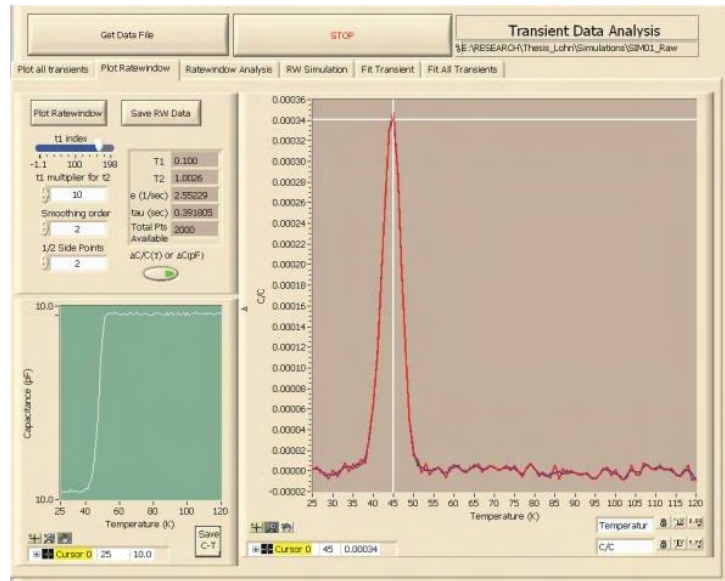
DLTS Data Fitting and Analysis window - Plot Ratewindow tab
Ratewindow of SIM01F5 simulation ($t_1 = 0.100/t_2 = 1.0026$)
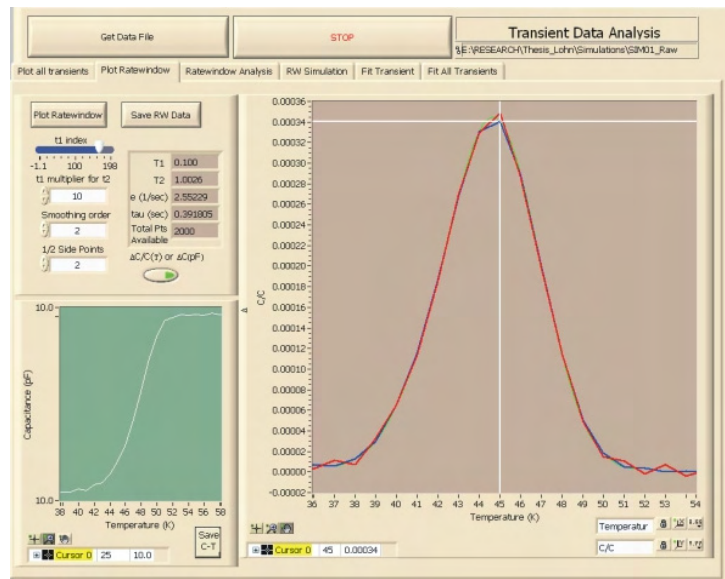
Plot Ratewindow – SIM01F5 zoomed in

The results of the ratewindow analysis gave comparable values (energy = 0.0863 to 0.0872 eV, sigma = 2.1E-15 to 2.7E-15). However additional points that did not fall on the linear curve in the Arrhenius plot were generated due to the noise. For this reason, care must be taken when selecting points used in the calculation.
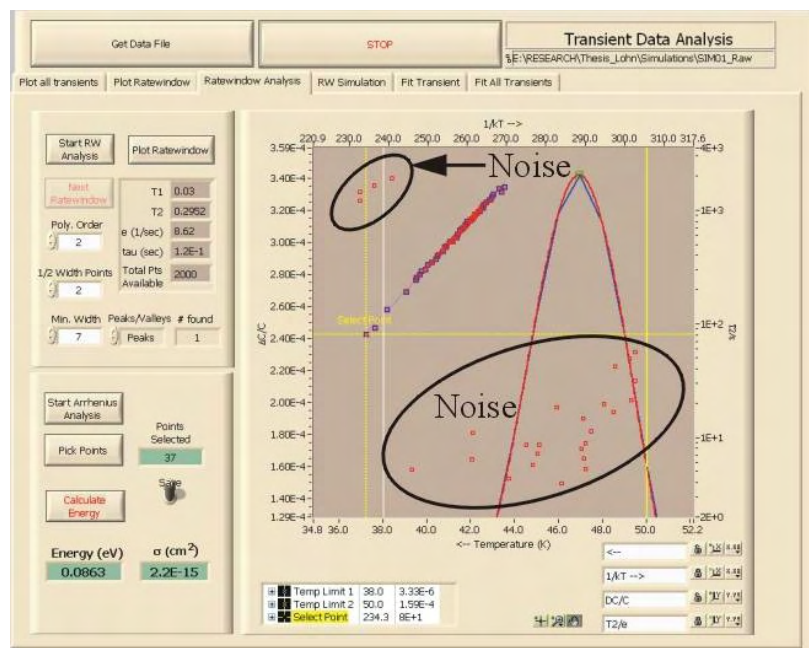
Ratewindow Analysis of SIM01F5

The additional points attributed to the noise are due the algorithm determining peaks found in the noise variation.
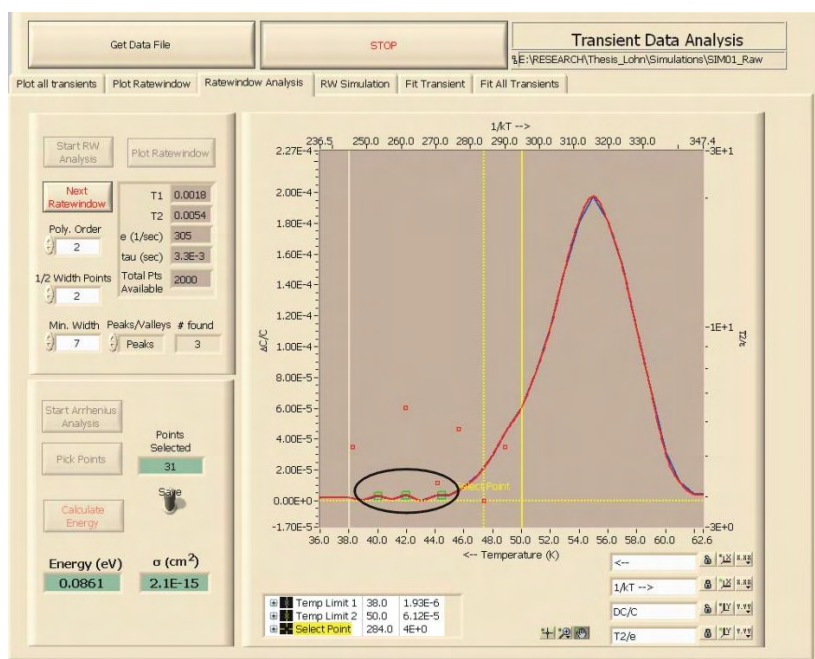
The amount of invalid data points created due to noise will vary upon the temperature limits of the ratewindow analysis. As the temperature range is decreased, fewer points attributed to noise are created.
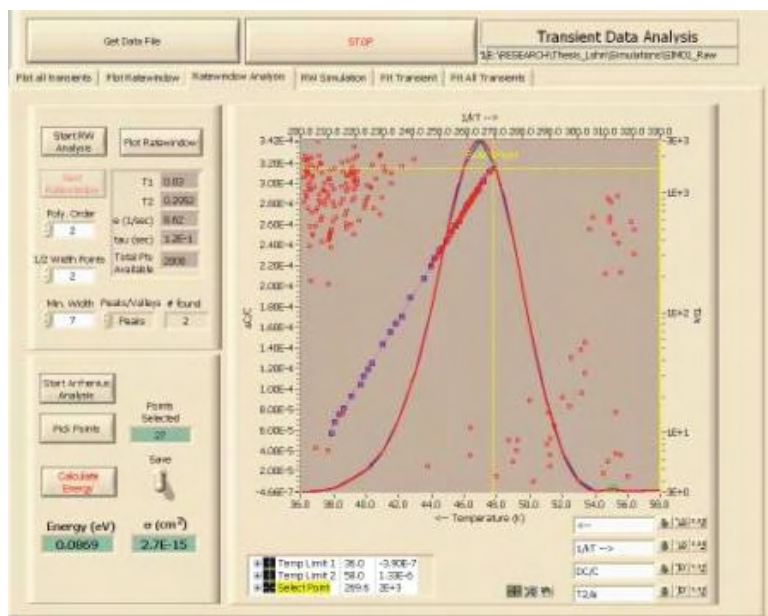
Ratewindow Analysis of SIM01F5
Temperature range: 36 to 58K
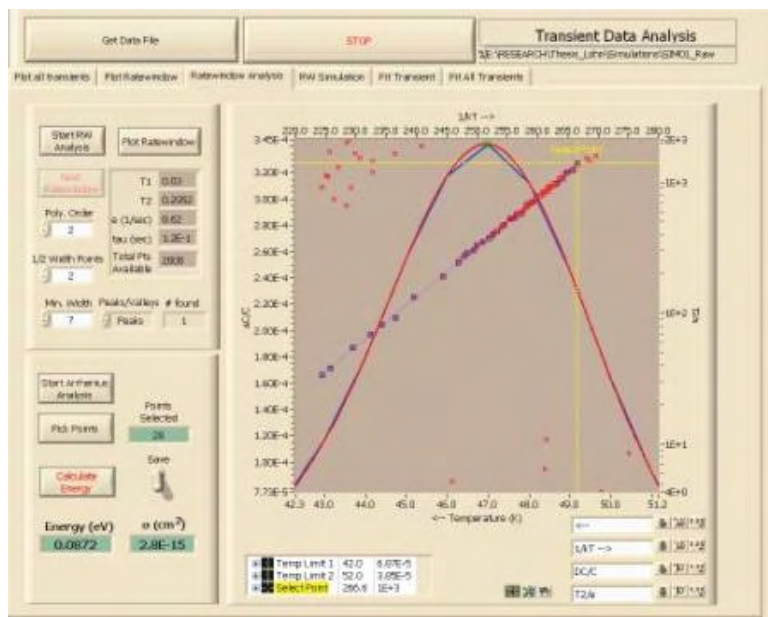
Ratewindow Analysis of SIM01F5
Temperature range: 42 to 52K

If the temperature range is too large or the measurement is too noisy, you run the risk of drowning out the linear curve due to the data points created by the noise. In the plot below, the linear curve is easily identifiable.
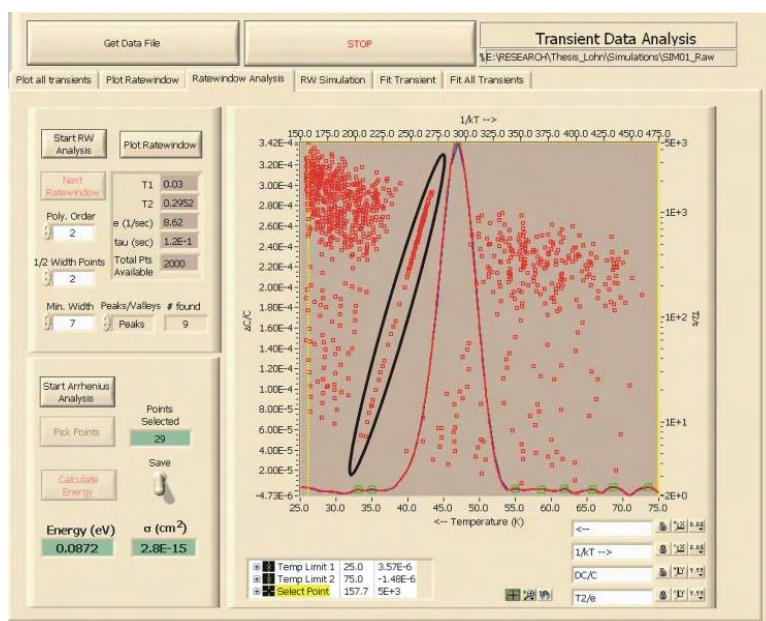
Ratewindow Analysis of SIM01F5
Temperature range: 25 to 75K

2. Transient Analysis

The Fit All Transients algorithm was performed on the SIM01F5 data and analyzed in a similar manner to the SIM01A data. The error limit on the Arrhenius Plot – Select Points window for the SIM01F5 data was set two orders of magnitude higher to display all of the points within the valid data range. The energy values matched closely with the value used in the simulation (0.087 eV), but the capture cross section still differed by an order of magnitude.

|	All Temps?	Start Temp	End Temp	Use initial values	Amp1	e1	Amp2	e2	Energy (eV)	Sigma (cm^2)	MSE
Fit 1	On	NA	NA	On	0.9	0.1	0	0	0.0868	1.4E-14	1.8E-04
Fit 2	On	NA	NA	Off	NA	NA	NA	NA	0.0869	1.4E-14	1.7E-04
Fit 3	Off	36	58	On	0.9	0.1	0	0	0.0868	1.4E-14	1.8E-04
Fit 4	Off	36	58	Off	NA	NA	NA	NA	0.0868	1.4E-14	1.8E-04

C. Two Traps – without noise

1. Ratewindow Analysis

A similar analysis can be performed on two closely spaced traps (E1 = 0.087 eV, E2 = 0.107 eV). The ratewindow of the SIM02A3 simulation shown below has two clearly identifiable peaks. In addition to the two peaks in the ratewindow, there is a deviation in the C-T curve at approximately 51K.
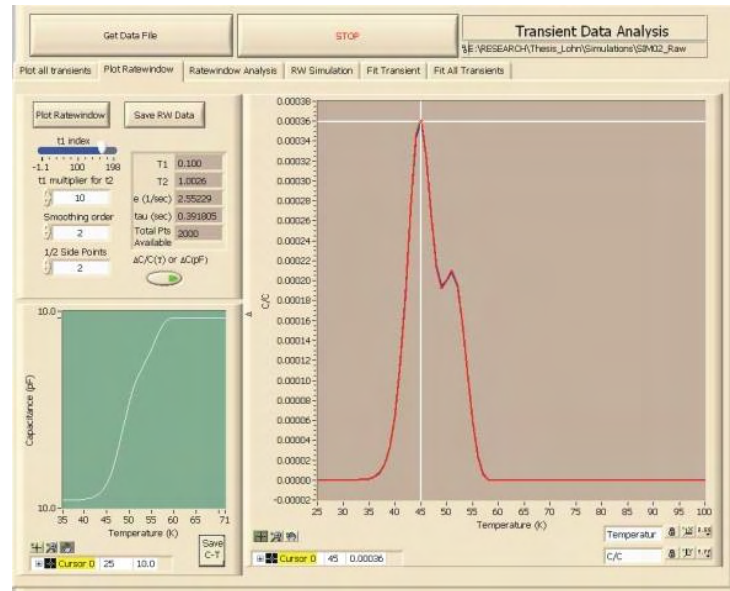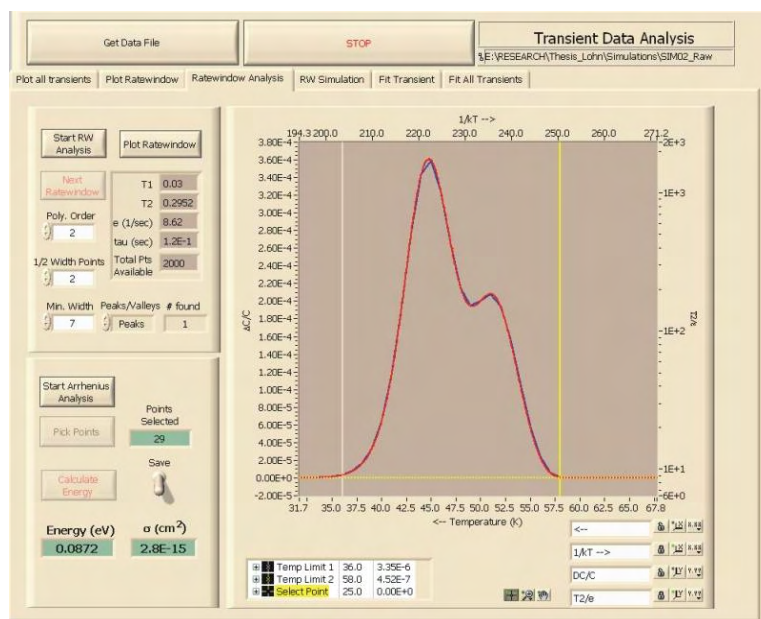

DLTS Data Fitting and Analysis window - Plot Ratewindow tab
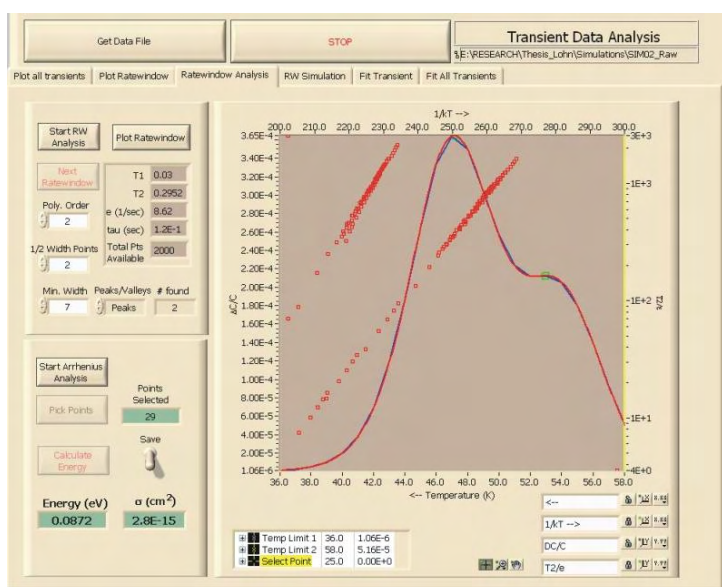**Ratewindow of SIM02A3 simulation (t_1 = 0.100/t_2 =1.0026)**
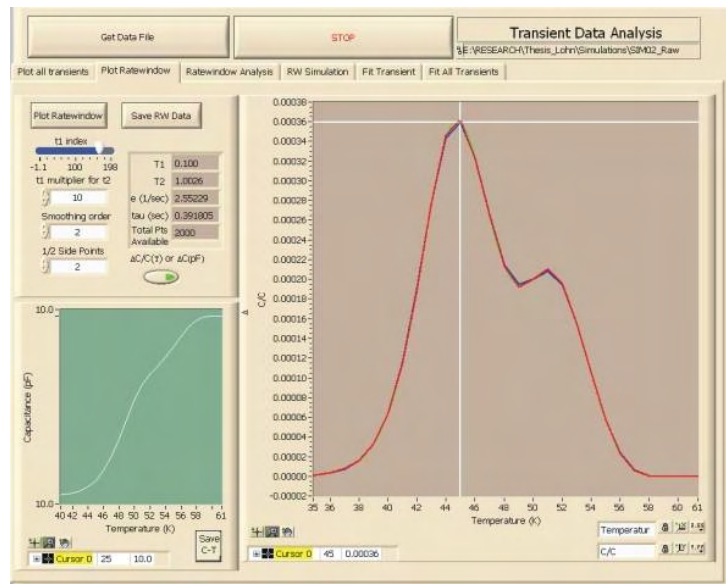
Plot Ratewindow – SIM02A3 zoomed in

The ratewindow analysis was performed over the temperature range 36 to 58K.

Ratewindow Analysis – SIM02A3

After all of the data points were found, the resulting plot displayed two linear curves, one for each trap.

Each trap must be analyzed separately when you perform the Arrhenius analysis. Press the "Start Arrhenius Analysis" button and the select the points from one of the curves and then press the "Calculate Energy" button. You will then press the "Start Arrhenius Analysis" button and do the same for the second curve.

The analysis of the first curve gave an energy value of 0.0852 eV and capture cross section of 1.6E-15 cm^2 for the simulated values of 0.087 eV and 2.5E-15 cm^2.
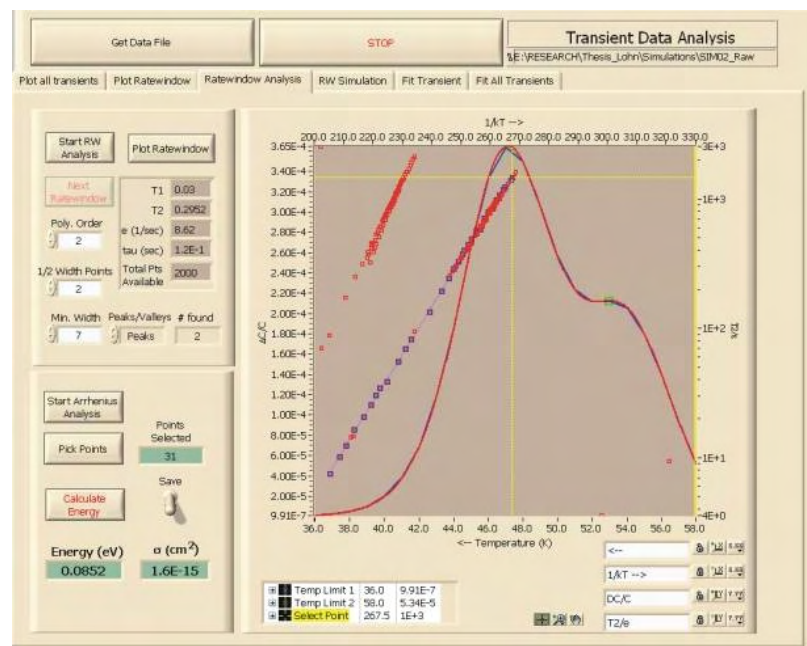
The analysis of the second curve gave an energy value of 0.109 eV and capture cross section of 1.7E-14 cm^2 for the simulated values of 0.107 eV and 1.0E-14 cm^2.
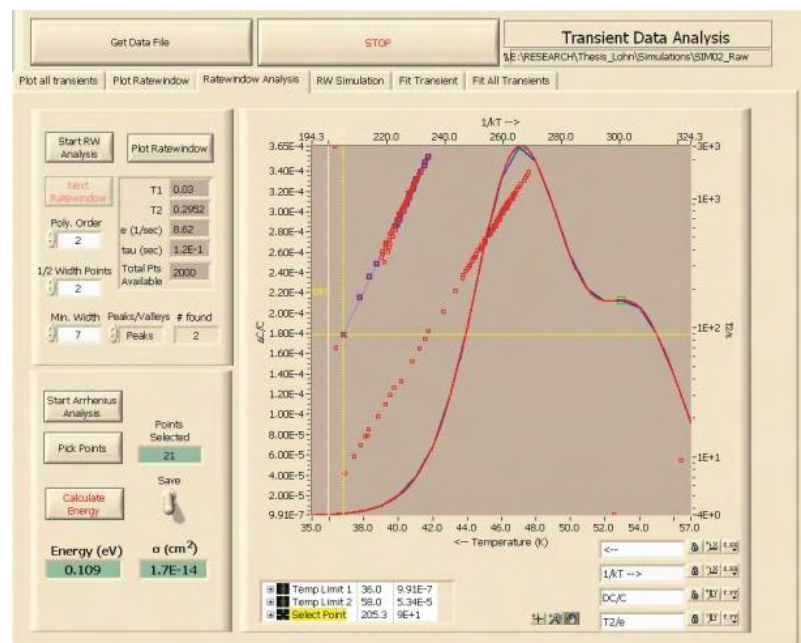
2. Transient Analysis

The Fit All Transients algorithm was performed on the SIM02A3 data over the entire temperature range (All Temps? – On) and with the "Use Initial Value" button off. The other parameters displayed below, had the same settings as previous analysis.

All fits used
Start Index: 1   Number of points: 2000
Smooth: On   Polynomial Order: 2   Side points: 3

When viewed in the Arrhenius Plot – Select Points window with the No. fit set to 1, the curve appears to have a kink in it, suggesting two traps.
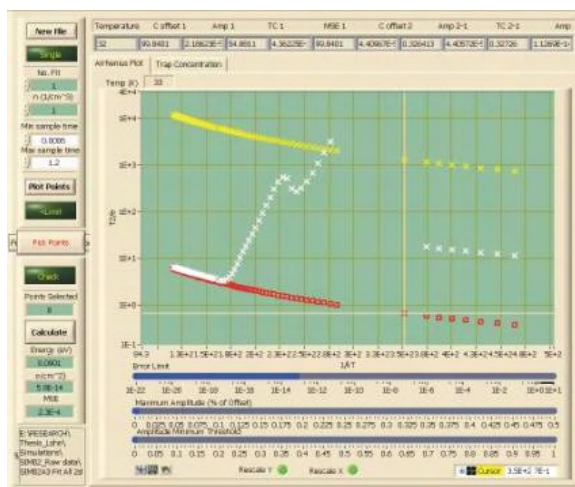
SIM02A3 Fit – No. Fit = 1

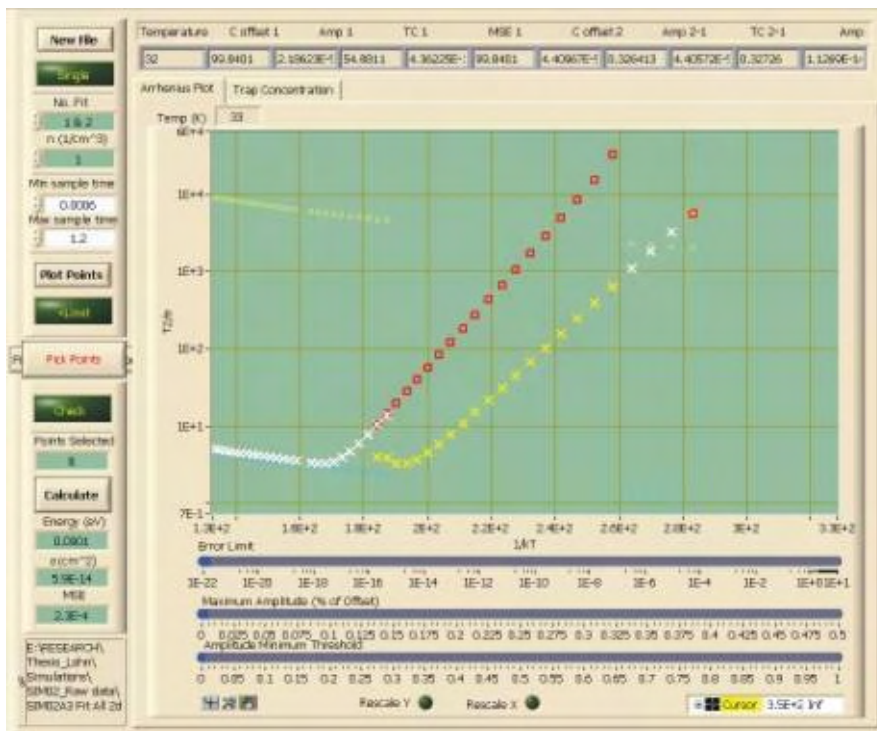The two traps are clearly visible when the No. fit is set to 2.
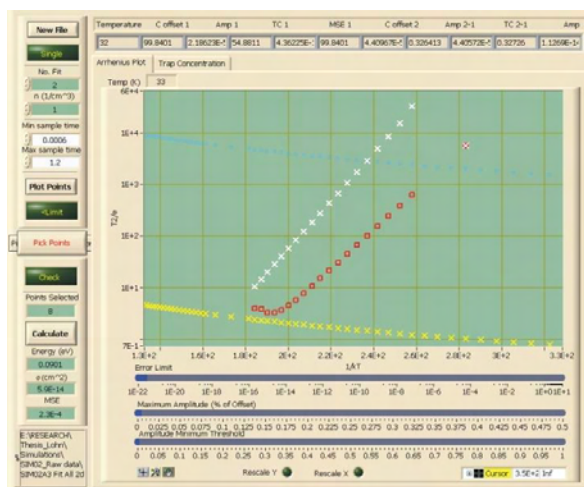
SIM02A3 Fit – No. Fit = 2
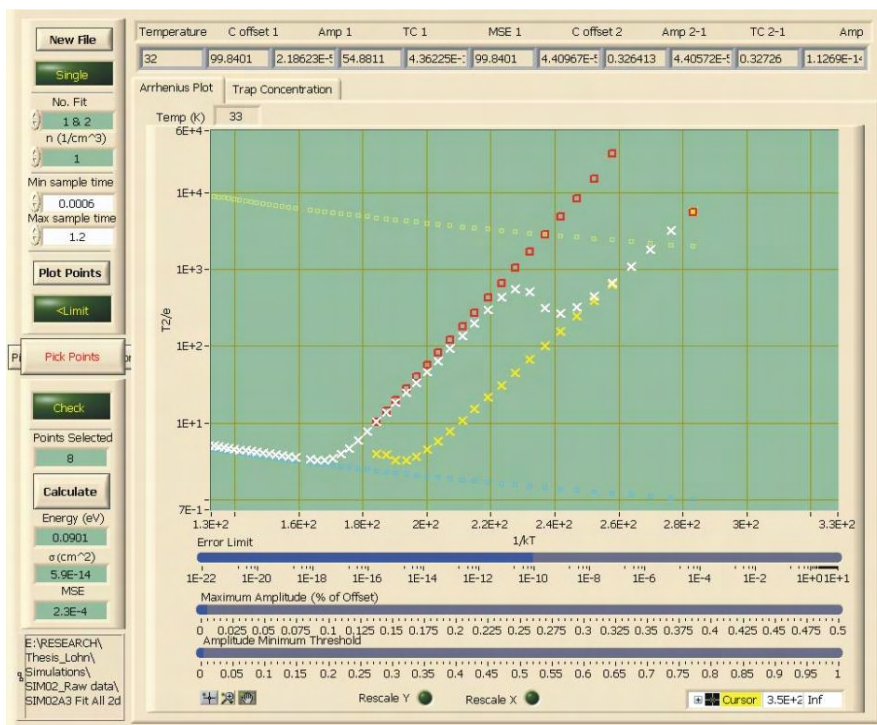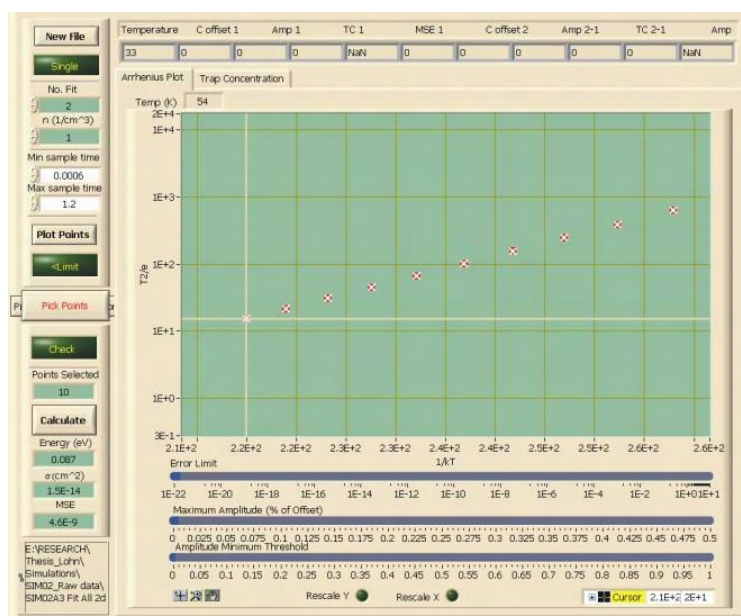
SIM02A3 Fit – No. Fit = 1&2

As the error is reduced using the slider bar, the one exponent fit is removed.
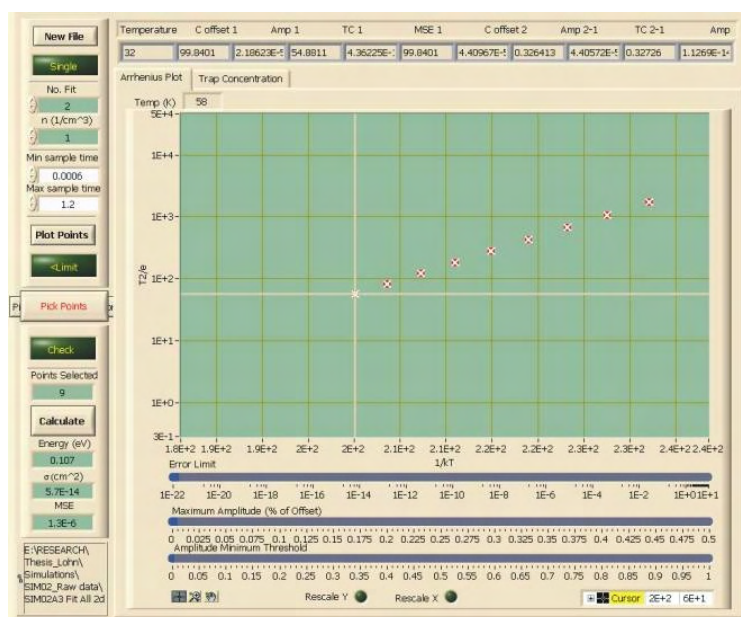

SIM02A3 Fit – No. Fit = 1&2

The energy calculation was performed on each trap. Similar to the ratewindow analysis, each trap must be done separately.

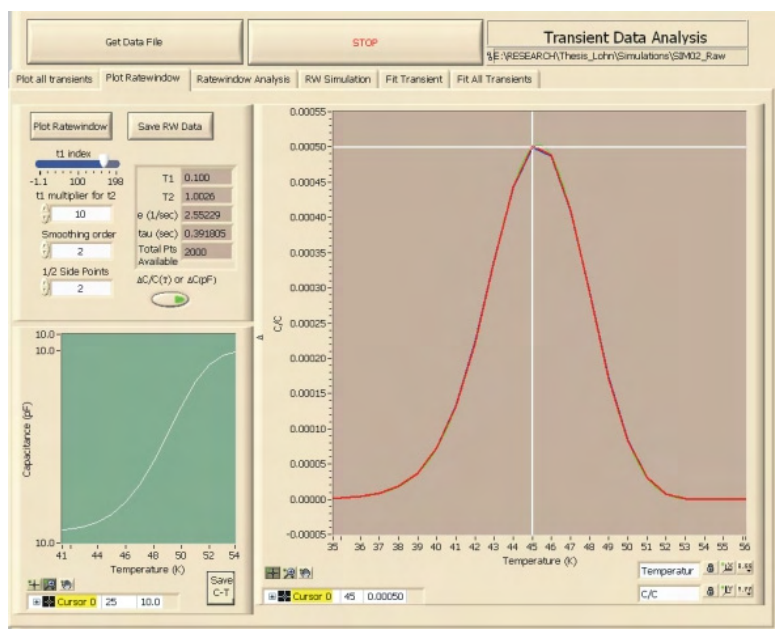|	Simulated		Calculated		
	Energy (eV)	Sigma (cm^2)	Energy (eV)	Sigma (cm^2)	Mean Square Error
Trap 1	0.087	2.5E-15	0.087	1.5E-14	4.6E-09
Trap2	0.107	1.0E-14	0.107	5.7E-14	1.3E-06

SIM02A3 Fit – No. Fit = 2 calculation (1st Trap)

SIM02A3 Fit – No. Fit = 2 calculation (2nd Trap)

1. Ratewindow Analysis

The ratewindow analysis was also performed on SIM02A1 where the trap energies differ by 0.01 eV compared to 0.02 eV for SIM02A3. Due to the close spacing of the traps, there are not two discernable peaks in the ratewindow.
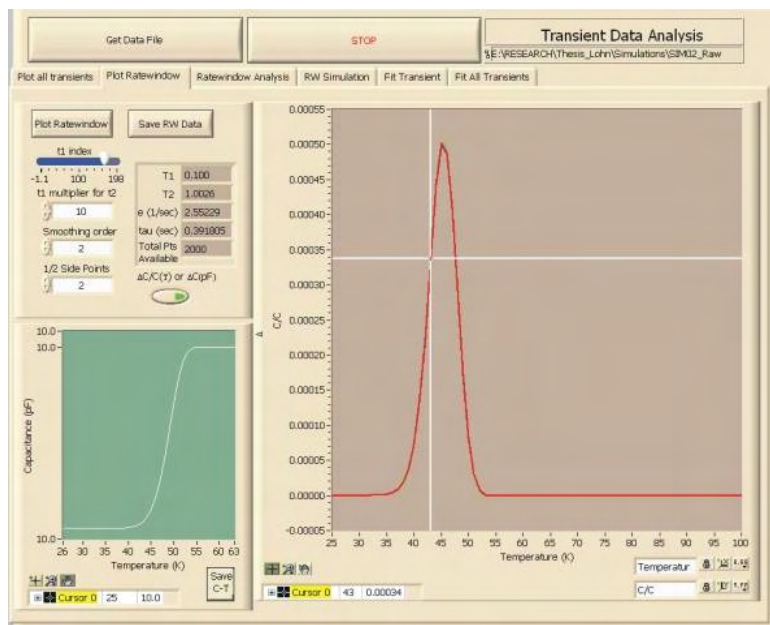

DLTS Data Fitting and Analysis window - Plot Ratewindow tab
Ratewindow of SIM02A1 simulation ($t_1 = 0.100/t_2 = 1.0026$)

Plot Ratewindow – SIM02A1 zoomed in

The ratewindow analysis was performed over the temperature range 36 to 58K giving the result below. The calculated energy was 0.089 eV and a sigma of 3.2E-15 cm^2. The second trap is not easily identifiable in the ratewindow analysis.
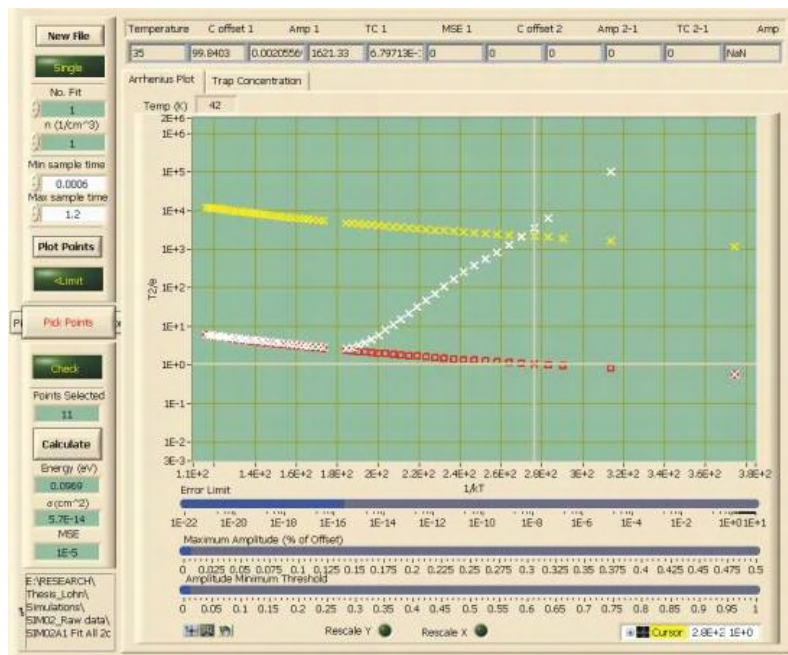
Simulation parameters: E1 = 0.087 eV, sigma1 = 2.5E-15 cm^2
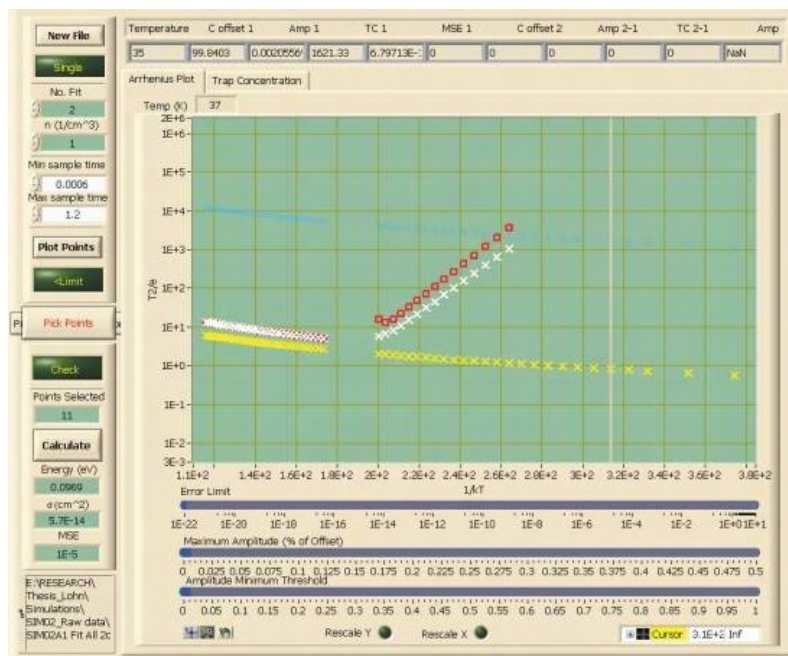E2 = 0.097 eV, sigma2 = 1.0E-14 cm^2)
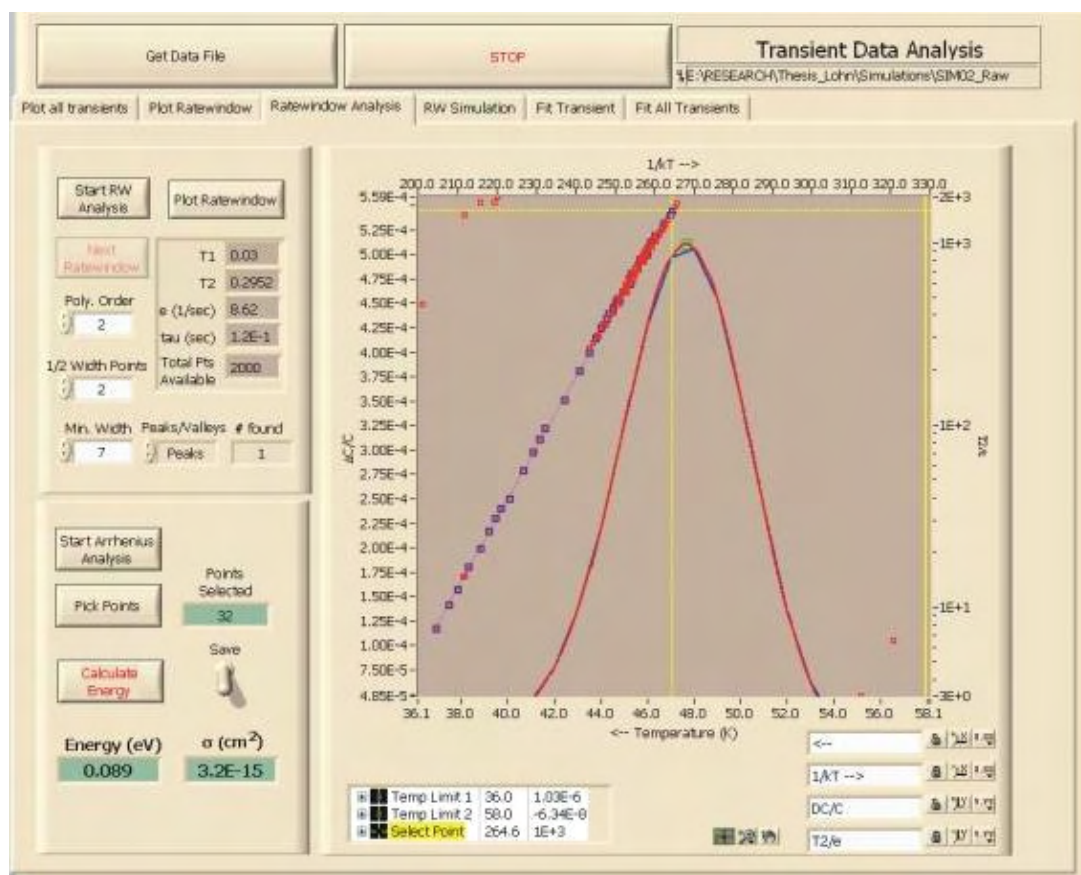
Ratewindow Analysis – SIM02A1
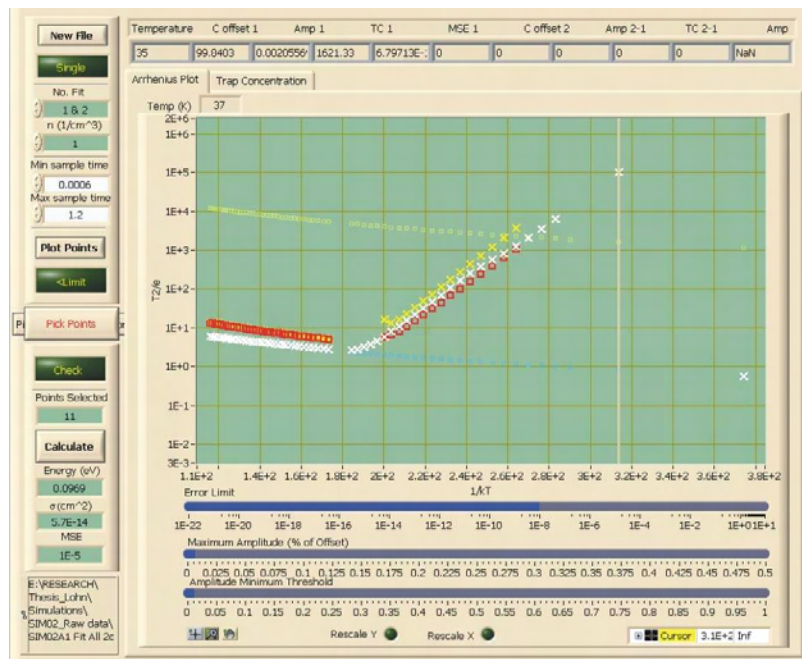
2. Transient Analysis

The Fit All Transients algorithm was performed on the SIM02A1 data with the same settings as were done on the SIM02A3 data.

SIM02A1 Fit – No. Fit = 1
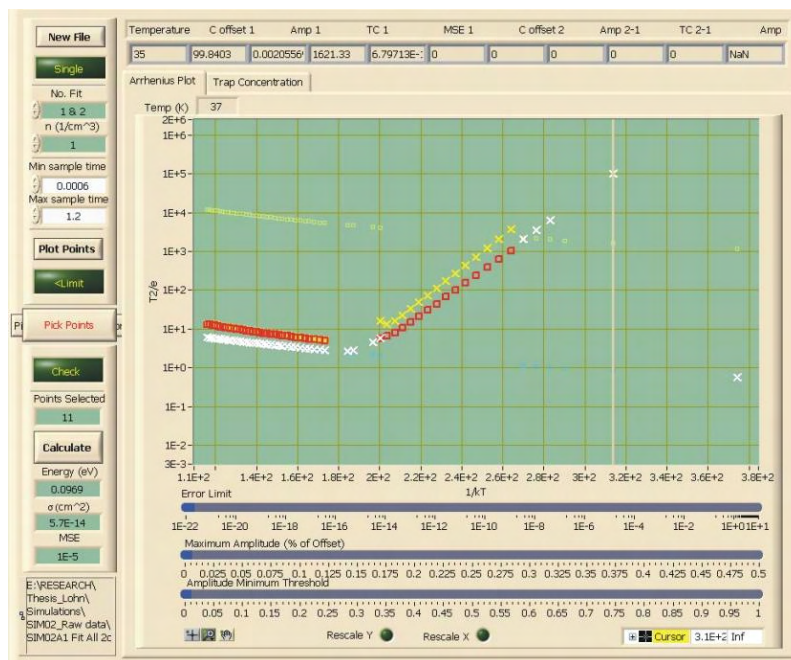

SIM02A1 Fit – No. Fit = 2
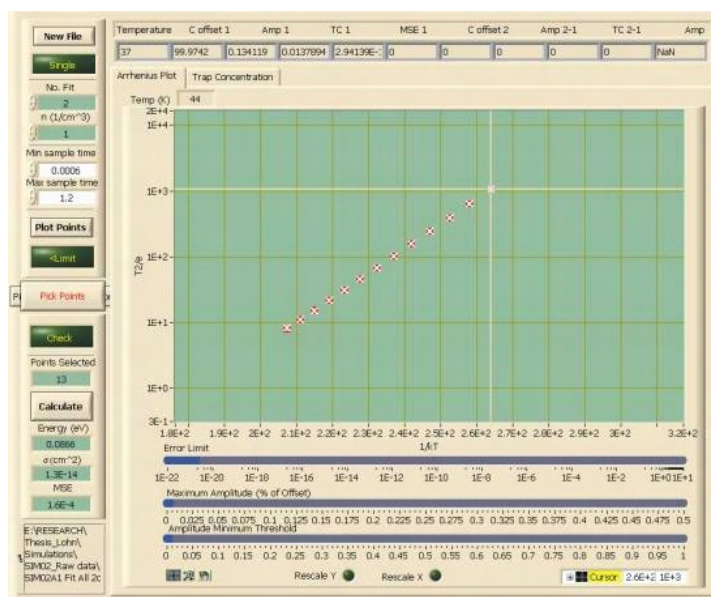
SIM02A1 Fit – No. Fit = 1&2

As the error is reduced using the slider at the bottom of the window, the data fit to the single exponent is removed.

SIM02A1 Fit – No. Fit = 1&2 with error reduced

The energy calculation was performed on each trap.

	Simulated		Calculated		
	Energy (eV)	Sigma (cm^2)	Energy (eV)	Sigma (cm^2)	Mean Square Error
Trap 1	0.087	2.5E-15	0.0866	1.3E-14	1.6E-04
Trap2	0.097	1.0E-14	0.0969	5.7E-14	1.0E-05

SIM02A1 Fit – No. Fit = 2 calculation (1st Trap)
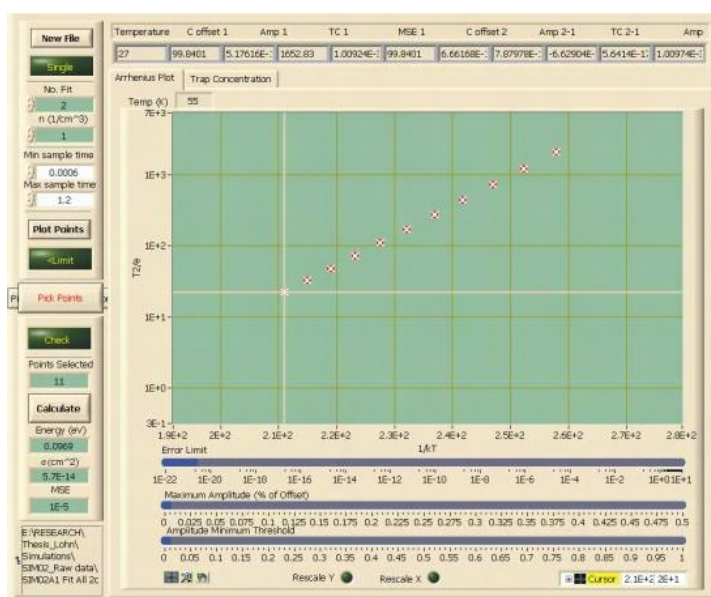
SIM02A1 Fit – No. Fit = 2 calculation (2nd Trap)

1. Ratewindow Analysis

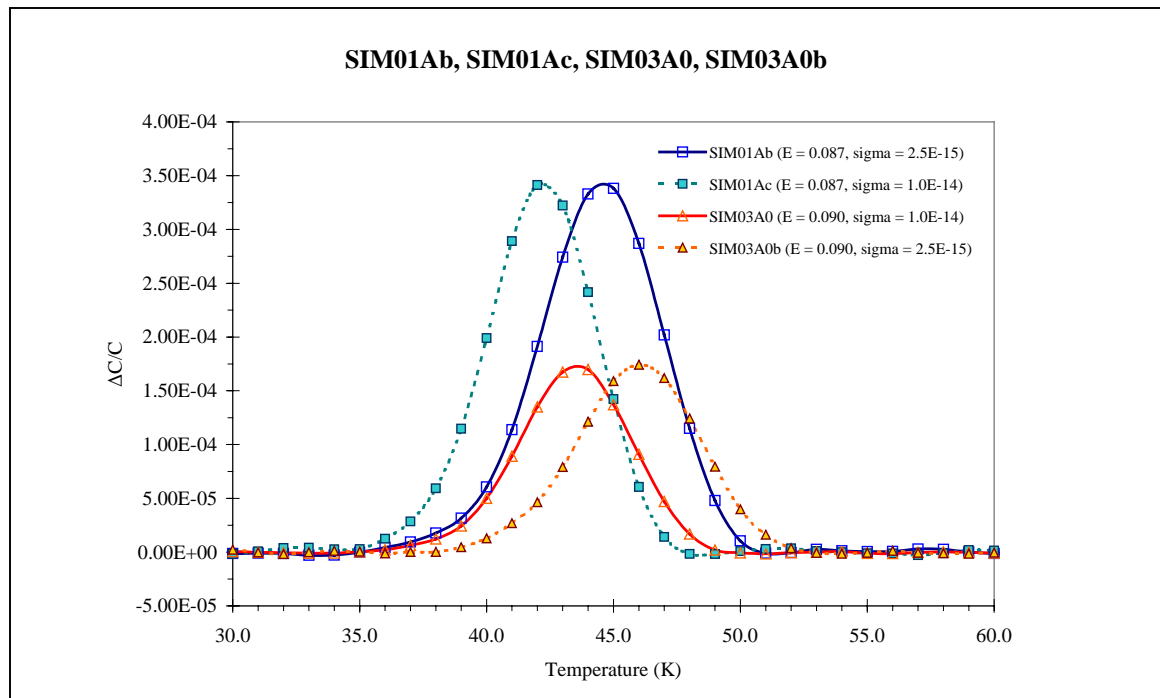A final simulation SIM03A was performed to demonstrate the effectiveness of fitting transients as compared to the ratewindow analysis. The difference in energy of the two traps was decreased to 0.003 eV, the trap density of the second trap was slightly reduced to NT2 = 2.0E15 and low level of noise was added (0.00005 pF – ~1% of ΔC). The parameters of the simulations and the resulting ratewindow plot can be seen below.

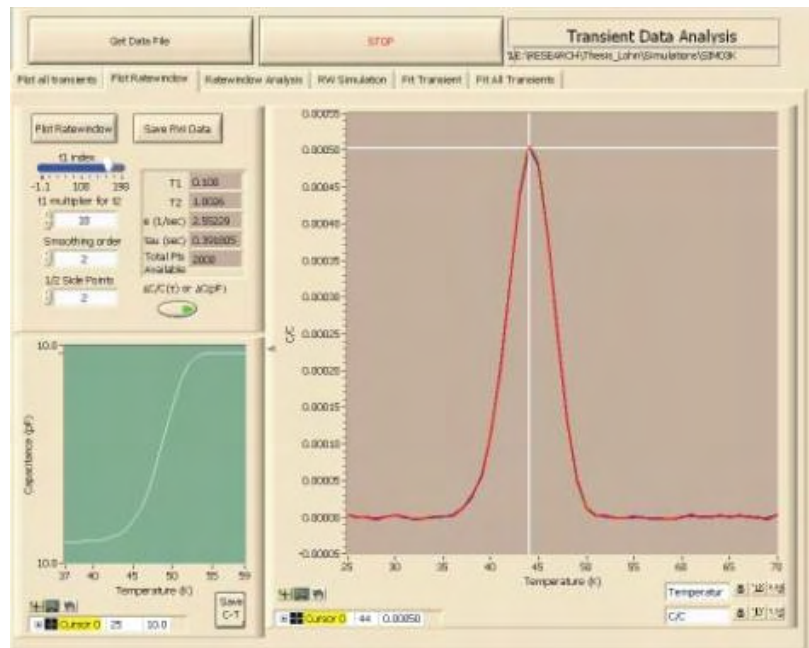| Filename:	SIM01A	SIM03A	SIM03A0
Comments:	Standard - 10 pF		
Parameter			
E1 (eV)	0.087	0.087	0.00
Sigma1 (cm^2)	2.50E-15	2.50E-15	0.00
NT1 (cm^{-3})	1.00E+13	1.00E+13	0.00
E2 (eV)	0.00	0.090	0.090
Sigma2 (cm^2)	0.00	1.0E-14	1.0E-14
NT2 (cm^{-3})	0.00	5.0E+12	5.0E+12
T-low (K)	25.00	25.00	25.00
T-high (K)	71.00	71.00	71.00
T-step (K)	1.00	1.00	1.00
Sample Period (s)	6.00E-04	6.00E-04	6.00E-04
Samples	2000	2000	2000
C0(pF)	10.00	10.00	10.00
Noise (pF)	0.00	0.00005	0.00005
Ns	1.00E+16	1.00E+16	1.00E+16
View (ms)	1200	1200	1200
Effective Mass	1.07	1.07	1.07
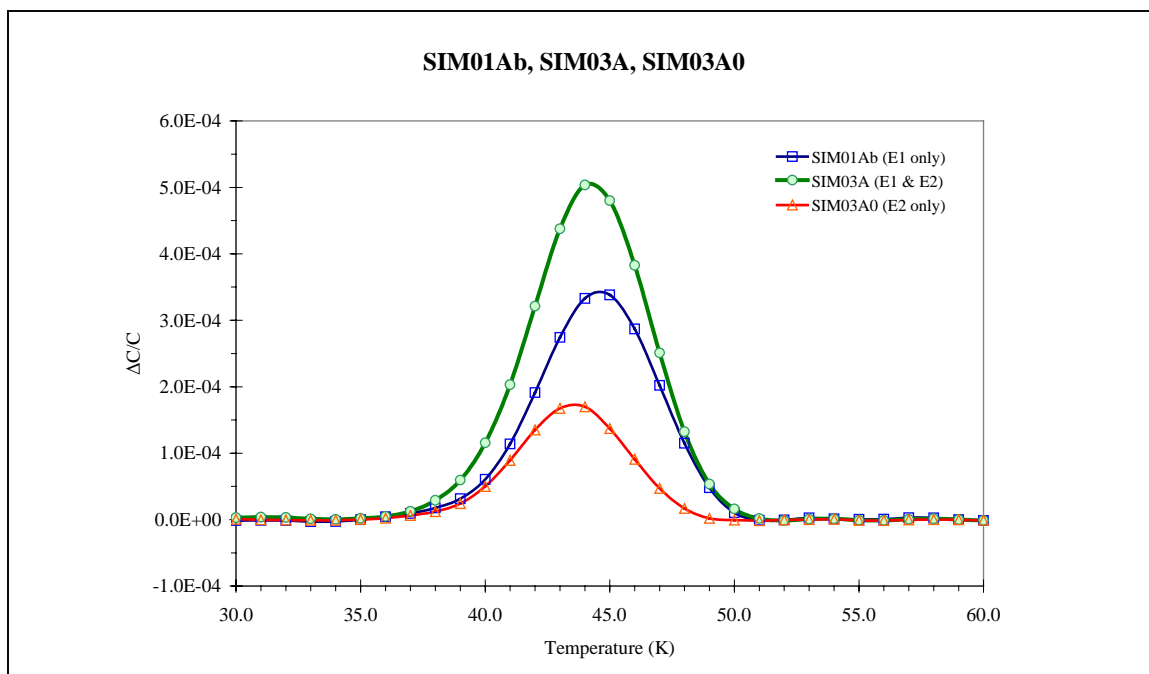
At first glance, it appears that there is an error in the simulated data when comparing the simulations of the individual traps. The peak of the second trap (SIMA30), which has a higher energy value than the first trap (SIM01Ab) occurs to the left of the peak of the first trap. The shift in the peaks is attributed to the difference in the sigma value, which also influences the peak position. For comparison, the individual peaks were compared with simulated peaks with comparable sigma values.

Filename:	SIM01Ab	SIM01Ac	SIM03A0	SIM03A0b
Parameter				
E1 (eV)	0.087	0.087	0.00	0.00
Sigma1 (cm^2)	2.50E-15	1.00E-14	0.00	0.00
NT1 (cm^{-3})	1.00E+13	1.00E+13	0.00	0.00
E2 (eV)	0.00	0.00	0.090	0.090
Sigma2 (cm^2)	0.00	0.00	1.0E-14	2.5E-15
NT2 (cm^{-3})	0.00	0.00	5.0E+12	5.0E+12
T-low (K)	25.00	25.00	25.00	25.00
T-high (K)	71.00	71.00	71.00	71.00
T-step (K)	1.00	1.00	1.00	1.00
Sample Period (s)	6.00E-04	6.00E-04	6.00E-04	6.00E-04
Samples	2000	2000	2000	2000
C0(pF)	10.00	10.00	10.00	10.00
Noise (pF)	0.00005	0.00005	0.00005	0.00005
Ns	1.00E+16	1.00E+16	1.00E+16	1.00E+16
View (ms)	1200	1200	1200	1200
Effective Mass	1.07	1.07	1.07	1.07

SIM01Ab, SIM01Ac, SIM03A0, SIM03A0b

Legend:
- SIM01Ab (E = 0.087, sigma = 2.5E-15)
- SIM01Ac (E = 0.087, sigma = 1.0E-14)
- SIM03A0 (E = 0.090, sigma = 1.0E-14)
- SIM03A0b (E = 0.090, sigma = 2.5E-15)

Y-axis: ΔC/C

X-axis: Temperature (K)

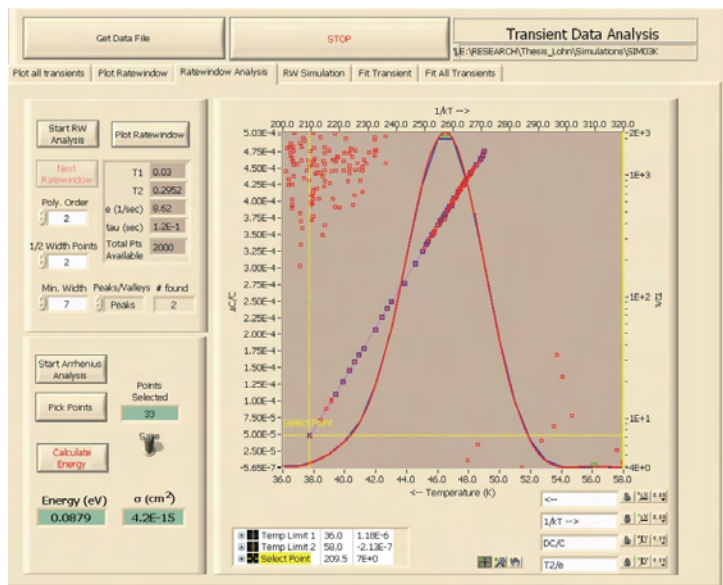The rate window plots for SIM03A can be seen below.

DLTS Data Fitting and Analysis window - Plot Ratewindow tab
Ratewindow of SIM03A simulation (t_1 = 0.100/t_2 =1.0026)
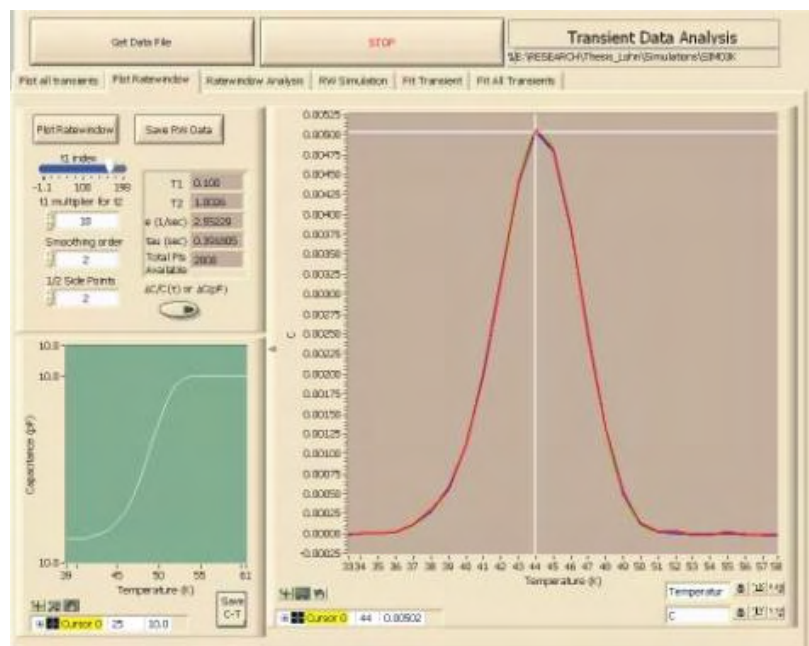
Plot Ratewindow – SIM03A zoomed in

The rate window analysis gave a single identifiable peak with calculated energy of 0.0879 eV and sigma of 4.2E-15 cm^2.

Ratewindow Analysis – SIM03A

2. Transient Analysis

The Fit All Transients algorithm was performed on the SIM03A data over the entire temperature range with initial values off similar to the SIM02A3 and SIM02A1 data. When viewed in the Arrhenius Plot – Select Points window, two distinct traps are visible.
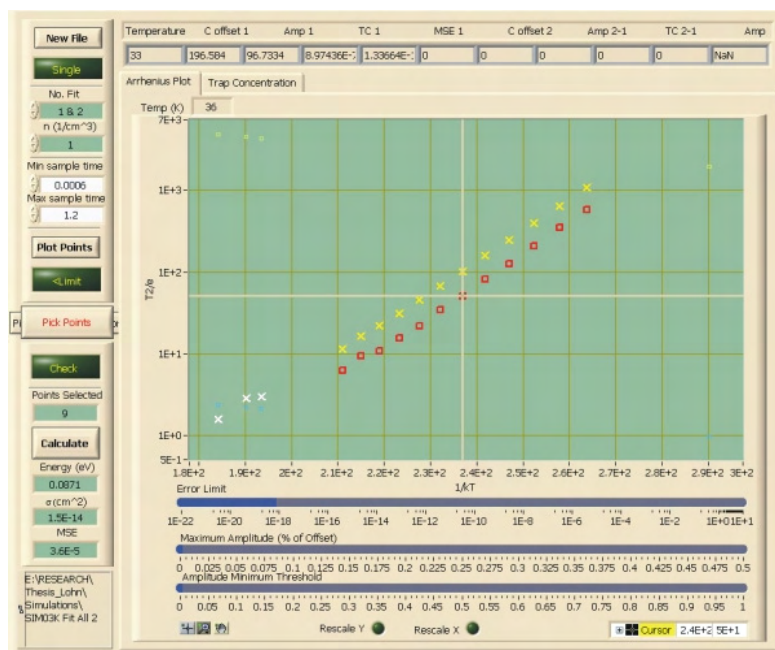
SIM03A Fit – No. Fit = 1&2

The resulting Arrhenius plots for each trap were analyzed to calculate the energy and capture cross section. The results are given below along with the simulated and ratewindow values for comparison.
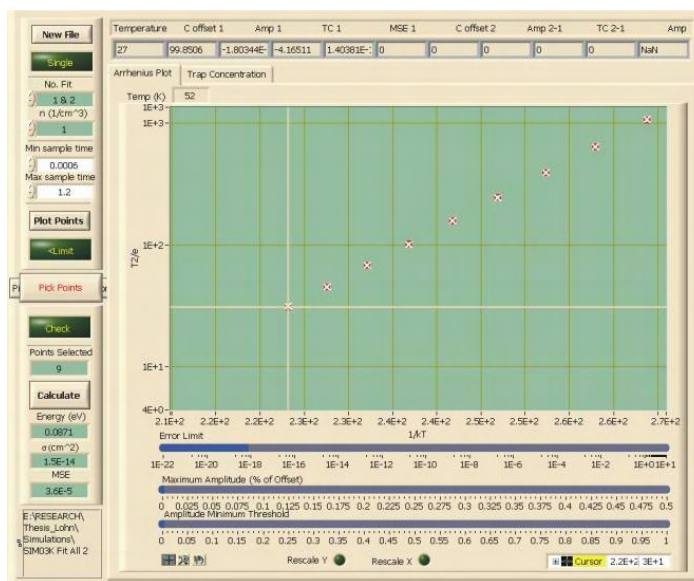

SIM03A Fit – No. Fit = 1&2 calculation (1st Trap)
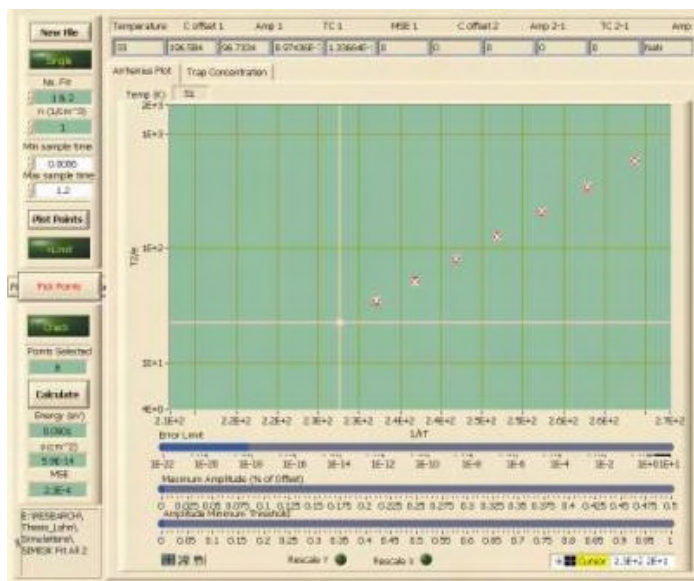
SIM03A Fit – No. Fit = 1&2 calculation (2nd Trap)

	Simulated		Calculated - RW Analysis		Calculated - Transient Analysis		
	Energy (eV)	Sigma (cm^2)	Energy (eV)	Sigma (cm^2)	Energy (eV)	Sigma (cm^2)	MSE
Trap 1	0.087	2.5E-15	0.0879	4.2E-15	0.0871	1.5E-14	3.6E-05
Trap2	0.090	1.0E-14	NA	NA	0.0901	5.9E-14	2.3E-04

REFERENCES

[1]David Halliday, Robert Resnick, and Jearl Walker, <u>Fundamentals of Physics</u>,4th ed. (John Wiley & Sons, Inc., New York, 1993).

[2]<u>Dictionary of Physics</u>, edited by Valerie Illingworth, 2nd ed. (Market House Books Ltd., 1990).

[3]George Gamow, <u>The Great Physicist from Galileo to Einstein</u>, (Dover Publications, Inc., New York, 1961).

[4]William S. Seese and G. William Daub, <u>Basic Chemistry</u>, 5th ed. (Prentice Hall, Englewood Cliffs, NJ, 1988).

[5]Darrell D. Ebbing, <u>General Chemistry</u>, 5th ed. (Houghton Mifflin Company, Boston, 1996).

[6]J. J. Thomson, Philosophical Magazine, Series 6, Vol.7, Number 39, p237-265, March 1904.

[7]Linda Edwards-Shea, <u>The Essence of Solid-State Electronics</u>, (Prentice Hall, 1996).

[8]S. O. Kasap, <u>Principles of Electronic Materials and Devices</u>, 2nd ed. (McGraw-Hill Companies, Inc., New York, 2002).

[9]Ben G. Streetman, <u>Solid State electronic Devices</u>, 4th ed. (Prentice Hall, Englewood Cliffs, NJ, 1995).

[10]M. N. Rudden and J. Wilson, <u>Elements of Solid State Physics</u>, 2nd ed. (John Wiley & Sons, 1993).

[11]Stephen A. Campbell, <u>The Science and Engineering of Microelectronic Fabrication</u>, 2n ed. (Oxford University Press, Inc., 2001).

[12]Stanley Wolf and Richard N. Tauber, <u>Silicon Processing for the VLSI Era, Volume 1: Process Technology</u>, (Lattice Press, Sunset Beach, CA, 1986).

[13]Dieter K. Schroder, <u>Semiconductor Material and Device Characterization</u>, 2nd ed. (John Wiley & Sons, Inc., New York, 1998).

[14]Albert Einstein, Annalen der Physik, "Über die von der molekularkinetischen Theorie der Wärme geforderte Bewegung von in ruhenden Flüssigkeiten suspendierten Teilchen [On the Motion Required by the Molecular Kinetic Theory of Heat of Small Particles Suspended in Stationary Liquid]", 17, May 1905.

[15]P. M. Mooney, Identification of Defects in Semiconductors, edited by Michael Stavola (Academic Press, 1999) Vol. 51B, Ch. 2, pp. 93-152.

[16]D. V. Lang, Thermally Stimulated Relaxation in Solids, edited by P. Bräunlich (Springer-Verlag, 1979) Vol. 37, Chap. 3, pp. 93-133.

[17]Tudor E. Jenkins, Semiconductor Science, (Prentice Hall International (UK) Limited, 1995).

[18]A. Broniatowski, A. Blosse, P. C. Srivastava, and J. C. Bourgoin, J. Appl. Phys. 54(6), 3023 (June 1983).

[19]Peter Blood and John W. Orton, The Electrical Characterization of Semiconductors: Majority Carriers and Electron States, (Academic Press Limited, 1992).

[20]G. L. Miller, D. V. Lang, and L. C. Kimerling, Annual Review of Material Science, edited by Robert A. Huggins, Richard H. Bube, and Richard W. Roberts (Annual Reviews Inc., Palo Alto, CA, 1977), Vol. 7, Chap. "Capacitance Transient Spectroscopy", pp. 377-448.

[21]Gary E. McGuire, Characterization of Semiconductor Materials, (William Andrews Publishing/Noyes, Park Ridge, NJ, 1989).

[22]D. V. Lang, J. Appl. Phys. 45(7), 3023 (July 1974).

[23]Lakeshore Model 331 Temperature Controller User's manual

[24]http://en.wikipedia.org/wiki/PID_controller

[25]http://en.wikipedia.org/wiki/PID_controller – editor: Samil Korkmaz

[26]Diodes Incorporated, 1N4001/L-1N4007/L (1.0 A Rectifier) Datasheet

VITA

Christopher Lohn was born in San Marcos, Texas on October 24, 1971. He attended Southwest Texas State University and completed his Bachelor of Science in Physics in December 1994. After completing his degree, he worked seven years in the semiconductor industry in the areas of device engineering, sustaining engineering and process engineering. He is the co-inventor on US patent (5,985,731) from his work at Motorola, Inc. After his career in the semiconductor industry, he returned to school to pursue his Master of Science in Materials Physics at Texas State University-San Marcos. During his graduate studies, he was employed as a lab instructor, research assistant and teaching assistant and was co-author in one professional publication. He completed his Master of Science in Materials Physics in May 2008.

Permanent Address: 4809 Airport Highway 21

Maxwell, Texas 78656

This thesis was typed by Christopher Lohn.